



Developing a 3D organotypical model to  
assess gum penetrating implant soft tissue  
outcomes and implant device development

By

Cleo Laura White

A thesis submitted to the University of Birmingham for the degree of  
DOCTOR OF PHILOSOPHY

Biomaterials Unit

School of Dentistry

College of Medical and Dental Sciences

University of Birmingham

December 2018

UNIVERSITY OF  
BIRMINGHAM

**University of Birmingham Research Archive**

**e-theses repository**

This unpublished thesis/dissertation is copyright of the author and/or third parties. The intellectual property rights of the author or third parties in respect of this work are as defined by The Copyright Designs and Patents Act 1988 or as modified by any successor legislation.

Any use made of information contained in this thesis/dissertation must be in accordance with that legislation and must be properly acknowledged. Further distribution or reproduction in any format is prohibited without the permission of the copyright holder.

## ABSTRACT

Dental implants are routinely used to replace missing teeth, to restore function or improve aesthetics. Research concentrating on implant-soft tissue interactions is a recent area of interest, owing to increased cases of soft tissue recession around the implants, which can lead to implant failure. Previous research initially investigating these interactions have utilised three-dimensional cell culture techniques to generate oral organotypic cultures. However, development of those cultures involve the use of animal-derived products such as foetal bovine serum. This project aimed to develop 3D oral organotypic cultures using animal-free products, to be utilised as research tools to analyse implant-soft tissue interactions.

Monolayer and two-dimensional cultures were initially used to select an appropriate commercially available animal-component-free medium. Three-dimensional oral organotypic cultures were then generated using human H400 keratinocyte and primary gingival fibroblast cultures on de-epidermalised dermis.

Histological and RT-PCR analysis of cytokeratins 1, 5, 10, and 13, Ki-67, e-cadherin, n-cadherin, vimentin and collagen VII, indicated that animal-component-free cultures were able to support 3D oral organotypic cultures with a stratified epithelium. These structures have the potential to be utilised to analyse implant-soft tissue interactions. Further work is required to optimise these models to ensure mimicking of the *in vivo* environment.

This thesis is dedicated to my parents,  
Len and Fiona White.

## ACKNOWLEDGMENTS

Firstly, I would like to express my gratitude to my supervisors: Dr Richard Shelton, Professor Owen Addison, Professor Gabriel Landini and Professor Paul Cooper for providing support and guidance during my PhD.

I would like to acknowledge and thank my funding body, Animal Free Research UK for funding my research and Dr Alpesh Patel for providing technical advice. Your enthusiasm has fuelled my passion for animal free research; a movement in Science that I hope to see continue to grow.

I would like to greatly thank the technical team within the School of Dentistry research labs, especially Michelle Holder, Helen Wright and Jianguo Liu, for taking the time to support me during the last 4 years. Much of my data collection would not have been possible without your patience, willingness to teach and guidance.

My fourth expression of thanks goes to Dr Penny Martens and her team at the University of New South Wales (UNSW): Dr Josef Gooding, Dr Alex Pattern and Ulises Aregueta-Robles. Thank you for giving me the opportunity to come to UNSW – teaching me in your field and allowing me to work alongside you. I truly learnt a lot and had the most unforgettable time.

I have been fortunate enough to have had amazing colleagues and friends who have supported me along the way. Ilaria Chicca, Hannah Serrage, Nina Vyas, Sean Lewin, Farha Ariffin Isabel Lopez-Oliva, Amirpasha Moetazedian, Rachel Flight, Helen Roberts, Fatemeh Moghimi, Naveed Saeed, Ali Abdulkareem, Firas Albaaj and Anna Karina Costa. I can't think of better people to have gone on this journey with (or share an office with).

A massive thank you to Jade Adams-White, Amy Butkus, Alice Lane, Lauren Schafer, Anne Luges, Suzanne Di Capite, Chloe Carpenter, Lois Hayward and housemates past and present, for your support and encouragement. A major shout out and whole heartedly 'thank you' to Dr Abisola Asuni. When the going got tough, I could always rely on you for support, pep talks, phone calls and a whole lot of tough love to keep me in check and helping me reach the end (I owe you one)!

I would like to specially thank William Jenkins. You have been a constant source of support and positivity, especially on the bad days.

Finally, I would like to profoundly express my thanks to my family, particularly my parents Len and Fiona and my brother Tom. These last four years have been verging on impossible, but your endless love, support, prayers, and encouragement, have made it possible. You taught me very early on to trust in God, never give up, do my very best and always be the best version of me - principles that have guided my path and will forever shape me. Without you, I couldn't have completed this journey.

# CONTENTS

ABSTRACT .....	2
ACKNOWLEDGMENTS.....	i
CONTENTS.....	iii
LIST OF FIGURES .....	xv
LIST OF TABLES .....	xxi
LIST OF EQUATIONS.....	xxiii
LIST OF ABBREVIATIONS AND ACRONYMS .....	xxiv
CHAPTER 1: INTRODUCTION.....	1
1.1. Oral mucosa .....	2
1.1.1. Function of oral mucosa .....	2
1.1.2. Structure of the oral mucosa.....	2
1.1.3. Types of oral epithelium .....	2
1.1.3.1. Stratified keratinized epithelium .....	3
1.1.3.2. Parakeratinized epithelium .....	4
1.1.3.3. Non-keratinized epithelium .....	4
1.1.3.4. Specialised epithelium - oral papillae.....	5
1.1.4. Oral epithelium representation.....	6
1.1.5. Keratinisation.....	7
1.1.5.1. Keratins .....	7

1.1.6.	Epidermal diseases associated with keratin mutations	10
1.1.7.	Junctional complexes within oral epithelia .....	11
1.1.7.1.	Occluding junctions .....	12
1.1.7.2.	Anchoring junctions.....	13
1.1.7.2.1.	Adherens junctions .....	13
1.1.7.2.2.	Desmosomes.....	14
1.1.7.2.3.	Focal adhesions.....	16
1.1.7.2.4.	Hemidesmosomes .....	17
1.1.8.	Basement membrane .....	19
1.1.8.1.	Lamina lucida .....	19
1.1.8.2.	Lamina densa .....	19
1.1.8.3.	Lamina propria .....	20
1.1.9.	Submucosa.....	20
1.2.	Supporting anatomical structures .....	21
1.2.1.	Alveolar bone .....	22
1.2.2.	Root cementum.....	22
1.2.3.	Periodontal ligament.....	23
1.2.4.	Periodontal epithelium .....	23
1.2.4.1.	Sulcular epithelium .....	24

1.2.4.2.	Junctional epithelium .....	25
1.2.4.3.	Oral gingival epithelium .....	25
1.3.	Tooth loss .....	25
1.3.1.	Periodontitis .....	26
1.4.	Dental implants .....	28
1.4.1.	History of dental implants .....	29
1.4.1.1.	Osseointegration .....	30
1.4.1.2.	Osseointegration process .....	31
1.4.1.3.	Factors affecting osseointegration .....	32
1.4.1.3.1.	Surface topography .....	33
1.4.1.3.2.	Implant composition .....	34
1.4.2.	Success of titanium .....	35
1.4.3.	Alternative dental implant materials .....	35
1.4.4.	Peri-implant mucosa attachment to implant surfaces	36
1.4.5.	Anatomical differences between post and peri implant gingiva .....	37
1.4.6.	Dental implant failure .....	39
1.4.6.1.	Peri-implant mucositis .....	40
1.4.6.2.	Peri-implantitis .....	41
1.4.6.2.1.	Pathogenesis of peri-implantitis .....	42

1.5. Animal use in dental research .....	43
1.6. Tissue engineering.....	47
1.6.1. Two-dimensional cell culture.....	48
1.6.2. Three-dimensional cell culture .....	49
1.6.2.1. Selection of appropriate cells .....	50
1.6.2.2. Selection of an appropriate scaffold.....	52
1.6.2.2.1. Naturally derived scaffolds .....	53
1.6.2.2.2. Synthetic Scaffolds .....	55
1.6.2.3. Culture media and use of animal supplementation..	56
1.6.2.4. Use of foetal bovine serum and bovine pituitary extract.....	59
1.6.2.5. Serum free oral organotypical models .....	60
1.6.2.6. Oral organotypic model applications .....	63
1.7. Research aims and objectives.....	64
<b>CHAPTER 2: MATERIALS AND METHODS .....</b>	<b>67</b>
2.1. Isolation, expansion and cultivation of primary human gingival keratinocytes and fibroblasts .....	68
2.2. Cultivation of human oral squamous cell carcinoma cell line (H400 cells).....	70
2.3. Passaging of confluent cell cultures .....	70

2.4. H400 cell culture in animal-component-free media using Trypan Blue stain .....	71
2.5. Calculation of population doubling times .....	72
2.6. Sensitivity of Alamar Blue and MTT assays for cell culture analysis.....	73
2.7. Alamar Blue calibration curve .....	76
2.8. pHGF and H400 cell culture analysis in different animal-component-free media using Alamar Blue.....	77
2.9. Analysis of calcium concentration in different animal-component-free media .....	78
2.10. Morphological analysis of pHGFs and H400 cells cultured in different animal-component-free media.....	78
2.11. Processing of de-epidermalised dermis (DED).....	79
2.12. Development of 3D oral organotypical cultures using DED as a scaffold.....	80
2.13. Preparation of sodium alginate solution and hydrogels.....	82
2.14. Preparation of RGD-modified sodium alginate solution and hydrogels .....	82
2.15. Analysis of the effect of hydrogel cross-linking and dissociation reagents on pHGF cultures. ....	83

2.16. Analysis of the effect of encapsulation within RGD modified alginate hydrogels on pHGF cultures .....	84
2.17. Analysis of pHGF released from encapsulation within RGD modified alginate hydrogels.....	85
2.18. Analysis of H400 attachment on RGD modified alginate hydrogels .....	86
2.19. Fabrication and synthesis PEG-DM .....	87
2.20. Characterisation and calibration of the UV light system ...	88
2.21. Analysis of hydrogel disc swelling mass and loss properties .....	89
2.22. Compressive testing of hydrogels.....	90
2.23. Fixation of the processed de-epidermalised dermis (DED) .	91
2.24. Haematoxylin and Eosin staining of DED .....	93
2.25. Preparation of TiZr samples .....	95
2.26. Cell adhesion and growth on prepared TiZr samples.....	96
2.27. Preparation of TiZr for SEM imaging .....	97
2.28. Image analysis of surface attachment.....	99
2.29. Non-contact profilometry .....	100
2.30. Extraction of RNA from H400 keratinocyte cultures .....	100
2.31. Extraction of RNA from pHGF cultures .....	101
2.32. Extraction of RNA from 3D oral mucosa cultures .....	102

2.33. Isolation of RNA.....	102
2.34. Quantification and visualisation of RNA.....	104
2.35. Primer development.....	105
2.36. Semi-quantitative reverse transcription PCR analysis.....	105
2.37. PCR product visualisation by gel electrophoresis .....	108
2.38. Real Time-PCR analysis .....	109
2.39. Identification of a suitable housekeeping gene for assay normalisation .....	110
2.40. Image analysis of surface attachment.....	114
2.41. Data and statistical analysis .....	114
CHAPTER 3: RESULTS .....	116
Results Section 1 .....	117
3.1. Influence of serum supplementation on H400 keratinocyte cultures.....	117
3.2. Identification of a suitable mitomycin C concentration for use in pHGF cultures .....	121
3.3. Influence of commercially available animal-component-free culture media on H400 keratinocyte cultures .....	123
3.4. Influence of commercially available animal-component-free culture media on pHGF cultures.....	127

3.5. Influence of commercially available animal-component-free culture media on pHGK cultures .....	132
3.6. Generation of an Alamar Blue calibration curve.....	135
3.7. Alamar Blue growth curves in DMEM supplemented with Human Serum and KGM-CD .....	137
3.8. H400 gene expression analysis.....	140
3.8.1. H400 keratinocytes gene expression analysis of cytokeratin 1 (CK1).....	140
3.8.2. H400 keratinocyte gene expression analysis of cytokeratin 5 (CK5).....	141
3.8.3. H400 keratinocyte gene expression analysis of cytokeratin 6 (CK6).....	141
3.8.4. H400 keratinocyte gene expression analysis of cytokeratin 13 (CK13).....	141
3.8.5. H400 keratinocyte gene expression analysis of cytokeratin 19 (CK19).....	142
3.8.6. H400 keratinocytes gene expression analysis of vimentin .....	144
3.8.7. H400 keratinocytes gene expression analysis of e-cadherin.....	144

3.8.8. H400 keratinocytes gene expression analysis of n-cadherin.....	144
3.9. pHGF gene expression analysis .....	146
3.10. Measuring calcium levels in the different animal-component free media.....	147
Results Section 2 .....	152
3.11. H400 keratinocyte culture growth on commercially pure (Grade IV) titanium (Ti) .....	152
3.12. pHGF culture on commercially pure (Grade IV) Ti.....	156
3.13. Characterisation of the initial pHGF culture response to TiZr metals.....	159
3.14. Characterisation of long term pHGF growth on TiZr alloys .....	164
3.15. SEM analysis of surface topography of commercially pure (Grade IV) Ti, commercially pure Zr and TiZr alloys after complete polishing.....	167
3.16. Image analysis of pHGF attachment on commercially pure (Grade IV) Ti, commercially pure Zr and TiZr alloy surfaces ....	170
3.17. Surface roughness analysis on polished TiZr discs .....	172
Results Section 3 .....	177

3.18. Analysis of the efficacy of preparing de-epidermalised dermis (DED) using two different approaches.....	177
3.19. Histological analysis of 3D oral organotypic models generated in animal-component-free culture media. ....	179
3.20. Quantification of epithelial thickness .....	181
3.21. Gene expression analysis of 3D oral organotypic models generated in animal-component-free culture media. ....	185
Results Section 4 .....	189
3.22. Mechanical properties of RGD modified alginate.....	189
3.23. The effect of hydrogel reagents on pHGF cultures.....	192
3.24. Biological influence of RGD modified alginate .....	196
3.25. Mechanical properties of polyethylene glycol di-methacrylate .....	199
CHAPTER 4: DISCUSSION .....	203
Discussion of Section 1 Results.....	204
4.1. The effects of human serum supplementation .....	204
4.2. Identification of a suitable mitomycin C concentration for the generation of pHGF feeder layers .....	205
4.3. Influence of commercially available animal-component free culture media on H400 keratinocyte cultures .....	207

4.4. Influence of commercially available animal-component free culture media on pHGF cultures.....	210
4.5. Influence of commercially available animal-component free culture media on pHGK cultures .....	211
4.6. Calcium concentration of commercially available animal-component free culture media .....	213
Discussion of Section 2 Results.....	215
4.7. Understanding pHGF and H400 keratinocyte culture growth on commercially pure (Grade IV) Ti .....	215
4.8. Understanding pHGF culture response to TiZr metals....	216
Discussion of Section 3 Results.....	222
4.9. Analysis of the efficacy of preparing de-epidermalised dermis (DED) from two approaches .....	222
4.10. Analysis of 3D oral organotypic cultures in animal-component-free culture media .....	223
4.11. Gene expression analysis of 3D oral organotypic cultures in animal-component-free culture media .....	227
Discussion of Section 4 Results.....	231
4.12. Understanding the mechanical properties of RGD modified alginate.....	231

4.13. Understanding the biological properties of RGD modified alginate .....	233
4.14. Understanding the effect of hydrogel reagents on pHGF cultures.....	235
4.15. Understanding the mechanical properties of PEG-DM237	
CHAPTER 5: CONCLUSIONS .....	240
Future Work .....	242
Optimisation of animal-component-free environments:.....	242
TiZr analysis .....	243
3D oral organotypic culture development .....	244
Hydrogel scaffold development.....	245
LIST OF REFERENCES.....	246
APPENDIX .....	276
Outputs from this research.....	277

## LIST OF FIGURES

Figure 1: Diagram of keratinized and non-keratinized epithelium .....	5
Figure 2: Diagram representing the locations of the differing types of oral epithelium .....	7
Figure 3: Diagram of an occluding junction .....	12
Figure 4: Diagram of an adherens junction .....	14
Figure 5: Diagram of a desmosome .....	15
Figure 6: Diagram of a focal adhesion.....	17
Figure 7: Diagram of a hemidesmosome .....	18
Figure 8: Diagram of the relationship of the periodontal tissues .....	22
Figure 9: Diagram of the periodontal epithelia and other periodontal tissues .....	24
Figure 10: Diagram of the structural components of a 3-part dental implant system. ....	29
Figure 11: Diagram highlighting the structural differences between natural mucosa and peri-implant mucosa.....	38
Figure 12: Emission and excitation spectrum for Irgacure 2959 .....	89
Figure 13: H400 keratinocyte growth curves in DMEM supplemented with different concentrations of serum .....	118
Figure 14: Viability of H400 keratinocytes in DMEM supplemented with different concentrations of human serum.....	120
Figure 15: The effect of varying concentrations of mitomycin C on pHGF cultures .....	122

Figure 16: Viability of pHGF cultures after exposure to different concentrations of mitomycin C.....	123
Figure 17: Growth curves of H400 keratinocyte cultures in three animal-component-free culture media.....	125
Figure 18: Average population doubling times of cultures of H400 keratinocytes grown in different animal-component-free media .....	126
Figure 19: Cell viability of H400 keratinocyte cultures grown in three animal-component-free culture media.....	127
Figure 20: Growth curves of pHGF cultures in three animal-component-free culture media .....	128
Figure 21: Average population doubling times of pHGF cultures grown in different animal-component-free media.....	130
Figure 22: Viability of pHGF cultures grown in three animal-component-free culture media .....	131
Figure 23: Growth curves of pHGK cultures in three animal-component-free culture media. ....	133
Figure 24: pHGK average population doubling times calculated for cultures in different animal-component-free medium .....	134
Figure 25: Viability of pHGK cultures grown in three animal-component-free culture media .....	135
Figure 26: Alamar Blue calibration curve for H400 keratinocytes ....	136
Figure 27: Alamar Blue calibration curve for pHGF cultures.....	137

Figure 28: Alamar Blue growth curves of H400 keratinocytes grown in either DMEM supplemented with 10% human serum or KGM-CD ..	138
Figure 29: Alamar Blue growth curves for pHGF cultures grown in either DMEM supplemented with 10% human serum or KGM-CD ..	139
Figure 30: H400 keratinocyte cytokeratin gene expression .....	143
Figure 31: H400 keratinocyte intermediate filament and cell adhesion gene expression .....	145
Figure 32: Calibration curve of calcium electrode. ....	149
Figure 33: Calcium concentrations of selected animal-component-free media.....	150
Figure 34: H400 keratinocyte growth curves grown on either tissue culture plasticware or commercially pure (grade IV) Ti discs.....	153
Figure 35: Viability of H400 keratinocyte cultures grown on tissue culture plasticware or commercially pure (Grade IV) Ti discs.....	155
Figure 36: Viable pHGF culture growth curves on either tissue-culture plasticware or commercially pure (grade IV) Ti discs.....	157
Figure 37: Viability of pHGF cultures grown on tissue culture plasticware or on commercially pure (Grade IV) Ti discs.....	158
Figure 39: Viability of pHGF cell attachment on TiZr alloys .....	162
Figure 40: Viability of pHGF cultures grown on either TiZr alloys, commercially pure (Grade IV) Ti, commercially pure Zr or tissue culture plasticware .....	163

Figure 41: Alamar Blue growth curves of pHGF cultures grown on either TiZr alloys, commercially pure (grade IV) Ti, commercially pure Zr or tissue culture plasticware .....	165
Figure 42: Average population doubling times of cultures of pHGF cultures grown on either TiZr alloys, commercially pure (grade IV) Ti, commercially pure Zr or tissue culture plasticware .....	166
Figure 43 (a-e): Representative SEM images of the surface topography of TiZr alloys.....	168
Figure 44 (a-e): Representative SEM images of pHGFs attached to the surface of TiZr alloys.....	169
Figure 45: Representative SEM images of pHGF cells attached to the surface of different TiZr alloys with their corresponding segmented images.....	171
Figure 46: Non-contact profilometry representative images of TiZr discs.....	174
Figure 47: Average surface roughness values for polished TiZr discs	175
Figure 48: Haematoxylin and eosin stained sections of unprocessed and processed de-epideramised dermis. ....	178
Figure 49: Haematoxylin and eosin stained sections of 3D oral organotypic models generated within either DMEM supplement with 10% human serum or KGM-CD.....	180

Figure 50: Haematoxylin and eosin stained sections of 3D oral organotypic models cultured in DMEM supplemented with 10% human serum, with their corresponding segmented images .....	182
Figure 51: Haematoxylin and eosin stained sections of 3D oral organotypic models cultured in KGM-CD, with their corresponding segmented images. ....	183
Figure 52: Calculated epithelium thickness from the segmented images of haematoxylin and eosin stained sections of 3D oral organotypic model.....	184
Figure 53: Gene expression levels of 3D oral organotypic models. ....	188
Figure 54: Stress-strain curves of different weight percent alginate hydrogel discs and RGD modified alginate hydrogel discs.....	190
Figure 55: Mass loss graphs for different weight percent alginate hydrogel discs and RGD modified alginate hydrogel discs.....	192
Figure 56: pHGF growth curves after exposure to different reagents involved in fabricating and dissolving alginate hydrogel discs.....	194
Figure 57: Viability of pHGF cultures exposed to different reagents involved in fabricating and dissolving alginate hydrogel discs.....	195
Figure 58: Growth curves of pHGF cell cultures following release from encapsulation within RGD modified alginate hydrogel discs.....	197
Figure 59: Growth curves of H400 cell cultures attached to the surface of RGD modified alginate hydrogel discs. ....	198

Figure 60: Stress-strain curves of different modulations of PEG-DM hydrogels under compressive force .....	200
Figure 61: Mass loss graphs for 10wt% or 20wt% PEG-DM hydrogel discs.....	202

## LIST OF TABLES

<b>Table 1:</b> Location, structure and function of oral papillae .....	6
<b>Table 2:</b> Details of oral epithelium keratin pairings .....	10
<b>Table 3:</b> Epidermal diseases associated with cytokeratin mutations .	11
<b>Table 4:</b> Stages of biological sample dehydration and fixation .....	92
<b>Table 5:</b> The various stages of Haematoxylin and Eosin staining .....	94
<b>Table 6:</b> Details of the silicon carbide grit sizes at respective grades.	96
<b>Table 7:</b> Component reagents forming the master mix for reverse transcription .....	106
<b>Table 8:</b> Reagents and volumes used in the primer master mix for the polymerase chain reaction. ....	107
<b>Table 9:</b> Details of the different stages of PCR .....	107
<b>Table 10:</b> Details of the components of each well used for qRT-PCR plate set-up. ....	109
<b>Table 11:</b> Primers and their details used for pHGK and H400 cell semi-quantitative RT-PCR analysis .....	111
<b>Table 12:</b> Primers used to quantify gene expression in H400 cultures and pHGFs using Real Time PCR .....	112
<b>Table 13:</b> Population doubling times of H400 kerationcytes cultured in different animal-component free media. ....	119
<b>Table 14:</b> Equations of the lines of best fit calculated from Alamar Blue calibration curves.....	137

<b>Table 15:</b> RT-PCR analysis showing fold changes in transcription of characterising genes of pHGF cells cultured in animal-component free media.....	147
<b>Table 16:</b> Calculated compressive moduli of the different weight percent alginate hydrogel discs and RGD modified alginate hydrogel discs.....	191
<b>Table 17:</b> Calculated compressive moduli of different compositions of PEG-DM hydrogel discs .....	201

## LIST OF EQUATIONS

Equation 1: Calculation of population-doubling time .....	72
Equation 2: Calculation of the percentage of reduced Alamar Blue ....	75
Equation 3: Calculation of hydrogel swelling ratio.....	90
Equation 4: Calculation of percentage surface coverage .....	100
Equation 5: Calculation of relative gene expression.....	109

## LIST OF ABBREVIATIONS AND ACRONYMS

°C	Degrees Celsius
µg	Microgram
µl	Microlitre
µm	Micromolar
2D	Two-dimensional
3D	Three-dimensional
ACTB	Beta (β)-actin
ALI	Air liquid interface
ANOVA	Analysis of variance
B2M	Beta-2-microglobulin
Bp	Base pair
Ca <sup>2+</sup>	Calcium ion
CaCl <sub>2</sub>	Calcium chloride
cDNA	Complementary de-oxyribonucleic acid
CK	Cytokeratin
Cm	Centimetre
Cm <sup>3</sup>	Centimetre cubed
CP Ti	Commercially pure (Grade IV) titanium
DED	De-epidermalised dermis
DM -	Dimethactylate
DMEM	Dulbecco's modified Eagle's medium
DMSO	Dimethyl sulfoxide
DNA	Deoxyribonucleic acid
Dnase I	Deoxyribonuclease I
dPBS	Dulbeccos phosphate buffered saline
ECM	Extracellular matrix
EDTA	Ethylenediaminetetraacetic acid
FBS	Foetal bovine serum
g	Gram
GAPDH -	Glyceraldehyde 3-phosphate dehydrogenase
HEPES -	4-(2-hydroxyethyl) piperazine-1-ethanesulfonic acid
HMDS	Hexmethylidisilazane
IL-8	Interleukin 8
IMS 99	Industrial methylated spirit 99 %
Irgacure 2959	2-Hydroxy-4'-(2-hydroxyethoxy)-2 methylpropiophenone
IU/ml	International units per millilitre

KGM-CD	Keratinocyte growth media – chemically defined
kV	Kilo volts
L	Litre
M	Molar
ml	Millilitre
mm	Millimetre
mm <sup>3</sup>	Millimetre cubed
mM	Millimolar
MMP	Matrix metalloproteinases
MPa	Megapascal
mRNA	Messenger ribonucleic acid
mV	Millivolts
MW	Molecular weight
MTT	3-(4,5-Dimethylthiazol-2-yl)-2,5-diphenyltetrazolium bromide
NaCl	Sodium chloride
Pa	Pascals
PBS	Phosphate buffered saline
PCR	Polymerase chain reaction
PEG	Polyethylene glycol
PEG-DM	Polyethylene glycol – methacrylate
PMN	Polymorphonuclear neutrophils
Ppm	Parts per million
Ra	The arithmetic mean deviation of the roughness profile from the mean line.
RGD	Arginine-Glycine-Aspartic Acid
RNA	Ribonucleic acid
RO	Reverse osmosis
rpm	Revolutions per minute
RT-PCR	Reverse transcription polymerase chain reaction
RUNX2	Runt-related transcription factor 2
S7	Supplement S7
SiC	Silicon carbide
SEM	Scanning electron microscope
sqRT-PCR	Semi quantitative reverse transcriptase
Ti	Titanium
TiZr	Titanium zirconium alloys
VII	Seven
v/v	Volume per volume
w/v	Weight per volume

YWHAZ	Tyrosine 3-monooxygenase/tryptophan 5-
	monooxygenase activation protein zeta
Zr	Zirconium

# **CHAPTER 1:**

# **INTRODUCTION**

## 1.1. Oral mucosa

### 1.1.1. *Function of oral mucosa*

The oral mucosa is a soft tissue membrane that lines the oral cavity and acts as a biological barrier to separate the underlying tissue, protecting from mechanical and pathogenic damage. Depending on location, the mucosa also provides additional functions, such as taste, touch and synthesis of saliva. Despite being categorized as a mucous membrane, owing to the secretions produced by the salivary glands, the structure is comparable with that of skin, although noticeably different in appearance due to lack of appendages such as hair follicles and sweat glands (Brogden and Squier, 2011; Cruchley and Bergmeier, 2018).

### 1.1.2. *Structure of the oral mucosa*

The oral mucosa consists of three different tissue components; **epithelium**, the outer lining consisting of layers of epithelial cells, the **lamina propria**, a loosely arranged connective tissue layer that supports the epithelium tissues and the **submucosa**, a layer of highly irregular and dense connective tissue containing epithelial salivary glands (Squier and Kremer, 2001).

### 1.1.3. *Types of oral epithelium*

The epithelium acts as the direct protective barrier between the body and environment. There are four subtypes of oral epithelium located in

different regions of the mouth; stratified keratinized epithelium, stratified parakeratinized epithelium, stratified non-keratinized epithelium and specialised epithelium. Oral epithelium is also classified as ‘stratified squamous’, meaning that it is composed of tightly packed multiple cell layers regardless of subtype. Both keratinized and non-keratinized epithelia have a basal layer (stratum basale) composed of cuboidal progenitor cells, that either i) migrate up and differentiate into large polygonal shaped keratinocytes, forming the spinous (prickle) cell layer or ii) remain as progenitor cells which maintain the keratinocyte population and can be used in tissue repair (Brogden and Squier, 2011).

#### *1.1.3.1. Stratified keratinized epithelium*

Keratinized epithelium is an abrasive resistant and tough epithelium, commonly found in locations within the oral cavity constantly exposed to repeated stresses from the environment, such as the ones derived from mastication. From the prickle layer, cells migrate towards the surface forming a granular cell layer, aptly named due the presence of keratohyalin granules within the cells. These granules are understood to be involved in the keratinization process by promoting cell dehydration, cell aggregation and the cross-linking of keratin fibres within the dehydrated cells. Moving more superficially from the granular layer, cells terminally differentiate forming the keratinized layer, which comprises cornified (non-viable) surface keratinocytes that

contain keratin protein and lack visible nuclei. The cornified envelope surrounds these cells, which contains lipids and cross-linked proteins and acts as a vital component of the epithelial barrier (Fukuyama and Epstein, 1986; Presland and Dale, 2000; Hand and Frank, 2015).

#### *1.1.3.2. Parakeratinized epithelium*

Parakeratinized epithelium is another type of masticatory mucosa, commonly located in regions of the hard palate and gingiva. Despite histologically presenting a similar structure to keratinized epithelium there is one key difference; the presence of shrunken nuclei within the superficial keratinized layers (Nanci, 2008).

#### *1.1.3.3. Non-keratinized epithelium*

Non-keratinized epithelium includes buccal and soft palate tissues and is known as lining mucosa; due to not experiencing the same level of environmental stresses as keratinized epithelium. Above the prickle layer, is the intermediate layer which consists of large flattened keratinocytes, containing a large amount of cytoplasmic protein filaments known as cytokeratins.. Non-keratinized epithelium has a superficial layer consisting of viable keratinocytes with nuclei (Brogden and Squier, 2011). Structural differences between keratinized and non-keratinized layers are presented in Figure 1.

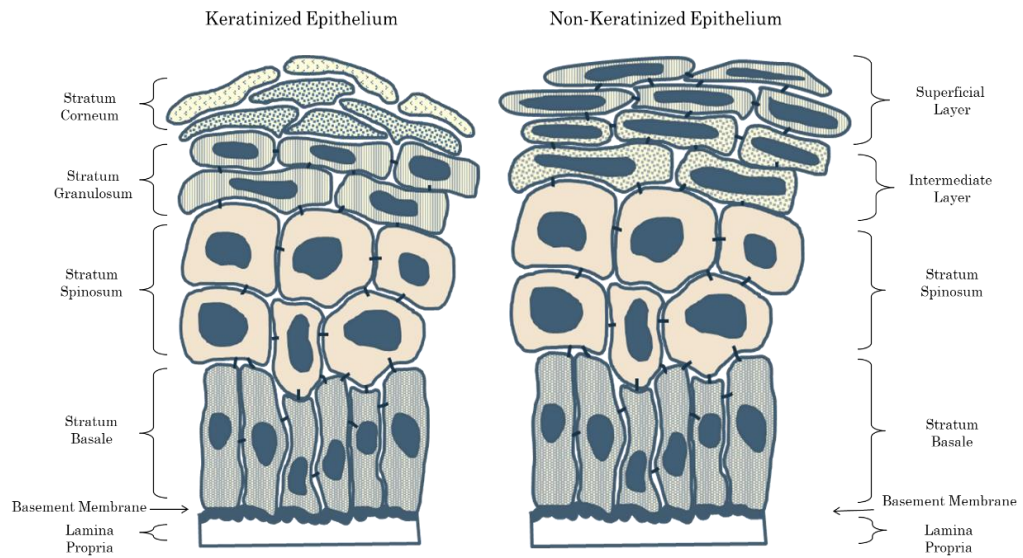


Figure 1: Schematic diagram highlighting the different layers of keratinized and non-keratinized oral epithelium. Image drawn by author, adapted from Nanci (2008).

#### 1.1.3.4. *Specialised epithelium - oral papillae*

Epithelium unique to the dorsal surface of the tongue contains oral papillae. There are four types of papillae: filiform, fungiform, circumvallate and foliate (Nanci and Bosshardt, 2006). Locations, structure, and function of each are presented in Table 1.

Table 1: Location, structure and function of oral papillae

<b>Type of Papillae</b>	<b>Location</b>	<b>Structure</b>	<b>Function</b>
Filiform	Anterior two thirds of tongue	Small cone shaped structures that protrude out of the surface.	Provides texture to the tongue and touch sensations.
Fungiform	Tip of tongue	Smooth round structures covered with non-keratinised epithelium	Provides perception of taste
Circumvallate	Posterior aspect of tongue.	Truncated dome shaped structure	Provides perception of taste (particularly bitter tastes)
Foliate	Side of tongue	Short, vertical folds covered in non-keratinised epithelium	Provides taste sensations

#### *1.1.4. Oral epithelium representation*

Representation of the distribution of oral mucosa in relation to the type of epithelium is presented in Figure 2. Lining mucosa, which is structurally categorised as non-keratinised epithelium equates to approximately 60% of the oral lining. Masticatory mucosa, categorised as stratified epithelium equates to 25% and specialised epithelium, typically identified due to the presence of oral papillae equates to 15% of the oral lining (Collins and Dawes, 1987).

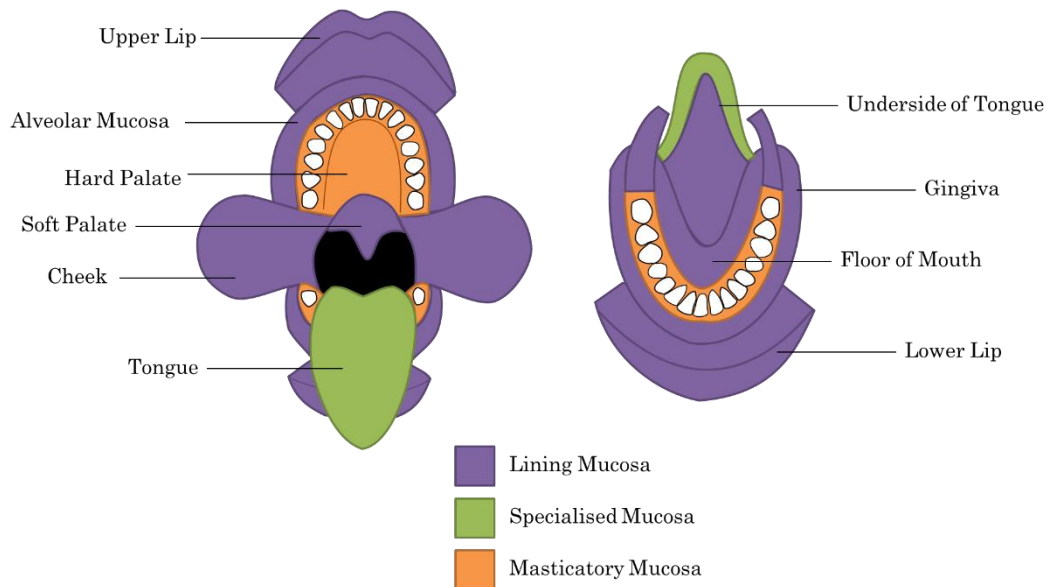


Figure 2: A schematic diagram representing the locations of the differing types of oral epithelium. Image drawn by author, adapted from Roed-Petersen and Renstrup (1969).

### 1.1.5. Keratinisation

To form the structure of keratinised oral epithelium, keratinocytes undergo a process known as keratinisation. This is where keratinocytes undergo terminal differentiation upon migration from the basal layer to form a flattened hardened cell filled with protein without nuclei; also known as the cornified layer (Shetty and Gokul, 2012).

#### 1.1.5.1. Keratins

Keratins are intermediate filament forming proteins, with molecular weights ranging from 40-66 kDa which are the structural proteins of epithelia. Studies by Schweizer *et al* (2006) have shown that there are 54 functional genes for keratins which either code for cysteine-rich

keratins, specific to tissues forming epidermal appendages or keratin proteins involved in forming intermediate filaments found within keratinocytes. These proteins are commonly used as fundamental markers of epithelial differentiation due to the specificity of distribution within epithelia. Commonly categorised by molecular weight and charge, there are two main types of keratins: type I, which have acidic properties and type II which have basic properties and are approximately 8 kDa larger. There are 17 type I and 20 type II keratins distributed within epithelia and when paired with their respective other, form intermediate filaments (for pairings see

Table 2 overleaf). Upon analysis, expressions patterns of keratins can determine the type of epithelia and anatomical location (Presland and Dale, 2000; Belaldavar *et al.*, 2016).

Table 2: Details of oral epithelium keratin pairings

<b>Keratin Type</b>		
Acidic	Basic	<b>Expression</b>
1	10	Epithelium: Keratinized Epithelium layer: Suprabasal Anatomical location: Oral gingival epithelium
4	13	Epithelium: Non-keratinized Epithelium layer: Suprabasal Anatomical location: Alveolar epithelium, gingival margin, sulcular epithelium
5	14/15	Epithelium: Keratinized and non-keratinized Epithelium layer: Basal Anatomical location: Junctional epithelium, sulcular epithelium, gingival margin, oral gingival epithelium, alveolar epithelium
6	16	Epithelium: Keratinized Epithelium layer: Hyperproliferative (Suprabasal) Anatomical location: Oral gingival epithelium
8	18	Epithelium: Simple Epithelium layer: Suprabasal Anatomical location: Junctional epithelium
19		Epithelium: Non-keratinized Epithelium layer: Basal Anatomical location: Junctional epithelium, sulcular epithelium, alveolar epithelium

#### *1.1.6. Epidermal diseases associated with keratin mutations*

Mutations of cytokeratin genes can cause a variety of disorders that predominately affect the skin and occasionally the oral mucosa, such as epidermolysis bullosa simplex and white sponge naevus (Johnston and Johnston, 2012; Shetty and Gokul, 2012). Details of these genetic disorders are provided in Table 3.

Table 3: Epidermal diseases associated with cytokeratin mutations

<b>Disease</b>	<b>Mutation</b>	<b>Inheritance</b>	<b>Oral Appearance</b>
Epidermolysis Bullosa Simplex	CK5, CK14	Autosomal Dominant	Dependant on type. Includes, blistering of oral mucosa and soft tissue lesions.
Pachyonychia Congenita	CK6a+b, CK16, CK17	Autosomal Dominant	Oral leukoplakia
White Sponge Naevus	CK4, CK13	Autosomal Dominant	Symmetrical, thick plaques, spongy in texture, usually on the buccal mucosa
Congenital Ichthyosiform Erythroderma	CK1, CK10	Autosomal recessive	Fine white scales

#### 1.1.7. *Junctional complexes within oral epithelia*

Junctional complexes are necessary to organise cells to form the required tissues and organs and can either be present between cells or between cells and the extracellular matrix, with the greatest prevalence occurring in epithelia. Cell junctions are classified into three main groups; occluding, anchoring, and communicating. These complexes are required to form the protective barrier of the epithelium observed within oral mucosa (stratified epithelium) by forming attachments between keratinocytes in different layers and the underlying basement membrane; anchoring cells together (Alberts *et al.*, 2002).

### 1.1.7.1. Occluding junctions

The main function of occluding junctions (also known as tight junctions or zonula occludens) is to minimise the space between adjacent cells, preventing the loss of molecules and moisture. These junctions also aid in supporting the barrier role of the epithelia by maintaining the polarity of cells and preventing lateral diffusion of certain membrane (Giepmans and van Ijzendoorn, 2009). The structure of occluding junctions is illustrated in Figure 3.

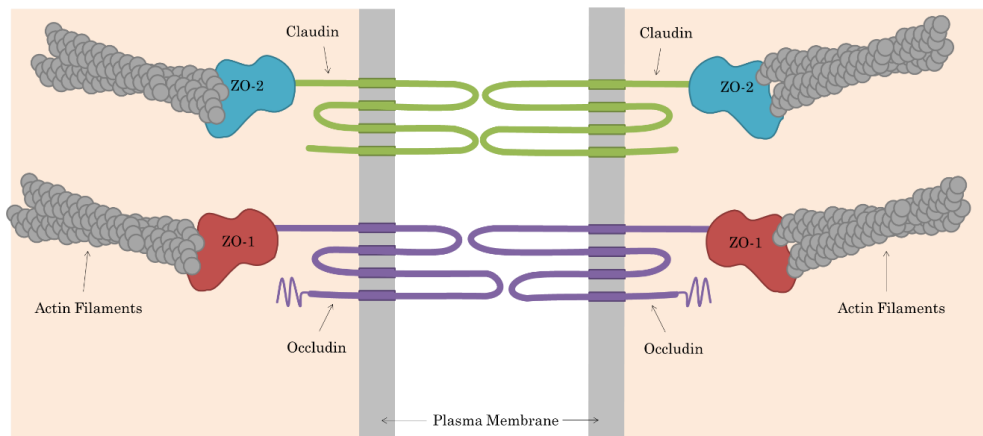


Figure 3: Structure of an occluding junction highlighting key proteins involved in the formation of this junction. Image drawn by author, adapted from Alberts *et al.* 2002) and Mateo *et al.* (2015).

Briefly, occluding junctions are comprised of sealing strands of claudin and occludin, which embed into the two adjacent plasma membranes which are key in the formation of these junctions. Both proteins interact with intracellular membrane proteins located within the structure known as zonula occludens, which in turn anchors the

strands of claudin or occludin actin fibres within the skeleton (Alberts *et al.*, 2002; Shen, 2012).

#### 1.1.7.2. *Anchoring junctions*

Anchoring junctions are found in tissues that undergo significant mechanical stresses, such as the heart and skin, and provide the necessary strength to transfer these stresses between cells and the ECM. There are two distinct types of anchoring junctions, 1. adherens junctions and desmosomes and 2. focal adhesions and hemidesmosomes (Alberts *et al.*, 2002; Giepmans and van Ijzendoorn, 2009).

##### 1.1.7.2.1. *Adherens junctions*

Adherens junctions have multiple functions including regulating the cytoskeleton, intracellular signalling and stabilising cell-cell adhesion; reinforcing occluding junctions, typically found above. Adherens junctions form an adhesion belt (also known as zonula adherens), that runs continuously in adjacent cells. Transmembrane adhesion proteins, specifically cadherins and catenins, anchor the adhesion belt together to the actin cytoskeleton within the cell (Alberts *et al.*, 2010; Harris and Tepass, 2010). Figure 4 illustrates the structure of an adherens junction.

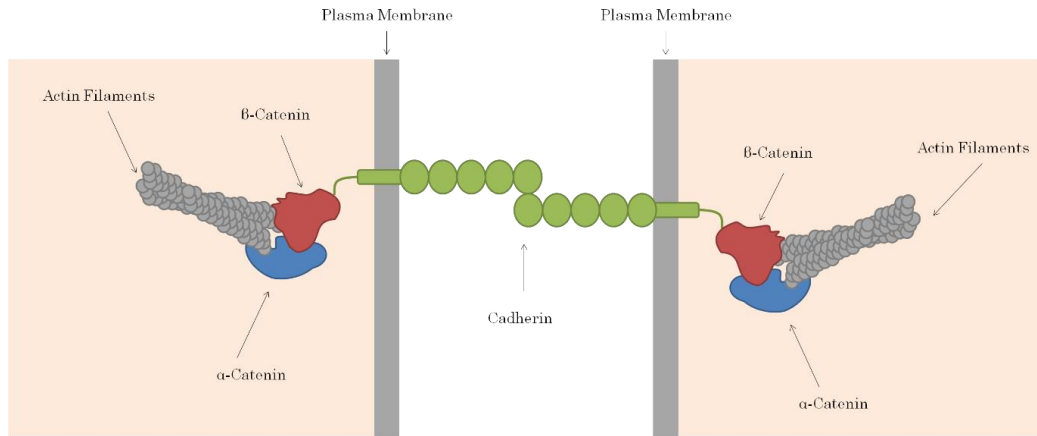


Figure 4: Structure of an adherens junction highlighting key proteins involved in the formation of this junction. Image drawn by the author, adapted from Alberts *et al.* (2002) and Aktary and Pasdar, (2012).

E-cadherin is a particularly noteworthy transmembrane protein due to commonly being used as a molecular marker for epithelial cells. Changes in expression levels of this protein are associated with physiological events such as epithelial-mesenchymal transition (EMT), which is the process where epithelial cells lose their epithelial phenotype and acquire mesenchymal cell phenotype such as an increased migratory capacity due to a series of biochemical changes (Giepmans and van Ijzendoorn, 2009; Lamouille, Xu and Derynck, 2014).

#### 1.1.7.2.2. *Desmosomes*

Similarly to adherens junction, desmosomes are located within tissues that experience high mechanical stresses and need to maintain tissue integrity. These junctions comprise a dense region of intracellular anchor proteins, keratin intermediate filaments and adhesion

molecules known as desmosomal cadherins (Alberts *et al.*, 2002; Garrod and Chidgey, 2008). This structure is illustrated in Figure 5.

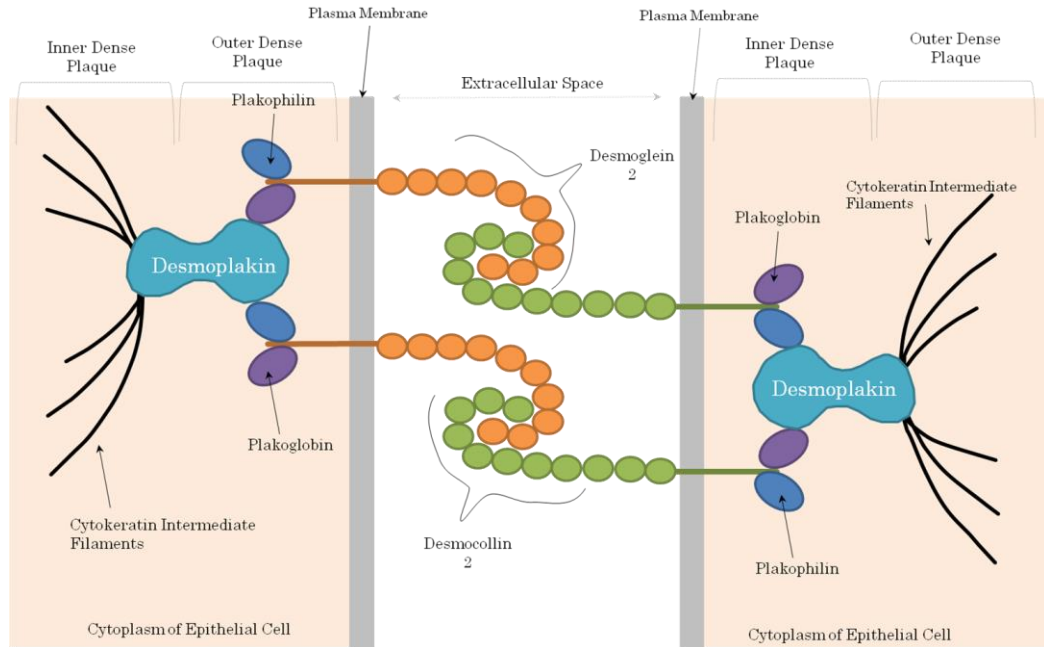


Figure 5: Structure of a desmosome highlighting key proteins involved in the formation of this junction. Image drawn by author, adapted from Garrod and Chidgey, (2008); Delva *et al.*, (2009).

Desmosomal anchor proteins (desmoplakin and plakoglobin) connect the keratin intermediate filaments to the desmosomal adherens (desmocollin 1-3 and desmoglein 1-4), forming a connection between two adjacent cells. Mutations within the desmosomal proteins, especially plakophilin 1 can lead to skin blistering disease, skin fragility ectodermal dysplasia syndrome, an autosomal recessive disorder (McGrath, 2005; Garrod and Chidgey, 2008).

#### 1.1.7.2.3. *Focal adhesions*

Focal adhesions are junctions that link the cytoskeleton of integrin receptor basal cells to the underlying extracellular matrix. The main proteins involved in forming these junctions are integrins and actin filaments. Actin fibres of the cytoskeleton are anchored through junctional plaque proteins vinculin and  $\alpha$ -actinin, filamin or talin to integrin proteins which in turn are bound to proteins within the extracellular matrix. (Alberts *et al.*, 2002; Wehrle-Haller, 2012).

Depending on which extracellular matrix protein the basal keratinocyte forms a junction with, influences which integrin subunits are present within this junction. Key ECM proteins include Laminin 1 (which forms attachment  $\alpha 2\beta 1$ ), laminin 5 (which forms attachment  $\alpha 5\beta 1$ ), collagen IV (which forms an attachment  $\alpha 9\beta 1$ ) and collagen VII (which forms an attachment  $\alpha 6\beta 4$ ) (Larjava *et al.*, 2011). The generic structure of a focal adhesion is presented in Figure 6.

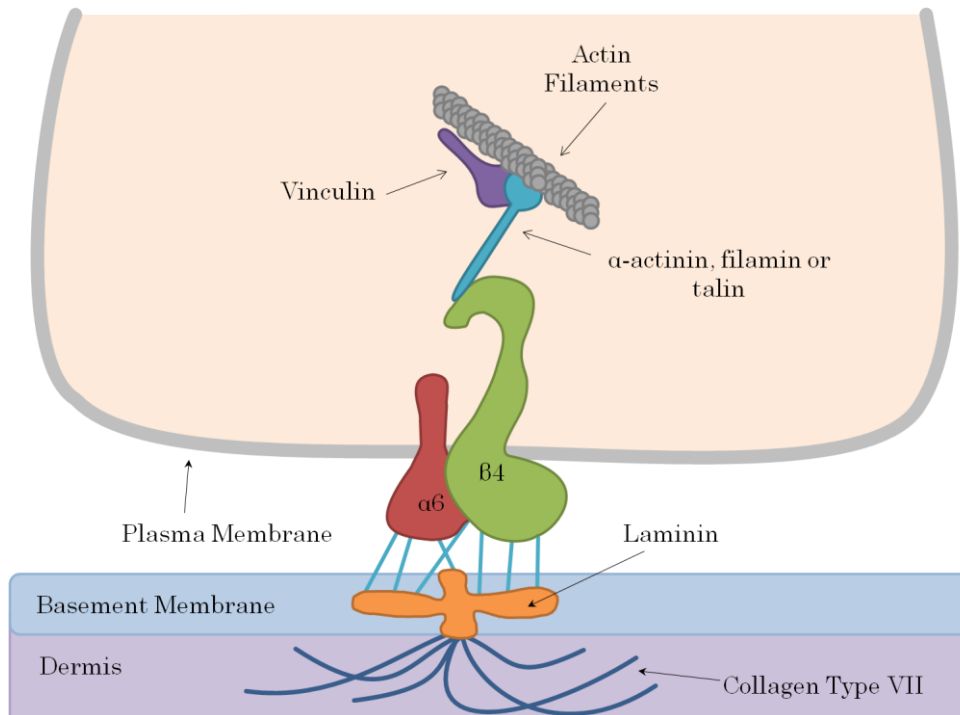


Figure 6: Structure of a focal adhesion highlighting key proteins involved in the formation of this junction. Image drawn by author, adapted from Garrod and Chidgey., (2008); Delva *et al.*, (2009).

#### 1.1.7.2.4. Hemidesmosomes

Hemidesmosomes have a similar morphology to that of a desmosome, although are responsible for adhering cells to the underlying extracellular matrix via integrins rather than adjacent cells. These junctions evenly distribute any tensile or shear forces that the epithelium may experience, and this occurs due to interactions through the protein components that form this complex. The core protein components of these structures are integrin  $\alpha6\beta4$ , laminin-332, an extracellular matrix protein and plectin, a cytoskeletal linker. Other important proteins include bullous pemphigoid antigen 1 (BPAG1) and

2 (BPAG2), these are proteins which form part of the adhesive junctional plaques (Alberts *et al.*, 2002; Walko *et al.*, 2015). The process by which these components interact to form hemidesmosomes is illustrated below in Figure 7.

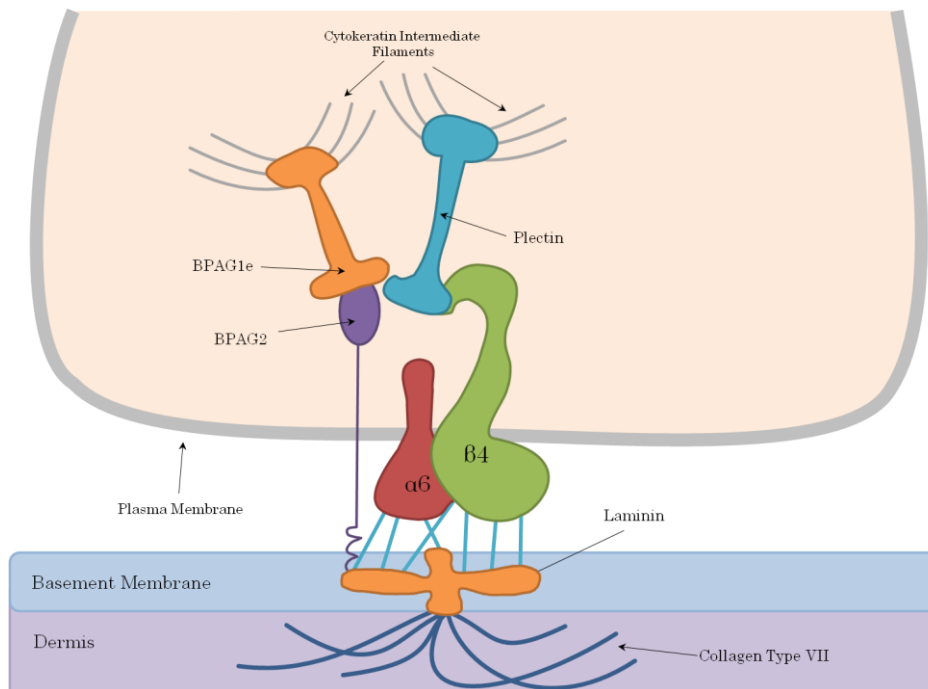


Figure 7: Structure of a hemidesmosome, highlighting key proteins involved in the formation of this junction. Image drawn by author, adapted from Alberts *et al.*, (2002) and Walko *et al.*, (2015).

Mutations that lead to structurally altered or missing proteins components, result in blistering skin diseases such as bullous pemphigoid and contribute to the disorders previously outlined in Table 3 (Zillikens, 1999).

### *1.1.8. Basement membrane*

The basement membrane (BM) is a semi-permeable extracellular matrix (ECM) that acts as an interface layer between the underlying connective tissue layers and the epidermis. This highly organised glycoprotein scaffold, elastic yet tough in nature, structurally supports the progenitor cells of the basal layer and through outside-in signalling, can modify cell behaviour. There are two morphologically distinct areas within the epidermal basement membrane: the lamina densa (an electron dense region) and the lamina lucida (Yurchenco and Patton, 2009; Hand and Frank, 2015).

#### *1.1.8.1. Lamina lucida*

The lamina lucida, is located directly above the lamina densa and is a relatively thin layer (20-40nm thick) composing of adhesive glycoproteins and laminin-5. Anchoring filaments extending from the hemidesmosomes formed between the basal cells and the lamina densa, perpendicularly traverse this layer (Merker, 1994; Ikeda *et al.*, 2000).

#### *1.1.8.2. Lamina densa*

The lamina densa layer is synthesized by the basal cells of the epithelium and can range from 30-150nm in thickness. The main structural components of this layer are collagen type IV and collagen type VII. Collagen type IV forms an open network providing strength

and easy passage to necessary fluids and macromolecules to the upper epidermis. Collagen type VII, forms part of the hemidesmosome anchoring filaments and glycoproteins such as laminin, which aids cell attachment to type IV collagen and fibronectin (Rohrbach and Martin, 1982; Yurchenco and Patton, 2009).

#### 1.1.8.3. *Lamina propria*

The lamina propria supports epithelium and basement membrane and is split into two layers: papillary and reticular. The more superficial layer of the two is the papillary layer which contains loosely arranged type 1 collagen fibres. This layer is often grooved, due to rete ridges (or rete-pegs) which are downward processes that extend from the epithelium to increase the attachment area between epithelium and underlying tissues. This layer also contains fibroblasts, peripheral nerves, vascular channels, and elastic fibres. Beneath the papillary layer is the reticular layer which consists of thick and dense collagen and elastic fibres, arranged into a lattice-like network (Paulsen and Thale, 1998; Chen *et al.*, 2015).

#### 1.1.9. *Submucosa*

In all areas of the oral mucosa, apart from the anterior portion of the hard palate and attached gingiva, the submucosa is located below the lamina propria. This layer consists of bands of collagen and elastic tissue which are highly vascularised and contain numerous nerve

fibres. Salivary glands, which secrete onto the mucosal surface are sometimes present, dependent upon location (Squier and Kremer, 2001).

## 1.2. Supporting anatomical structures

Masticatory mucosa is the 'umbrella' term given to all the soft tissues within the oral cavity that are able to withstand the forces of mastication. Tissues considered to be masticatory include the hard palate and the periodontium, which surrounds and supports teeth. The periodontium can be divided into four tissue sections: alveolar bone, root cementum, periodontal ligaments, and gingiva; and are illustrated below in

Figure 8.

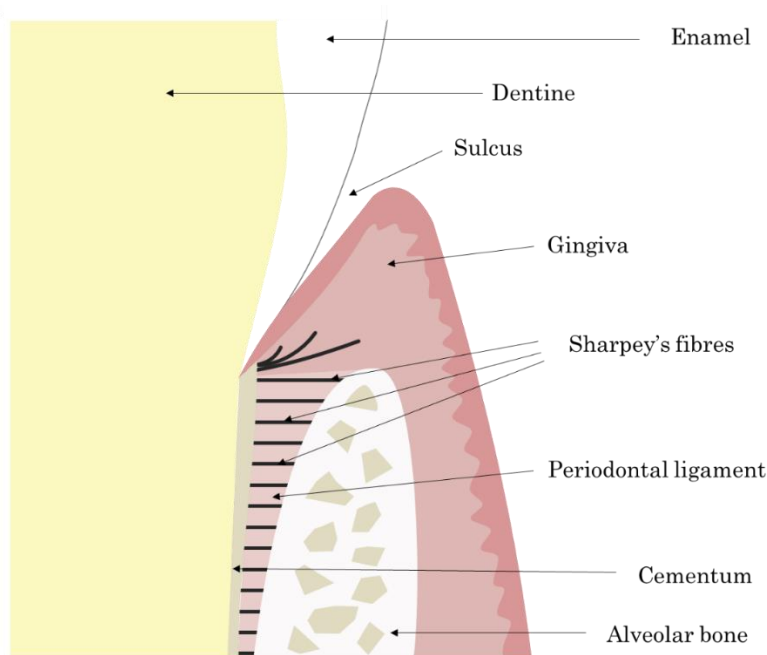


Figure 8: Relationship of the periodontal tissues, forming the periodontium. Image drawn by author, adapted from Barczyk *et al.*, (2013); Lindhe *et al.*, (2015).

### *1.2.1. Alveolar bone*

Alveolar bone is part of the mandibular and maxillary bones which contains pockets, known as alveoli, where teeth are located. It comprises three anatomical components, two plates of compact bone which form the shape of the alveoli, and spongy bone, which not only lines the alveoli but also acts as an attachment site for the bundles of periodontal ligament fibres and the associated tooth (Matalová *et al.*, 2014).

### *1.2.2. Root cementum*

Root cementum is a hard-mineralised tissue that covers the tooth root providing an attachment surface to periodontal ligament fibres.

Cementum is secreted by cementoblasts through a process known as cementogenesis which is where cementum matrix (composition dependant on the type of cementum) is secreted and deposited onto the exposed dentine, which then crystallises and mineralises, forming cementum. There are two forms of cementum, categorised as acellular and cellular. Acellular cementum is composed of mineralised non-collagenous proteins and perpendicularly arranged collagen fibres. Cellular cementum has a similar composition to acellular cementum; however it is less mineralised and has cementocytes located throughout the matrix. The perpendicular collagen fibres that traverse

cementum, connect to Sharpey's fibres that originate from the periodontal ligament, thus connecting cementum to dentine and alveolar bone (Lindhe *et al.*, 2015; Yamamoto *et al.*, 2016).

### *1.2.3. Periodontal ligament*

The periodontal ligament (PDL) is an attachment between the cementum and the underlying alveolar socket. This attachment comprises a matrix of perpendicularly or obliquely aligned (to the tooth surface) collagen fibres, which are arranged into bundles known as principal fibres. These fibres are surrounded by cells including osteoblasts, keratinocytes, fibroblasts, cementoblasts and immune response cells such as macrophages. The extremities of these fibres traverse the periodontal ligament and embed into the cementum or alveolar bone, providing mechanical support and stability to the teeth (Hughes, 2014).

### *1.2.4. Periodontal epithelium*

There are three types of periodontal epithelium which can be categorised into three types based on their location: 1) sulcular epithelium, which interfaces with the tooth without forming attachments, 2) junctional epithelium which interfaces with the tooth and forms direct attachments to the enamel surface and 3) gingival epithelium – which lines the oral cavity. All three epithelium form the dentinogingival junction, which functions to attach the gingiva to the

tooth as illustrated in Figure 9 (Lindhe *et al.*, 2015). Cytokeratin distribution also varies per epithelium location, and differences in distribution are presented detailed in Figure 9 (Pöllänen, *et al.*, 2003).

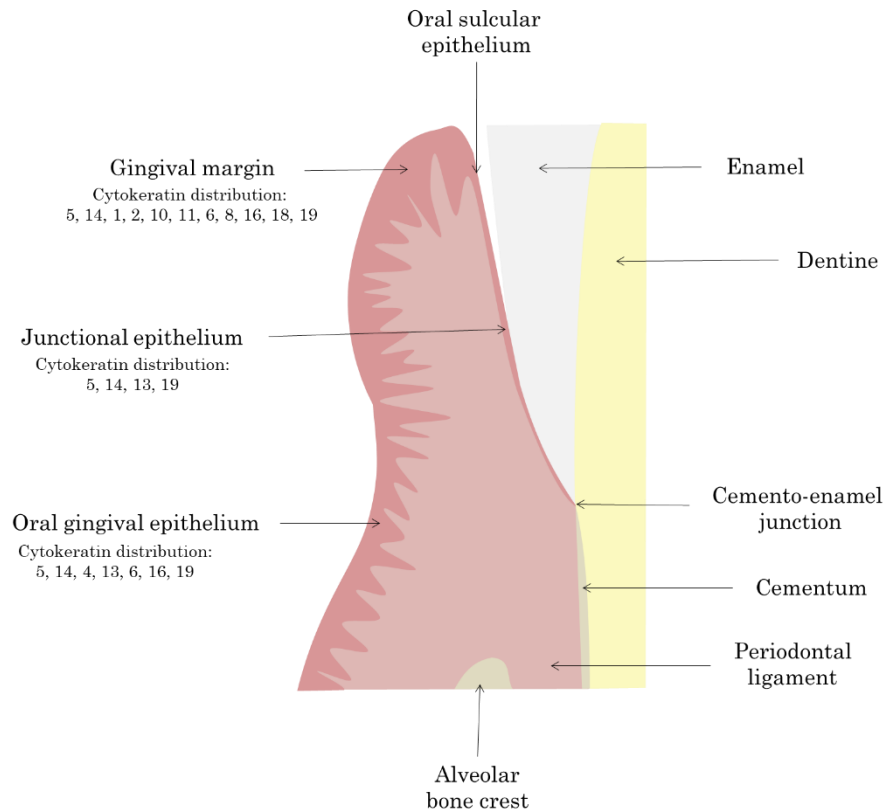


Figure 9: A schematic of the periodontal epithelia and other periodontal tissues, forming the periodontium. Cytokeratin distribution is also detailed. Image drawn by author adapted from Bosshardt and Lang, (2005).

#### 1.2.4.1. *Sulcular epithelium*

Sulcular epithelium is located at the coronal part of the free gingiva, lining the gingival sulcus. Although structurally similar to oral epithelium (stratified squamous) it is often classed as non-keratinized owing to the extremely low frequency of surface keratinized layers (Newman *et al.*, 2015).

#### 1.2.4.2. *Junctional epithelium*

Junctional epithelium plays a crucial role in maintaining the integrity and health of the periodontium as it attaches to the enamel or cementum via hemidesmosomes located within a basement membrane like structure. This attachment seals the underlying periodontal tissues from the oral environment and is constantly regenerating through basal layer proliferation. Although categorised as non-keratinised stratified epithelium, the morphology of cells within this epithelium exhibits subtle differences, for example, basal cells are more cuboidal in morphology, with more cytoplasm, while suprabasal cells are elongated, orientated parallel to the tooth (Nanci and Bosshardt, 2006; Lindhe *et al.*, 2015).

#### 1.2.4.3. *Oral gingival epithelium*

Oral gingival epithelium lines and faces the oral cavity and is closely attached to the alveolar bone. This epithelium is classed as keratinised stratified epithelium and follows the mucogingival line, which signifies the boundary between the non-keratinised lining mucosa (Lindhe *et al.*, 2015).

### 1.3. **Tooth loss**

Whilst the periodontal tissues are structured in a way to provide mechanical support and structure to the associated tooth, the presence of risk factors can result in inflammation, which subsequently leads to the damage and destruction of these tissues. Factors resulting in the destructive inflammation include smoking habits, trauma, systemic diseases and poor oral hygiene which has led to the development of periodontitis.

### *1.3.1. Periodontitis*

Periodontitis is the term used to describe inflammation of the periodontium, caused by an aberrant host immune response towards bacteria found within biofilms of the subgingival plaque on the tooth surface. If not treated, the pathogenic process can lead to chronic inflammation and progressive destruction of the periodontal tissues resulting in tooth loss. Within the subgingival plaque, if there is a shift (dysbiosis) in composition of the biofilm in favour of pathogenic opportunistic bacteria, a destructive host immune response can occur, initiating the pathogenesis of periodontitis (Page and Kornman, 1997; Hernández *et al.*, 2011; Lindhe *et al.*, 2015).. Three important pathogenic bacteria involved in the pathogenesis of periodontitis are *Porphyromonas gingivalis*, *Fusobacterium nucleatum* and *Aggregatibacter actinomycetemcomitans*. Extensive research has shown that pathogenic bacteria colonise the gingival crevice and gingival pocket and the presence of bacterial components in this area such as

lipopolysaccharides (LPS), proteases and toxins, induces exaggerated inflammation of the soft tissues (Page and Kornman, 1997; Hernández *et al.*, 2011; Lindhe *et al.*, 2015). Inflammation of the soft tissues initiated by keratinocytes releasing interleukin 8 (IL-8), a chemokine that attracts immune cells, which causes an influx of immune cells such as lymphocytes and polymorphonuclear neutrophils (PMNs). Lymphocytes and PMNs release cytokines, reactive oxygen species, matrix metalloproteinases (MMP) and other proteolytic enzymes in an attempt to kill the pathogenic bacteria (Cekici *et al.*, 2015). The release of MMPs (particularly MMP8) and reactive oxygen species degrades the ECM and induces apoptosis in the surrounding fibroblasts, therefore significantly reducing the level of collagen VII synthesis (Sorsa *et al.*, 2004). This degradation and reduction in collagen synthesis results in the weakening and eventually destruction of the periodontal ligaments and supporting structural fibres (Sharpey's fibres). Upon destruction of the periodontal ligament, fibroblasts located in the area release tumour necrotic factor -alpha (TNF- $\alpha$ ), a chemokine that activates osteoclast activation, proliferation and differentiation (Sorsa *et al.*, 2004). This initiates bone resorption, where osteoclasts attach to the newly exposed matrix and creates a sealing zone, which forms a micro-environment (Teitelbaum, 2000). Within the sealing zone, ion transportation occurs, which causes the bone to demineralise. Following this, osteoclast cells then release

cathepsin K, a lysosomal protease that degrades the demineralised bone, resulting in bone destruction. Once the bone within the sealing zone has been destroyed, the osteoclast detaches and re-attaches along the exposed surface (Teitelbaum, 2000). Continual destruction of the alveolar bone eventually leads to tooth loss if this is untreated.

Tooth loss can have a significant impact on quality of life. Teeth enable mastication, articulation and contribute to overall aesthetic appearance, therefore loss of a tooth or teeth can have a detrimental effect on one or all for the three aspects of a patient's wellbeing. To restore previously lost function, dental implants can be used to artificially replace a missing tooth or teeth.

#### **1.4. Dental implants**

Dental implants are increasingly being used as a restorative treatment to replace missing teeth. The replacement of teeth has been widely performed throughout history with varying degrees of success. At present, the most common dental implants systems consist of three parts: the implant root (a permanent surgical device that is implanted into either the mandible or maxilla providing anchorage and support to the overall prosthesis), the abutment (a structure that connects the implant root to the prosthetic attachment) and lastly, the crown (the artificial replacement for the tooth) (Lindhe *et al.*, 2015). Three-part systems (illustrated in Figure 10) have been developed over time

through trial and error and can be traced back to the Ancient Egyptians.

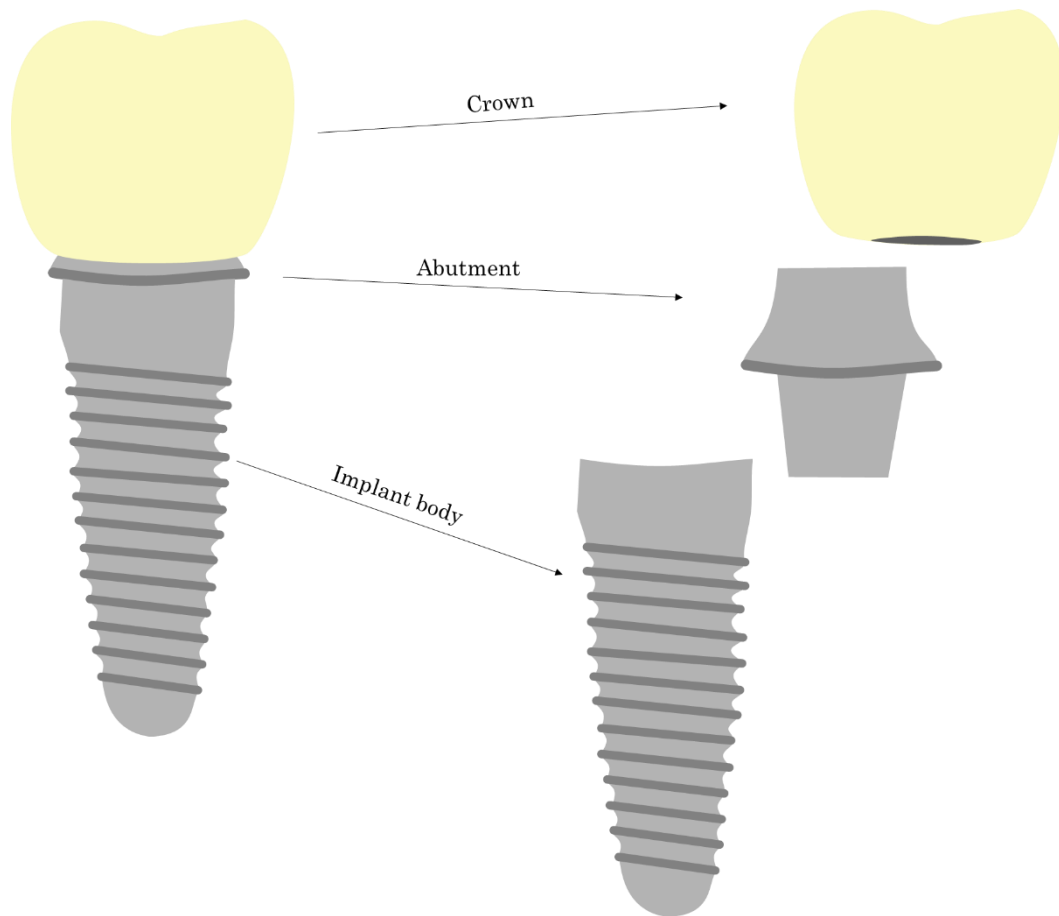


Figure 10: Structural components of a commercially pure Ti (Grade IV) 3-part dental implant consisting of a crown commonly made of a ceramic such as zirconia, abutment and implant body. Image drawn by author.

#### *1.4.1. History of dental implants*

Throughout history, civilisations have attempted to replace missing teeth with a wide range of materials such as semi-precious metals (Ancient Egyptians, 2500BC), shells (Mayans, ~500 BC) and gold rods (Maggiolo, ~1800s) however, it wasn't until the mid-1930s that shape and materials of implants were more thoroughly investigated

(Abraham, 2014). Having observed the placements of hip implants, Dr Alvin Strock began to study the potential use of vitallium (chromium - cobalt alloy) orthopaedic screws and implanted them within the mandible as a replacement root for missing teeth. They found that the screws became anchored to the bone and provided support for a restored tooth structure. However, in subsequent years, a variety of implant designs: endosteal (within bone), subperiosteal (on top of bone) and transosteal (through bone) in a variety of materials became available for clinical use. The success of these implants (classed as retention of the implant) has been extremely variable and many subsequently failed. It was a further 20 years before insight of interactions between implanted materials and bone were better understood (Abraham, 2014).

#### *1.4.1.1. Osseointegration*

In the 1950s, Professor Per-Ingvar Brånemark, a Swedish orthopaedic surgeon, was researching bone regeneration and healing, and he subsequently discovered that bone grew and adhered to the surface of titanium chambers that he had inserted within rabbit fibulae to provide an opportunity for intra-vital imaging of bone remodelling (Brånemark *et al.*, 1969). Upon analysis using light microscopy, the implant site showed the bone grew in close proximity to the inserted titanium with no apparent adverse side effects (as determined by a lack of inflammation or presence of immune cells in the surrounding

soft tissue). This phenomenon was subsequently termed 'osseointegration' and is described as 'a process whereby clinically asymptomatic rigid fixation of alloplastic materials is achieved, and maintained, in bone during functional loading' (Albrektsson *et al.*, 2009). This discovery, pioneered studies using Ti that investigated its potential use for root implants and much of Brånemark's subsequent work involved modifying and developing Ti implants for use in dental applications (Brånemark *et al.*, 1977). An example of this application was a long term (15 years) clinical study conducted by Adell *et al.* (1981) where 2768 Ti fixtures were placed in 371 patients. The clinical trial yielded an extremely high success rate with 81% and 91% Ti fixtures placed in the maxilla and mandible, respectively, remaining stable during the follow up period, which was defined as the implant being a non-moveable fixture upon manual stability testing and the application of rotational forces. The results of this study reinforced the importance of osseointegration for root implant success.

#### 1.4.1.2. *Osseointegration process*

As a process, successful osseointegration is a cellular and extracellular cascade of biological events. Upon insertion of the implant body within the prepared bone site, matrix proteins from tissue fluid and blood adsorb and desorb onto the implant surface. Blood cells, inflammatory cells such as leukocytes and platelets migrate from surrounding capillaries into the adjacent tissue and onto the implant surface

(Monjo, *et al.*, 2008). Fibrin also adheres to the implant surface which activates the complement pathway and creates a fibrin scaffold.

Platelets become activated upon interaction with the implant surface and fibrin scaffold, causing the release cytokines such as transforming growth factor beta 1 (TGF- $\beta$ 1), and platelet derived growth factor (PDGF) are released. The release of these chemoattractant factors cause migration of mesenchymal stem cells and osteoblasts to the implant surface (Baylink, *et al.*, 1993; Monjo, *et al.*, 2008). This then causes an upregulation of bone morphogenetic proteins (BMPs), which activates the expression of runt-related transcription factor 2 (RUNX2) a transcription factor that initiates the differentiation of mesenchymal stem cells to osteoblasts (Rutkovskiy *et al.*, 2016). Once fully differentiated, osteoblasts start to produce matrix vesicles that produce osteoid in response to the presence of bone formation factors such as TGF-beta 1 (Baylink, *et al.*, 1993; Monjo, *et al.*, 2008). Once the osteoid has formed, osteoblasts secrete alkaline phosphatase which promotes mineralisation of calcium and phosphate which was also deposited on the surface by osteoblasts, forming bone (Orimo, 2010).

#### *1.4.1.3. Factors affecting osseointegration*

A systematic review conducted by Smeets *et al* (2016), indicated that there are currently over 1300 different dental implant systems available, all with varied designs. Some of the more common modifications to dental implants include, shape, thread design,

presence of bioactive coatings and differences in surface topography. Of these factors which influence osseointegration, there is strong evidence that implant surface topography and chemical composition directly affects the likelihood of long term osseointegration and implant success (Elias *et al.*, 2012).

#### 1.4.1.3.1. *Surface topography*

Modifications to implant surface topography such as roughness, wettability, and surface chemistry have been found to influence the rate of osseointegration. In particular introducing a roughened micro-topology (~1-2 $\mu$ m surface roughness) with pit features of between 10 and 50 microns in lateral dimensions, has been shown to increase adhesion of osteoblasts to the implant surface, promote osteoblast differentiation and proliferation leading to improved osteointegration (Albrektsson and Wennerberg, 2004; Smeets *et al.*, 2016).

Larsson *et al.* (1996) conducted research using rabbit tibial bone formation surrounding threaded titanium implants that had either been machined or electropolished with or without anodizing. After 6 weeks, the animals were sacrificed and contact ratio between bone tissue and implant surface, and the presence of mineralised bone between threads was observed. It was found that implants with a smoother surface after electropolishing, without anodizing treatment, exhibited a significantly lower ratio of bone growth surrounding the implant in comparison with implants that had a rougher surface

topography due to being electropolished or machined with or without anodizing. Similarly, Wennerberg *et al.* (1998) evaluated the effect of four surface modifications (grit blasted with Al<sub>2</sub>O<sub>3</sub> particles of the following sizes: 25µm, 75µm and 250µm) on screw shaped implants. Implants were inserted into rabbit tibiae and histomorphometrically analysed for the bone to metal contact percentage and bone percentage within the screw threads. Screws modified with 75µm Al<sub>2</sub>O<sub>3</sub> particles had a greater percentage of implant to bone contact in comparison with smoother surface finishes and other Al<sub>2</sub>O<sub>3</sub> particle blast sizes. Both Larsson *et al.* (1996) and Wennerberg *et al.* (1998) suggested that modifying the surface roughness of implant bodies would create a surface that promoted osteoblast differentiation and proliferation, thereby increasing the overall rate of osseointegration.

#### *1.4.1.3.2. Implant composition*

Implant composition has also been recognized as an important factor for successful osseointegration and selecting a material that is not compatible within the body, can increase the potential of implant rejection and ultimately failure. Since Brånemark's discovery of osseointegration, titanium has been classed as the 'gold standard' for dental implant materials due to favourable mechanical properties, favourable host response (osseointegration of the implant) and long-term clinical success when used as an implant (Saini *et al.*, 2015).

#### 1.4.2. Success of titanium

The success of titanium (Ti) as an implant material is reportedly due to the formation and presence of a nontoxic passive oxide layer (Gotman, 1997). When Ti is in the presence of oxygen a rapid chemical reaction occurs resulting in the formation of a surface layer of titanium oxide (TiO<sub>2</sub>). The formation of this oxide layer significantly reduces the rate of corrosion, by acting as a protective barrier, preventing the release of metal ions and metal dissociation *in vivo* (Noort, 1987). It has been assumed that the oxide layer makes Ti corrosion resistant *in vivo*, which factors in long term osseointegration and implant success (Lindhe *et al.*, 2015).

#### 1.4.3. Alternative dental implant materials

The identification of Ti as a successful implant material, means many dental implant systems have been manufactured using commercially pure grades of Ti, with Grade IV being the more favourable to produce dental implant systems. Whilst commercially pure Ti dental implants have had wide clinical success, the mechanical properties are not as desirable when compared with implants fabricated from Ti alloys. This has led to extensive research into Ti alloys with improved mechanical properties, which enable smaller diameter implant systems to be produced which require less bone volume to be removed when preparing the implant site. Developed alloys include, Ti-6Al-4V and Ti-6Al-7Nb (Saini *et al.*, 2015). Whilst these alloys are suitable

alternatives to commercially pure Ti and provide improved mechanical properties, no alloy is exempt from corrosion, and use of these alloys has been highly disputed due to suggested aluminium (Al) and vanadium (V) ion release, which elicit immunological responses (Li *et al.*, 2010). As a result of this controversy, other Ti alloys have been investigated and recently, attention has turned to binary alloys of titanium and zirconium (TiZr alloys).

Previous research, has established that binary TiZr alloys, when used as dental implant materials, have increased cell attachment (Ikarashi *et al.*, 2007), have a higher yield strength (Gottlow *et al.*, 2012) and have greater corrosion resistance when compared with commercially pure Ti dental implants (Zhang *et al.*, 2018). The superior properties of binary alloys of Ti (~85%) and zirconium (Zr) (~15%) have led to the clinical success and widespread use of these alloys as dental implants under the trade name of Roxolid® (Straumann, Basel, Switzerland).

#### *1.4.4. Peri-implant mucosa attachment to implant surfaces*

Whilst osseointegration has been extensively studied to determine the long-term success of dental implant, recent data has shown that the peri-implant mucosa also plays a major role in implant success and longevity by its isolation of the implant site from potential bacterial invasion. This process is known as the biological seal (Chai, Razali and Ngeow, 2016). The peri-implant epithelium, which is equivalent to junctional epithelium found within natural gingiva, forms a direct

interface with the implant surface. Fibroblasts located within the peri-implant epithelium attach to the extracellular matrix proteins adsorbed onto the implant surface by hemidesmosome complexes, and secrete laminin 1 and 5. These proteins influence keratinocytes to orientate parallel to the implant surface and differentiate to form basal and suprabasal cell layers of non-keratinised stratified epithelium connecting the basal lamina synthesised by fibroblasts adhered to the implant surface via desmosomes. It has been found that these interaction only occur within the lower regions of peri-implant epithelium, with the uppermost regions exhibiting rare and often absent epithelium attachment to the implant surface (Ikeda *et al.*, 2000; Yamaza and Kido, 2011).

#### *1.4.5. Anatomical differences between post and peri implant gingiva*

Whilst there are some similarities between periodontal tissues surrounding osseointegrated dental implants and periodontal tissues surrounding the natural tooth, namely the direct attachment of the epithelium to the dental implant surface as described in the previous section, there are also many anatomical differences (Ivanovski and Lee, 2018). Within a natural tooth environment attachment of the tooth to the underlying bone is aided by Sharpey's fibres, which are orientated perpendicular to the tooth root surface and form attachments to cementum, anchoring the tooth. Whereas dental implants are connected to the underlying bone through osseointegration.

Additionally, Sharpey's fibres are present but orientated parallel to the implant surface and do not form attachments to the implant surface (illustrated in Figure 11).

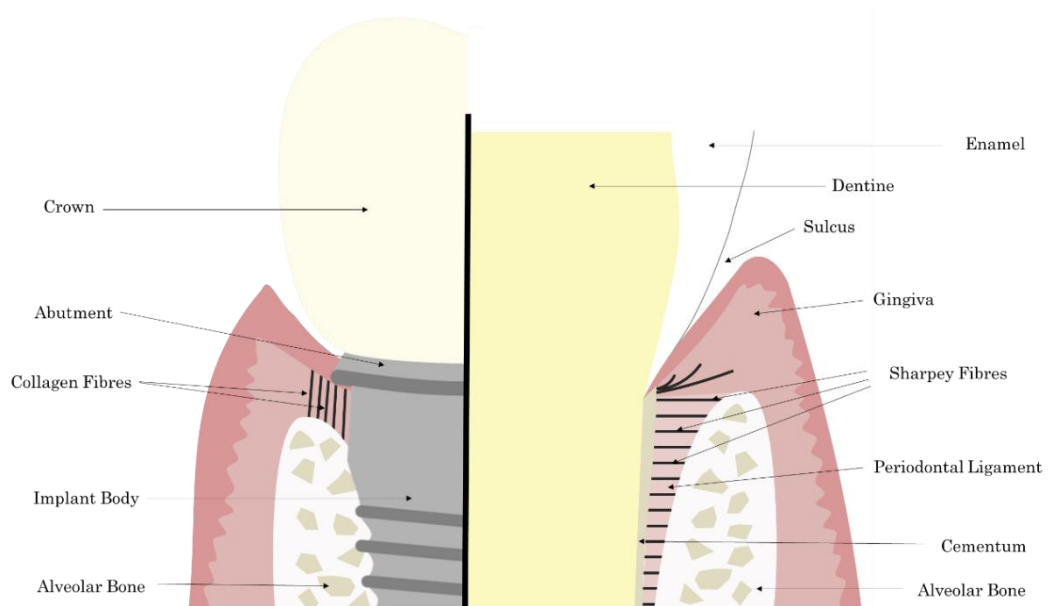


Figure 11: A schematic diagram highlighting the structural differences between natural mucosa and peri-implant mucosa. Image drawn by author Bosshardt and Lang, (2005).

There is an increased susceptibility to apical progression of bacteria due to the previously mentioned anatomical difference, and the lack of epithelium attachment to the implant surface of the uppermost regions of the junction epithelium. This results in the increased likelihood of contracting bacteria induced peri-implant diseases such as peri-implant mucositis and peri-implantitis, which are caused by infection. Peri-implant mucositis is a reversible inflammatory reaction occurring in the periodontium, and peri-implantitis is an inflammatory response

which can cause the loss of bone supporting the dental implant, leading to implant failure (Dhir *et al.*, 2013; Ivanovski and Lee, 2018).

#### 1.4.6. *Dental implant failure*

Despite the high success rate of dental implants, failure does occur which requires removal of the whole implant system. Implant failure is defined as '*the total failure of the implant to fulfil its purpose because of mechanical or biologic reasons*' (el Askary *et al.*, 1999). In accordance with the timing of the failure, this can be categorised into early failure (within one year of implantation) or late failure (after one year of implantation). Early implant failure is understood to be caused by failed osseointegration, however there are many factors that can contribute, which can be categorised as patient related or implant characteristics (Levin, 2008). Research has identified that the most common patient related factors associated with early failure include: smoking (Bain and Moy, 1993), poor oral hygiene (Lambert, Morris and Ochi, 1997), bacterial contamination of the implant site (Lambert, Morris and Ochi, 1997), poor bone density and quality (Malik *et al.*, 2010), surgical trauma (Annibali *et al.*, 2008) and systemic diseases and treatments (Donos and Calciolari, 2014). Implant characteristics associated with early implant failure include, surface characteristics (Sartoretto *et al.*, 2015), improper placement (Annibali *et al.*, 2008), lack of primary stability (Javed *et al.*, 2013) and overheating during implant site preparation (Eriksson and Albrektsson, 1984).

Late implant failure is described as '*failure to maintain established osseointegration*' (Esposito *et al.*, 1998). Factors identified as increasing the likelihood of late implant failure include, excessive implant loading (Sakka *et al.*, 2012) and improper implant construction resulting in implant fracture (Levin, 2008). Bacteria induced peri-implant related disease, peri-implantitis, is one of the major causes of late implant failure and is considered to be derived from peri-implant mucositis (el Askary *et al.*, 1999).

#### 1.4.6.1. *Peri-implant mucositis*

Peri-implant mucositis is classified as 'the localised inflammation of the peri-implant mucosa' (Albrektsson and Isidor, 1994). The cause of this disease is due to the accumulation of pathogenic oral bacteria such as *Porphyromonas gingivalis*, *Fusobacterium nucleatum* and *Aggregatibacter actinomycetemcomitans* contaminating the implant surface. This subsequently induces a host immune response caused by the presence of LPS and bacterial toxins causing the release of IL-8 from the surrounding epithelial cells, attracting and causing an influx of PMNs and lymphocytes leading to inflammation of the periodontal tissues. Clinically, peri-implant mucositis resembles gingivitis (a disease that occurs in natural periodontal tissues) and manifests as bleeding upon gentle probing, mucosa swelling and redness, however a stronger immune response is seen occurring within peri-implant tissues. This occurs due to an already elevated level of immune cells in

the surrounding tissues as well as an increase in osteoclasts due to bone remodelling after osteoid mineralisation after implantation. In the presence of LPS and bacterial toxins osteoclasts can act as antigen-presenting cells and can activate and recruit T-cells (Li *et al.*, 2010). The activation of T-cells results in the recruitment and influx of other lymphocytes which release MMP8. As mentioned in Section 1.3.1, MMP8 causes the breakdown of the ECM, therefore causing the structurally weak biological seal to become even weaker, resulting in an increase in pocket depth upon probing.

It has been found that removal of the bacteria causing the inflammatory response is an effective treatment and with time, the effects of the disease are reversed. However, if left untreated, peri-implant mucositis has the potential to progress into peri-implantitis (Leonhardt *et al.*, 1992; Zitzmann and Berglundh, 2008; Salvi *et al.*, 2012).

#### 1.4.6.2. *Peri-implantitis*

Peri-implantitis is defined as '*progressive peri-implant mucosa inflammation with associated bone loss*' and is caused by the ongoing presence of pathogenic bacteria on the dental implant surface, which leads to a destructive host immune response (Albrektsson and Isidor, 1994). Characteristics of this disease are soft tissue redness, swelling and bleeding upon probing and, upon radiographic imaging, visible bone loss caused by bone resorption and decreased osseointegration.

These clinical manifestations are similar to those of periodontitis, which occurs in periodontal tissues surrounding natural teeth (Zitzmann and Berglundh, 2008).

#### 1.4.6.2.1. Pathogenesis of peri-implantitis

Both peri-implant mucositis and peri-implantitis present similar clinical symptoms to gingivitis and periodontitis (respectively), however pathogenesis of these diseases differ. Within a healthy mouth, normal oral bioflora consists largely of gram-positive bacteria, however when bioflora composition shifts to mainly consist of gram-negative anaerobic bacteria, such as *Porphyromonas gingivalis*, *Fusobacterium nucleatum* and *Aggregatibacter actinomycetemcomitans*, induction of gingivitis occurs, which is a reversible disease that causes inflammation of the periodontal tissues. If not treated, gingivitis can in turn progress into periodontitis which is inflammation of the periodontal tissues with associated bone loss. Whilst the presence of the bacteria associated with gingivitis and periodontitis have been found in the bioflora of oral environments affected by peri-implant mucositis and peri-implantitis, it has been further identified that bacteria with have a high affinity to titanium such as *Staphylococcus aureus* are involved in the pathogenesis of these diseases (Salvi *et al.*, 2008; Subramani *et al.*, 2009).

Although scientific knowledge concerning the importance of the biological seal, and early clinical indicators of peri-implant related

diseases has reduced the likelihood of implant failure, the majority of the associated studies have involved the use of *in vivo* animal models.

### **1.5. Animal use in dental research**

Animals have been commonly used within biomedical research for centuries and their application has led to many significant contributions to medical knowledge. Whilst their use is an extremely controversial and philosophical topic, using animals as a model for human physiology has many benefits, such as the generation of long term studies, or conducting research that would be classed as unethical on human participants (Franco, 2013). An example of this is research by Liñares *et al.* (2013) which investigated the soft tissue integration with modified abutment surfaces. This study involved removing healthy premolars and the first molar in the mandible of minipigs, to create space for the test implants. After 3 months, 6 randomly allocated implants were placed and allowed to heal for 8 weeks and subsequently the animals were sacrificed with the mandibles removed to allow histological and histomorphometric analysis. No difference between the experimental abutment surfaces and soft tissue integration was identified.

A further example of where the use of animals has developed scientific knowledge has been in the discovery and characterisation of osseointegration (described in Section 1.4.1.1). Such experiments

conducted using human participants would be classed as wholly unethical, firstly due to the unnecessary removal of healthy teeth, the placement of implants or placement of titanium optical chambers in the fibula and the removal of bone to analyse biological responses (Brånemark *et al.*, 1977).

However, whilst animal models allow for research that would be unethical in humans, there has been an extensive ongoing scientific, ethical and philosophical debate regarding their use not only within the scientific community but also extending to public opinion. The ongoing debate within the UK led to the development of laws such as the Animals (Scientific Procedures) Act 1986, which regulates and protects the use of animals in research as well as compelling scientists to assess the level of harm that arises from experimental work (Franco, 2013). Additionally, extensive opinion polls by Ipos MORI (2016) have provided an insight into the public attitude. The results from the latest survey (2016) revealed that 65% of the public had a negative opinion of the use of animals which increased in negativity as the size of the animal increased, i.e. the reaction towards the use of rats was less negative than the reaction towards the use of primates. Additionally, 74% responded by stating that more research should be conducted in to alternatives to animal use, while 65% accepted animal testing as an absolute last option if there was no alternative available. As a response to the Animals (Scientific Procedures) Act 1986, inter-species variation

and public opinion, researchers are highly encouraged to undertake the 3R's: replacement, reduction and refinement, which has fundamental goal of substituting animal research, in the forefront of methodology planning (Clemence and Leaman, 2016; National Centre for the Replacement Refinement & Reduction of Animals in Research, 2018).

Alongside the ethical reasonings for the non-use of animals, there are also scientific drawbacks. With many experiments that have involved the use of animal models, the outcomes observed have been generally assumed to be a reflection or prediction for outcomes that will occur in humans. However, translating outcomes from a model organism to human response cannot be do so easily due to interspecies differences and unrealistic results due to experimental conditions (Shanks *et al.* 2009).

Within dental implant research, a wide range of animals have been used including, rat, rabbit, pig, and primates, with the most commonly used animal model being a dog (Martini *et al.*, 2001, Pearce *et al.*, 2007). The use of dogs has enabled many advancements within dental implant research due to the ability to conduct long term research with loaded or unloaded implants (Gotfredsen *et al.*, 2001), the ability to analyse peri-implantitis on osseointegrated implant (Lee *et al.*, 2016), and the ability to observe and assess healing around dental implants (Thoma *et al.*, 2011). However, directly translating the results of these studies to humans, is not without difficulty. It has been identified that

bone remodelling occurs at a significantly higher rate in dogs than humans as well as vastly varying per species (Anderson and Danylchuk, 1978; Bloebaum *et al.*, 1991). Furthermore, dogs have a higher likelihood of developing periodontitis and unlike humans, do not have routines in place such as the brushing of teeth to maintain oral health (Kortegaard *et al.*, 2008). This therefore questions the translatability of research investigating the pathogenesis of periodontitis and peri-implantitis in dogs to humans.

Alongside translatability, reliability of the results should be questioned. Whilst there are procedures and laws that require scientists to appropriately treat and care for animals used within scientific research (as discussed earlier), it has been suggested that routine laboratory procedures such as handling, cage moving and blood collection causes stress to animals.

Balcombe *et al.*, (2004) conducted a systematic review to identify the effect of handling, orogastric gavage and blood collection on physiological parameters. Eighty studies were identified which reported physiological parameters of particular interest which included: heart rate, blood pressure, behaviour, serum or plasma concentrations of glucose and corticosterone. It was identified that after handling, blood collection, orogastric gavage or a combination of the three, animal stress related responses were statistically significantly higher with responses ranging from 20 -100% higher than the animals' baseline or control.

This research highlights the importance of how routine laboratory procedures can significantly affect physiological data and reinforces the need for caution when interpreting physiological data from animal models.

Both the ethical and scientific drawbacks have led to a focus on tissue engineering to yield attainable solutions. This includes *in vitro* 3D models that retain the complexity of soft tissue architectures, normal *in vivo* cell behaviour and providing the necessary control ensuring reproducibility.

## **1.6. Tissue engineering**

Tissue engineering is a multidisciplinary field of science that combines and adapts cell biology with material science in order to generate a three-dimensional (3D) hybrid solution. Over the last 30 years tissue engineering has become more advanced due to increased understanding and developments within science and technology. This has enabled the engineering of complex tissues and organs *in vitro* that can be used to repair or replace failing or damaged tissues or organs (Mikos *et al.*, 2006). Additionally, from a research perspective, useful *in vitro* research models such as organ-on-a-chip, organoids and organotypic models have been developed.

### 1.6.1. Two-dimensional cell culture

Two-dimensional (2D) cell culture is a universal method which enables the relatively rapid analysis of cellular responses to stimuli at low cost and high throughput. Cells are typically cultured on rigid tissue culture plasticware or glass and grown as monolayers. Culture medium is heavily characterised with defined quantities of growth factors and nutrients resulting in homogenous proliferation and growth. Cell shape is determined by cell attachment and spreading on the surface and cells can only migrate out, from the point of initial seeding.

Despite the benefits of 2D cell culture (a well-accepted method that has significantly advanced scientific knowledge through the understanding of basic cell behaviour), this heavily controlled and unrelatable culture environment yields cell behaviour, morphology and signalling not typical to that found *in vivo*. Hakkienen *et al.*, (2011) used primary human fibroblasts isolated from foreskins to compare the morphology, migration and cell adhesion. Using sandwich culturing (the process of placing cell suspension between two layers of basement membrane extract or collage) and hydrogel scaffolds as 3D environments, migration and cell adhesion was compared to cells grown in a 2D environment. Time-lapse microscopy and quantification of collagen type I and fibrin, were used to determine the culture environment effect on migration. It was found that fibroblasts cultured within a 2D environment migrated at 1.3 times slower rate than fibroblasts

cultured on either 3D scaffold, highlighting the unrealistic environment to observe cell behaviour. Additionally, it has been found that polarization, a necessary phenomenon for the differentiation of certain cell types such as epithelial cells, is completely lost, affecting subsequent cell behaviour, highlighting the impact 2D cell culture method has on cells (Edmondson *et al.*, 2014; Jedrzejczak-Silicka, 2017). These deviations from *in vivo* like cell behaviour, has called into question the use of 2D cell culture for certain applications such as wound healing and cancer metastasis, leading to the development and refinement of 3D cell culture techniques.

#### *1.6.2. Three-dimensional cell culture*

To overcome the problems faced when using 2D culture methods and to fabricate physiologically similar tissues and organs, three-dimensional (3D) cell culture platforms, specifically organotypic cultures, have been employed to recreate the complex tissue architecture and properties found *in vivo*. Adapted from the basic principles of *in vitro* organ culture systems, these 3D structures are developed from the isolation and expansion of multiple cell types from tissue biopsies, within a controlled environment and are used within different fields of tissue engineering (Sun *et al.*, 2006; Li and Kilian, 2015). In recent years, 3D oral organotypic models have been developed and used to investigate drug toxicity (Barrila *et al.*, 2010), the efficacy of drug delivery systems

(Yadev *et al.*, 2011), and more recently, interactions and biocompatibility of dental implants (Chai *et al.*, 2011).

Developing a 3D oral organotypic model is a multifactorial process and requires three fundamental elements: a cell source, scaffold and appropriate culture conditions, especially culture medium that enables the production of correct biochemical signals and markers, which aim to determine if the engineered model is biologically appropriate (Izumi *et al.*, 2000).

#### *1.6.2.1. Selection of appropriate cells*

Oral immortalised cell lines such as hTERT fibroblasts derived from normal gingival fibroblasts that have been established with human telomerase reverse transcriptase gene transfection and H400 keratinocytes, derived from human alveolar tissue, are commonly used to generate 3D oral organotypic models (Khan *et al.*, 2012; Buskermolen *et al.*, 2016). Advantages of using a cell line are that they are relatively inexpensive, easier to handle, yield sufficient cell numbers for analyses and require no isolation from tissues by the user in comparison to cells derived from primary origin, particularly primary gingival keratinocytes. Whilst the use of immortalised cells are accepted as suitable alternatives to primary cells, one problem is that cell behaviour is not representative of cell behaviour *in vivo* due to their immortalised nature. Due to this lack of translatability, there is a preference for the use of primary gingival cells.

Primary gingival human keratinocytes and fibroblasts can be isolated using a variety of methods with the simplest being tissue brushings. Cells can also be isolated and expanded using different methods. Enzymatic digestion can be used to break down the proteins of the initial biopsy, resulting in a coculture suspension that can be subsequently seeded. Alternatively, the explant method can be utilised which involves finely dissecting the biopsy, to increase the surface area and the likelihood of cell outgrowth. A combination of both methods can be used which allows for independent isolation and expansion of keratinocytes and fibroblasts. Initially biopsies are undergo a short exposure to enzymatic dissociation, enabling mechanical separation of the epidermis from the dermis to occur. Following this the epidermis and the dermis are separately dissected to allow for clean isolation and expansion of primary human gingival fibroblasts and keratinocytes (Gowers *et al.*, 2018).

The main influence to use primary cells when developing 3D oral organotypic models is the retention of *in vivo* like behaviour due to cells being non-transformed or immortalised. This enables better translation of results in comparison to the results obtained from 3D oral organotypic models generated using cell lines. However, there are disadvantages in using primary cells which include, high cost of initial isolation, low yield from original tissue sample, slow growth in

comparison to cell lines, short life span and difficulty in handling due to culture sensitivity (Kaur and Dufour, 2012).

Dongari-Batzoglou and Kashleva (2006) developed an oral organotypic model to better understand oral mucosa and oral Candida interactions. Immortalized and primary keratinocyte and fibroblasts were used to generate separate models. It was found that only a small number of keratinocytes and fibroblasts could be isolated from oral tissue biopsies, therefore multiple biopsies from multiple donors were required. However, upon utilisation of the cells derived from multiple biopsies, it was found that cells exhibited different proliferation rates and life spans, subsequently affecting the developed 3D oral organotypic model.

Whilst both cell lines and primary cultures have their advantages and disadvantages, cell lines are more commonly used due to high yield generation and handling capabilities.

#### *1.6.2.2. Selection of an appropriate scaffold*

Scaffolds are porous 3D structures that provide structural shape and stability to the growing cells. Dependant on the overall organotypic application, these structures can be fabricated from temporary or permanent materials. Regardless of durability, scaffolds need to have the following characteristics: demonstrate biocompatibility with seeded cells and surrounding environment, porosity to enable cell and nutrient infiltration, promotion of attachment of cells and mechanical stability

to support the developing model. Within the development of 3D oral organotypic models, scaffolds are used to substitute for the lamina propria and previously, have been established without dermal components, however it was found epithelial stratification failed to occur due to lack of basal progenitor cell differentiation (Lamb and Ambler 2013). Furthermore, it is reasonably common to seed or encapsulate fibroblasts within the scaffold to aid development. Saintigny *et al.* (1993) investigated the effect of seeded fibroblasts within a chitosan cross-linked collagen glycosaminoglycan (GAG) lattice on the development of reconstructed epidermis.

Immunohistological analysis revealed that keratinocytes were not able to produce organised stratified epithelium on lattices without fibroblasts, this highlighted the influence of fibroblast-keratinocyte interactions on keratinocyte differentiation. As previously described, appropriate scaffold selection depends on the application of the organotypic model, and there are many different types of scaffolds available. These can be categorised into two main groups: naturally derived and synthetic scaffolds (Izumi *et al.*, 2000; Hosseinkhani *et al.*, 2014; Payne *et al.*, 2014).

#### *1.6.2.2.1. Naturally derived scaffolds*

Naturally derived scaffolds such as collagen and alginate hydrogels, acellular cadaveric dermis (AlloDerm™, LifeCell Corporation, Brachburg, New Jersey, USA) and de-epithelialized dermis (DED), are

the most commonly used scaffolds for generating 3D oral organotypic models due to retention of structural properties and histological similarity with natural mucosa following processing. Boadi *et al.* (2014) developed a 3D oral organotypic cancer model using DED and primary oral keratinocytes and fibroblasts. Briefly, the epidermis was mechanically separated from the dermis of cadaveric skin following 1M sodium chloride treatment. The resultant DED was then cut into 1.5×1.5 cm squares and a liquid tight seal was created using weighted down chamfered rings on top of the DED. Primary oral keratinocytes and fibroblasts were seeded within the rings at a ratio of 3:1 keratinocytes to fibroblasts. After two days, the structure was raised to the air liquid interface (ALI) to encourage epithelial stratification for up to 21 days. After 21 days at ALI the models were processed using histology and epithelial thickness was measured using optical coherence tomography. It was identified that the differentiation pattern observed was similar to that seen in a normal gingival biopsy (used as comparison), however, the thickness in epithelium was slightly thinner.

Whilst use of naturally derived scaffolds are extremely beneficial in terms of excellent cellular interactions achieved and scaffold architecture, they do possess disadvantages such as limited mechanical support and physical stability (Ophof *et al.*, 2002).

#### 1.6.2.2.2. Synthetic Scaffolds

Synthetic scaffolds such as polyethylene glycol (PEG), polylactic acid (PLL) and polyethylene terephthalate (PET) provide suitable alternatives to naturally derived scaffolds due to the ability to adapt and control their characteristics such as degradation rate and mechanical strength. In comparison with naturally derived scaffolds, synthetic scaffolds are cheaper, better suited for load bearing applications and, have high reproducibility, therefore enabling increased control of the developing 3D model. However, one major disadvantage is lack of biological cues that promote biological interactions such as cell attachment. To overcome this, many synthetic polymers (and natural polymers such as alginate) are chemically modified with peptides such as arginylglycylaspartic acid (RGD) and tyramine (Tyr), or proteins such as fibrin and chitosan, which promotes cell adhesion on synthetic surfaces (Gervaso *et al.*, 2013; Lim *et al.*, 2015).

Research conducted by Tsao *et al.* (2014) utilised PEG conjugated with chitosan to create hydrogel scaffolds for *in vitro* models of skin. Human foreskin fibroblast (HFF) and HaCat cell lines, HFF cells, at a concentration of  $1 \times 10^5$  cells, were suspended within the C-PEG hydrogel during gelation. Upon complete *in situ* gelation,  $5 \times 10^5$  HaCaT cells were seeded on the top of the C-PEG hydrogel. Models were initially submerged for 4 days, before culture medium volume

(DMEM supplemented with 10% human serum and 1% antibiotic-antimycotic solution) was reduced to expose the surface to the ALI. Using H&E staining and immunofluorescent staining, it was revealed that the *in vitro* models of skin using C-PEG as a scaffold, resembled wound healing environments found *in vivo*. Furthermore, there was also expression of relevant *in vivo* wound healing markers within this *in vitro* environment. Histological analysis revealed epithelium stratification and differentiation, highlighting the potential use of this synthetic scaffold.

While synthetic scaffolds are used, naturally derived polymers are more favoured due to the pre-existing biological cues, which vastly improves cellular attachment.

#### 1.6.2.3. *Culture media and use of animal supplementation*

Although cell and scaffold selection have a significant impact on generating 3D oral organotypic models that are characteristically similar to natural mucosa, it is the biochemical properties of the culture environment that fundamentally affects growth and development. This is specifically attributed to culture media and supplementation (Payne *et al.*, 2014). Early cell culture research utilised body fluids as a culture medium for *in vitro* cell culture, with research conducted by Ross G. Harrison (in 1907), being one of the earliest successful examples of *in vitro* animal cell culture. Harrison

used frog lymph fluid to outgrow frog nerve fibres, however it was soon identified that frog lymph fluid was unsuitable for warm-blooded cell culture (Harrison *et al.*, 1907). As a consequence of this work, alternative body fluids were explored and led to the identification and use of blood plasma as a culture medium, enabling Alexis Carrel (in 1912) to long-term cultivate chicken embryonic cells for several months. Carrel further identified that the addition of embryonic extract to blood plasma, increased cell proliferation and extended the culture period, which led to embryonic extract being regularly supplemented in blood media (Carrel., 1912). Concurrently, in 1911, Margaret R. Lewis and Warren H. Lewis developed the Locke-Lewis medium, which is composed of inorganic salts, amino acids, and glucose. The identification of embryonic extract and the development of Locke-Lewis medium, steered scientific endeavours towards synthetic medium (Lewis and Lewis., 1912). This led researchers to focus on identifying components within natural supplements that affected survival and growth of cells culture *in vitro*. In 1955, Harry Eagle developed Eagle's medium and minimum essential medium (MEM) that only contained glucose, inorganic salts, amino acids vitamins and dialyzed serum, all of which had been identified as essential for the successful *in vitro* culture of animal cells (Eagle., 1955). The advancements of these media led to cell specific improvements to

MEM, resulting in the development of cell specific basal media such as Dulbecco's modified MEM (DMEM) (Dulbecco and Freeman., 1959).

For specific keratinocyte cultivation, Rheinwald and Green (1975) were one of the first to successfully serially cultivate human keratinocytes *in vitro*. They used Green's medium (a specially adapted basal media for keratinocyte cultures, developed by Green) supplemented with foetal bovine serum (FBS) in conjunction with a mitotically inactive murine fibroblast (3T3) feeder layer, known to secrete soluble factors that facilitate the attachment and growth of primary keratinocytes.

Another significant development came from Barnes and Sato (1980), who created a culture environment without a fibroblast feeder layer. They combined DMEM with Ham's nutrient mixture F-12 (a medium rich in amino acid composition, specifically linoleic acid and putrescine and growth factor epidermal growth factor (EGF), which are required for colony formation and long term cultivation of keratinocytes *in vitro* (Yao and Asayama., 2017). This combination proved to be a successful feeder layer-free culture environment, due to the preferred composition of growth factors, amino acids and hormones, especially EGF. Whilst this medium was initially developed as a serum free alternative, it is now widely used with FBS supplementation and is classed as one of the more favourable supplemented mediums to culture keratinocytes and 3D oral organotypic models.

#### 1.6.2.4. *Use of foetal bovine serum and bovine pituitary extract*

The majority of commercially available keratinocyte culture media routinely require supplementation with FBS or bovine pituitary extract (BPE) to provide the necessary nutrients for the promotion of cell growth and proliferation. However, over the last decade, animal-component free media have begun to be increasingly used for *in vitro* cultivation due to the scientific drawbacks of serum and BPE. One major disadvantage is that there is a high degree of variability between batches. As a result, when testing the effect of certain variables such as growth factors, interpretation can be difficult as it is not obvious if the tested variable or inter-batch variability of FBS or BPE are influencing culture outcomes. Additionally, serious ethical concerns surrounding the harvesting of FBS have arisen, namely foetal awareness, which have led to members of the scientific community questioning whether the bovine foetus is conscious and experiences any pain or distress thus causing suffering as blood is drained and collected (Jochems *et al.*, 2002; van der Valk *et al.*, 2004). Strict animal welfare laws exist to ensure that the harvesting of FBS is conducted as humanely as possible. Whilst these laws are in place, there is a significantly large demand for FBS with over 500,000 litres used within the UK. This large supply and demand has attached with it a negative public opinion. As a result, there has been a shift in research to utilise alternatives that are serum free and animal-origin free

culture media. This would not only would eliminate the disadvantages mentioned previously, but also would enable development of culture systems that are more precisely defined and allow for more control *in vitro*, as well as removing concerns of potential biological contamination (Jochems *et al.*, 2002; van der Valk *et al.*, 2004).

Manufacturers have responded by developing serum-free media kits such as EpiLife® and Supplement S7® and Defined keratinocyte serum-free medium by Gibco® Life Technologies.

#### *1.6.2.5. Serum free oral organotypical models*

The first serum free 3D oral organotypic models were developed by Izumi *et al.* (2000) who used keratinocytes and fibroblasts isolated from tissue biopsies from human masticatory mucosa that had been dissociated using enzymes. Expanded cultures were then cultured on a naturally derived commercially available scaffold, AlloDerm™, an acellular nonimmunogenic cadaveric human dermis, and cultured using supplemented molecular, cellular and development biology media (MCDB) 153 - a serum-free culture media based on Ham's F-12, optimised through the addition of selective growth factors, vitamins and amino acids specific for keratinocyte cultivation. Cultures were submerged for 4 days before being raised to the ALI to induce epithelium stratification. Histological and immunohistochemical analyses were used to compare the models developed in a serum free environment to those developed in the serum supplemented

environment. It was found that there were no significant differences in tissue architecture and expression of stratified epithelium markers between the two culture environments, as both generated tissues with continuous stratified epithelial layers (3 - 6 keratinocyte layers thick). Furthermore, keratinocytes grown in serum free media, exhibited a faster proliferation rate (0.7 days) than those grown in serum supplemented media (2.9 days) and underwent a 98-fold increase in proliferation until passage 6.

The success of Izumi *et al.* (2000) paved the way for Yoshizawa *et al.* (2004) who adapted their method to develop organotypic models of human conjunctiva and oral mucosa. Although Izumi *et al.* (2000) and Yoshizawa *et al.* (2004) both generated oral organotypic models that had a similar architecture to that of natural human oral mucosa, including epithelium stratification. Briefly, oral keratinocytes and fibroblasts were enzymatically dissociated from oral biopsies and expanded using MCDB 153 supplemented with BPE. Using AlloDerm™, cells were seeded at a concentration of  $1.25 \times 10^5$  cells/cm<sup>2</sup> remaining submerged for 4 days. After 4 days the construct was raised to the ALI for a further seven days, which were then histologically analysed. These findings directly contrast studies by others including those of Lamb and Ambler (2013) who found that serum free environments failed to generate stratified epithelium. Neonatal human epidermal keratinocytes were expanded in commercially available

serum-free media Lonza KGM-Gold™ medium and subsequently seeded onto DED at a concentration of  $3 \times 10^5$  cells/cm<sup>2</sup>. 3D epidermal skin models were cultured using commercially available serum-free media Lonza KGM-Gold™ medium, Epilife® and FAD culture medium (a 3:1 mix of Dulbecco's modified Minimal Essential Medium (DMEM) and Ham's nutrient mixture F-12). Using haematoxylin and eosin (H&E) staining histological and immunofluorescent staining for CK14 and CK10, it was demonstrated that organotypic models grown in the commercially available serum free media failed to stratify and form mature epithelial layers as seen in organotypic models grown in serum supplemented medium or as occurs in natural human oral mucosa. Additionally, overall thickness of the epithelial layers were found to be significantly thinner in models cultured in serum free environments. These findings were in agreement with the previously published work of Costea *et al.* (2005), who investigated the direct effect of culture medium on the growth of keratinocyte monolayers and morphogenesis of oral organotypical models. From buccal biopsies, primary keratinocytes and fibroblasts were expanded and seeded onto collagen type I scaffolds for 10 days at ALI in chemically defined medium, Keratinocyte Serum Free Medium® (KSFM®)(Life Technologies™, Grand Island, New York, USA), FAD both supplemented with FBS and without. Using immunohistochemical staining to detect for CK13, and Ki-67, data indicated that chemically defined medium, KSFM® was

unable to support the growth and proliferation of keratinocyte cultures in comparison with FAD supplemented with serum and without serum supplementation. Additionally, organotypic models grown in KSF<sup>®</sup> exhibited the fewest epithelial layers, had fewer cell to matrix adhesions (collagen scaffold) and had the least differentiated layers.

#### 1.6.2.6. *Oral organotypic model applications*

Although there are some noted difficulties in using serum free culture conditions to develop oral organotypic models, these models are useful for *in vitro* research to enable drug toxicity testing (Barrila *et al.*, 2010), biocompatibility analysis of newly developed implants (McGinley, Moran and Fleming, 2013) and host-pathogen interactions (Yadev *et al.*, 2011). In addition they can be used to investigate soft tissue-dental implant interactions (Chai *et al.*, 2011).

In 2010, Chai *et al.* published the first research using 3D oral organotypic models for the purpose of analysing dental implant-soft tissue interactions. They used primary human oral keratinocytes and fibroblasts, isolated from oral mucosa biopsies, seeded onto AlloDerm<sup>™</sup> scaffolds and cultured these for 4 days. Using a punch biopsy, four different surface modified titanium rods (polished, sandblasted, machined and TiUnite) were implanted within the constructs, with the whole structure raised to the air liquid interface (ALI) to encourage epithelial stratification. Upon histological observation, two types of epithelial attachment were observed: *pocket type*, where a gap between

the epithelial layer and the implant surface was visible and *non-pocket type*, with no apparent gap. It was also identified that the various surface modifications had no significant effect on epithelial attachment. Chai *et al* also conducted further experiments using 3D organotypic oral mucosa models to assess i) ultrastructural features of various surface treated titanium implants and soft tissue interactions (Chai *et al.*, 2010), ii) the effect of varying implant topography biological seal (Chai *et al.*, 2011) and iii) the contours between the soft tissue and implant surface (Chai *et al.*, 2012).

Whilst there is no denying the importance of this research, all experimental work relied on the culture environment being supplemented with FBS or BPE, thus adding uncontrolled variables to the culture environment.

## **1.7. Research aims and objectives**

The development of relevant *in vitro* oral organotypic models enables the reduction and replacement of animals used within oral research, which has the potential to aid and advance current knowledge surrounding soft tissue-dental implant interactions. At present, this application in an entirely animal-component free environment has yet to be achieved. Therefore, the overall aim of this project was to:

- Develop a 3D oral organotypic model using an entirely animal-component free environment to enable analysis of soft tissue-implant interactions. Subsequent objectives include:
  - - Identification and development of an optimized protocol for isolating and culturing primary human oral keratinocytes and fibroblasts, to be used to construct 3D oral organotypic models.
    - Identification and selection of a suitable animal-component free culture media that has the ability to support and sustain growing immortalized keratinocyte (H400) and primary human oral fibroblast and keratinocyte cultures for long term culture (>21 days).
    - Determination of the effect of animal-component free culture media on H400 and primary keratinocyte cytoskeletal, cell adhesion and proliferative gene expression including, cytokeratins, 1, 5, 6, 19 and 19, Ki-67, e-cadherin, n-cadherin and vimentin.

- Development of an optimized protocol to separate the epidermis from the dermis and to remove all cells from allogenic skin.
  
- Analysis of H400 and primary keratinocyte interactions with different grades of titanium and zirconia alloys using viability and attachment assays and image analysis.
  
- Mechanical analysis of suitable hydrogel scaffolds for use as alternative to de-epidermalised dermis (DED), to enable fibroblast encapsulation and maintenance of fibroblast viability.
  
- Analysis of H400 and primary keratinocyte interactions with different grades of titanium and zirconia alloys using viability and attachment assays and image analysis.
  
- Mechanical analysis of suitable hydrogel scaffolds for use as alternative to de-epidermalised dermis (DED), to enable fibroblast encapsulation and maintenance of fibroblast viability.

**CHAPTER 2:**  
**MATERIALS AND**  
**METHODS**

## **2.1. Isolation, expansion and cultivation of primary human gingival keratinocytes and fibroblasts**

Oral fibroblasts and keratinocytes were isolated and expanded from buccal gingiva donated by 3 patients, through the University of Birmingham Dentistry Research Tissue Bank (NRES Research Ethics Committee approval 14/SW/1148). To reduce the potential of future microbial contamination, the patient's biopsy sites were rinsed with chlorhexidine for ~1-minute prior to 4 mm punch biopsy removal. Biopsies were then placed in KGM-CD (Lonza, Basel, Switzerland) supplemented with 100 I.U./ml penicillin, 100µg/ml streptomycin solution (Sigma-Aldrich, Dorset, UK) and 100µg/ml Amphotericin B (Sigma-Aldrich, Dorset, UK) and incubated at 4°C for up to 6 hours. To detach the oral epithelium from the lamina propria, and to isolate primary human gingival keratinocytes (pHGK) biopsies were washed in Dulbecco's modified phosphate buffered saline (dPBS) (pH 7.2) (Gibco, Thermo Fisher Scientific, Loughborough, UK) to remove any excess blood and placed in 1ml TrypLE™ Express (Life Technologies, Thermo Fisher Scientific, Loughborough, UK) supplemented 200 I.U./ml penicillin, 200µg/ml streptomycin solution (Sigma-Aldrich, Dorset, UK) and 200µg/ml Amphotericin B (Sigma-Aldrich, Dorset, UK), then placed at 4°C for 20 – 22 hours to promote detachment of the epidermis from dermis.

After enzymatic treatment, the epithelium was detached using a disposable surgical scalpel no:10 (Swann-Morten, Sheffield, UK), finely minced and placed within a Nunc™ T25cm<sup>2</sup> cell culture flask (Nunc™, Thermo Fisher Scientific, Loughborough, UK) with 1ml of KGM-CD supplemented with 100 I.U./ml penicillin, 100µg/ml streptomycin solution (Sigma-Aldrich, Dorset, UK), and 100µg/ml Amphotericin B (Sigma-Aldrich, Dorset, UK). To isolate and expand primary human gingival fibroblasts (pHGF), the separated lamina propria was dissected into pieces of approximately (~1mm<sup>2</sup>) and placed within a T25cm<sup>2</sup> cell culture flask (Nunc™, Thermo Fisher Scientific, Loughborough, UK) with 1ml Dulbecco's Modified Eagle Medium (DMEM) (Gibco, Thermo Fisher Scientific, Loughborough, UK) supplemented with 10% human serum (Sigma-Aldrich, Dorset, UK), 10mM HEPES (4-(2-hydroxyethyl)-1-piperazineethanesulfonic acid; Sigma-Aldrich, Dorset, UK), 100 I.U./ml penicillin, 100µg/ml streptomycin solution (Sigma-Aldrich, Dorset, UK) and 100µg/ml of Amphotericin B (Sigma-Aldrich, Dorset, UK). Samples were incubated overnight and 1ml of supplemented media was added to the cultures daily until a total volume of 5ml was reached. Media changes for primary keratinocytes and fibroblasts were performed 5 days after initial seeding and subsequent media changes were performed every 2-3 days.

## **2.2. Cultivation of human oral squamous cell carcinoma cell line (H400 cells)**

The H400 cell line is an immortalized keratinocyte cell line established from a human squamous cell carcinoma of the alveolar process (Prime *et al.*, 1990). Cells were cultured in KGM-CD (Lonza, Basel, Switzerland) and all cultures were incubated at 37°C in an atmosphere of 5% CO<sub>2</sub> and 95% humidity. H400 cell culture media changes were performed every 2-3 days.

## **2.3. Passaging of confluent cell cultures**

Once cultures reached ~80% confluency (based upon microscopic observation), culture media was aspirated, and cells were washed twice using dPBS (Gibco, Thermo Fisher Scientific, Loughborough, UK) before 5ml TrypLE™ Express (Life Technologies, Thermo Fisher Scientific, Loughborough, UK) was added and the flask was incubated until visible detachment of cells from the surface occurred based upon microscopic observation; this was at approximately 5 minutes incubation. The TrypLE™ Express -cell mix was then transferred to a 50ml universal tube (Nunc™, Thermo Fisher Scientific, Loughborough, UK) and centrifuged (Precision Durafuge®100; Thermo Fisher Scientific, Loughborough, UK) at 800 revolutions per minute (rpm) for 6 minutes to pellet the suspended cells. Subsequently the supernatant

was removed by aspiration and the cell pellet re-suspended in 5ml of supplemented culture medium.

#### **2.4. H400 cell culture in animal-component-free media using Trypan Blue stain**

To identify a suitable animal-component-free medium to develop a 3D oral organotypic cultures, growth and viability of H400 cells were analysed over a 21-day experimental period.

H400 cells were seeded at  $5 \times 10^3$  cells per well in 24 well plates (Nunc™, Thermo Fisher Scientific, Loughborough, UK) and were cultured in either DMEM (Gibco, Thermo Fisher Scientific, Loughborough, UK) supplemented with 10% human serum (Sigma-Aldrich, Dorset, UK) and 10mM HEPES (Sigma-Aldrich, Dorset, UK), CnT-Pr (CellnTEC Advanced Cell Systems AG, Bern, Switzerland), Epilife (Life Technologies, Thermo Fisher Scientific, Loughborough, UK) supplemented with S7 (Thermo Fisher Scientific, Loughborough, UK) or KGM-CD (Lonza, Basel, Switzerland). On days 2, 5, 7, 11, 14, 16, 19 and 21 of culture, media was replenished and six wells from each experimental group, had media removed, washed twice with dPBS (Gibco, Thermo Fisher Scientific, Loughborough, UK) and had 200µl of TrypLE™ Express (Life Technologies, Thermo Fisher Scientific, Loughborough, UK) added, to dissociate cells from the tissue culture surface. After five minutes of incubation, wells were observed

using a phase contrast microscope (Eclipse TE3000 Inverted Microscope, Nikon, Surrey UK Ltd, UK) to identify cell detachment. From the cell suspension, a 50µl aliquot was subsequently removed and combined with an equal volume of 0.4% Trypan Blue (Life Technologies, Thermo Fisher Scientific, Loughborough, UK) and the number of living (unstained) and dead cells (stained dark blue) were counted using an improved Neubauer haemocytometer (Hawksley, Sussex, UK). All viable cell counts were performed in triplicate.

## **2.5. Calculation of population doubling times**

To determine population doubling times data obtained between days 7 and 14 for all cultures was used in the following Equation 1.

$$\text{Doubling Time} = \frac{T \times \ln(2)}{(\lg(N_1 - N_2))}$$

**Equation 1:** Calculation of population-doubling time

Where:

*T* = Time difference (days) between  $N_0$  and  $N_1$

*Lg* = Log *x* base 10

$N_0$  = Number of cells at the start of linear region

$N_1$  = Number of cells at the end of linear region

## **2.6. Sensitivity of Alamar Blue and MTT assays for cell culture analysis**

The Alamar Blue (7-Hydroxy-3H-phenoxazin-3-one 10-oxide; Sigma-Aldrich, Dorset, UK) and the MTT (3-(4,5-dimethylthiazol-2-yl)-2,5-diphenyltetrazolium bromide; Sigma-Aldrich, Dorset, UK) assays were compared to determine the most sensitive high-throughput colourimetric assay.

Alamar Blue (Sigma-Aldrich, Dorset, UK) and MTT (3-(4,5-dimethylthiazol-2-yl)-2,5-diphenyltetrazolium bromide; Sigma-Aldrich, Dorset, UK) assays are both colorimetric assays and can be used to analyse population growth, metabolic activity and viability of growing cell cultures (Mosmann, 1983; O'Brien *et al.*, 2000; Hamid *et al.*, 2004). The reactive component of Alamar Blue is Resazurin; a blue compound that can permeabilise the cell membrane and if added to viable cell cultures, Resazurin is reduced to Resorufin (a bright red compound) by cellular metabolic reduction. Viable cells will actively continue to reduce Resazurin to Resorufin which results in a colourimetric media change from blue to red. If added to non-viable cells, no reduction occurs therefore the colour of the media will remain blue (O'Brien *et al.*, 2000).

MTT is a soluble tetrazolium dye that is yellow and following addition to viable cell cultures, mitochondrial dehydrogenases specifically,

NAD(P)H-dependent cellular oxidoreductase, reduce MTT to its insoluble form, formazan which is a deep purple. Similarly to the principles of Alamar Blue mentioned above, if added to non-viable cells, no reduction occurs therefore there is no colour change (Mosmann, 1983; Hamid *et al.*, 2004).

H400 cells (passage 26) and pHGFs (Biopsy 16, passage 5) were seeded at the following densities;  $5 \times 10^3$ ,  $1 \times 10^4$ ,  $5 \times 10^4$ ,  $1 \times 10^5$  and  $5 \times 10^5$ , in two sets of sextuplicates in 24-well plates (Nunc™, Thermo Fisher Scientific, Loughborough UK) in 1ml DMEM (Gibco, Thermo Fisher Scientific, Loughborough, UK) supplemented with 10% human serum (Sigma-Aldrich, Dorset, UK) and 0.1mM HEPES (Sigma-Aldrich, Dorset, UK) Cultures were then incubated for 24 hours in standard conditions, to allow attachment. Alamar Blue (Sigma-Aldrich, Dorset, UK) was dissolved in dPBS (Gibco, Thermo Fisher Scientific, Loughborough, UK) at a concentration of 1% and MTT reagent (Sigma-Aldrich, Dorset, UK) was dissolved in dPBS (Gibco, Thermo Fisher Scientific, Loughborough, UK) to form a working concentration of  $5 \text{mg ml}^{-1}$ . After the initial seeding period, to one set of culture wells, 100µl of Alamar Blue was added to give a final concentration of 10%, to the remaining sextuplicates initially prepared, 100µl of MTT solution was added to the each of the wells. Cultures were incubated for 4 hours in standard conditions. As negative controls, Alamar Blue solution and

MTT were added directly to wells containing culture medium without cells.

For cultures containing Alamar Blue, plates were covered to reduce exposure to light and placed on an orbital shaker (R100/TW; Luckham LTD, Sussex, England) for 2 minutes to promote an even colour distribution. 100µl of solution was removed from each well and transferred to a well on a fresh 96-well plate (Nunc™, Thermo Fisher Scientific, Loughborough, UK). Cultures containing the MTT reagent, had their media and MTT mix completely removed and 200µl dimethyl sulfoxide (DMSO; Sigma-Aldrich, Dorset, UK) was added. The plate was then covered in foil and placed on an orbital shaker for 2 minutes. 100µl from each well was then removed and placed into a well on a 96-well plate (Nunc™, Thermo Fisher Scientific, UK).

Absorbance readings for both the test and control wells were read at 570nm for Alamar Blue assay and 630nm for MTT cultures using an absorbance microplate reader (ELX 800; Biotek Instruments Inc, Swindon, UK).

To calculate the percentage of Alamar Blue that had been reduced, Equation 2 was applied:

$$\text{Percentage reduction of Alamar Blue} = \frac{(O2 \times A1) - (O1 \times A2)}{(R1 \times N2) - (R2 \times N1)} \times 100$$

**Equation 2:** Calculation of the percentage of reduced Alamar Blue

Where:

*O1 = molar extinction coefficient (E) of oxidized Alamar Blue at 570 nm (80586)*

*O2 = E of oxidized Alamar Blue at 600 nm*

*R1 = E of reduced Alamar Blue® at 570 nm*

*R2 = E of reduced Alamar Blue® at 600 nm*

*A1 = absorbance of test wells at 570 nm*

*A2 = absorbance of test wells at 600 nm*

*N1 = absorbance of negative control well (media plus Alamar Blue but no cells) at 570 nm*

*N2 = absorbance of negative control well (media plus Alamar Blue but no cells) at 600 nm*

## **2.7. Alamar Blue calibration curve**

H400 cells (P26) and pHGFs (Biopsy 16, passage 5) at the following densities;  $5 \times 10^3$ ,  $1 \times 10^4$ ,  $5 \times 10^4$ ,  $1 \times 10^5$  and  $5 \times 10^5$ , were seeded in sextuplicate in 24-well cell culture plates (Nunc™, Thermo Fisher Scientific, Loughborough, UK) and grown in either DMEM (Gibco, Thermo Fisher Scientific, Loughborough, UK) supplemented with 10% human serum (Sigma-Aldrich, Dorset, UK) and 0.1mM HEPES (Sigma-Aldrich, Dorset, UK) or KGM-CD (Lonza, Basel, Switzerland)

and incubated under standard conditions for 24 hours, to allow cell attachment.

Using the method and concentration outlined in Section 2.6, an Alamar Blue standard curve was generated and from Equation 2, reduction of Alamar Blue was calculated for each of the following seeding densities:  $5 \times 10^3$ ,  $1 \times 10^4$ ,  $5 \times 10^4$ ,  $1 \times 10^5$  and  $5 \times 10^5$ . Using the linear portion of the graph (cell number plotted against percentage reduction of Alamar Blue), cell number was read from % reduction of Alamar Blue.

## **2.8. pHGF and H400 cell culture analysis in different animal-component-free media using Alamar Blue**

To compare with results obtained from Trypan Blue assays,  $5 \times 10^3$  pGHFs (P5) or H400 cells (P27) per well were seeded in six wells (Nunc™, Thermo Fisher Scientific, Loughborough UK) and were grown in either DMEM (Gibco, Thermo Fisher Scientific, Loughborough, UK) supplemented with 10% human serum (Sigma-Aldrich, Dorset, UK) and 10mM HEPES (Sigma-Aldrich, Dorset, UK), CnT-Pr (CellnTEC Advanced Cell Systems AG, Bern, Switzerland), Epilife (Life Technologies, Thermo Fisher Scientific, Loughborough, UK) supplemented with S7 (Thermo Fisher Scientific, Loughborough, UK) or KGM-CD (Lonza, Basel, Switzerland). At the same time points as described in section 2.5, and using the method described above,

absorbance values at 570nm and 60nm were recorded from which the cell number was calculated.

## **2.9. Analysis of calcium concentration in different animal-component-free media**

Due to the reported effect of calcium on proliferation of both fibroblasts and keratinocytes, the calcium concentration was determined for each animal-component-free media using a calcium electrode (Orion™ Thermo Fisher Scientific, Loughborough UK (Tu and Bikle, 2013; Pinto *et al.*, 2015). Initially, the electrode was calibrated using 1, 10, 100 and 1000 Ca<sup>2+</sup> parts per million (ppm) solutions which were made serially diluting 1000 Ca<sup>2+</sup> (ppm) solution (EDT directION, Dover, UK) with reverse osmosis (RO) water. Once, calibrated, the electrode was placed in the different animal-component-free media and the output was recorded. From the calibration curve, the outputs from the calcium electrode were plotted and the calcium concentrations for each media determined.

## **2.10. Morphological analysis of pHGFs and H400 cells cultured in different animal-component-free media**

pHGFs (passage 6) and H400 cells (passage 21) were seeded at a density of  $1 \times 10^4$  cells per well in a 6 well plate (Nunc™, Thermo Fisher Scientific, Loughborough UK) and cultured in either DMEM

(Gibco, Thermo Fisher Scientific, Loughborough, UK) supplemented with 10% human serum (Sigma-Aldrich, Dorset, UK) and 10mM HEPES (Sigma-Aldrich, Dorset, UK), CnT-Pr (CellnTEC Advanced Cell Systems AG, Bern, Switzerland), Epilife (Life Technologies, Thermo Fisher Scientific, Loughborough, UK) supplemented with S7 (Thermo Fisher Scientific, Loughborough, UK) or KGM-CD (Lonza, Basel, Switzerland) for 7, 14 or 21 days. Subsequently at these time-points, cultures were removed from the incubator and a series of phase contrast images using a digital camera (Nikon D5300, Nikon, Japan) were captured and used to observe cell morphology.

### **2.11. Processing of de-epidermalised dermis (DED)**

To identify a suitable processing method to generate de-epidermalised dermis (DED) two commonly used methods were used and compared (Takami *et al.*, 1996; MacNeil, Shepherd and Smith, 2011). Cadaveric skin (Euro Tissue Bank, Beverwijk, Netherlands) was dissected into six  $\sim 1\text{cm}^2$  sections. Three samples were placed in dPBS (Gibco, Thermo Fisher Scientific, Loughborough, UK) and incubated at 37°C for 4 days before removing and placing into 1M NaCl (pH7.2; Sigma-Aldrich, Dorset, UK) incubated at 37°C for 3 days after which the epidermis was separated mechanically from the dermis using fine point forceps and a disposable surgical scalpel no:10 (Swann-Morten, Sheffield, UK). A further three samples were placed in 0.25% TypLE™ Express (Gibco,

Thermo Fisher Scientific, Loughborough, UK) and 0.5mM EDTA (ethylenediaminetetraacetic acid; Sigma-Aldrich, Dorset, UK) for 2 days at 4°C. Samples were then incubated in 0.5% Triton X-100 (Sigma-Aldrich, Dorset, UK) for 24h at room temperature with continuous agitation to promote epidermis detachment. Mechanical separation was also performed using fine point forceps and a disposable surgical scalpel no:10 (Swann-Morten, Sheffield, UK). To sterilise the resultant DED, samples were immersed in excess 0.1% peracetic acid (Sigma-Aldrich, Dorset, UK) solution – titrated using 1M sodium hydroxide (Sigma-Aldrich, Dorset, UK) to pH 7- for 5 hours at room temperature. Following sterilisation, the samples were stored in dPBS (Gibco, Thermo Fisher Scientific, Loughborough, UK) (Gibco, Thermo Fisher Scientific, Loughborough, UK) with 100 I.U./ml penicillin and, 100µg/ml streptomycin solution (Sigma-Aldrich, Dorset, UK) and 100µg/ml of Amphotericin B (Sigma-Aldrich, Dorset, UK) and stored at 4°C until further use. The dPBS (Gibco, Thermo Fisher Scientific, Loughborough, UK) was refreshed weekly.

## **2.12. Development of 3D oral organotypical cultures using DED as a scaffold**

The prepared DED sections as described above were transferred into fresh dPBS (Gibco, Thermo Fisher Scientific, Loughborough, UK) supplemented with 100 I.U./ml penicillin, 100µg/ml streptomycin

solution (Sigma-Aldrich, Dorset, UK) and 100µg/ml of Amphotericin B (Sigma-Aldrich, Dorset, UK) and incubated for 2 hours at 37°C in 5% CO<sub>2</sub> prior to use. Subsequently, the prepared samples were placed onto transwell tissue culture inserts (ThinCert™, pore size: 3.0µm, membrane: PET Membrane RoTac; Greiner Bio-One GmbH, Kremsmünster, Austria) which had been previously placed in a 6 well tissue culture plate (Nunc™, Thermo Fisher Scientific, Loughborough, UK) and supplemented media was added up to the base surface of the membrane. Confluent flasks of pHGF and H400 cell cultures were passaged using the method described in section 2.4. Resuspended pHGF cells were seeded at 2x10<sup>6</sup> cells per sample, reticular side down, in 2ml of supplemented culture media; equating to 1x10<sup>6</sup> pHGF cells seeded per 1cm<sup>2</sup> of processed DED. Supplemented culture medium (total volume 2ml) was then added to completely submerge the sample. The newly cell seeded samples were then incubated in a humidified environment at 37°C in 5% CO<sub>2</sub> for 3 days. Subsequently, medium was then removed and the DED with seeded cells was inverted so that the papillary surface was uppermost. Using the method described in section 2.4, H400 cell cultures were seeded at a density of 2x10<sup>6</sup> cells (suspended in 2ml of supplemented culture medium) per sample onto the papillary side of the processed DED and a further 2ml culture medium was added to completely submerge the sample prior to incubation. Culture medium was changed daily up to 4 days. On the

fourth day, medium was removed, and fresh supplemented culture medium was added to just beneath the papillary surface to enable exposure of the H400 keratinocytes to the air liquid interface (ALI); to encourage stratification. Culture media was changed every 2-3 days maintaining the ALI for 7, 14 or 21 days. The 3D cultures were then either processed for histological analysis (Section 2.24) or RT-PCR analysis (Section 2.37).

### **2.13. Preparation of sodium alginate solution and hydrogels**

Sodium alginate (Sigma-Aldrich, Dorset, UK) was dissolved in 0.1M MES buffer (2-(N-morpholino) ethanesulfonic acid; Sigma Aldrich, Dorset, UK) and RO water at room temperature to create a 1.2wt % solution (pH:7.2). To form hydrogels, 100mM calcium chloride ( $\text{CaCl}_2$ ; Sigma-Aldrich, Dorset, UK) was added to the solution which then cross-linked, forming a gel (Hwang, Varghese and Elisseeff, 2007).

### **2.14. Preparation of RGD-modified sodium alginate solution and hydrogels**

Using the method referenced above, sodium alginate solution was produced. To the solution, peptide arginine-glycine–aspartate (RGD) (Sigma-Aldrich, Dorset, UK) was added in the presence of EDC (1-ethyl-3-(dimethylaminopropyl) carbodiimide; Sigma-Aldrich, Dorset,

UK) and sulfo- NHS (N-hydroxysulfosuccinimide; Sigma-Aldrich, Dorset, UK) with constant stirring and left to react for 18 hours at room temperature. The RGD-modified alginate was then purified using dialysis (cellulose tubing with MW=14,000Da; Sigma-Aldrich, Dorset, UK) for 3 days; with 3 water changes performed per day. The resultant solution was then sterilized using a 0.22µm filter (Merck Milipore, Nottingham, UK) (Hwang, *et al.*, 2007). To form hydrogels, 100mM CaCl<sub>2</sub>, was added to the solution which cross-linked, forming a gel.

### **2.15. Analysis of the effect of hydrogel cross-linking and dissociation reagents on pHGF cultures.**

Confluent flasks of pHGF and H400 cell cultures were passaged using the method described in Section 2.4. Resuspended H400 and pHGF cell cultures were seeded at a density of 5 x 10<sup>3</sup> into 24 well plates (Nunc™, Thermo Fisher Scientific, Loughborough UK) and were cultured in DMEM (Gibco, Thermo Fisher Scientific, Loughborough, UK) supplemented with 10% human serum (Sigma-Aldrich, Dorset, UK) and 10mM HEPES (Sigma-Aldrich, Dorset, UK) and incubated overnight. Culture media was then removed and cultures were then washed with dPBS before being exposed to either 100mM CaCl<sub>2</sub> or 100mM sodium citrate (Sigma-Aldrich, Dorset, UK) for minutes. After exposure, the reagents were removed and cultures were washed using dPBS to remove any residual traces and 500µl of supplemented culture

medium was added. On days 1, 4, 7, 11, 14 and 21 days, media was replenished and six wells from each experimental group, had media removed, washed twice with dPBS (Gibco, Thermo Fisher Scientific, Loughborough, UK) and had 200µl of TrypLE™ Express (Life Technologies, Thermo Fisher Scientific, Loughborough, UK) added, to dissociate cells from the tissue culture surface. After five minutes of incubation, wells were observed using a phase contrast microscope (Eclipse TE3000 Inverted Microscope, Nikon, Surrey UK Ltd, UK) to identify cell detachment. From the cell suspension, a 50µl aliquot was subsequently removed and combined with an equal volume of 0.4% Trypan Blue (Life Technologies, Thermo Fisher Scientific, Loughborough, UK) and the number of living (unstained) and dead cells (stained dark blue) were counted using an improved Neubauer haemocytometer (Hawksley, Sussex, UK). All viable cell counts were performed in triplicate.

## **2.16. Analysis of the effect of encapsulation within RGD modified alginate hydrogels on pHGF cultures**

RGD modified alginate solutions outlined in Sections 2.13 and 2.14, were heated to 37°C prior to use for 30 minutes. Sterile filter paper (Whatman® Grade 1 100m, Sigma-Aldrich, Dorset, UK) was added to Petri dishes (100mm x 20mm; Sigma-Aldrich, Dorset, UK) and saturated with 3ml of 100mM CaCl<sub>2</sub>, with hydrogel moulds (M8 (28mm

x 20mm x 1mm) stainless steel washer, Amazon, Milton Keynes, UK) placed on the surface. Confluent flasks of pHGF cell cultures were passaged using the method described in Section 2.4. A volume of cell resuspension containing  $1 \times 10^6$  cells was added to a 5ml bijou tube (Sigma-Aldrich, Dorset, UK). An appropriate volume of RGD modified alginate solution was added to the cell suspension, making the total volume equal to 1ml and this was evenly mixed. 200 $\mu$ l of the of hydrogel/cell suspension mix were added to the hydrogel mould, with another piece of saturated sterile filter paper placed on the moulds. A further 10ml of 102mM  $\text{CaCl}_2$  was added to completely submerge the hydrogel moulds and the structures were incubated at 37°C until cross linking occurred (up to 5 minutes). Crosslinked hydrogels were then carefully removed from moulds and placed into a petri dish containing dPBS for 1 minute. Fabricated hydrogels were then placed within tissue culture inserts (ThinCert™, pore size: 3.0 $\mu$ m, membrane: PET Membrane RoTac; Greiner Bio-One GmbH, Kremsmünster, Austria) and submerged within 2ml supplemented culture medium.

### **2.17. Analysis of pHGF released from encapsulation within RGD modified alginate hydrogels**

To release previously encapsulated pHGF cell cultures (Section 2.16) culture media was removed from the wells and structures were washed in dPBS twice. Hydrogels were then exposed to 100mM sodium citrate

(Sigma-Aldrich, Dorset, UK) for up to 5 minutes to dissociate the hydrogel structure. The resultant cell/reagent solution was then centrifuged at 800rpm to pellet the cells.  $1 \times 10^4$  cells were seeded in 24 well plates (Nunc™, Thermo Fisher Scientific, Loughborough UK) and cultured in supplemented culture medium. After 1, 3, 5 and 7 days in culture, media was changed and 50µl of Alamar Blue solution (Section 2.6) was added to give a final concentration of 10% to each well. Cultures were incubated for 4 hours in standard conditions and as negative controls, Alamar Blue solution was added directly to wells containing culture medium without cells. Absorbance readings for both the test and control wells were read at 570nm and using Equation 2 and the calibration curve generated in Section 2.7, viable cell numbers were calculated.

## **2.18. Analysis of H400 attachment on RGD modified alginate hydrogels**

Using the methods described in Section 2.14, RGD modified alginate hydrogels were fabricated. Confluent flasks of H400 cell cultures were passaged using the method described in Section 2.4. Resuspended H400 cell cultures were seeded at a density of  $5 \times 10^3$  on top of RGD modified alginate hydrogels within 24 well tissue culture plates (Nunc™, Thermo Fisher Scientific, Loughborough UK). Cells were incubated for 30 minutes, before being submerged within

supplemented culture medium. After 1 day, RGD modified hydrogels with H400 cells attached to the surface were transferred to a fresh 24 well tissue culture plate (Nunc™, Thermo Fisher Scientific, Loughborough UK) and media was refreshed. 50µl of Alamar Blue solution (Section 2.6) was added to give a final concentration of 10% to each well. Cultures were incubated for 4 hours in standard conditions and as negative controls, Alamar Blue solution was added directly to wells containing culture medium without cells. Absorbance readings for both the test and control wells were read at 570nm and using Equation 2 and the calibration curve generated in Section 2.7, viable cell numbers were calculated. Media refreshing and Alamar Blue absorbance readings were repeated on days 3, 5 and 7.

### **2.19. Fabrication and synthesis PEG-DM**

Fabrication and synthesis of poly(ethylene glycol) dimethacrylate (PEG-DM) was performed as previously described (Martens and Anseth, 2000). PEG was combined with 5mg hydroquinone (Sigma-Aldrich, Dorset, UK) and purged with nitrogen for 30s by flooding the vial with nitrogen gas using a 19-gauge needle attached to a rubber tube attached to a nitrogen tank. The two reagents were heated using a microwave (Easy Chef II; Sharp, Uxbridge, UK) at 400W for 5 minutes. 157.4µl of methacrylic anhydride (Sigma-Aldrich, Dorset, UK) was added. The solution was then cooled for 10 minutes at room

temperature, vortexed then microwaved again for 5 minutes at 400W until molten. To purify the solution, ice cold ethyl ether (Sigma-Aldrich, Dorset, UK) was slowly dripped into the solution with constant stirring. The precipitated polymer solution was then vacuum-filtered to remove the excess ethyl ether (Sigma-Aldrich, Dorset, UK). The polymer was then removed from the filter and placed into a new beaker. The extracted polymer was then subjected to a high vacuum (~25 psi) for up to 60 minutes. This process was repeated a further two times. After the final precipitation, the precipitate was placed again in a high vacuum for at least 2 hours then placed within a desiccator for up to 6 months.

## **2.20. Characterisation and calibration of the UV light system**

PEG-DM is a solution that requires the addition of a photoinitiator and exposure to UV light to form a hydrogel (Martens and Anseth, 2000; Martens *et al.*, 2007; Young, Poole-Warren and Martens, 2012). The photoinitiator selected for this research was from Irgacure® 2959 (2-hydroxy-4'-(2-hydroxyethoxy)-2-methylpropiophenone; BASF Schweiz AG, Basel, Switzerland) and was used due to its reported extremely low cytotoxicity (Williams *et al.*, 2005). Although the excitation maximum for Irgacure® 2959 (BASF Schweiz AG, Basel, Switzerland) is between 200-300nm (see Figure 12), due to potential DNA damage to

cells from these wavelengths, higher wavelengths of between 350-400nm are commonly used to photoinitiate these hydrogel systems to minimise cyto- and geno-toxicity.

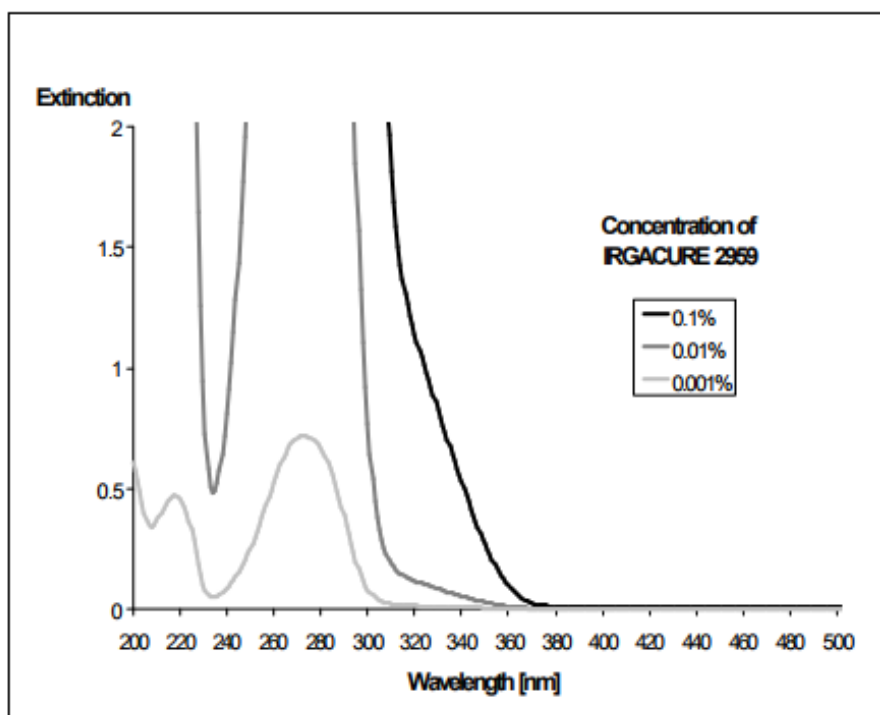


**Figure 12:** Emission and excitation spectrum for Irgacure 2959 at a range of concentrations. Image obtained from Ciba Speciality Chemicals (2011).

## 2.21. Analysis of hydrogel disc swelling mass and loss properties

Changes in wet mass for the different hydrogels were monitored for up to 14 days. Sodium alginate and PEG-DM discs with a volume of 220 $\mu$ l were created and initially weighed after fabrication. Samples were then placed in 0.9% saline solution for 1, 3, 5, 7 and 14 days at 37°C in a humidified incubator. On the aforementioned days, samples were

carefully removed and excess moisture was removed by blotting using filter paper (Whatman® Filter Paper No.1, 7.0cm; Camlab, Cambridge, UK) and samples weighed using laboratory scales (Fisherbrand™ Analytical Balance; Fisher Scientific, Loughborough, UK). The swelling ratio was then calculated using Equation 3.

$$\text{Swelling Ratio (\%)} = \frac{W_t - W_0}{W_0} \times 100$$

**Equation 3:** Calculation of hydrogel swelling ratio

Where:

$W_0$  = *Weight immediately after fabrication*

$W_t$  = *Weight at experimental time point*

## 2.22. Compressive testing of hydrogels

A series of hydrogel discs were created using the methods described in Section 2.13 and 2.14. After initial manufacture, 6 randomly selected discs from each set were immediately compressed using a 50N load cell on a universal compressive testing instrument (Instron 5544; Instron Ltd, Buckinghamshire, UK) at a cross-head speed of 1 mm/min, until failure, to determine the load-displacement behaviour of the different hydrogels. From the data obtained, stress and strain were calculated and graphs were plotted which enabled calculation of the Young's Modulus for each sample. For the remaining samples, these were

incubated in 0.9% saline solution at 37°C for 1, 3 or 5 days to identify what effect swelling mass/loss had on the compressive strength of the fabricated hydrogels. The compression test was performed as previously described.

### **2.23. Fixation of the processed de-epidermalised dermis**

#### **(DED)**

To compare the efficacy of removing the epidermis from the underlying connective tissue, samples were examined histologically on sections stained with Haematoxylin and Eosin. DED samples were fixed in 10% neutral buffered formalin (Sigma-Aldrich, Dorset, UK) overnight, then placed in Cellsafe biopsy cassettes (CellPath Ltd, Newton, UK) and tissue processing cassettes (CellPath Ltd, Newton, UK) and passed through serial dilutions of ethanol followed by xylene as detailed in Table 4.

**Table 4:** Stages of biological sample dehydration and fixation

<b>Tissue Processing Stage</b>	<b>Duration</b>	<b>Temperature (°C)</b>
Initial rinse of sample in dPBS	5 minutes	25
10% neutral buffered formalin	24 hours	
30% Ethanol	20 minutes	
40 % Ethanol		
50% Ethanol		
60% Ethanol		
70% Ethanol		
80% Ethanol		
90% Ethanol		
100 % Ethanol	10 minutes	
100% Ethanol		
Xylene	25 minutes	
Xylene		
Molten paraffin wax	30 minutes	
Molten paraffin wax		
Molten paraffin wax		

Samples were then submerged in molten paraffin wax (Histoplast, Thermo Scientific, UK) for 20-30 minutes, and this was repeated twice. Wax impregnated samples were then removed from the tissue cassettes and embedded in paraffin wax using thermal embedding and cryo-console (Sakura Tissue–Tek TEC IV Embedding Console System 4714, Netherlands). Samples were then removed from the processing cassette and the cellsafe pad (CellPath Ltd, Newton, UK) and placed in molten paraffin wax. Fresh molten paraffin wax was added to stainless steel base moulds and samples were placed perpendicular to the base of the mould using tweezers. The mould was then placed immediately on the cryo-console Sakura Tissue–Tek TEC IV Embedding Console System 4714, Netherlands) that was set at a temperature of -5°C and

allowed to cool until the wax became solid. The sample was then removed from the mould and sections of thicknesses ranging between 4 - 5µm cut using a rotary microtome (Leica RM 2035, Leica instruments GmbH, Germany) and mounted on super frost plus glass slides (Thermo Fisher Scientific, Loughborough, UK).

#### **2.24. Haematoxylin and Eosin staining of DED**

Haematoxylin and Eosin is a widely used histological staining procedures to examine tissue architecture (Alturkistani, Tashkandi and Mohammedsaleh, 2015). Prior to histological staining, slides were incubated in a 60°C oven (Hotbox Oven Size 1; Gallenkamp, Weiss Technik, Loughborough, UK) overnight to bake the sections onto the slide. The procedure used for Haematoxylin and Eosin staining is outlined in Table 5.

**Table 5:** The various stages of Haematoxylin and Eosin staining

<b>Reagent</b>	<b>Duration (Minutes)</b>
Xylene	5
Xylene	1 (with agitation)
100% Ethanol	2 (with agitation)
95% Ethanol	2 (with agitation)
70% Ethanol	1
50% Ethanol	1
35% Ethanol	1
Haematoxylin Gills II	5
0.3% w/v Acetic Acid	0.5
0.3% Hydrochloric acid	0.5
Scott's tap water substitute	2
Eosin	2
95% Ethanol	
100% Ethanol	2
Xylene	2 (with agitation)

Slides were agitated in xylene to deparaffinise the wax, rinsed in tap water then rehydrated in a series of ethanol dilutions. Sections were then placed in Gills II Haematoxylin (Surgipath Europe Ltd, Peterborough, UK) for 5 minutes, rinsed in water to remove any excess dye then placed in 0.3% acetic acid (Merck Ltd, Middlesex, UK) for 30 seconds followed by 0.3% hydrochloric acid (HCl; Sigma-Aldrich, Dorset, UK). Sections were then rinsed in running tap water before being placed into Scott's Tap Water Substitute (Surgipath Europe Ltd, Peterborough, UK) for 2 minutes. Following this, sections were rinsed in tap water for a minute then placed in Eosin (Surgipath Europe Ltd, Peterborough, UK) which stains for non-specific proteins for 2 minutes

before being rinsed in running water and dehydrated twice in 100% ethanol for 1 minute and twice in xylene for 2 minutes. Sections were then mounted using XAM neutral mounting medium (VWR, International Ltd, Lutterworth, UK).

### **2.25. Preparation of TiZr samples**

Experimental discs were prepared from metal rods (American Elements®, California, USA) that had been cast and melted in excess of three times to ensure homogeneity throughout the rods. The composition of rods ranged from commercially pure grade IV titanium (Ti) and commercially pure zirconium (Zr) to TiZr alloyed rods which contained varying atm% of Zr; 5, 15 and 50%. Following manufacture, each disc was sectioned to a thickness of 0.1mm, then individually polished using a series of silicon carbide papers (Struers, Ballerup, Denmark) from P80 up to P4000, on a polishing machine (DAP-7, Struers, Denmark) lubricated with water using a standardized time of 3 minutes per silicon carbide grade. Table 6 shows the subsequent order and information regarding grit size.

**Table 6:** Details of the silicon carbide (Struers, Ballerup, Denmark) grit sizes at respective grades

<b>Silicon Carbide Grade</b>	<b>Diameter of Grit (<math>\mu\text{m}</math>)</b>
P80	201
P100	162
P220	68
P320	46
P500	30
P800	22
P1000	18
P1200	15
P2400	10
P4000	5

Following the sequential polishing, the discs were prepared to an apparent mirror-like finish by using an MD Chem 200mm polishing disc (Struers, Ballerup, Denmark) using OP-S, a colloidal dispersion of  $0.04\mu\text{m}$  silica particles for 5 minutes (Struers, Ballerup, Denmark).

Once mirror-like finishes were achieved, the discs were then degreased and cleaned in acetone, ethanol then RO water each for 10 minutes in a sonicator bath (Vitasonic II; VITA, Bad Säckingen, Germany). Discs were then allowed to air dry prior to autoclaving ( $121^{\circ}\text{C}$ , 100kPa, 60 minutes; MIS 3781L; Sanyo, Cardiff, UK) before use.

### **2.26. Cell adhesion and growth on prepared TiZr samples**

Sterilised discs were placed in a 12-well tissue culture plate (Nunc<sup>TM</sup>, Thermo Fisher Scientific, Loughborough, UK), using one disc per well. DMEM supplemented with 10% human serum (Sigma-Aldrich, Dorset, UK) or KGM-CD (Lonza, Basel, Switzerland) were added to 4 wells of

each TiZr composition. In three of the wells for each media type, pHGF cells were seeded at a density of  $5 \times 10^3$  cells per well. Using the concentrations and procedure described in Section 2.9, 200 $\mu$ l Alamar Blue was added to each well and incubated under standard culture conditions for 4 hours. 100 $\mu$ l solution was then removed from each well and placed within a well on a 96 well plate (Nunc™, Thermo Fisher Scientific, Loughborough, UK), and the absorbance was determined at 570nm and 600nm using a microplate reader (Biotek Instruments Inc, UK). Subsequently the culture media and the Alamar Blue mix was aspirated, wells were then washed twice in dPBS (Gibco, Thermo Fisher Scientific, Loughborough, UK) and fresh culture media was added to each well. The absorbance of each well was read every 2-3 days for 21 days. Discs with no cells seeded were used as a negative control and cells cultured directly onto the well surface was used a positive control.

### **2.27. Preparation of TiZr for SEM imaging**

After experimental use, each disc was re-polished using the procedure described in section 2.26, pHGFs (Biopsy 16 Passage 4) were seeded at  $5 \times 10^3$  cells per well in either DMEM (Gibco, Thermo Fisher Scientific, Loughborough, UK) supplemented with 10% human serum (Sigma-Aldrich, Dorset, UK) or KGM-CD (Lonza, Basel, Switzerland) and 100 I.U./ml penicillin, 100 $\mu$ g/ml streptomycin solution (Sigma-Aldrich,

Dorset, UK) and 100µg/ml Amphotericin B (Sigma-Aldrich, Dorset, UK); media was changed every other day. At days 7, 14 and 21, discs from each composition with cells adhered to were placed at 4°C for 30 minutes prior to culture media removal. Discs were then washed twice in dPBS (Gibco, Thermo Fisher Scientific, Loughborough, UK) to remove non-adherent cells. 1ml of fixative solution; 2.5% glutaraldehyde (Sigma-Aldrich, Dorset, UK) buffered in 0.1M sodium cacodylate (Sigma-Aldrich, Dorset, UK); pH 7.2, for 30 minutes at 4°C. Discs were then dehydrated in a series of serial ethanol dilutions, 20, 30, 40, 50, 70 and 90%, each at 10 minutes. Discs were then placed in 95% ethanol for 10 minutes with 2 changes and then placed into 100% ethanol, with 2 changes within 15 minutes. Discs were then placed in hexamethyldisilazane (HMDS) (Sigma-Aldrich, Dorset, UK) for 5 minutes, and this was repeated twice. Excess HMDS (Sigma-Aldrich, Dorset, UK) was removed and allowed to evaporate overnight. Samples were then mounted onto 25mm aluminium stubs (Agar Scientific, Essex, UK) using conductive carbon mounting tape (Agar Scientific, Essex, UK) and sputter coated with gold (K550X, Quorum Technologies, Kent, UK) for 2 minutes at 25mA, which provided a coating of approximately 15nm thickness. Standardized images of pHGF cells attached to the mirror-like surface of the different TiZr discs were captured using a high vacuum scanning electron microscope (SEM) (Zeiss EVO® MA10; Carl Zeiss Microscopy GmbH, Jena,

Germany) using an accelerating voltage of 10.00kV and a working distance of 10.00mm. Images were captured at a range of magnifications.

## **2.28. Image analysis of surface attachment**

Using the method previously described in Vyas *et al* (2016), surface coverage of attached pHGF cells on different TiZr surfaces was performed using FIJI (ImageJ, U. S. National Institutes of Health, Bethesda, Maryland, USA) (Schindelin *et al.*, 2012). SEM images obtained in Section 2.27 were pre-processed by enhancing the contrast to 0.5% and applying a rolling background subtraction to correct for uneven illumination. Using the Trainable Weka Segmentation plug-in (Arganda-Carreras *et al.*, 2017), cells were segmented from the surface of the polished TiZr discs by providing pixel samples to initially train the classifier in a semi-supervised way. Pixel samples consisted of square regions measuring 6 x 6 pixels, determined to be optimal to fit between clusters of cells which had exposed TiZr surfaces as well as providing enough pixel values for training. Following segmentation, objects that were less than 30 pixels were removed using 'The Analyse Particles plug-in', as they were considered to be noise. Histograms of each image were used to calculate the number of pixels corresponding to pHGF cell coverage and the percentage of surface coverage was calculated using the equation below:

$$\begin{aligned}
 & \text{Surface coverage (\%)} \\
 &= \frac{\text{number of pixels corresponding to cell surface coverage}}{\text{total number of pixels}} \\
 & \times 100
 \end{aligned}$$

**Equation 4:** Calculation of percentage surface coverage

### **2.29. Non-contact profilometry**

The surface roughness of polished TiZr discs was measured by using a Zygo Optical Profilometer (Zygo, USA) with a 10x Mirau objective lens, a magnification of 2.0x, a resolution of 0.56µm, and a field of view of 0.36x0.27mm to compare the surface finish of the different polished alloys. A random 2D area from 3 arbitrarily selected disks of each alloy was measured.

### **2.30. Extraction of RNA from H400 keratinocyte cultures**

RNA was extracted from H400 keratinocyte cultures that had been grown in either DMEM (Gibco, Thermo Fisher Scientific, Loughborough, UK) supplemented with 10% human serum (Sigma-Aldrich, Dorset, UK) and 10mM HEPES (Gibco, Thermo Fisher Scientific, Loughborough, UK), CnT-Pr (CellnTEC Advanced Cell Systems, Switzerland), Epilife (Life Technologies, Thermo Fisher Scientific, Loughborough, UK) supplemented with S7 (Life Technologies, Thermo Fisher Scientific, Loughborough, UK) or KGM-CD (Lonza, Basel, Switzerland) 7, 14 or 21 days using RNeasy Kit

(Qiagen N.V, Netherlands) following the instructions provided by the manufacturer. Culture media was removed, and cultures were washed with dPBS. 350µl Buffer RLT (Qiagen N.V, Netherlands) was added directly to the culture flask (T25cm<sup>2</sup> cell culture flask; Nunc™, Thermo Fisher Scientific, Loughborough, UK), to cover the culture. The lysate was removed and placed into a sterile 1ml PCR tubes (Eppendorf, Thermo Fisher Scientific, Loughborough, UK) and mixed with an equal volume of 70% ethanol.

### **2.31. Extraction of RNA from pHGF cultures**

To extract RNA from pHGF cultures grown at either 7, 14 or 21 days in the various animal component-free media previously listed, a phenol isolation approach was conducted (owing to limited RNA extraction using the method described in Section 2.30). This involved removing culture media, washing flasks in dPBS (Gibco, Thermo Fisher Scientific, Loughborough, UK) ensuring any residual media was removed, and detaching cells using 1ml TrypLE™ Express (Gibco, Thermo Fisher Scientific, Loughborough, UK). After cells had fully detached (following observation using a light microscopy) the cell suspension was placed into a sterile 2ml centrifuge tubes (Eppendorf, Thermo Fisher Scientific, Loughborough, UK) and centrifuged at 10,000rpm for 3 minutes. Following this, the supernatant was removed and 1ml Trizol (Sigma-Aldrich, Dorset, UK) was added to the cell pellet

and incubated for 5 minutes at room temperature. 200µl chloroform was then added to the same centrifuge tube (Eppendorf, Thermo Fisher Scientific, Loughborough, UK) and was agitated vigorously and incubated at room temperature for 2 minutes. The sample was then centrifuged at 12,000rpm for 15 minutes to enable separation between the precipitate and the aqueous layers. The aqueous layer was carefully aspirated and placed into a clean 2ml centrifuge tube (Eppendorf, Thermo Fisher Scientific, Loughborough, UK) and 650µl 70% ethanol was carefully added to the sample.

### **2.32. Extraction of RNA from 3D oral mucosa cultures**

To extract and isolate RNA from 3D oral mucosa cultures, these were initially carefully washed in dPBS (Gibco, Thermo Fisher Scientific, Loughborough, UK) and then placed in RNAlater (Sigma-Aldrich, Dorset, UK) to prevent RNA from degradation. Samples were then snap frozen using liquid nitrogen (BOC, West Bromwich, UK) and ground using a pestle and mortar. Following this, a phenol isolation was conducted as described previously in Section 2.31.

### **2.33. Isolation of RNA**

The 70% ethanol and aqueous samples mix was transferred to an RNAeasy (Qiagen N.V, Netherlands) spin column in a 2ml collection tube and centrifuged (Model 5415 D, Eppendorf, Thermo Fisher Scientific, Loughborough, UK) at 10,000 rpm for 30s . The flow-through

was then discarded and 350µl Buffer RW1 (Qiagen N.V, Netherlands) was added to the column before centrifuging at 10,000 rpm for 30s. 10µl DNase I (Sigma-Aldrich, Dorset, UK), which had been previously dissolved and mixed in 550µl RNA free water (Sigma-Aldrich, Dorset, UK), was then added to 70µl Buffer RDD (Sigma-Aldrich, Dorset, UK) and placed directly onto the spin column membrane and incubated at room temperature for 15 minutes. This was repeated for each sample. 350µl Buffer RW1 (Qiagen N.V, Netherlands) was added to the column, which was then centrifuged at 10,000rpm for 30s and the flow through was discarded. 500µl Buffer RW1 (Qiagen N.V, Netherlands) was then added to the column, and was centrifuged at 10,000 rpm for 20s, and the flow – through was discarded. 500µl Buffer RPE (Qiagen N.V, Netherlands) was added to the column before the column was centrifuged at 10,000 rpm for 2 minutes. The flow through was discarded and the column was placed into a new collection tube (Qiagen N.V, Netherlands) and centrifuged at full speed for 1 minute. The column was then removed and placed into a 1.5ml collection tube (Qiagen N.V, Netherlands) and 30µl RNase water (Qiagen N.V, Netherlands) was added to the membrane and centrifuged at 10,000 rpm for 1 minute to elute the RNA.

### **2.34. Quantification and visualisation of RNA**

Using a spectrophotometer (BioPhotometer Plus, Eppendorf, Stevenage, UK) the concentration of RNA was measured. To initially calibrate, the spectrophotometer, 70 $\mu$ l RNA-free water (Qiagen N.V, Netherlands) was added to a cuvette and the absorbance was read. Parameters of the dilutions used (68 $\mu$ l RNA-free water, 2 $\mu$ l RNA sample) were inputted and the concentrations ( $\mu$ g/ml) and purity (260/280) of each diluted RNA sample was measured and recorded. After every 4 readings, the spectrophotometer was recalibrated with RNA-free water (Qiagen N.V, Netherlands).

To visualise RNA integrity, a 1% agarose gel was prepared by dissolving 0.7g agarose (Thermo Scientific, Loughborough, UK) in 70ml TAE (Tris-acetate-EDTA; Thermo Scientific, Loughborough, UK) buffer by heating for 2 minutes in a microwave (Easy Chef II; Sharp, Uxbridge, UK) at 850W. The gel was cooled with gentle agitation under running cold water, ensuring homogeneous solidification. 3 $\mu$ l SYBR Gold (Life Technologies, Thermo Fisher Scientific, Loughborough, UK) – which was created by diluting 10,000x SYBR Green into TAE Buffer to form a 1x SYBR Green solution and added to the solution before the gel was poured and the well forming combs were inserted. After cooling, Hyperladder IV (GeneFlow, Lichfield, UK) was loaded into the first lane followed by RNA samples mixed with 1 x buffer in the subsequent wells. The loaded gel was electrophoresed at 120V for 20

minutes, then visualised using G:BoxChemi HR16 (Syngene, Cambridge, UK) under illumination from an ultraviolet light source.

### **2.35. Primer development**

To conduct semi-quantitative reverse transcription PCR and Real-Time PCR, primers for the genes of interest need to be created. To do this, the gene accession number, a unique identifiable number given to a specific gene, was identified from The National Center for Biotechnology Information (NCBI) website (2018) ensuring that the accessions numbers corresponded to genes specifically present in humans. Following this, using the NCBI prime-Blast® website (2018) primers were designed with the maximum PCR product size for real-time PCR primers being capped at  $\leq 100$  base pairs and designed to span exon-exon junctions where possible. Finally, using the NCBI Blast®, Blastn suite website (2018) the specificity of the designed primer was checked prior to being ordered from either Invitrogen or ThermoFisher, UK.

### **2.36. Semi-quantitative reverse transcription PCR analysis**

Using the Tetro Kit (Bioline, Taunton, USA) and following guidelines provided by the manufacturer, the master mix described in Table 7 was created for each sample:

**Table 7:** Component reagents forming the master mix for reverse transcription

<b>Reagent</b>	<b>Volume (<math>\mu</math>l)</b>
Oligo dT <sub>18</sub>	1
dNTP (10mM)	1
5x RT Buffer	4
RNase inhibitor	1
Reverse Transcriptase (200u/ $\mu$ l)	1
RNase free Water	2

The master mix was added to 2 $\mu$ l RNA (for each sample) in a sterile 1ml PCR tube (Eppendorf, Thermo Fisher Scientific, Loughborough, UK) and placed within a thermal cycler (Master Gradient, Eppendorf, Thermo Fisher Scientific, Loughborough, UK) and samples were incubated at 45°C for 40 minutes for cDNA synthesis, then 85°C for 5 minutes to terminate the enzymatic reaction. Following this, RNA-free water was added to the complementary DNA (cDNA) to give a volume of 500 $\mu$ l per sample. This was then placed in a YM-30 microcon filter assembly (Millipore UK, Stevenage, UK) and centrifuged at 10,000 rpm for 2 minutes, then 8,000rpm for 1 minute twice, with levels assessed in between spins using a pipette. Filters were then removed from the construct, inverted into fresh 1ml centrifuge tubes (Eppendorf, Thermo Fisher Scientific, Loughborough, UK) and centrifuged at 800rpm for 1 minute. This filtering approach aimed to remove impurities which may have inhibited the PCR.

Using BioMix™Red (Bioline, Taunton, USA) sq-RT-PCR assays were performed. This involved creating a primer mastermix (Table 8) for each sample consisting of, 12.5µl BioMix Red, 9.5µl or RNA-free water and 2µl of forward and reverse primer mix, which was made prior to this by adding 10µl of both the forward and reverse primers (see Table 11 for sequences) per gene to 60µl RNase free water and mixing evenly. The primer mastermix was then added to 1µl cDNA and this was then placed within a Thermo Cycler (Master Gradient, Eppendorf, Thermo Fisher Scientific, Loughborough, UK) to complete the reaction. Details of the thermal cycling conditions are provided in Table 9.

**Table 8:** Reagents and volumes used in the primer master mix for the polymerase chain reaction.

Reagent	Volume (µl)
BioMix Red	12.5
Forward & reverse primer mix (see Table 11)	2
RNase free water	9.5
cDNA	1

**Table 9:** Details of the different stages of PCR including temperatures and incubation times used

Stage	Temperature (°C)	Time
Denaturing	94	5 minutes
Amplification (25 – 33 cycles)	94	20 seconds
	65	20 seconds
	75	20 seconds
Final Extension	72	10 minutes

### **2.37. PCR product visualisation by gel electrophoresis**

Whilst PCR products were being synthesized, a 1.5% agarose gel which was prepared by dissolving 0.9g agarose (Thermo Scientific, Loughborough, UK) in 60ml TAE buffer (Tris-acetate-EDTA; Thermo Scientific, Loughborough, UK) buffer by heating for 2 minutes in a microwave (Easy Chef II; Sharp, Uxbridge, UK) at 850W. The gel was cooled with gentle agitation under running cold tap water, ensuring homogeneous solidification. Three  $\mu$ l 1x SYBR Gold (Life Technologies, Thermo Fisher Scientific, Loughborough, UK) was added to the solution before the gel was poured and the combs inserted to generate the loading wells. Following this, 6 $\mu$ l of the PCR products were loaded into the wells (with expectation of the first which was loaded with Hyperladder IV (GeneFlow, Lichfield, UK) and the gel was electrophoresed at 120V for 30 minutes before being transferred for ultraviolet visualization using G:Box Chemi HR16 (Syngene, Cambridge, UK).

To quantitate PCR products, Gene Tools software (Syngene, Cambridge, UK) was used to generate equal sized rectangular boxes surrounding each amplified PCR band on the captured gel images. The pixel intensity was adjusted for the background intensity and the PCR product with the highest intensity was set to 100%, and from this, comparative volume density values were calculated. Expression of each gene was normalised against the housekeeping gene amplification

product of glyceraldehyde 3-phosphate dehydrogenase (GAPDH) using Equation 5.

$$\text{Relative Gene Expression} = \frac{\text{Sample volume density}}{\text{GAPDH volume density}} \times 100$$

**Equation 5:** Calculation of relative gene expression

After normalization, expression of each gene was converted to a percentage of expression levels of the highest normalized volume density.

### 2.38. Real Time-PCR analysis

Using a thermal cycler (LightCycler® 480 system, Roche, Switzerland), real time-PCRs were performed in a 96-well plate (LightCycler®, Roche, Switzerland) with each well containing a final volume of 17µl. The composition of the final volume per well is shown in Table 10.

**Table 10:** Details of the components of each well used for qRT-PCR plate set-up.

Reagent	Volume (µl)
SYBR Green I Master PCR Mix	10
PCR Primer mix	2
DNase free water	3
cDNA	2

Samples were carefully mixed by aspiration, loaded into wells and the PCR plate was sealed using foil (LightCycler®, Roche, Switzerland).

The plate was then centrifuged at 1500g for 2 minutes to capture all samples and loaded into the plate holder of the LightCycler® (LightCycler®, Roche, Switzerland). Samples were amplified in duplicate and 2 blank controls per primer were included in each plate. Using the second derivative max method which was computed from the LightCycler software (Version 1.5; Roche Diagnostics, Roche, Switzerland) Cp values were calculated which subsequently enabled relative expression levels to be determined. The efficiency for each primer (forward and reverse) was calculated from a series of serial dilutions of cDNA (1:1 – 1:1000) generated using the LightCycler®480 software (Version 1.5; Roche Diagnostics, Roche, Switzerland).

### **2.39. Identification of a suitable housekeeping gene for assay normalisation**

The Excel (Microsoft, US) add-on software tool BestKeeper (Pfaffl *et al.*, 2004) was used to identify the most suitable housekeeping gene for sample analysis. Housekeeping genes with a SD <1 were deemed stable and YWHAZ housekeeping gene (protein 14-3-3ζ) was considered to be the most suitable reference gene for normalisation of target gene expression.

**Table 11:** Primers and their details used for pHGK and H400 cell semi-quantitative RT-PCR analysis developed using the method described in Section 2.30

<b>Gene</b>	<b>GenBank Accession Number</b>	<b>Primer sequence (5' → 3')</b>	<b>Product Length (Base Pairs)</b>	<b>Primer Melting Temperature (T<sub>m</sub>) (°C)</b>	<b>Cycle Number</b>	<b>Supplier</b>
Cytokeratin 1	NM_0061521.2	F - TGG CAA GAC CGA GGT CGA TT R - TGT GGG TGG TGG TCA CTG CT	202	60	30	Thermohybaidd
Cytokeratin 5	NM_000424.2	F - CCA AGC CAA TTG CAG AAC CA R - AAA TTT GGG ATT GGG GTG GG	407	60	30	Thermohybaidd
Cytokeratin 6	NM_005554 (KRT6A)	F - GTC CTC AGG CCC CTC TCT GG R - CCC CTG GCA ATT TTC TGC AA	317	60	30	Thermohybaidd
Cytokeratin 16	AF061812.1	F - CTT GGC ACC ATG ACC ACC TG R - CAC CGA AGC CAG CAC CAA G	294	60	30	Thermohybaidd
Cytokeratin 19	NM_002276.3	F - CCT ACA GCT ATC GCC AGT CG R - ATG GTT AGC TTC TCG TTG CC	243	60	33	Thermohybaidd
E-cadherin	NM_004360	F - CAA GTG CCT GCT TTT GAT GA R - GCT TGA ACT GCC GAA AAA TC	339	60	30	Invitrogen
Vimentin	NM_00380.2	F - AGT TTT TCA GGA GCG CAA GA R - TTG GTT GGA TAC TTG CTG GA	194	60	30	Thermohybaidd
Involucrin	NM_005547	F - GAA CAG CAG GAA AAG CAC CT R - TAG CGG ACC CGA AAT AAG TG	332	60	30	Invitrogen

**Table 12:** Primers used to quantify gene expression in H400 cultures and pHGFs using Real Time PCR developed using the method described in Section 2.32

Type of Gene	Primer Name	Ascension Number	Primer Sequence (5' → 3')	Product Length (Base Pairs)	Supplier
Housekeeping	GAPDH	NM_002046	F - CTCCTGTTTCGACAGTCAG R - GCCCAATACGACCAAATC	111	Thermohybid
	B2M	NM_004048	F - ACCCCCACTGAAAAAGATGA R - ATCTTCAAACCTCCATGATG	114	Thermohybid
	YWHAZ	NM_004048	F - ACTTTTGGTACATTGTGGCTTCAA R - CCGCCAGGACAAACCAGTAT	94	Thermohybid
	ACT B	NM_001101	F - CATCGAGCACGGCATCGTCA R - TAGCACAGCCTGGATAGCAAC	211	Thermohybid
Target Gene	Vimentin	NM_003380	F - GGACCAGCTAACCAACGACA R - TCCTCCTGCAATTTCTCCCG	93	Thermohybid
	Collagen VII	NM_000094.3	F - GGGTGAACGGGGAGTGAAG R - GGGACCAGCTTCTCCCTTG	70	Thermohybid
	FSP-1 (S100A)	NM_019554.2	F - TCTTGTTTGGTGCTTCTGAG R - CAGCAGTCAGGATCAACACG	72	Thermohybid
	E cadherin	Z13009	F - GTCTCCTCTTGGCTCTGCC R - CACCGTGAACGTGTAGCTCT	75	Thermohybid
	CK1	NM_006121.3	F - TGGACCTTCAGGCCAAACTT R - TGCATCTGAGACAACTCTGCTT	85	Thermohybid
	CK10	NM_000421.3	F - TCCCAACTGGCCTTGAACA R - TGAGAGCTGCACACAGTAGC	75	Thermohybid
	CK4	NM_002272.3	F - GGGCGAGGAGTACAGAATGT R - CCTAATCCTCCGCTGATGCC	99	Thermohybid
	CK13	NM_002274.3	F - GGACGCCAAGAAGCGTCAG R - GGCGACCAGAGGCATTAGAG	90	Thermohybid

Ki-67	NM_001145966.1	F – CTGACCCTGATGAGAGTGAGGG R - ATAGTTCAGGTCTTAGGTGCC	78	Thermohybrid
N - cadherin	NM_001308176.1	F – GGC GTTATGTGTGTATCTTCACTG R CAGTTGCTAAACTTCACTGAAAGGA	82	Thermohybrid
Integrin subunit alpha 6	NM_001316306.1	F - TTGCCAGCAAGGTGTAGCA R- GGTCAAAAACAGCAGGCCTTT	100	Thermohybrid

#### **2.40. Image analysis of surface attachment**

Using the Trainable Weka Segmentation plug-in (Arganda-Carreras *et al.*, 2017) method as outlined in Section 2.28, and the histological images obtained from Section 2.24, the epithelium was segmented from the dermis and the background. Pixel regions of 8 x 8 were used as this was deemed appropriate to distinguish the epithelium and the dermis. Following segmentation, objects that were less than 30 pixels were removed using 'The Analyse Particles plug-in', as they were considered to be noise. The segmented epithelium was then measured using the straight-line function, which had been previously calibrated using a scale bar at the same magnification which the H&E stained images were taken. Three measurements from three different 3D oral organotypic models were taken for each day at the ALI, were used to calculate the average epithelium thickness.

#### **2.41. Data and statistical analysis**

Microsoft Excel (Version 1712; Microsoft, Washington, USA) was used for basic data analysis, including the calculation of the average and standard deviation. Following this, statistical analysis of data was conducted using the SPSS statistical package (Version 24; IBM SPSS Statistics, New York, USA). Depending on the nature of the data, determined through the conduction of a Shapiro-Wilk normality test,

specific statistical tests were conducted to identify significances within data sets.

For parametric data sets either a Students t-test, a one-way or a two-way analysis of variance (ANOVA) were conducted. Where ANOVA analysis determined statistical significance ( $p < 0.05$ ), a *post hoc* Tukey test was conducted. For non-parametric data sets, either a Mann Whitney U or Kruskal Wallis-H test were conducted. Where either test found significance ( $p < 0.05$ ) a Student Newman-Keuls *post hoc* test was conducted to identify which groups were significantly different.

Biological replicates were performed in triplicate and are expressed as N numbers per dataset.

# **CHAPTER 3:**

# **RESULTS**

# Results Section 1

Due to the animal-component-free nature of this research, the results presented in this chapter are obtained from experiments designed to identify a suitable animal-component-free media to enable development of 3D oral organotypic cultures. The three commercially available animal-component-free media namely CnT-Pr, Epilife supplemented with S7 and KGM-CD were selected based on the frequency of use reported within previous literature. Additionally, human serum supplementation was used as the control culture environment.

To study the effects of long-term culture of the cells grown within the three-selected media, an array of techniques were employed, including proliferation, viability curves and gene expression assays. Furthermore, to provide an insight into the differences between the commercially available media, due to reluctance of manufacturers to release the composition of their products, the calcium concentration was analysed.

## **3.1. Influence of serum supplementation on H400 keratinocyte cultures**

Within cell culture, FBS is routinely used to provide supplementation to the culture environment, however due to the animal-component-free nature of this research, a suitable alternative supplement was required. Previous research identified that there was no significant differences in proliferation and viability of cells that had been cultured in FBS or human serum (Issac *et al.*, 2011), therefore it was decided to use human serum as the

comparative culture environment. However before comparing the animal-component-free media to human serum supplementation, understanding the influence of varying serum supplementation on cell cultures was essential to enable the identification of the most suitable percentage of serum to supplement with.

Figure 13 shows that lowering the concentration of human serum had a profound effect on cell number. A Kruskal- Wallis H test was executed, due to the non-parametric nature of the data which revealed that from day 9, cultures grown in either 5% or 2% had a significantly lower number of viable cells than cultures grown in 10% human serum ( $p < 0.05$ ;  $n = 3$ ).

Additionally, population doubling times, which are presented in Table 133 further supported the growth curve data obtained.

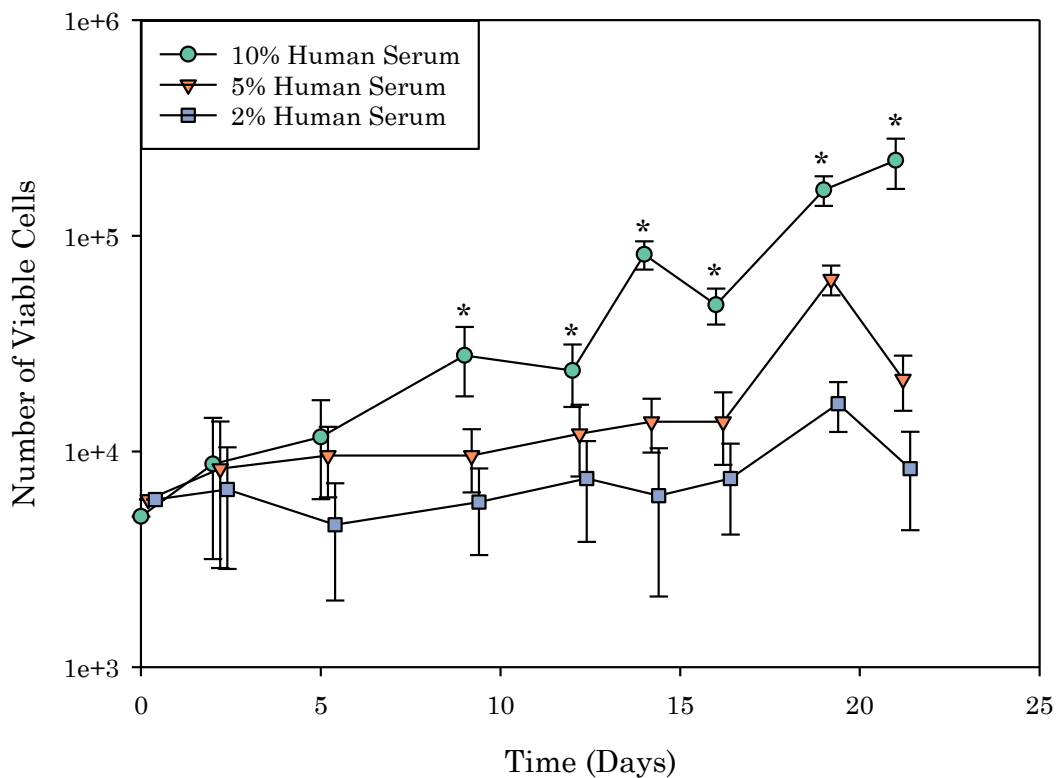


**Figure 13:** H400 keratinocyte growth curves in DMEM supplemented with different concentrations of human serum (2, 5 or 10%) for 21 days. A Kruskal-

Wallis H test identified that H400 keratinocytes grown in 10% human serum generated statistically significantly higher cell numbers compared with H400s grown in 2% human serum from day 7 ( $p < 0.05$ ) and 5% human serum from day 9 ( $p < 0.05$ ) (denoted by \*). No significant difference in cell number was identified between 5% and 2% human serum supplements. Error bars represent one standard deviation from the mean and each group has been jittered 0.2 days along the x-axis for clarity ( $n=3$ ).

**Table 13:** Population doubling times calculated from days 9 to 19 from Figure 13.

<b>Human serum concentration</b>	<b>Average population time <math>\pm</math> standard deviation (Days)</b>	<b>Significance when compared to 10% human serum supplementation</b>
2%	7.41 $\pm$ 0.4	$p < 0.001$
5%	2.14 $\pm$ 0.3	$p < 0.001$
10%	1.84 $\pm$ 0.3	-

Varying the concentration of human serum supplementation had no detectable effect on cell viability; presented in Figure 14. A Kruskal-Wallis H test was performed which revealed that there was no significant differences between any of the groups as  $p > 0.05$  ( $n=3$ ), further supporting the observed results presented in Figure 14.

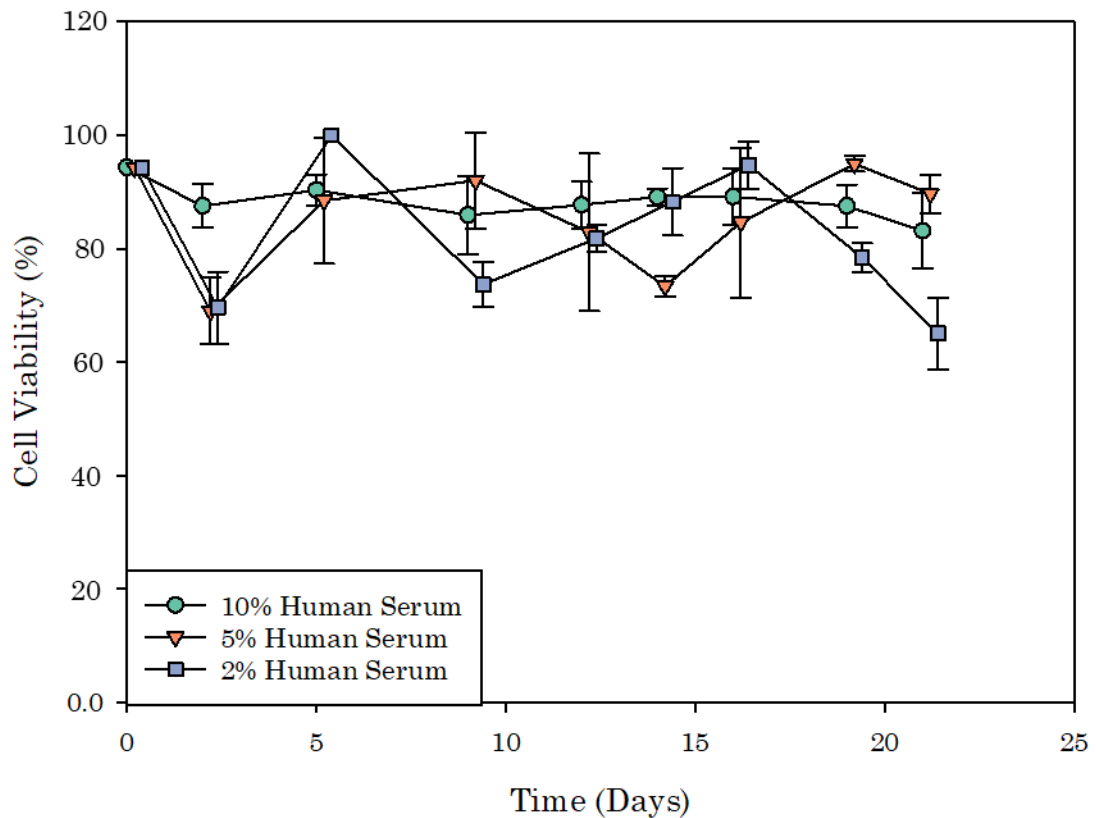


**Figure 14:** Viability of H400 keratinocytes in DMEM supplemented with different concentrations of human serum (2, 5 or 10%) for 21 days. A Kruskal-Wallis H test revealed that there were no significant difference between the different levels of human serum supplementation in terms of cell viability ( $p=0.939$ ). Error bars represent one standard deviation from the mean and each group has been jittered 0.2 days along the x-axis for clarity ( $n=3$ ).

Data presented in Figures 13 and 14 and Table 13 showed that human serum supplementation had a direct effect on cell number during the experimental period as Figure 13 and Table 13 suggested that reducing human serum supplementation acted a limiting factor, hindering increases in cell number. Therefore, to be able to compare the effect of the animal component-free culture media in subsequent cell culture experiments, 10% human serum supplementation was selected and was used as a control.

### **3.2. Identification of a suitable mitomycin C concentration for use in pHGF cultures**

Previous research has shown that feeder layers (commonly consisting of non-proliferating fibroblasts) are typically required to grow primary keratinocyte cultures *in vitro*, due to providing and releasing the necessary extracellular signals and growth factors that keratinocyte cultures require to proliferate. (Blacker, Williams and Goldyne, 1987; Llames *et al.*, 2015).

To convert actively growing populations of fibroblasts into a non-proliferating feeder layer, confluent cultures are treated with mitomycin C, which prevents proliferation by inhibiting DNA synthesis. However, exposure to mitomycin C needs to be controlled as it can induce cell death, therefore, testing the suitable concentrations presented in previous research to ensure efficacy of inhibition of proliferation was performed (Rheinwald and Green, 1975; Lu *et al.*, 2012; Llames *et al.*, 2015).

Using cell number as an indication of inhibition of proliferation, it can be seen in Figure 15, that mitomycin C had an inhibitory effect on all experimental group cell numbers, when compared with the control. A Kruskal-Wallis H test followed by *post-hoc* Student-Newman-Keuls test was performed (due to the non-parametric nature of the data) and it was found that there were no significant differences between any of the experimental groups ( $p=0.895$ ;  $n=3$ ). Furthermore, it was found that from Day 3, all cultures treated with mitomycin C, regardless of concentration, had a statistically lower number of viable cells when compared with the control populations ( $p<0.05$ ).

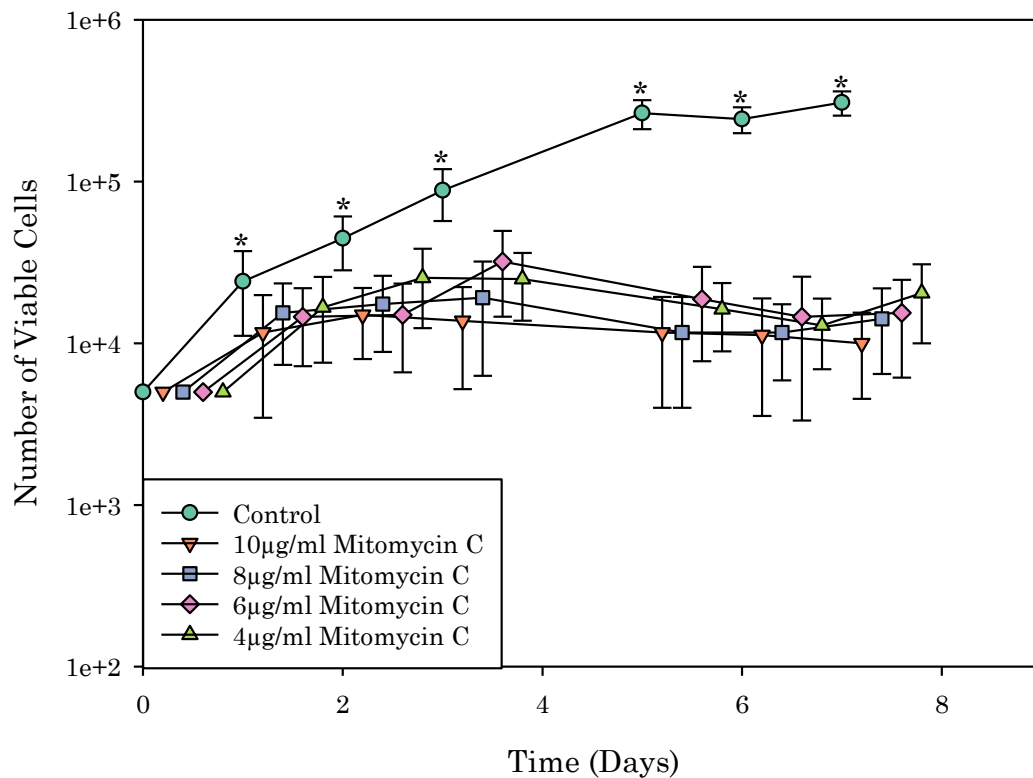


**Figure 15:** The effect of varying concentrations of mitomycin C on pHGF cultures over 7 days. Statistical analysis revealed that there was no significant differences between the experimental cultures when compared to the control ( $p > 0.05$ ). The control yielded statistically higher cell numbers than pHGF cultures exposed to mitomocycin C ( $p < 0.05$ , denoted by \*). Error bars represent one standard deviation from the mean and each group has been jittered 0.2 days along the x-axis for clarity ( $n=3$ ).

Viability of the cultures presented in Figure 16, was also monitored during the experimental period and it was found that there were no significant differences ( $p > 0.05$ ;  $n=3$ ) between any of the cultures as determined by a Kruskal-Wallis H test which was conducted due to the non-parametric nature of the data.

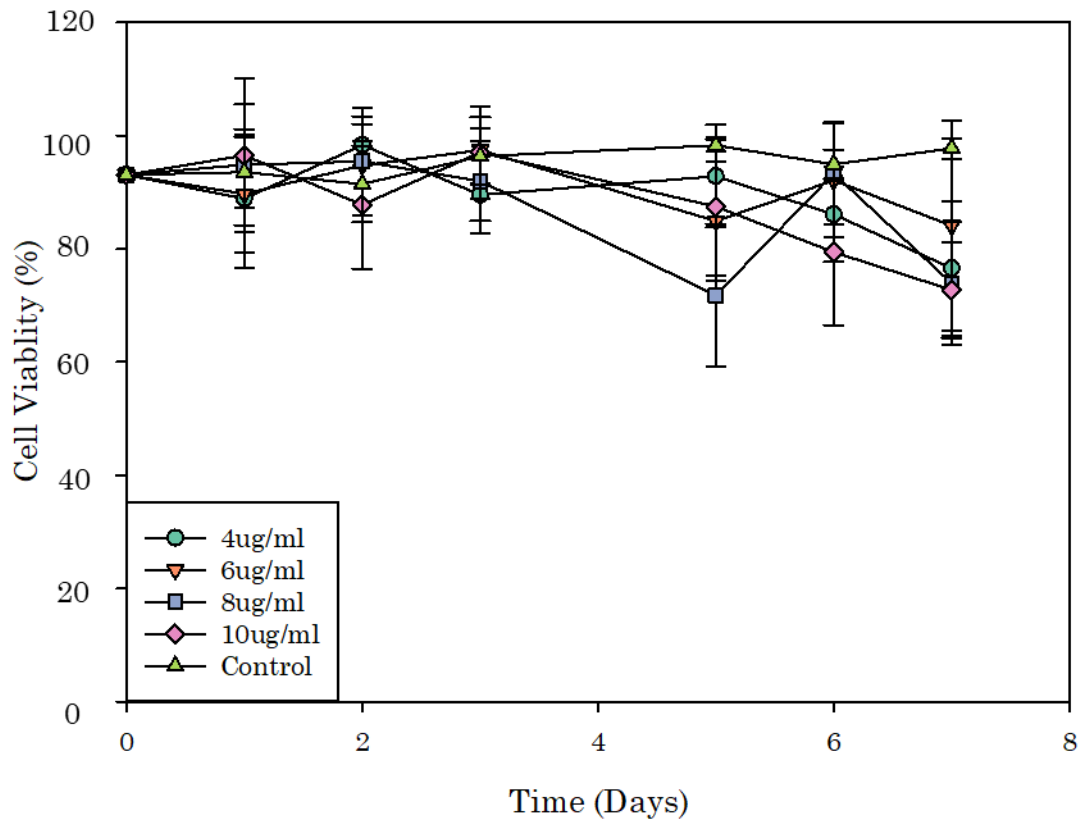


**Figure 16:** Viability of pHGF cultures after exposure to different concentrations of mitomycin C. No significant differences were identified in the percentage of viable cells between the different cultures and controls using the Kruskal- Wallis H Test. Error bars represent one standard deviation from the mean and each group has been jittered 0.2 days along the x-axis for clarity (n=3).

Results presented in Figures 15 and 16 coupled with statistical analysis indicated that 4 $\mu$ g/ml of mitomycin c was a suitable concentration to use to generate fibroblast feeder layers.

### **3.3. Influence of commercially available animal-component-free culture media on H400 keratinocyte cultures**

The selected animal-component-free culture media were tested for their ability to support proliferating culture of H400 keratinocytes and the ability to retain viability of the cultures under long-term culture conditions. Whilst

human serum supplementation could be used, commercially available animal-component-free culture media is more beneficial due to the highly defined composition, despite not being available within the public domain. In comparison to this, human serum is still not fully characterized, and has a degree of variability of known factors which vary per source. Using media that have defined compositions is extremely beneficial as it allows for a consistent culture environment, enabling the development of more standardized 3D oral organotypic cultures.

Data presented in Figure 17 shows that despite the identical cell number upon initial seeding, cultures grown in KGM-CD had higher cell numbers from day 2 when compared to the other animal-component-free media. A Kruskal-Wallis H test followed by a Student-Newman-Keuls *post-hoc* test (conducted due to the non-parametric nature of the data) revealed that the difference in cell number was significantly higher from day 7 ( $p < 0.05$ ;  $n = 3$ ). When comparing the cell numbers of cultures grown in KGM-CD and DMEM supplemented with 10% human serum, although apparent visible differences in cell number (Figure 5), the differences in cell number was not deemed significant (Kruskal-Wallis H test;  $p < 0.05$ ;  $n = 3$ ). Comparing cultures grown in CnT-PR and Epilife supplemented with S7 to DMEM supplemented with 10% human serum, statistical analysis (Kruskal-Wallis H test followed by a Student-Newman-Keuls *post-hoc* test) determined that cultures grown in DMEM supplemented with 10% human serum had statistically higher cell numbers ( $p < 0.05$ ;  $n = 3$ ) from day 7.

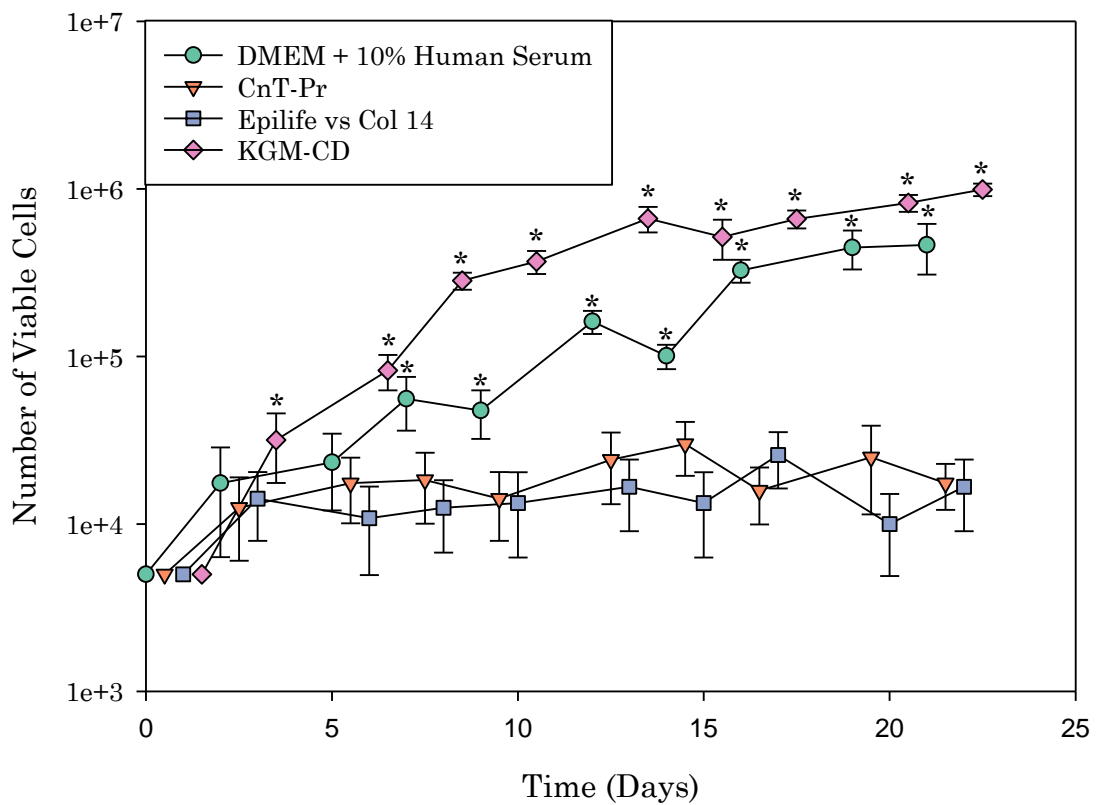


**Figure 17:** Growth curves of H400 keratinocyte cultures in three animal-component-free culture media for an experimental period of 21 days. From day 7, cell counts of cultures of H400 keratinocytes grown in both KGM-CD and DMEM supplemented with 10% human serum had statistically higher cell numbers compared to cultures of H400 keratinocytes cultured in Epilife supplemented with S7 and CnT-PR ( $p < 0.05$ , denoted by \*). Error bars represent one standard deviation from the mean and each group has been jittered 0.5 days along the x-axis for clarity ( $n=3$ ).

Average population doubling times presented in Figure 18 were calculated using the data obtained between days 7 and 14 from Figure 17. It was found that KGM-CD had the shortest population doubling time followed by DMEM supplemented with 10% human serum. CnT-Pr and Epilife had the longest population doubling times at 6.26 and 14.95 days respectively. However, statistical analysis (Kruskal-Wallis H test), revealed that there was no

significant differences between any of the average population doubling times as  $p > 0.05$ .

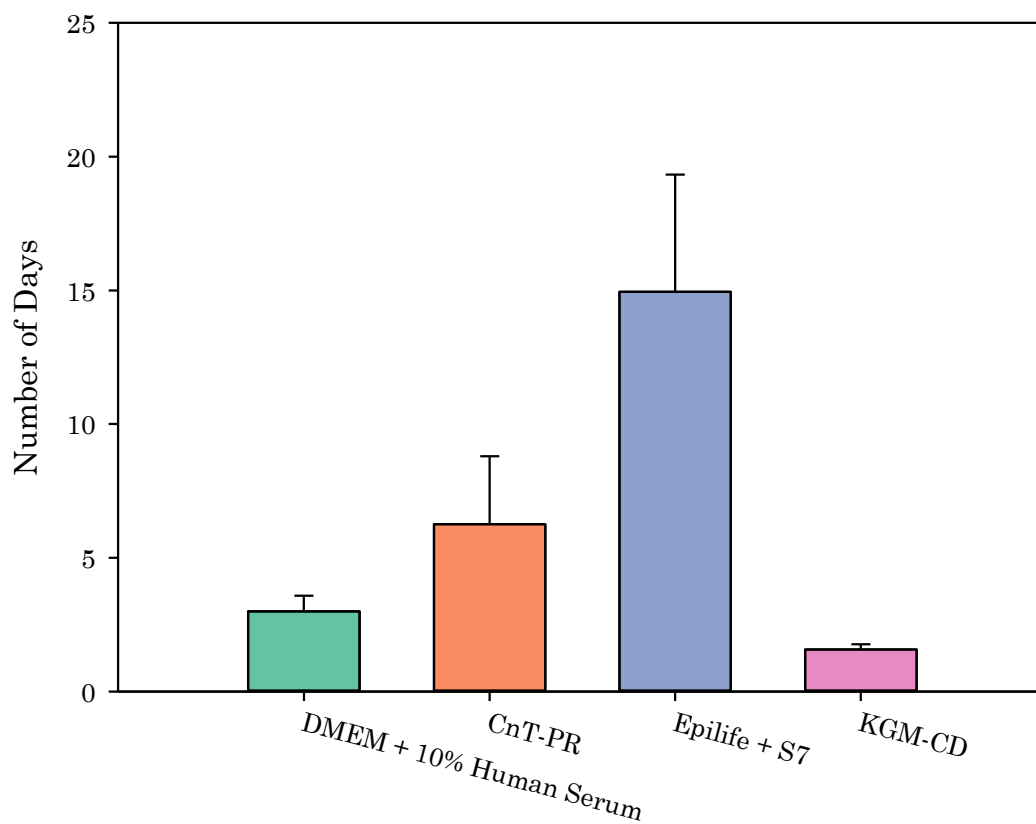


**Figure 18:** Average population doubling times of cultures of H400 keratinocytes grown in different animal-component-free media for 7 days. Although upon observations H400 keratinocyte cultures grown in KGM-CD and DMEM supplemented with 10% human serum appear to have shorter average population times, statistical analysis revealed that the observed differences were not significant as  $p > 0.05$ . Error bars represent one standard deviation from the mean ( $n=3$ ).

In addition to cell number, cell viability was monitored over the experimental period with the data presented in Figure 19. The results obtained spanned extreme viability ranges making it difficult to deduce (using a Kruskal-Wallis H test;  $p > 0.05$ ;  $n=3$ ) any significant differences between groups. However, from Day 15 it can be seen that there is substantial cell death for cultures grown in KGM-CD. The significance of

this result relates to the pattern of growth observed in Figure 17 where from Day 15, the number of viable cells appear to remain constant for the remainder of the experiment, suggesting that confluency had been achieved.

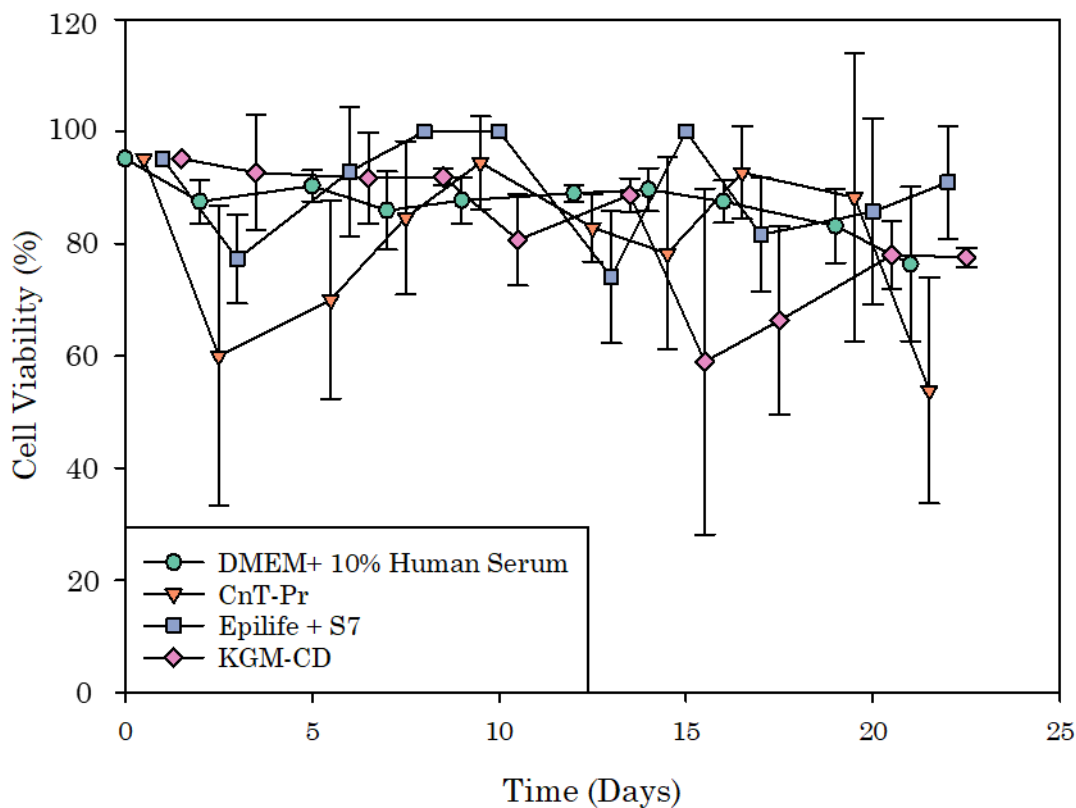


**Figure 19:** Cell viability of H400 keratinocyte cultures grown in three animal-component-free culture media for an experimental period of 21 days. Due to the extreme range of viabilities obtained, no conclusions could be drawn which was further supported by statistical analysis which found no significant difference ( $p>0.05$ ). Error bars represent one standard deviation from the mean and each group has been jittered 0.5 days along the x-axis for clarity ( $n=3$ ).

### 3.4. Influence of commercially available animal-component-free culture media on pHGF cultures

From the data presented above (Section 3.3) it was evident that H400 keratinocyte cultures were able to achieve higher cell numbers when grown in KGM-CD with comparison to the other commercially available animal-component-free media. However, in oral mucosa, other cell types are found

namely fibroblasts, therefore the next stage was to analyse how fibroblasts (pHGF cells) responded to the selected animal-component-free culture media.

Figure 20 shows that pHGF cultures in all the commercially available animal-component-free media did not generate comparable cell numbers at any time-point as was evident in the control cultures; pHGF cultures grown in DMEM supplemented with 10% human serum. Cultures grown in KGM-CD appeared to undergo increased proliferation (observation drawn from increased cell numbers) compared with the other media used although a Kruskal-Wallis H test, a non-parametric statistical test, revealed that the observed differences were not significant ( $p > 0.05$ ;  $n = 3$ ).

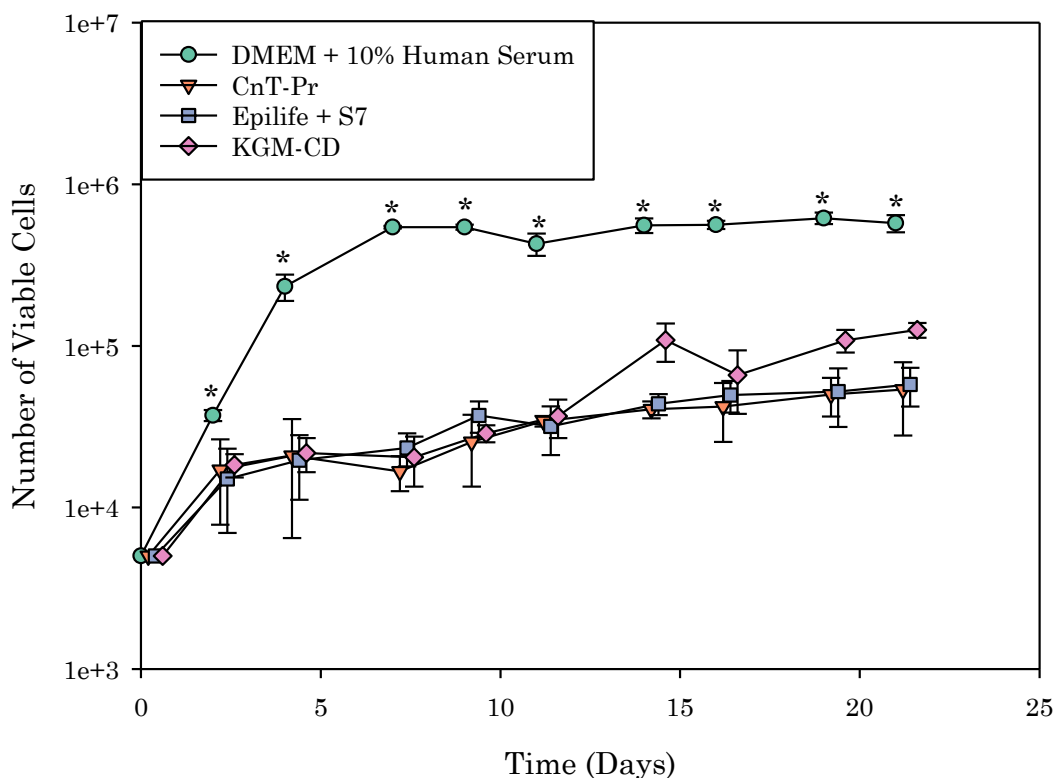


**Figure 20:** Growth curves of pHGF cultures in three animal-component-free culture media for an experimental period of 21 days. From day 2, cell counts of pHGF cultures grown in DMEM supplemented with 10% human serum had statistically higher cell numbers compared to cultures of H400 keratinocytes cultured in CnT-PR, Epilife supplemented with S7 and KGM-CD ( $p < 0.05$ , denoted

by \*). Cultures grown in KGM-CD appear to produce higher cell numbers than cultures grown in CnT-PR and Epilife, however statistical analysis revealed that there was no significance ( $p > 0.05$ ). Error bars represent one standard deviation from the mean and each group has been jittered 0.5 days along the x-axis for clarity ( $n=3$ ).

Average population doubling times (presented in Figure 21) were calculated using data obtained between days 7 and 14 of Figure 20. DMEM supplemented with 10% human serum had the shortest average population doubling time followed by cultures grown in KGM-CD. Due to the non-parametric nature of this data, a Kruskal-Wallis H test followed by a Student-Newman-Keuls *post-hoc* test was conducted to identify any significance between the differences. It was found that pHGF cultures grown in DMEM supplemented with 10% human serum had significantly shorter average population doubling times compared with cultures grown in CnT-PR ( $p < 0.001$ ;  $n=3$ ), Epilife supplemented with S7 ( $p < 0.001$ ;  $n=3$ ) and KGM-CD ( $p=0.009$ ;  $n=3$ ). Additionally, pHGF cultures grown in KGM-CD had significantly shorter average population doubling times than cultures grown in both Epilife supplemented with S7 ( $p=0.002$ ;  $n=3$ ) and CnT-PT ( $p < 0.001$ ;  $n=3$ ).

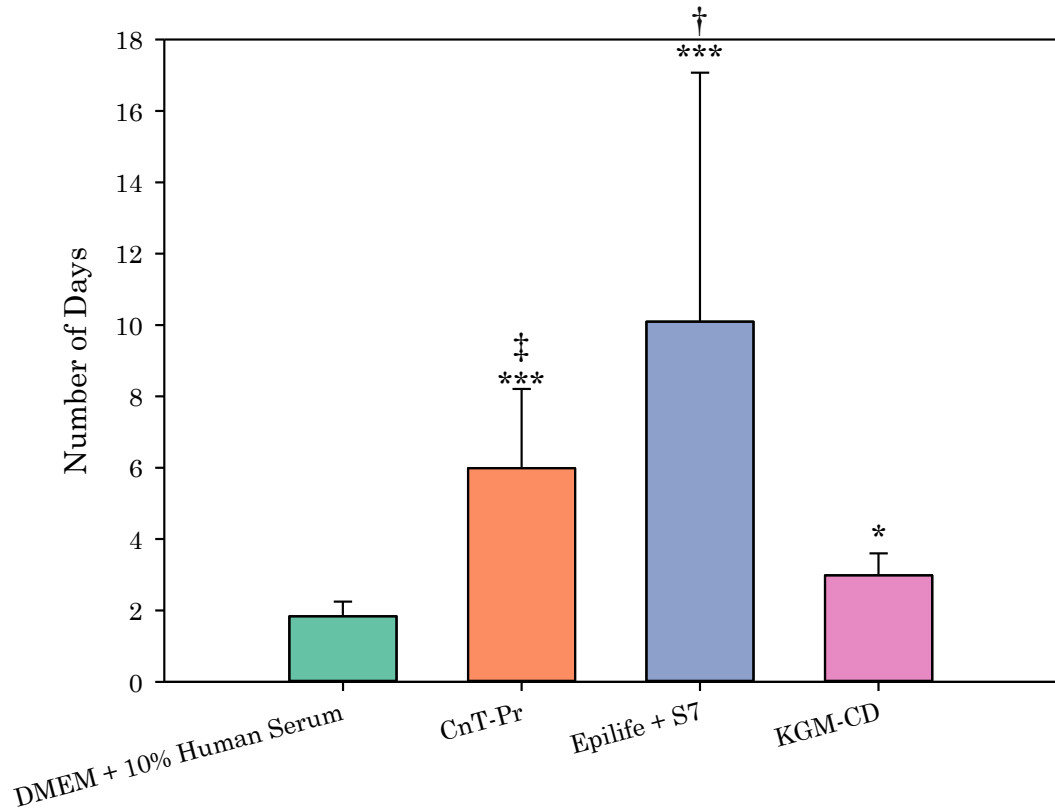


**Figure 21:** Average population doubling times of pHGF cultures grown in different animal-component-free media for 7 days. Cultures grown in DMEM supplemented with 10% human serum had significantly shorter average population doubling times than cultures grown in CnT-PR ( $p < 0.001$ , denoted by \*\*\*), Epilife supplemented with S7 ( $p < 0.001$ , denoted by \*\*\*) and KGM-CD ( $p = 0.009$ , denoted by \*). Cultures grown in KGM-CD had significantly shorter average population doubling times than cultures grown in both Epilife supplemented with S7 ( $p = 0.002$ , denoted by †) and CnT-PT ( $p < 0.001$ , denoted by ‡). Error bars represent one standard deviation from the mean ( $n = 3$ ).

Viability of cultures (see data presented in Figure 22) were also analysed but revealed no significant differences between the different culture media used.

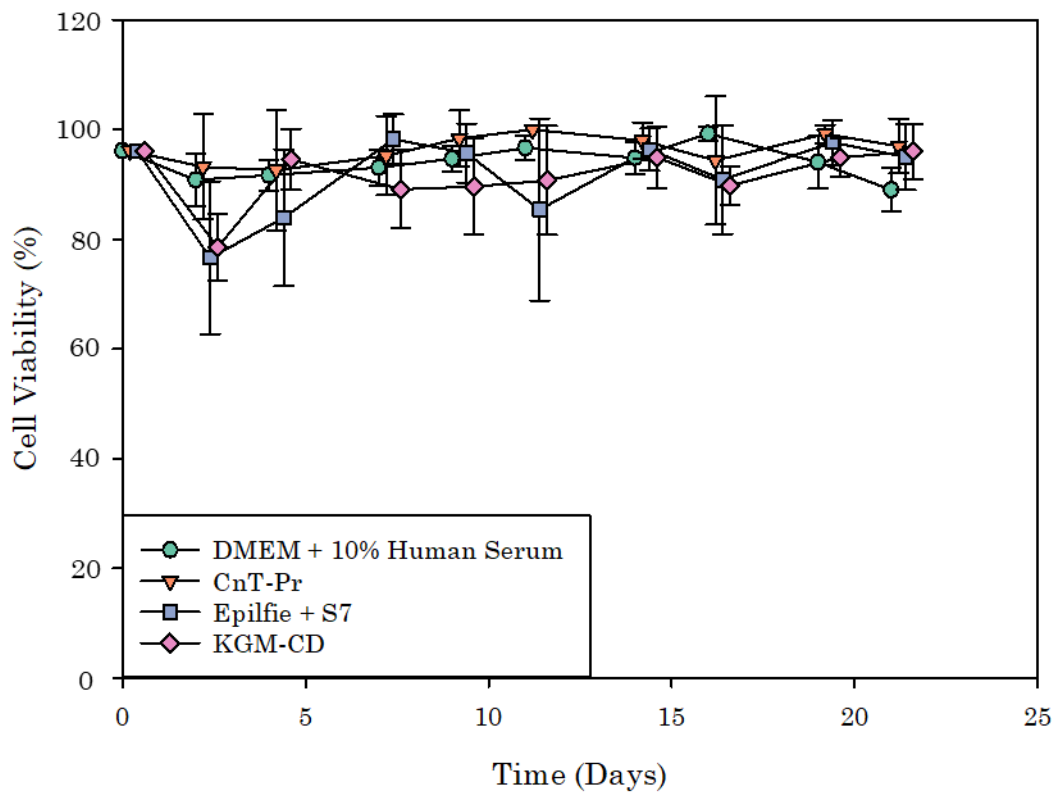


**Figure 22:** Viability of pHGF cultures grown in three animal-component-free culture media for an experimental period of 21 days. Due to the extreme range of culture viabilities obtained, no conclusions could be drawn which was further supported by statistical analysis which found no significant difference ( $p > 0.05$ ). Error bars represent one standard deviation from the mean and each group has been jittered 0.5 days along the x-axis for clarity ( $n=3$ ).

Although the data presented did not yield any significant differences between the selected animal-component-free media and showed inhibition of pHGF culture proliferation, it should be noted that the media selected have been specifically formulated and optimised to support keratinocyte cultures. The use of keratinocyte media was decided upon, due to fibroblast cultures having a shorter population doubling time than keratinocyte cultures and over dominating when grown as a co-culture in a non-specific environment,

enabling the development of a biologically relevant 3D oral organotypic model.

### **3.5. Influence of commercially available animal-component-free culture media on pHGK cultures**

Although immortalized keratinocytes are commonly used to generate 3D models, due to the low yield in primary keratinocytes from biopsies and short survival rates – keratinocytes differentiate after 4 passages, immortalised keratinocytes have been genetically altered which results in behaviour not typical of keratinocytes found *in vivo* (Sigurdson *et al.*, 2002; Dongari-Bagtzoglou and Kashleva, 2006).

Upon successful isolation and cultivation of pHGK cells these were cultured in selected animal-component-free media; KGM-CD due to the ability to maintain large numbers of viable cultures of both H400 keratinocytes and pHGF cells, as shown in data presented in the previous sections, Epilife supplemented with S7 selected due to being commonly used in previous research and DMEM supplemented with 10% human serum was used as a control (Song *et al.*, 2004; Lekhanont *et al.*, 2009). For cell experiments using pHGK cells, cell growth and viability were observed for a relatively short cultivation period (16 days) due to the short survival time of pHGK cells when cultured *in vitro*.

Figure 23 shows that all pHGK cultures appeared to proliferate at a similar level and statistical analysis (Kruskal-Wallis H test; due to non-parametric nature of the data) revealed that there were no significant differences between groups. Although no individual culture medium could be selected

on the basis of this data, it showed that pHGK cells were able to grow in all three animal-component-free media (Lamb and Ambler, 2013).

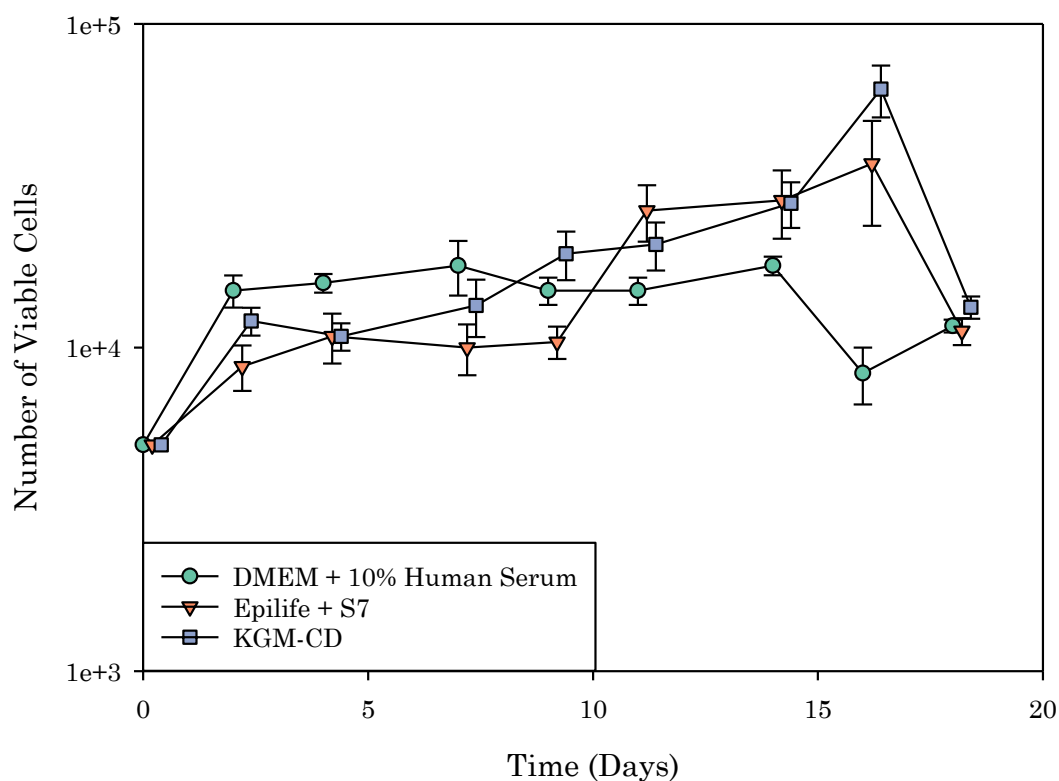


**Figure 23:** Growth curves of pHGK cultures in three animal-component-free culture media for an experimental period of 21 days. Although no significant difference between cell numbers in the different cultures was identified ( $p>0.05$ ), the graph highlights that all cultures were able to proliferate in all environments. Error bars represent one standard deviation from the mean and each group has been jittered 0.2 days along the x-axis ( $n=3$ ).

Average population doubling times (presented in Figure 24) were calculated using data obtained between days 7 and 14 as presented in Figure 23. The graph shows that pHGK cultures grown in DMEM supplemented with 10% human serum, took longer to proliferate, however when statistically analysing this result using a one-way ANOVA, this observation was not deemed significant.

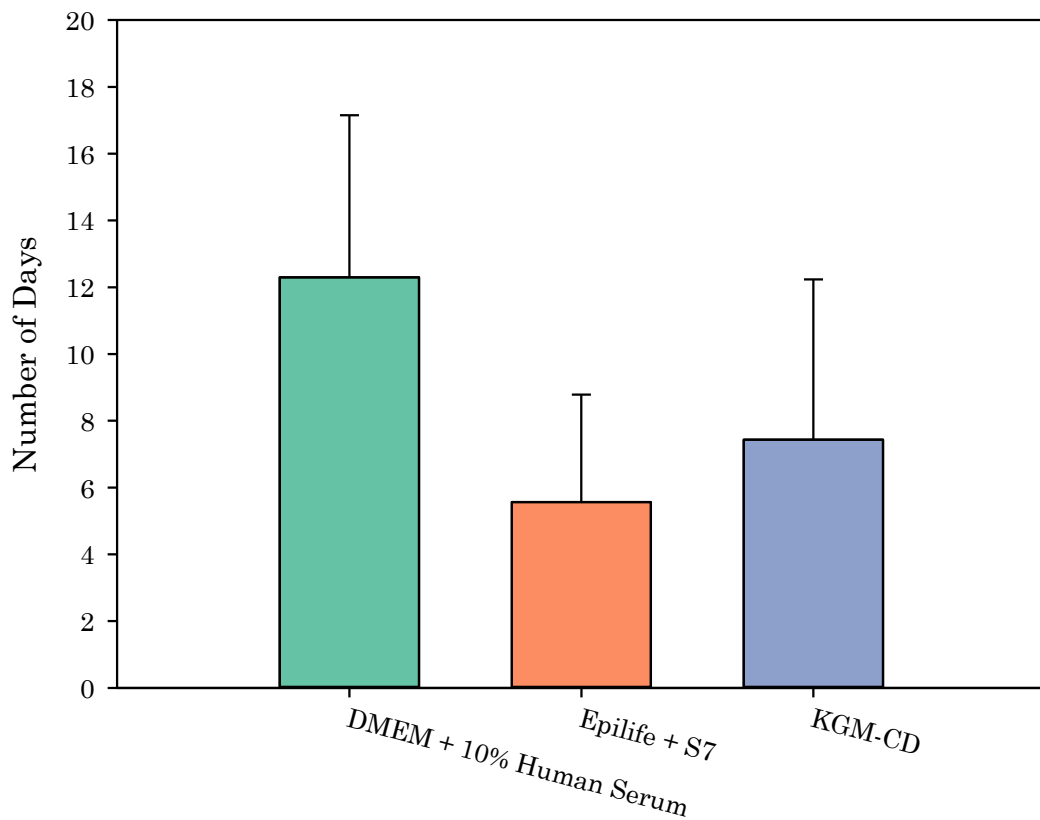


**Figure 24:** pHGK average population doubling times calculated for cultures in different animal-component-free medium for 7 days. Although upon observations pHGK cultures grown in DMEM supplemented with 10% human serum appear to have increased average population times, statistical analysis revealed that the observed differences were not significant as  $p > 0.05$ . Error bars represent one standard deviation from the mean ( $n=3$ ).

Viability of cultures (presented in Figure 25) were also analysed but revealed no significant differences between the different culture media.

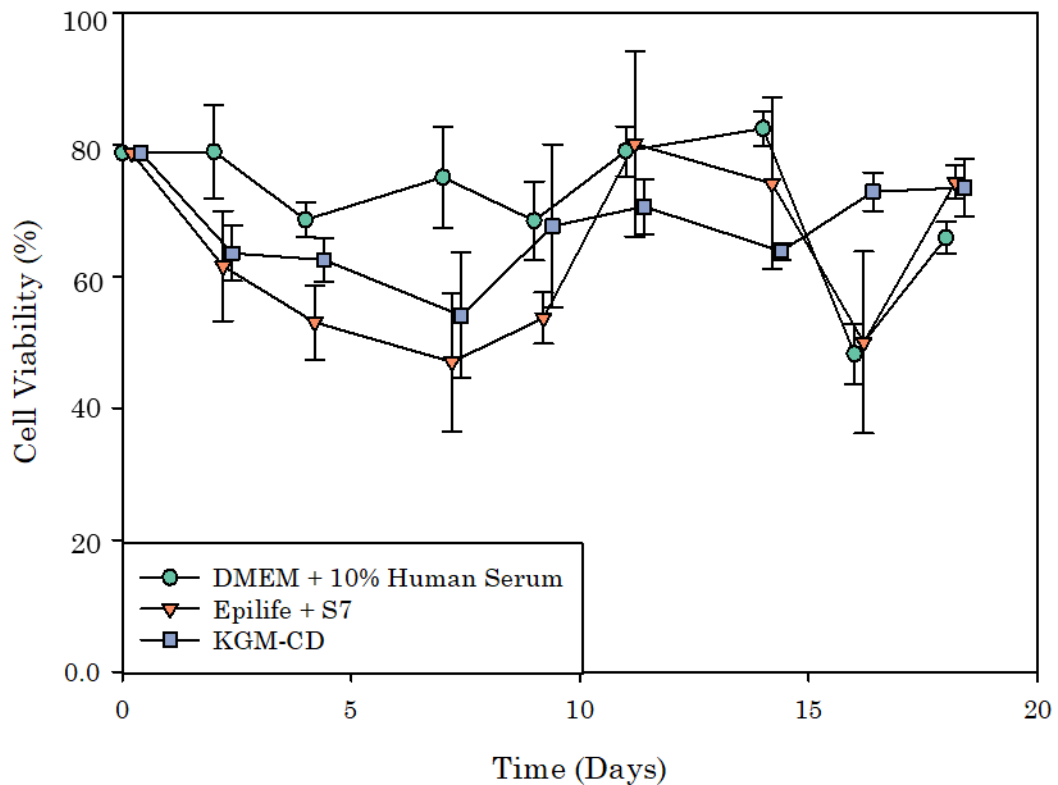


**Figure 25:** Viability of pHGK cultures grown in three animal-component-free culture media for an experimental period of 19 days. Due to the extreme range of culture viabilities obtained, no conclusions could be drawn which was further supported by statistical analysis which found no significant difference ( $p > 0.05$ ). Error bars represent one standard deviation from the mean and each group has been jittered 0.2 days along the x-axis for clarity ( $n=3$ ).

Due to difficulties experienced when utilising pHGK cultures, including extremely low yield, short culture life span and slow initial proliferation, it was decided that H400 keratinocyte cultures would be used when developing 3D oral organotypic models.

### 3.6. Generation of an Alamar Blue calibration curve

To confirm data generated by Trypan Blue assays shown in Figures 17 and 20, an Alamar Blue assay was undertaken which enabled the same cultures to be used throughout the growth period for monitoring cell number.

Calibration curves were generated to enable spectrophotometric output from the Alamar Blue assay to be related to cell number. The equations of the line and  $R^2$  values are presented in Table 14.

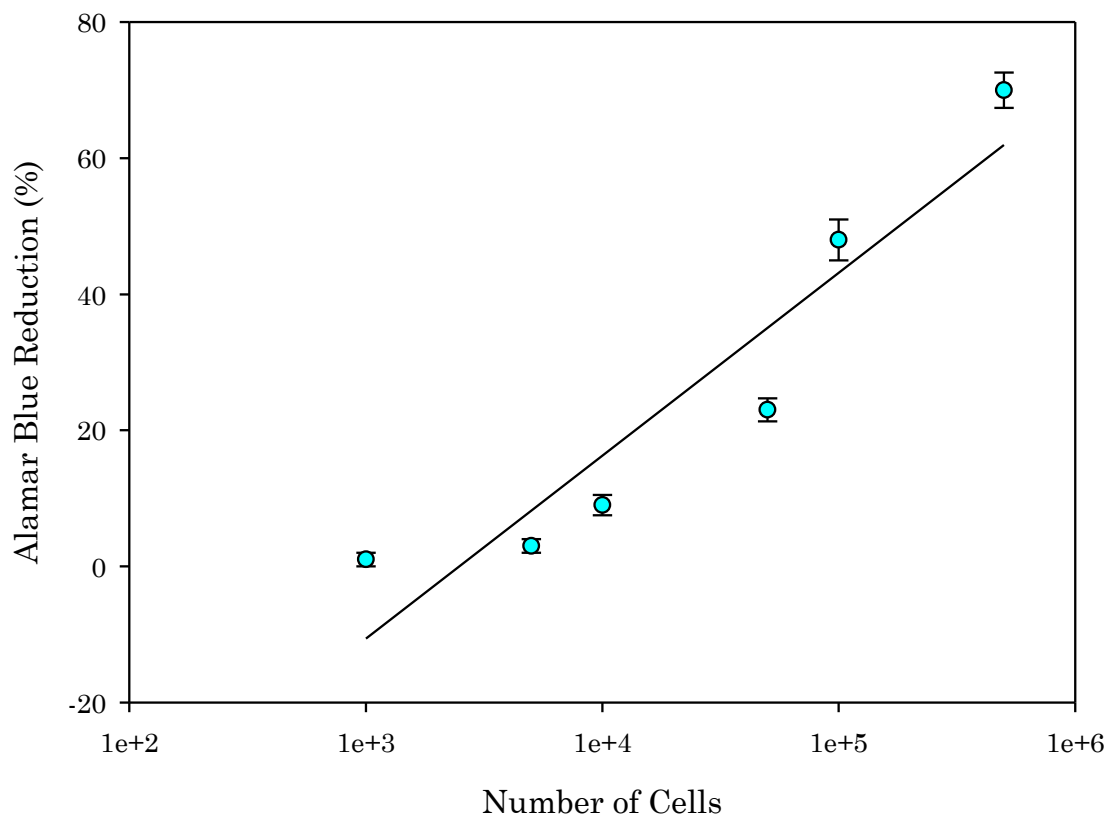


**Figure 26:** Alamar Blue calibration curve for H400 keratinocytes seeded at known concentrations. The line of best fit was calculated using linear regression and the equation of the line was used in future experiments to relate Alamar Blue reduction (%) to cell number. The equation of the Error bars represent one standard deviation from the mean (n=3).

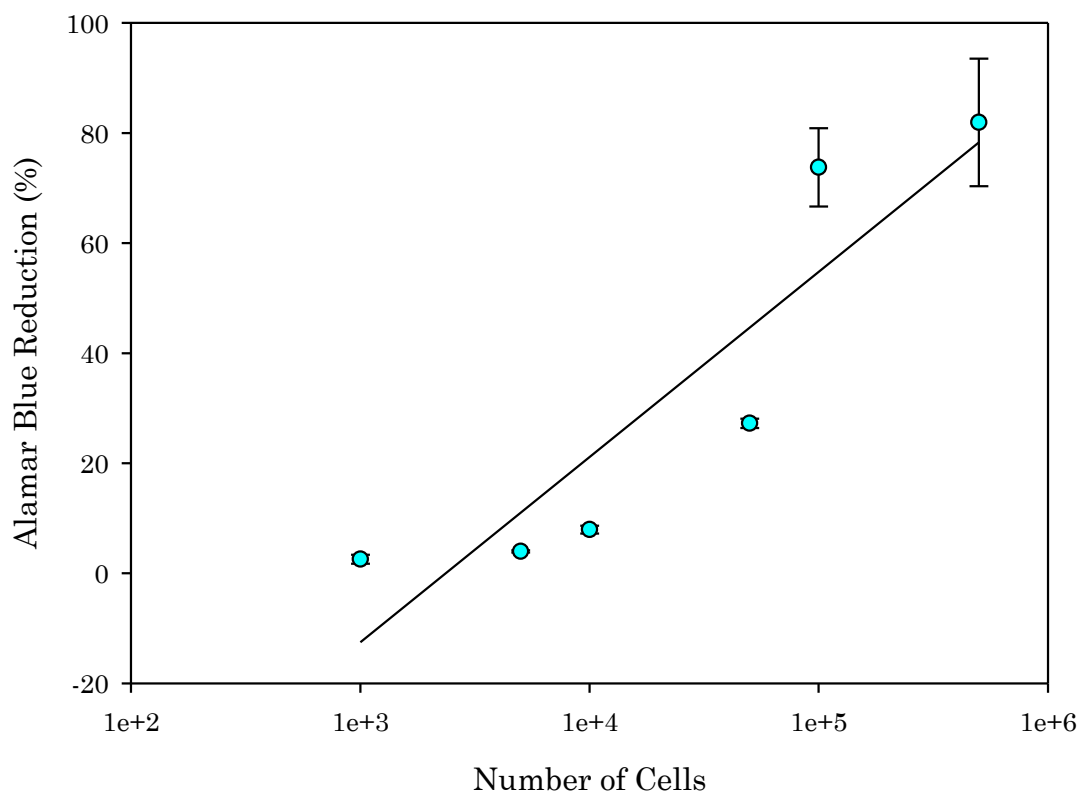


**Figure 27:** Alamar Blue calibration curve for pHGF cultures seeded at known concentrations. The line of best fit was calculated using linear regression and the equation of the line was used in future experiments to relate Alamar Blue reduction (%) to cell number. Error bars represent one standard deviation from the mean (n=3).

**Table 14:** Equations of the lines of best fit calculated from Figures 26 and 27.

Cell Type	Equation of line	R <sup>2</sup>
H400 Keratinocytes	$y = (1.25 \times 10^{-5})x + 0.116$	0.991
pHGF	$y = (1.48 \times 10^{-6})x + 0.162$	0.826

### 3.7. Alamar Blue growth curves in DMEM supplemented with Human Serum and KGM-CD

Using the equations in Table 14, Alamar Blue growth curves were generated with the y-axis converted from percent reduction of Alamar Blue to number

of cells. It should be noted that upon conversion from percent reduction of Alamar Blue to number of cells, it was apparent that both cultures did not reach the number of cells previously seen in the Trypan Blue exclusion assay analysis over the same study period (Figures 17 and 20).

Figure 28 presents Alamar Blue data for H400 keratinocytes grown in either DMEM supplemented with either 10% human serum or KGM-CD. Similar to the Trypan Blue assay (Figure 17), H400 keratinocyte cultures grown in KGM-CD proliferated at a quicker rate than cultures grown in DMEM supplemented with 10% human serum as demonstrated by the increase in cell number. However, upon statistical analysis (Student t-test) no significance was found in this observation ( $p > 0.05$ ).

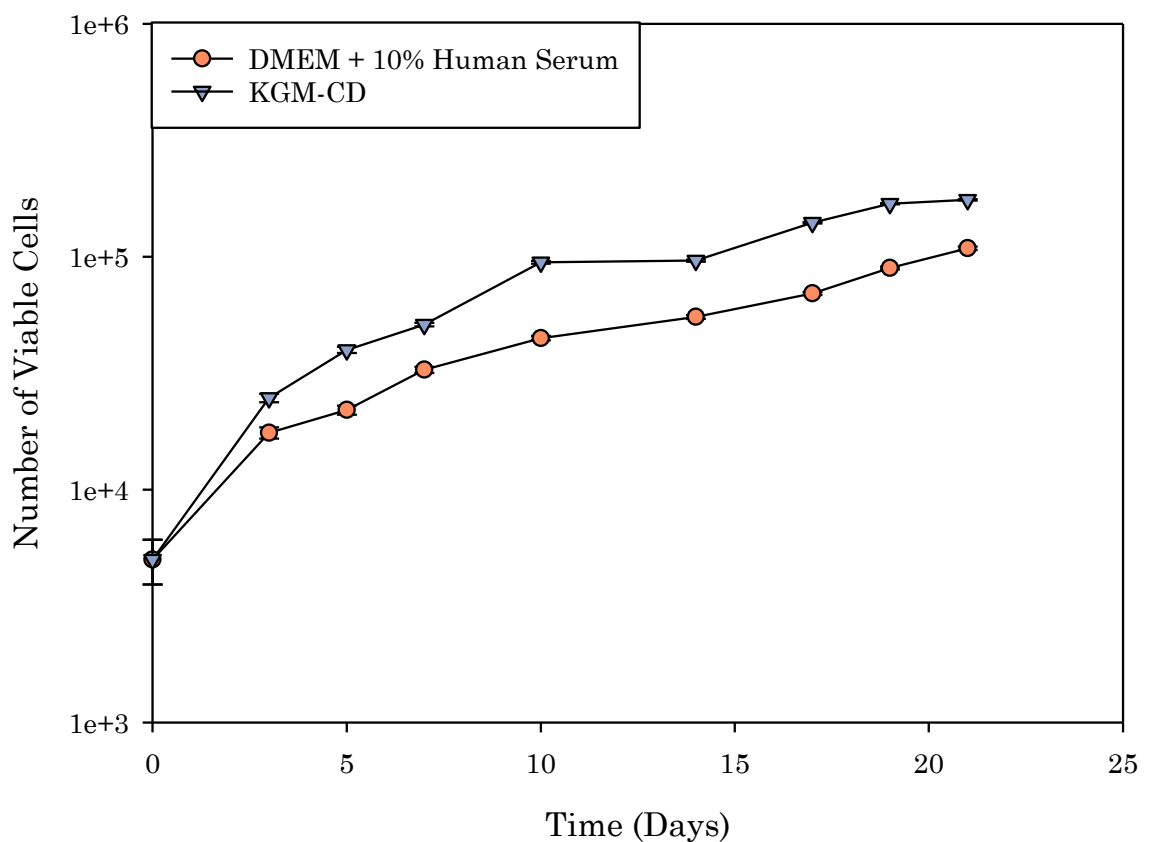


**Figure 28:** Alamar Blue growth curves of H400 keratinocytes grown in either DMEM supplemented with 10% human serum or KGM-CD. No statistical

significance was found at any time point and error bars represent one standard deviation from the mean ( $p > 0.05$ ;  $n = 3$ ).

Alamar Blue growth curves for pHGF cultures are presented in Figure 29. pHGF cultures grown in KGM-CD appear to proliferate at a comparable to cultures grown in DMEM supplemented with 10% human serum. Upon comparison to the equivalent Trypan Blue assay (Figure 20), culturing in KGM-CD does not appear to have an apparent limiting effect on proliferation as seen in Figure 20. Using a Student's t-test, due to the parametric nature of this data, it was identified that that this observation was not statistically significant.

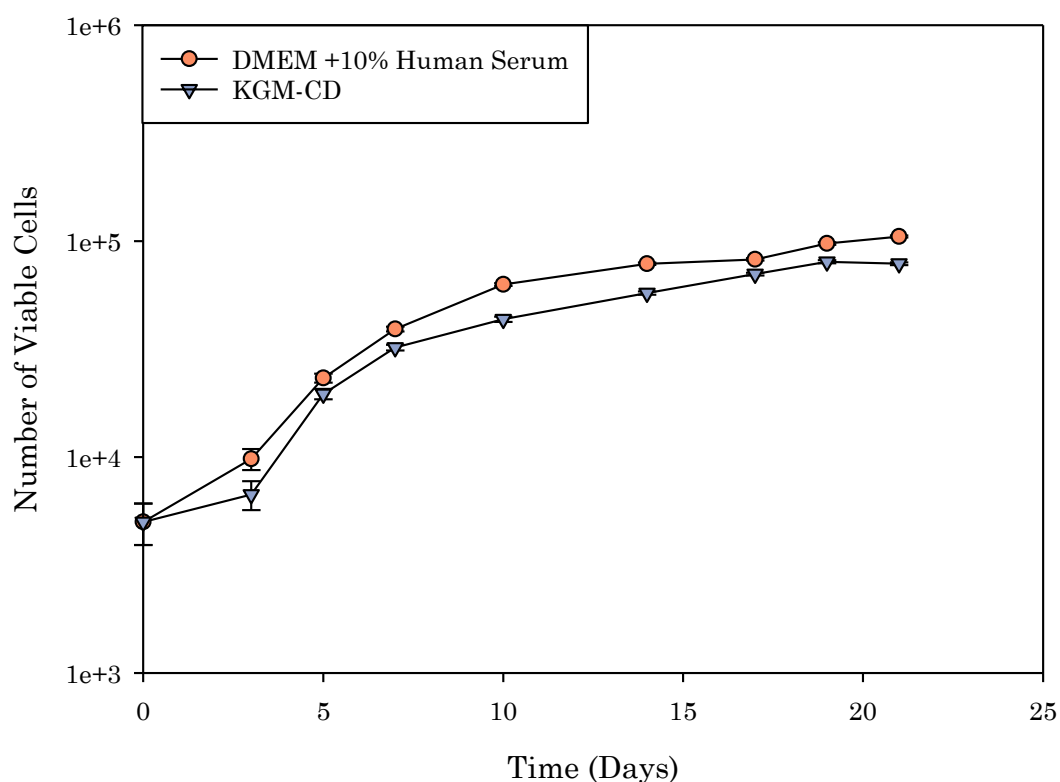


**Figure 29:** Alamar Blue growth curves for pHGF cultures grown in either DMEM supplemented with 10% human serum or KGM-CD. Using a Student's t-test, no statistical significance was found at any time point and error bars represent one standard deviation from the mean ( $p > 0.05$ ;  $n = 3$ ).

### 3.8. H400 gene expression analysis

Animal-component-free media is known to influence cell proliferation and viability (Lamb and Ambler, 2013). To understand the effect of those media on H400 keratinocyte and pHGF molecular phenotype, semi-quantitative reverse polymerase chain transcription (sqRT-PCR) was used to investigate the effects on structural protein and cell adhesion encoding genes typically expressed in these cell types, namely, CK -1, -5, -6, -13 and -19, e-cadherin, n-cadherin and vimentin.

#### 3.8.1. H400 keratinocytes gene expression analysis of cytokeratin 1 (CK1)

Figure 30a shows that in all the commercially available animal-component-free media, there was increased expression of CK1 as the number of days in culture increased. A two-way ANOVA followed by a *post-hoc* Tukey test was conducted, due to the parametric nature of the data, identified that the number of days had an effect on CK1 expression with cultures grown for 14 days expressing significantly increased levels in comparison with cultures grown for 7 days ( $p=0.031$ ;  $n=3$ ). Interestingly cultures grown in DMEM supplemented with 10% human serum, did not appear to follow the trend observed in the cultures grown in commercially available animal-component-free media, with highest expression level occurring in day 14 cultures. Statistical analysis also revealed that H400 keratinocyte cultures grown in KGM-CD always expressed higher levels of CK1 when compared with expression levels of cultures grown in DMEM supplemented with 10% human serum ( $p=0.028$ ;  $n=3$ ).

### 3.8.2. H400 keratinocyte gene expression analysis of cytokeratin 5 (CK5)

From Figure 30b, it can be seen that expression levels of CK5 decreased as the length of culture increased, with day 14 having lower expression than day 7. Statistical analysis (Two-way ANOVA followed by a *post-hoc* Tukey test) determined that this observation was significant ( $p=0.021$ ;  $n=3$ ).

Between groups, it was identified that cultures grown in DMEM supplemented with 10% human serum had significantly lower expression of CK5 than cultures grown in CnT-PR ( $p=0.041$ ;  $n=3$ ) and KGM-CD ( $p=0.030$ ;  $n=3$ ).

### 3.8.3. H400 keratinocyte gene expression analysis of cytokeratin 6 (CK6)

Figure 30c shows that in all cultures, grown for 14 days there was a slight decrease in CK6 expression when compared with day 7 expression levels.

Upon statistical analysis, using a (two-way ANOVA followed by a *post-hoc* Tukey test), it was identified that this decrease in expression was significant. ( $p=0.001$ ;  $n=3$ ). Furthermore it was also identified that H400 keratinocyte cultures grown in DMEM supplemented with 10% human serum expressed significantly less CK6 when compared to Epilife supplemented with S7 ( $p=0.023$ ;  $n=3$ ), CnT-PR ( $p=0.041$ ;  $n=3$ ) and KGM-CD ( $p=0.008$ ;  $n=3$ ).

### 3.8.4. H400 keratinocyte gene expression analysis of cytokeratin 13 (CK13)

Using the data presented in Figure 30d, it was observed and found that H400 keratinocyte cultures grown in DMEM supplemented with 10% serum demonstrated increased expression levels of CK13 when compared with CnT-PR ( $p=0.021$ ;  $n=3$ ), Epilife supplemented with S7 ( $p=0.014$ ;  $n=3$ ), and KGM-CD ( $p=0.007$ ;  $n=3$ ). Statistical significance was identified by

conducting a two-way ANOVA followed by a *post-hoc* Tukey test.

Furthermore, all day 14 H400 keratinocyte cultures showed significantly higher expression levels of CK13 in comparison with day 7 cultures (p=0.001; n=3).

#### *3.8.5. H400 keratinocyte gene expression analysis of cytokeratin 19 (CK19)*

Results presented in Figure 30e show that as the number of days in culture increased, the expression levels of CK19 also increased regardless of culture media used. Day 14 cultures grown show an increase of expression regardless of culture medium. A two-way ANOVA followed by a *post-hoc* Tukey test revealed that there was no significant difference between cultures however, it was revealed that day 14 cultures, for all media tested, had significantly higher expression levels for CK19 compared with day 7 cultures (p=0.03 n=3).

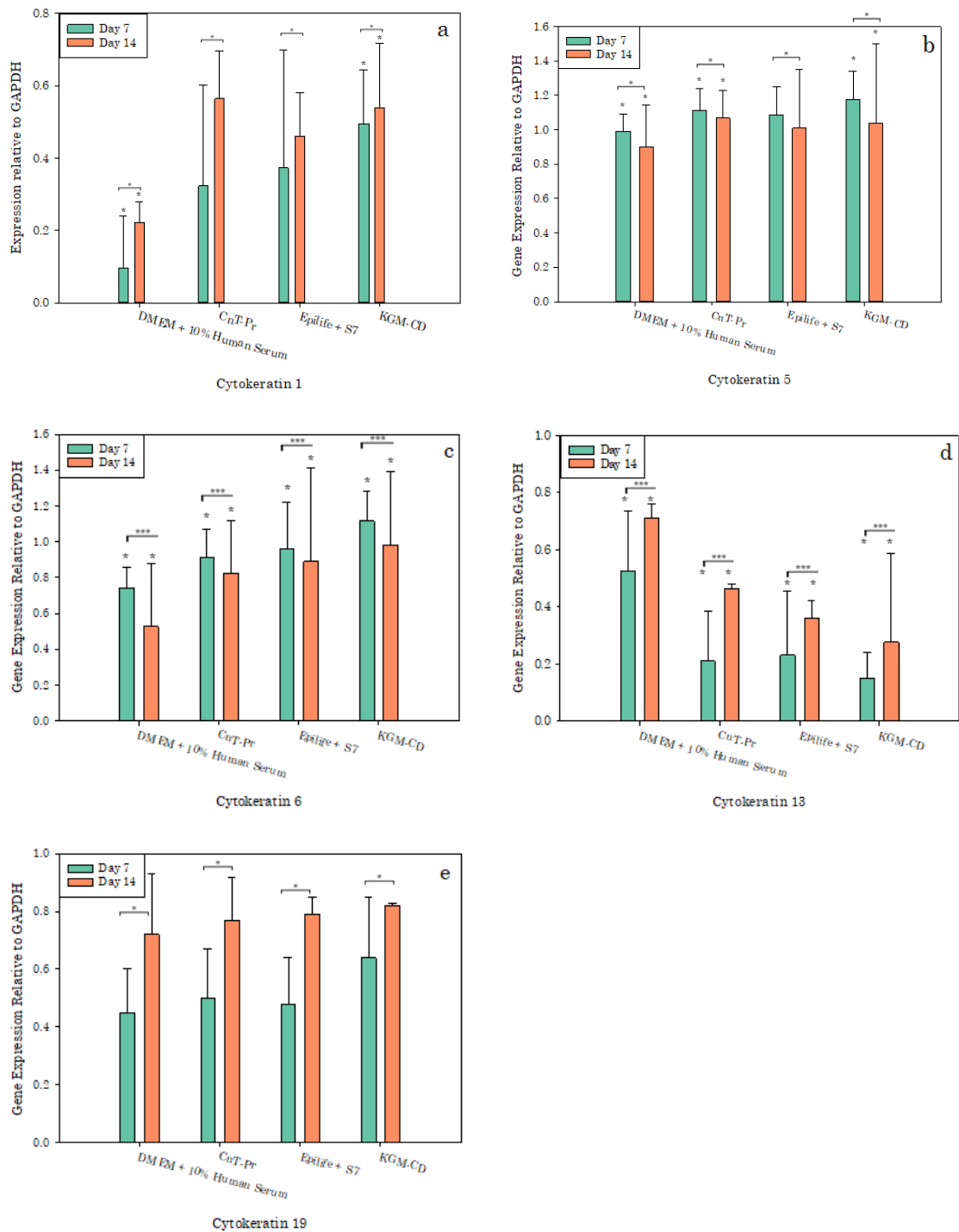


**Figure 30 a-e:** H400 keratinocyte cytochrome gene expression after cultivation in the experimental animal-component-free media for either 7 or 14 days. Cytochrome expression is expressed as a ratio to the reference gene GAPDH.  $p < 0.05$  is denoted by \* and  $p < 0.001$  is denoted by \*\*\*. Error bars represent one standard deviation from the mean ( $n=3$ ).

### *3.8.6. H400 keratinocytes gene expression analysis of vimentin*

Figure 31a shows that vimentin expression levels increased as the time in culture increased, with the exception of cultures grown in CnT-Pr, where the highest expression level was observed on day 14. Statistical analysis (Two-way ANOVA) identified that day 14 had significantly higher expression of vimentin than Day 7 ( $p=0.035$ ;  $n=3$ ). It was also identified that culture media had no significant effect ( $p>0.05$ ;  $n=3$ ).

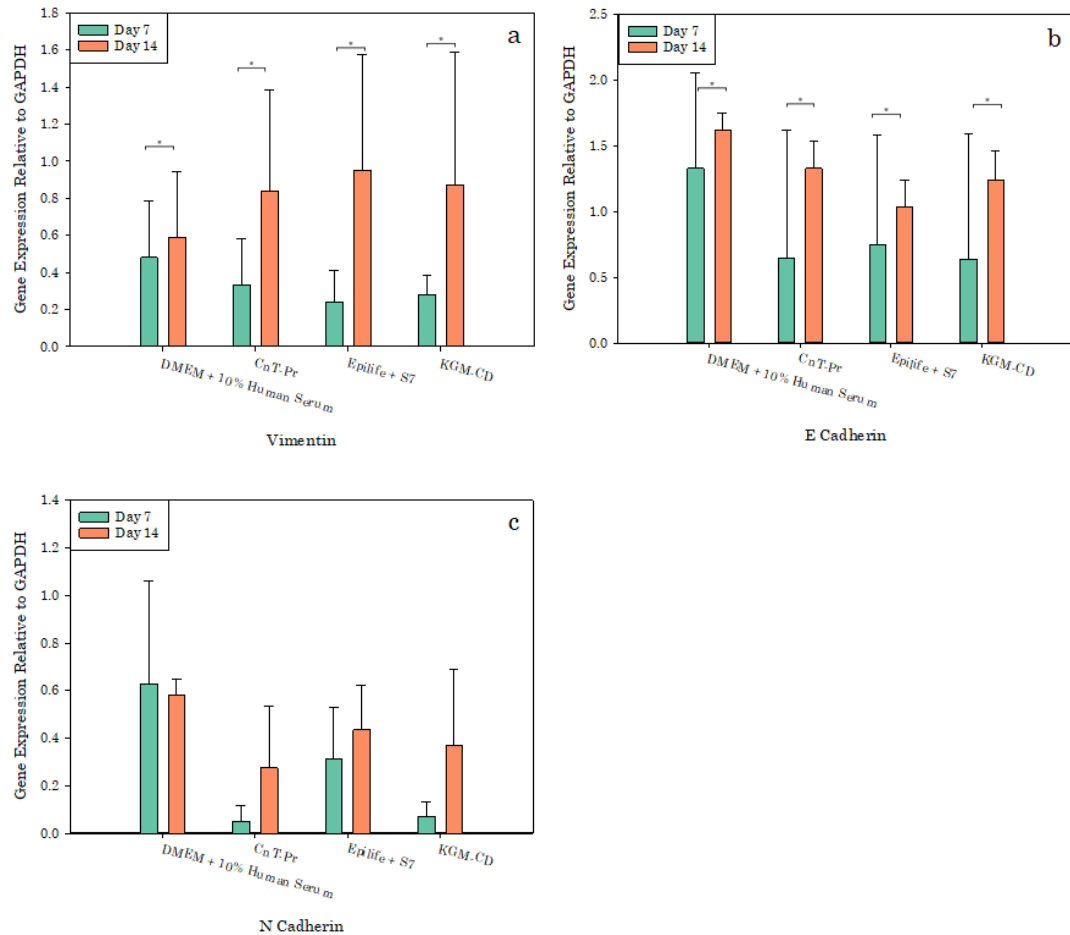
### *3.8.7. H400 keratinocytes gene expression analysis of e-cadherin*

Figure 30b shows that expression of e-cadherin increased from day 7 to day 14 cultures. Statistical analysis revealed that there was no significant difference between H400 keratinocytes grown in the different culture media ( $p=0.091$ ;  $n=3$ ) however, there was a significant between the length of culture. Cultures grown for 14 days expressed e-cadherin more markedly than cultures grown for 7 days ( $n=0.020$ ;  $n=3$ ) regardless of culture media used.

### *3.8.8. H400 keratinocytes gene expression analysis of n-cadherin*

Cultures grown in DMEM supplemented with 10% human serum appeared to express the highest level of n-cadherin (Figure 30c) after 7 days in cultures, with expression levels reducing as culture period increased. Whereas H400 keratinocyte cultures grown in both CnT-Pr and Epilife supplemented with S7 appeared to express the highest level of n-cadherin after 14 days; with expression increasing as culture

period increased. Statistical analysis (two-way ANOVA) revealed that expression of n-cadherin was not affected by culture media ( $p=0.072$ ;  $n=3$ ) or length of culture period ( $p=0.139$ ;  $n=3$ ).



**Figure 31 a-c:** H400 keratinocyte intermediate filament (a) and cell adhesion (b and c) gene expression after cultivation in the experimental animal-component-free media for either 7 or 14 days. Intermediate filament and cell adhesion gene expression is expressed as a ratio to the reference gene GAPDH.  $p < 0.05$  is denoted by \* Error bars represent one standard deviation from the mean ( $n=3$ ).

The results presented in both Figures 30 and 31 indicate that cultures grown in KGM-CD express the tested genes in a similar pattern to cultures grown in DMEM supplemented with human serum, signifying normal gene expression. Cytokeratin 6 and vimentin are expressed at significantly greater levels, particularly at Day 21, which could be attributed to the 'over-confluency' of the cultures, causing H400 cells to become stressed.

### **3.9. pHGF gene expression analysis**

Due to low yields of cDNA acquired from pHGF cultures when using normal isolation techniques, a phenol isolation followed by real-time polymerase chain reaction (RT-PCR) was employed to analyse the effect of the different media on mesenchymal gene expression levels of vimentin and n-cadherin. Cytokeratin 14 was included as a negative control. Due to time constraints it was not possible to undertake RT-PCR analysis at more than the one-culture time point of day 21.

However this provided an indication of the effect of long term culture on pHGF cultures in the different animal-component-free media.

There was no expression of cytokeratin 14 after 21 days in culture detected. Furthermore, pHGF cultures grown in DMEM supplemented with 10% human serum had greater fold changes of both vimentin (2.5 fold increase) and n-cadherin (3.1 fold increase) relative to the

housekeeping gene YWHAZ. Cultures grown in CnT-PR had the lowest fold changes of vimentin and n-cadherin when compared with the fold changes observed in the other culture conditions (Table 15).

**Table 15:** RT-PCR analysis showing fold changes in transcription of characterising genes of pHGF cells grown in the experimental culture media for 21 days (n=3).

Gene Name	Gene Symbol	Fold changes relative to housekeeping gene YWHAZ			
		DMEM + 10% human serum	CnT-PR	Epilife + S7	KGM-CD
N-cadherin	CDH2	3.1	2.2	2.7	2.4
Vimentin	VIM	2.5	1.8	2.3	2.2
Cytokeratin 14	KRT14	-	-	-	-

The biological implication of this result indicates that pHGF cells are able to strongly express fibroblastic marker genes despite culturing within a keratinocyte specific medium. Therefore, when using animal-component-free media to develop 3D oral organotypic cultures, it is suggested that the only effect will be inhibition of proliferation.

### **3.10. Measuring calcium levels in the different animal-component free media**

Calcium levels in culture media are known to influence cell proliferation, differentiation and gene expression (Durham and

Walton, 1982; Cao, Chen and Schreyer, 2012; Pinto *et al.*, 2015).

Calcium is also known to affect epithelial stratification, with culture media containing low calcium concentrations ( $\leq 0.1\text{mM}$ ) resulting in the development of 3D oral organotypic cultures with fewer stratified layers in comparison to cultures grown in higher calcium concentrations (Lamb and Ambler, 2013).

Based on the data presented in the previous sections, it was hypothesised that there could be a difference in calcium concentration between the different media used, however before measuring the calcium levels, a calcium calibration curve was created. Using non-linear regression, due to the logarithmic nature of the graph, a line of best fit was calculated enabling conversion of electrode potential to calcium ions (ppm). The calibration curve is presented in Figure 32.

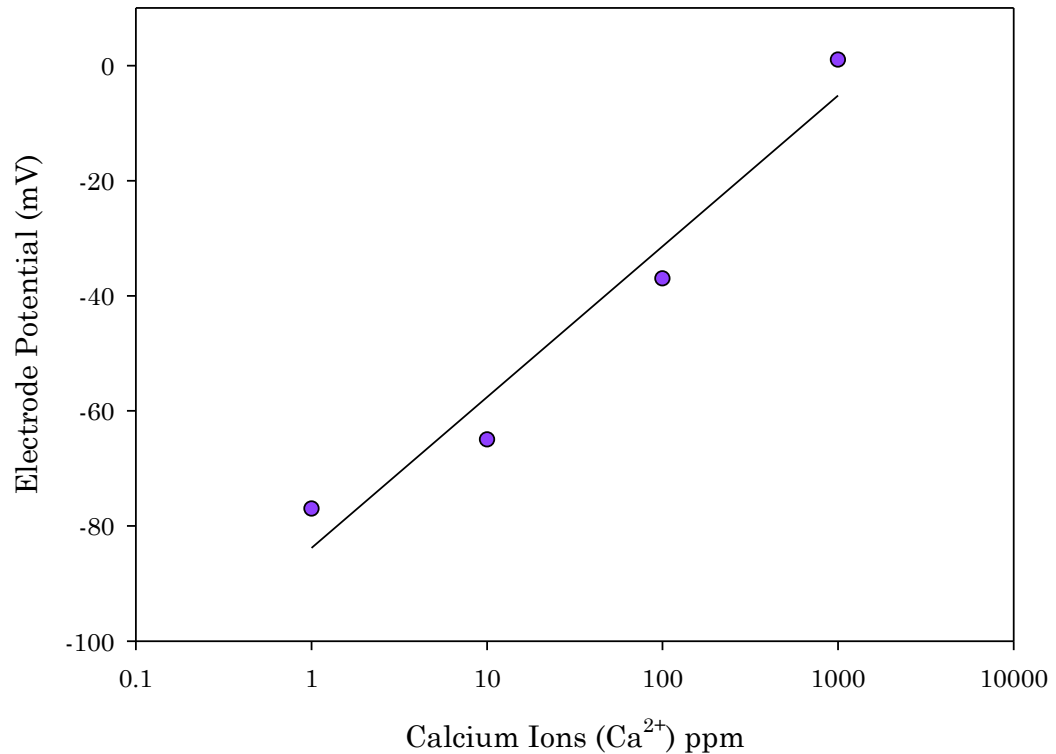


**Figure 32:** Calibration of calcium electrode using standard calcium solutions at 37°C. The equation of the line of best fit is  $y = 11.379\ln(x) - 83.8$ ;  $R^2 = 0.9526$  ( $n=3$ ).

Figure 33 shows that DMEM supplemented with 10% human serum had higher levels of  $\text{Ca}^{2+}$  when compared with the three commercially animal-component-free media. Due to the parametric nature of the data, a one-way ANOVA followed by a *post-hoc* Tukey test was conducted to determine any significance between the observed differences. It was found that DMEM supplemented with 10% human serum had significantly higher levels of  $\text{Ca}^{2+}$  compared with the three commercially available animal-component-free media ( $p < 0.001$ ;  $n=3$  for all comparisons). No  $\text{Ca}^{2+}$  was detected in KGM-CD.

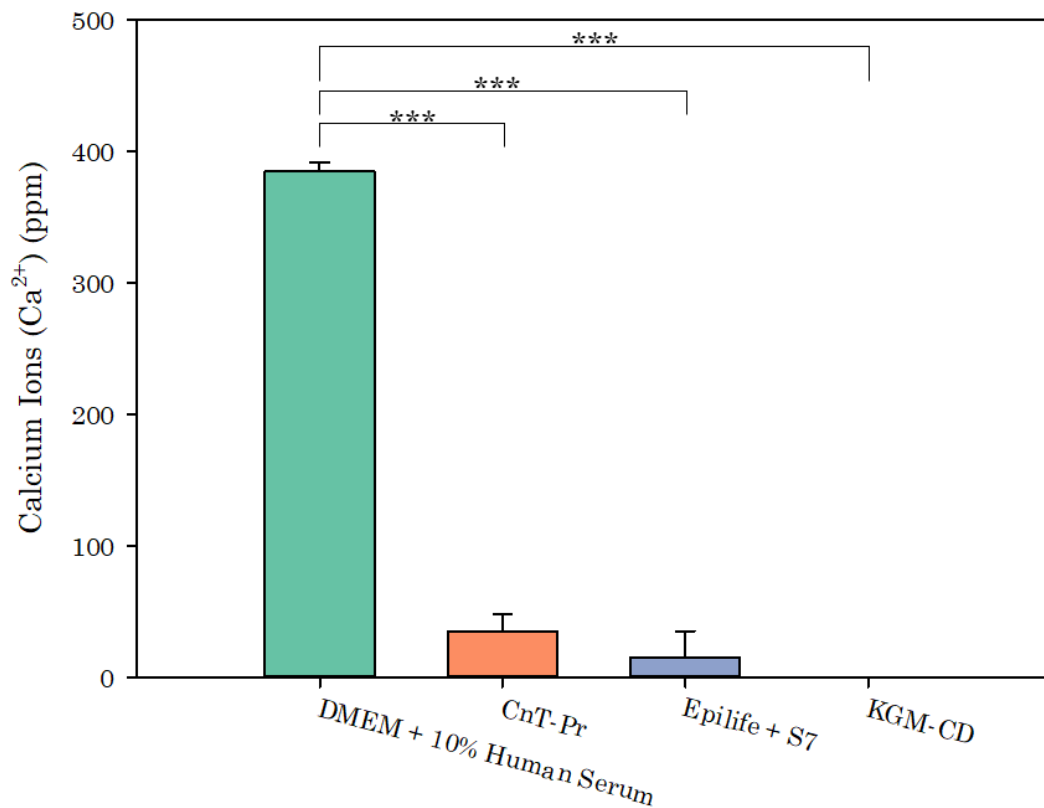


**Figure 33:** Calcium concentrations of selected animal-component-free media. Using a one-way ANOVA followed by a *post-hoc* Tukey test determined that DMEM supplemented with 10% human serum had significantly greater levels of Ca<sup>2+</sup> when compared with the other animal-component-free media ( $p < 0.001$ , denoted by \*\*\*). Error bars represent one standard deviation from the mean ( $n=3$ ).

The results from this section, indicated that all the tested animal component-free media selected, had potential to be used to generate 3D oral organotypic cultures. However, it was decided that KGM-CD would be used to generate 3D oral organotypic cultures due to H400 keratinocyte culture outperforming those which were cultured in DMEM supplemented with 10% human serum, inhibition of pHGF proliferation yet retaining high viability and fewer variations in

genetic expression when compared to DMEM supplemented with 10% human serum.

## Results Section 2

The data presented in this chapter were derived from experiments designed to investigate the biological response in terms of cell viability and attachment to binary titanium zirconium (TiZr) alloys, with the aim of identifying optimum compositions for use as a dental implant material.

Prior to investigating how cell cultures proliferated on, and responded to, the TiZr alloys a better understanding of how H400 keratinocytes and pHGF cultures responded to existing Ti dental implant substrates was necessary.

### **3.11. H400 keratinocyte culture growth on commercially pure (Grade IV) titanium (Ti)**

H400 keratinocyte cultures were able to grow and proliferate on commercially pure (Grade IV) Ti however cultures did not generate comparable cell numbers (at any time point) with the control cultures grown on tissue culture plasticware as shown in Figure 34, despite being cultured on equal surface areas. At day 2, there were  $58 \pm 5\%$  fewer cells attached to the Ti surfaces when compared with the control cultures. The biggest percentage difference in number of viable cells attached to Ti surfaces occurred on days 12 and 14 where there were

94% and 94% fewer cells attached to the Ti disc surface when compared with control cultures, respectively.

Due to the non-parametric nature of the data, confirmed by failure of Shapiro-Wilk normality test, a Mann-Whitney U test was performed which revealed that from day 2, H400 keratinocyte cultures grown on tissue culture plasticware contained a statistically higher number of viable cells ( $p=0.038$ ;  $n=3$ ).

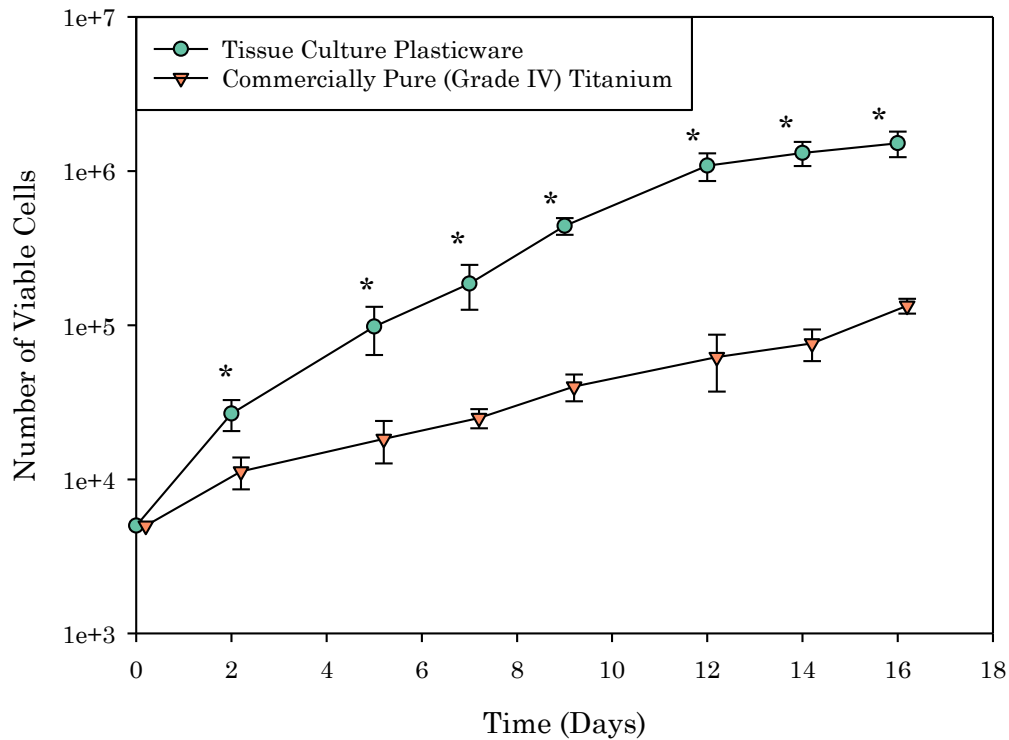


**Figure 34:** H400 keratinocyte growth curves grown on either tissue culture plasticware or commercially pure (grade IV) Ti discs. From day 2, H400 keratinocyte cultures grown on tissue culture plasticware had statistically higher cell numbers compared with H400 keratinocyte cultures grown on commercially pure (Grade IV) Ti discs ( $p=0.032$ , denoted by \*). Error bars

represent one standard deviation from the mean and each group has been jittered 0.2 days along the x-axis for clarity (n=3).

Additionally, population doubling times, presented further supported that H400 keratinocyte cultures grown on tissue culture plasticware had a shorter population doubling time than those grown on commercially pure (Grade IV) Ti. This difference was statistically significant, following a Student's t-test due to the parametric nature of the data as  $p < 0.001$  (n=3).

H400 keratinocyte culture viability during the experimental period depicted in Figure 35 showed that varying the surface had no effect on cell viability, which was further supported by a Student's t-test, which revealed no significant differences between any of the cultures ( $p = 0.455$ ; n=3).

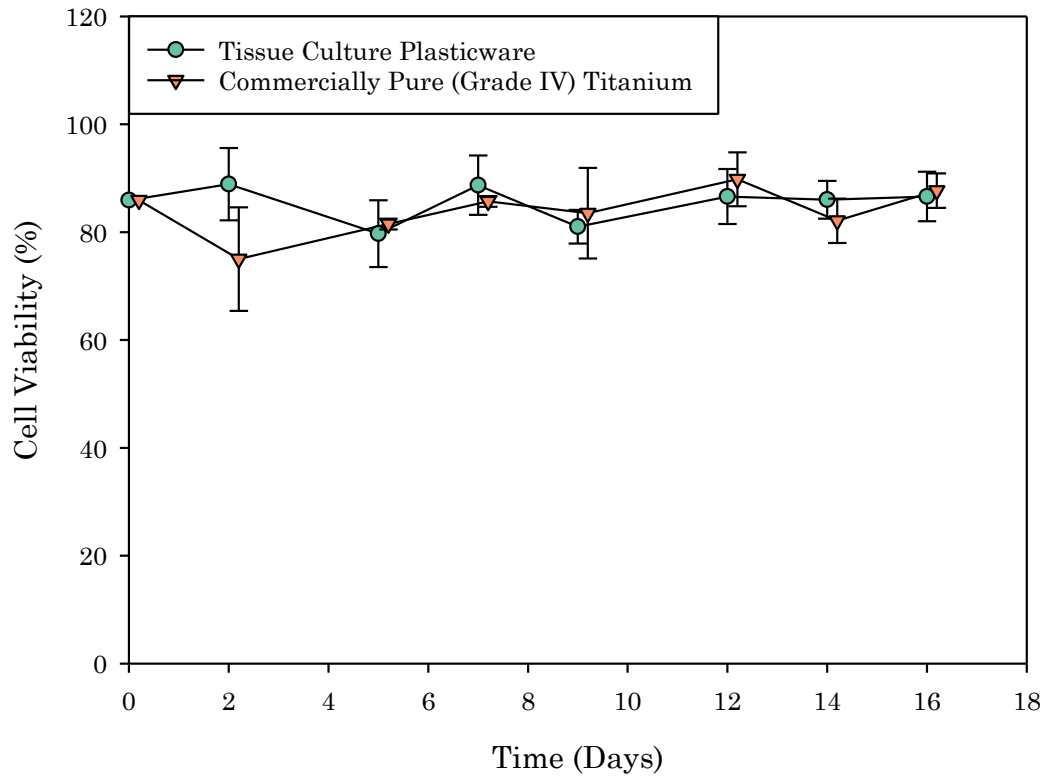


**Figure 35:** Viability of H400 keratinocyte cultures grown on tissue culture plasticware or commercially pure (Grade IV) Ti for 16 days. No significant differences were identified in the percentage of viable cells between the different cultures using a Student's t-test at any time-point. Error bars represent one standard deviation from the mean and each group has been jittered 0.2 days along the x-axis for clarity (n=3).

### **3.12. pHGF culture on commercially pure (Grade IV) Ti**

pHGF cultures were able to grow and proliferate on commercially pure (Grade IV) Ti, however cultures did not generate comparable cell numbers to those of the control cultures (Figure 36) grown on tissue culture plasticware, at any time point analysed despite being cultured on equal surface areas.

Differences in cell number were apparent from day 2, where pHGF cultures grown on Ti surfaces exhibited  $41\pm 3\%$  fewer cells when compared with control cultures. Unlike the H400 cultures grown on Ti surfaces, where the greatest difference in number of cells was observed on days 12 and 14, the greatest difference in viable cell numbers was observed on both days 7 and 9 where there were  $53\pm 4\%$  and  $53\pm 12\%$  fewer cells attached to the Ti disc surface when compared with control cultures, respectively.

A Student's t-test revealed that from day 2, pHGF cultures grown on tissue culture plasticware had statistically 1.6 times higher number of viable cells than cultures grown on Ti surfaces ( $p=0.012$ ;  $n=3$ ).

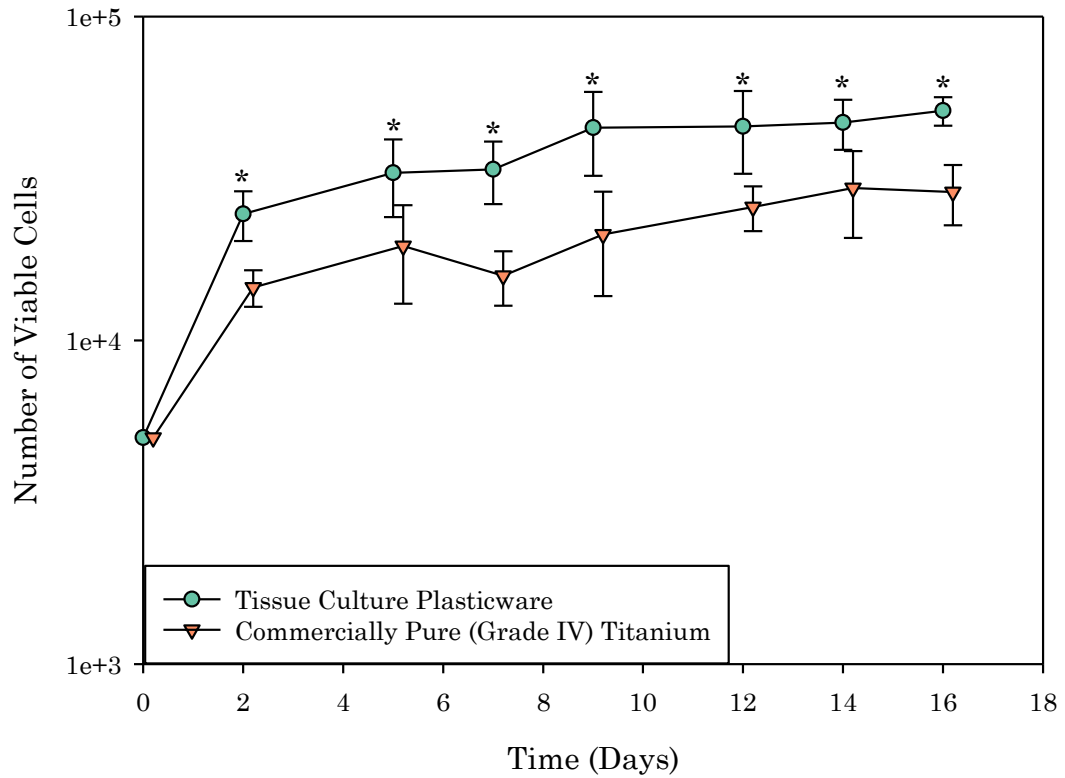


**Figure 36:** Viable pHGF culture growth curves on either tissue-culture plasticware or commercially pure (grade IV) Ti discs. From day 2 onwards, pHGF cultures grown on tissue culture plasticware had statistically higher cell numbers compared with pHGF cultures grown on commercially pure (Grade IV) Ti discs ( $p=0.012$ , denoted by \*). Error bars represent one standard deviation from the mean and each group has been jittered 0.2 days along the x-axis for clarity ( $n=3$ ).

Average population doubling times indicated that pHGF cultures grown on tissue culture plasticware had a shorter population doubling time compared with the H400 keratinocyte cultures grown on commercially pure (Grade IV) Ti, however this difference was not statistically significant (Student's t-test,  $p>0.05$  ( $n=3$ )).

pHGF culture viability over 16 days during the experimental period (Figure 37) was not influenced by the surface the cells were cultured on. A Student's t-test revealed that there were no significant differences in cell viability between the two cultures ( $p>0.05$ ;  $n=3$ ).

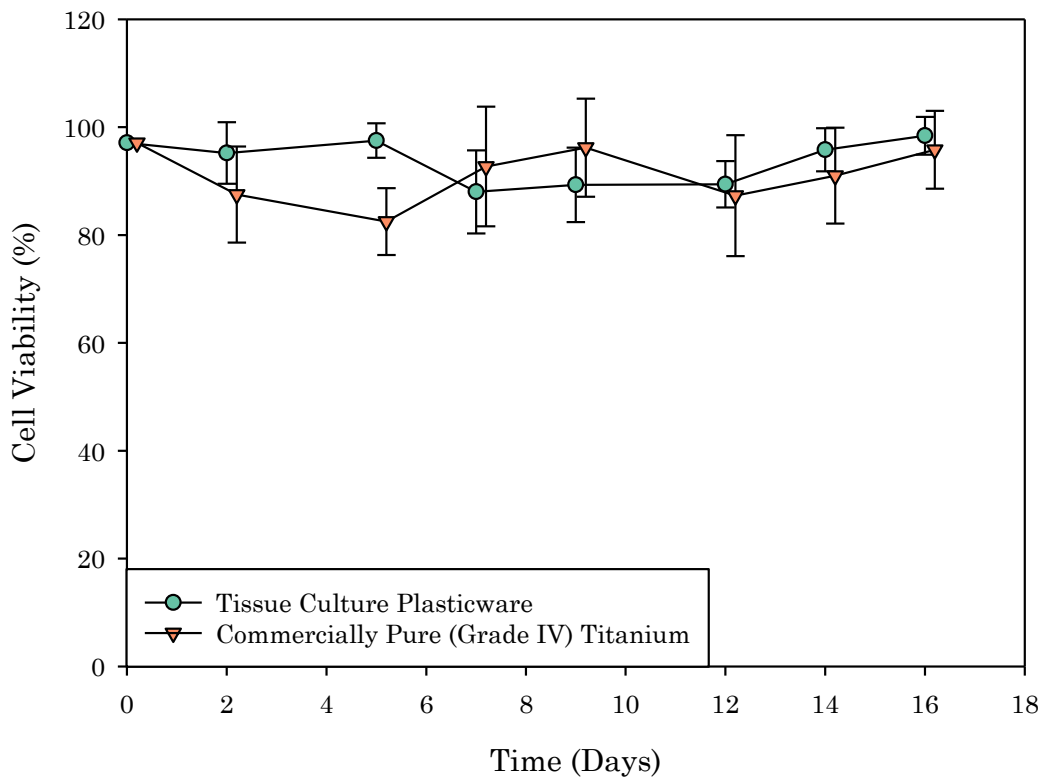


**Figure 37:** Viability of pHGF cultures grown on tissue culture plasticware or on commercially pure (Grade IV) Ti for 16 days. No significant differences were identified in the percentage of viable cells between the different cultures using a Student's t-test ( $p>0.05$ ). Error bars represent one standard deviation from the mean and each group has been jittered 0.2 days along the x-axis for clarity ( $n=3$ ).

### **3.13. Characterisation of the initial pHGF culture response to TiZr metals**

In the following sections TiZr alloys are referred to in terms of percentage of Zr composition. Commercially pure (Grade IV) Ti and Zr are described as 0% and 100% Zr, respectively. Additionally, only pHGF cells cultured in DMEM supplemented with 10% human serum were used for subsequent biological experiments. This was to ensure biological relevancy, as fibroblast cells are the predominate cell type that interact and form hemidesmosomal complexes with the proteins adsorbed onto the dental implant surface upon implantation -leading to the generation of a biological seal.

The data from pHGF cultures that had been grown for 24 hours on tissue culture plasticware, commercially pure (Grade IV) Ti and Zr and TiZr alloys is shown in Figure 38. Tissue culture plasticware supported the highest number of viable cells attached to the surface after 24 hours in comparison with the other surfaces, whilst of the TiZr surfaces, 50% Zr had the highest number of viable cells attached to the surface.

A Kruskal-Wallis H test followed by a Student-Newman-Keuls post-hoc test (due to the parametric nature of the data), showed that the pHGF cultures grown on tissue culture plasticware had statistically significant higher numbers of viable pHGF cells attached to the surface

compared with 0% Zr (difference of  $2.17 \times 10^4$  cells,  $p=0.008$ ;  $n=3$ ), 5% Zr (difference of  $1.47 \times 10^4$  cells,  $p=0.009$ ;  $n=3$ ), 15% Zr (difference of  $1.75 \times 10^4$  cells,  $p=0.049$ ;  $n=3$ ), 50% Zr (differences of  $1.39 \times 10^4$  cells,  $p=0.008$ ;  $n=3$ ) and 100% Zr (difference of  $1.78 \times 10^4$  cells,  $p=0.008$ ;  $n=3$ ). Additionally, 0% Zr had statistically lower numbers of viable pHGFs on the surface when compared with the other TiZr surfaces: 5% Zr ( $p=0.022$ ;  $n=3$ ), 15% Zr ( $p<0.001$ ;  $n=3$ ), 50% Zr ( $p=0.024$ ;  $n=3$ ) and 100% Zr ( $p=0.030$ ;  $n=3$ ).

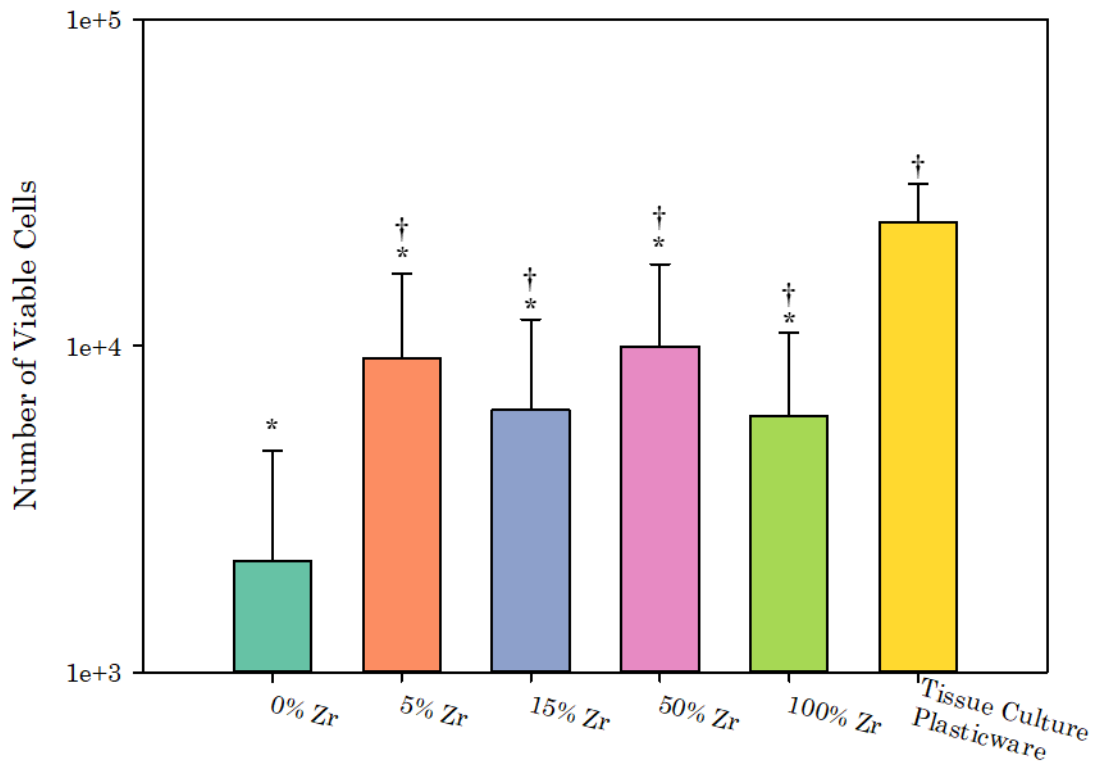


**Figure 38:** Viable pHGF cell attachment on TiZr alloys (5%, 15% and 50% Zr), commercially pure (Grade IV) Ti (0% Zr), commercially pure Zr (100% Zr) or tissue culture plasticware for 24 hours. Differences between groups were assessed using a Kruskal-Wallis H test followed by a Student-Newman-Keuls post-hoc test. Statistically lower viable cell numbers are denoted with \*,

statistically higher viable cell numbers are denoted by †. Error bars represent one standard deviation from the mean (n=3).

Data from pHGFs incubated on the different TiZr alloy surfaces for 48 hours are shown in Figure 39. Cultures grown on the TiZr alloys (5% Zr, 15% Zr and 50% Zr) exhibited higher numbers of viable cells attached to the surface when compared with culture cells grown on 0% Zr, 100% Zr and tissue culture plasticware. A one-way ANOVA followed by a *post-hoc* Tukey test revealed that 15% Zr had statistically higher numbers of cells attached to the surface than 0% Zr (p=0.01; n=3), tissue culture plasticware (p=0.012; n=3), 5% Zr (p=0.014; n=3) and 100% Zr (p=0.02; n=3). 50% Zr had statistically higher numbers of cells attached to the surface than 0% Zr (p=0.016; n=3), tissue culture plasticware (p=0.018; n=3), 5% Zr (p=0.021; n=3) and 100% Zr (p=0.03; n=3).

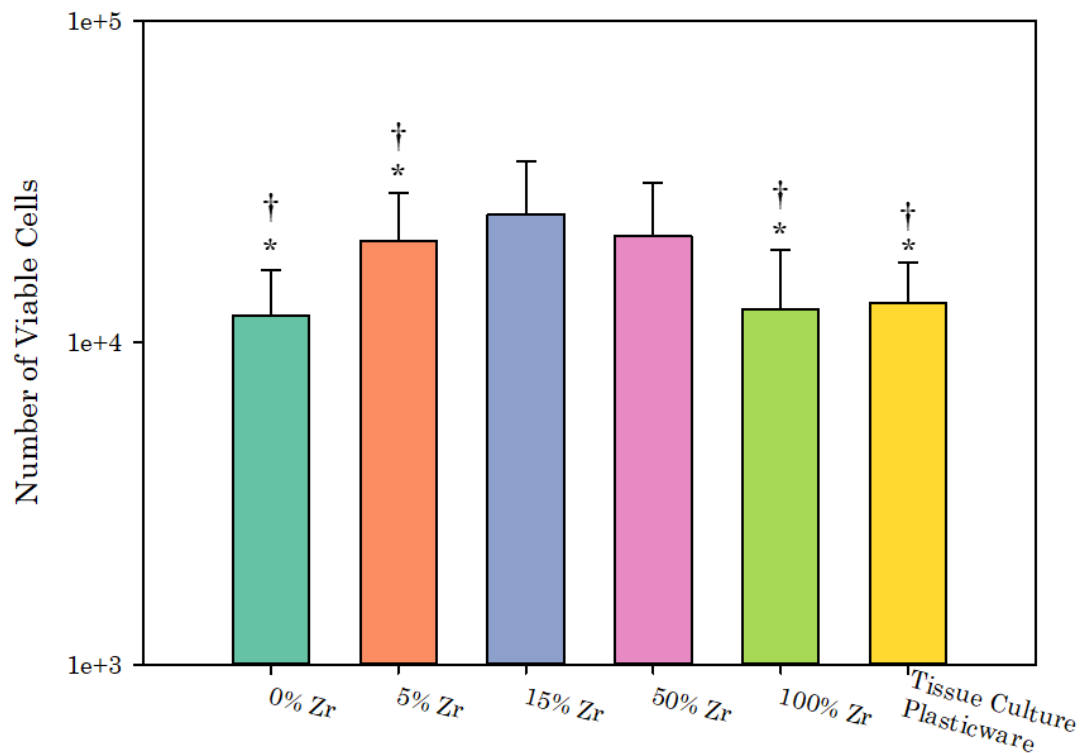


**Figure 39:** Viable pHGF cell attachment on either TiZr alloys (5%, 15% and 50% Zr), commercially pure (Grade IV) Ti (0% Zr), commercially pure Zr (100% Zr) or tissue culture plasticware for 48 hours. Differences between groups were assessed using a one-way ANOVA followed by a *post-hoc* Tukey test. \* and † denote statistically ( $p < 0.05$ ) lower cell numbers to 15% Zr and 50% Zr respectively. Error bars represent one standard deviation from the mean ( $n=3$ ).

pHGF culture viability following 24 hour and 48-hour attachment periods are shown in Figure 40. pHGF cultures that were incubated on the surface for 48 hours, exhibited higher viability than cultures that were only incubated for 24 hours, with the exception of tissue culture plasticware, where the viability remained at a similar level. A two-way ANOVA followed by a post-hoc Tukey test, revealed that pHGF

cultures grown for 48 hours on 0% Zr and 15% Zr had a significantly higher viability than the same cultures which were grown for 24 hours ( $p < 0.001$  and  $p = 0.014$  respectively;  $n = 3$ ). When comparing the viability of cultures grown on the different surfaces for 24 hours, 0% Zr had statistically lower pHGF culture viabilities than pHGF cultures grown on 5% Zr ( $p = 0.013$ ;  $n = 3$ ), 50% Zr ( $p = 0.019$ ;  $n = 3$ ) 100% Zr ( $p = 0.021$ ;  $n = 3$ ) and tissue culture plasticware ( $p < 0.001$ ;  $n = 3$ ). Furthermore, when comparing the viability of cultures grown on the different surfaces for 48 hours, no significant difference between pHGF culture viability was found.

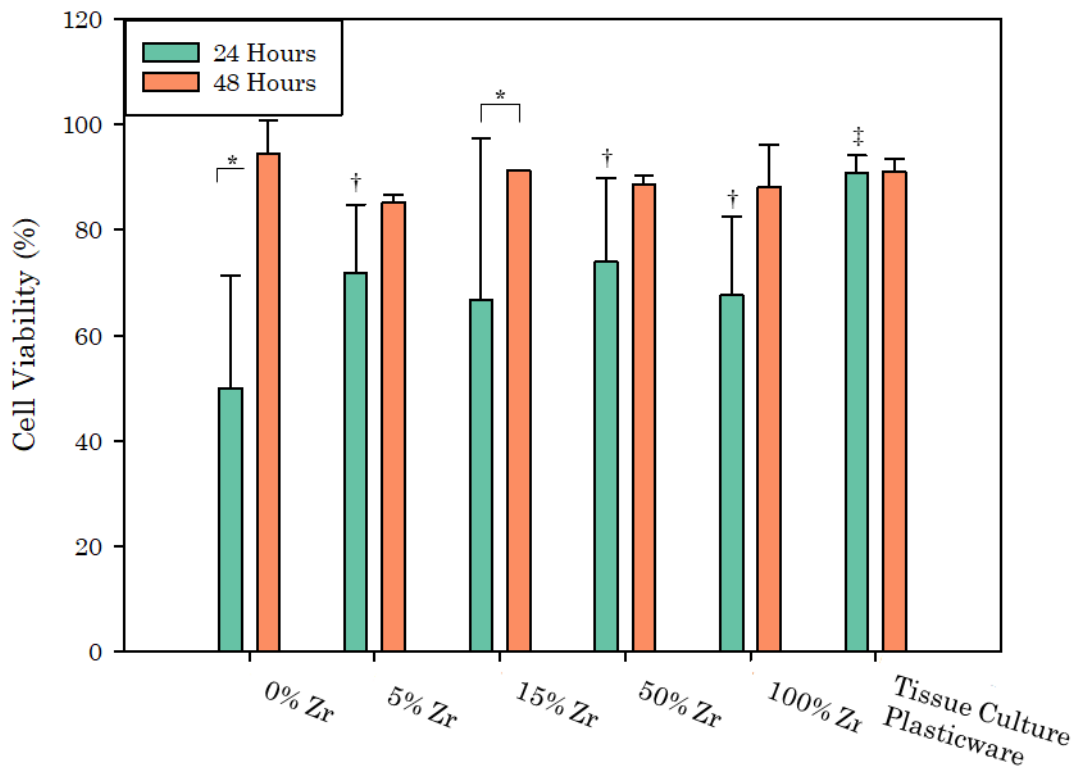


**Figure 40:** Viability of pHGF cultures grown on either TiZr alloys (5%, 15% and 50% Zr), commercially pure (Grade IV) Ti (0% Zr), commercially pure Zr (100% Zr) or tissue culture plasticware for 24 and 48 hours. A two-way

ANOVA followed by a *post-hoc* Tukey test to compare the effect of surface material, the effect of attachment time and a combination of the two on pHGF cell culture viability. \* denotes  $p < 0.05$ . Statistically higher culture viabilities compared to 0% Zr are denoted by † ( $p < 0.05$ ) and ‡ ( $p < 0.001$ ). Error bars represent one standard deviation from the mean ( $n=3$ ).

### **3.14. Characterisation of long term pHGF growth on TiZr alloys**

The data obtained from pHGF cultures grown on the different TiZr alloys, commercially pure (Grade IV) Ti and Zr and tissue culture plasticware for up to 19 days is shown in Figure 41. As the number of days increased, so did the number of viable cells attached to the surface, regardless of material composition. Using a two-way ANOVA followed by a *post-hoc* Tukey test, it was found that day 14, 16 and 19, had significantly higher viable cell numbers in comparison to day 0, 1, 3, 5, 7 and 9 regardless of culture surface composition, owing to the increased length in culture ( $p < 0.05$  for all;  $n=3$ ). Upon observation, it appeared that pHGF cultures grown on 5% Zr and 50% Zr supported higher numbers of viable pHGFs than 0%, 15% and 100% Zr towards the end of the experimental period. However, statistical analysis revealed that only pHGF cultures grown on tissue culture plasticware generated statistically higher numbers than pHGFs grown on 0% Zr and 100% Zr ( $p=0.025$ ,  $p=0.029$  respectively  $n=3$ ).

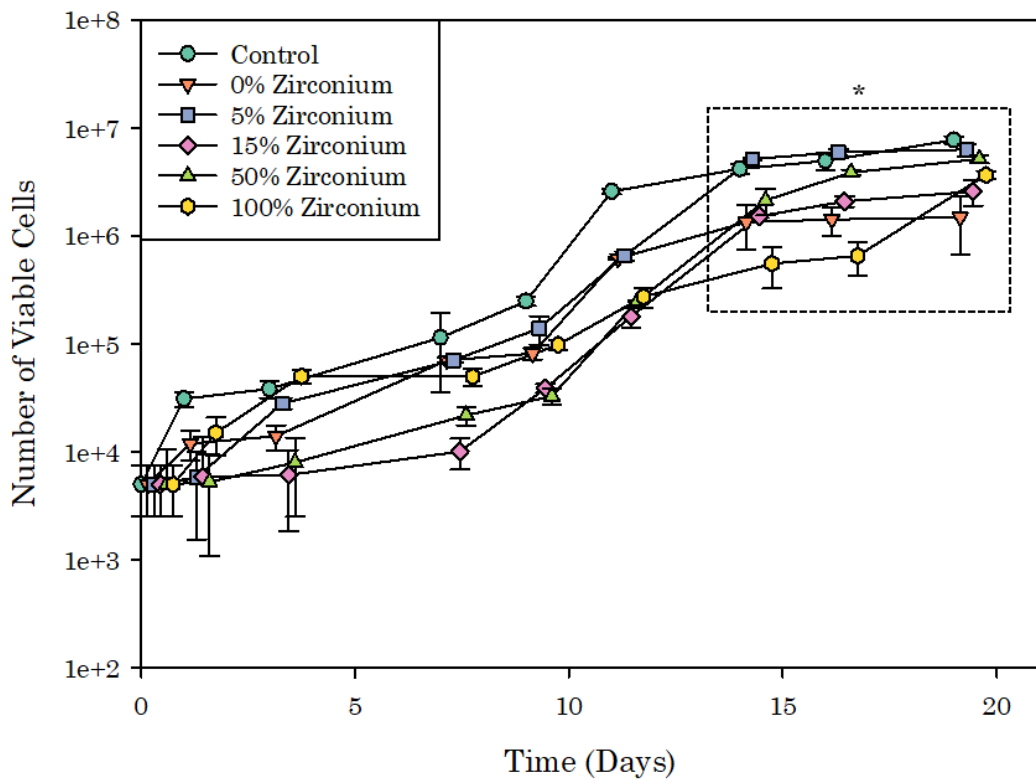


**Figure 41:** Alamar Blue growth curves of pHGF cultures grown on either TiZr alloys (5%, 15% and 50% Zr), commercially pure (grade IV) Ti (0% Zr), commercially pure Zr (100% Zr) or tissue culture plasticware for up to 19 days. A two-way ANOVA followed by a *post-hoc* Tukey test found that day 14, 16 and 19, had significantly higher viable cell numbers in comparison to day 0, 1, 3, 5, 7 and 9 regardless of culture surface composition ( $p < 0.05$  for all, denoted by \*). Error bars represent one standard deviation from the mean and each group has been jittered 0.15 days along the x-axis for clarity ( $n=3$ ).

Average population doubling times (Figure 42) were calculated using data obtained between days 7 and 14 shown in Figure 41. pHGFs grown on 15% Zr had statistically shorter population doubling times than 0% and 100% Zr, which was determined by a Student's t-test ( $p < 0.001$ ;  $n=3$ ).

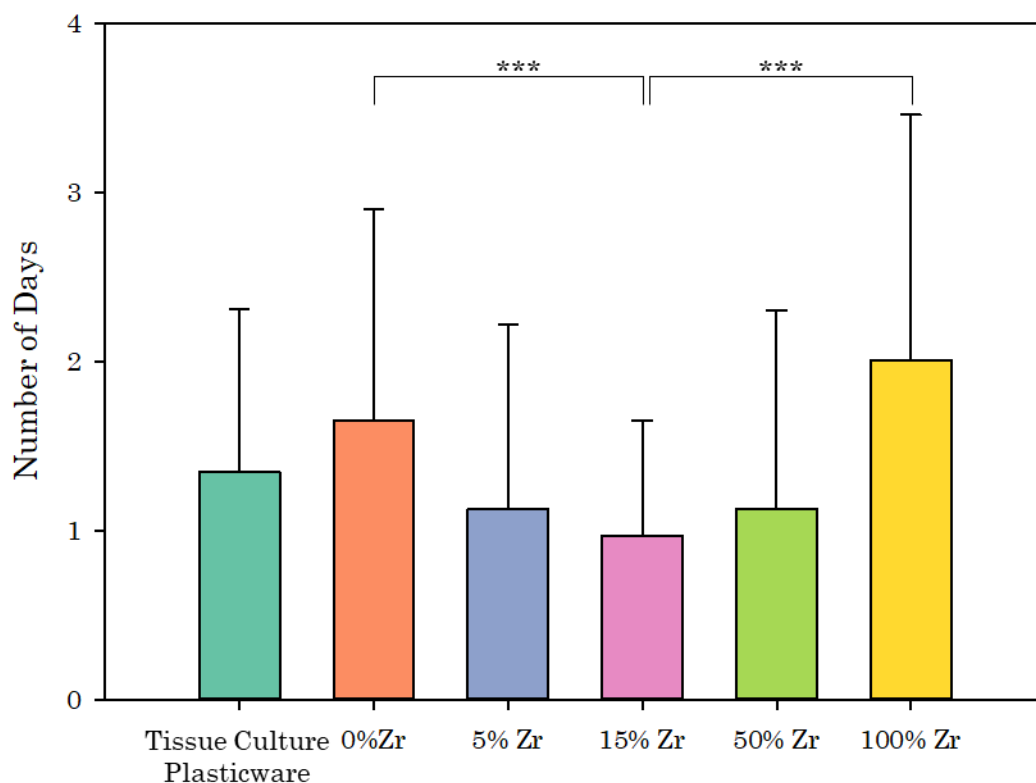


**Figure 42:** Average population doubling times of cultures of pHGF cultures grown on either TiZr alloys (5%, 15% and 50% Zr), commercially pure (Grade IV) Ti (0% Zr), commercially pure Zr (100% Zr) or tissue culture plasticware grown for 7 days. pHGF cultures grown on 15% Zr had shorter average population doubling times than all the other surfaces and using a Student's t-test to statistically analyse, this observation was found to be significant ( $p < 0.001$ , denoted by \*\*\*). Error bars represent one standard deviation from the mean ( $n=3$ ).

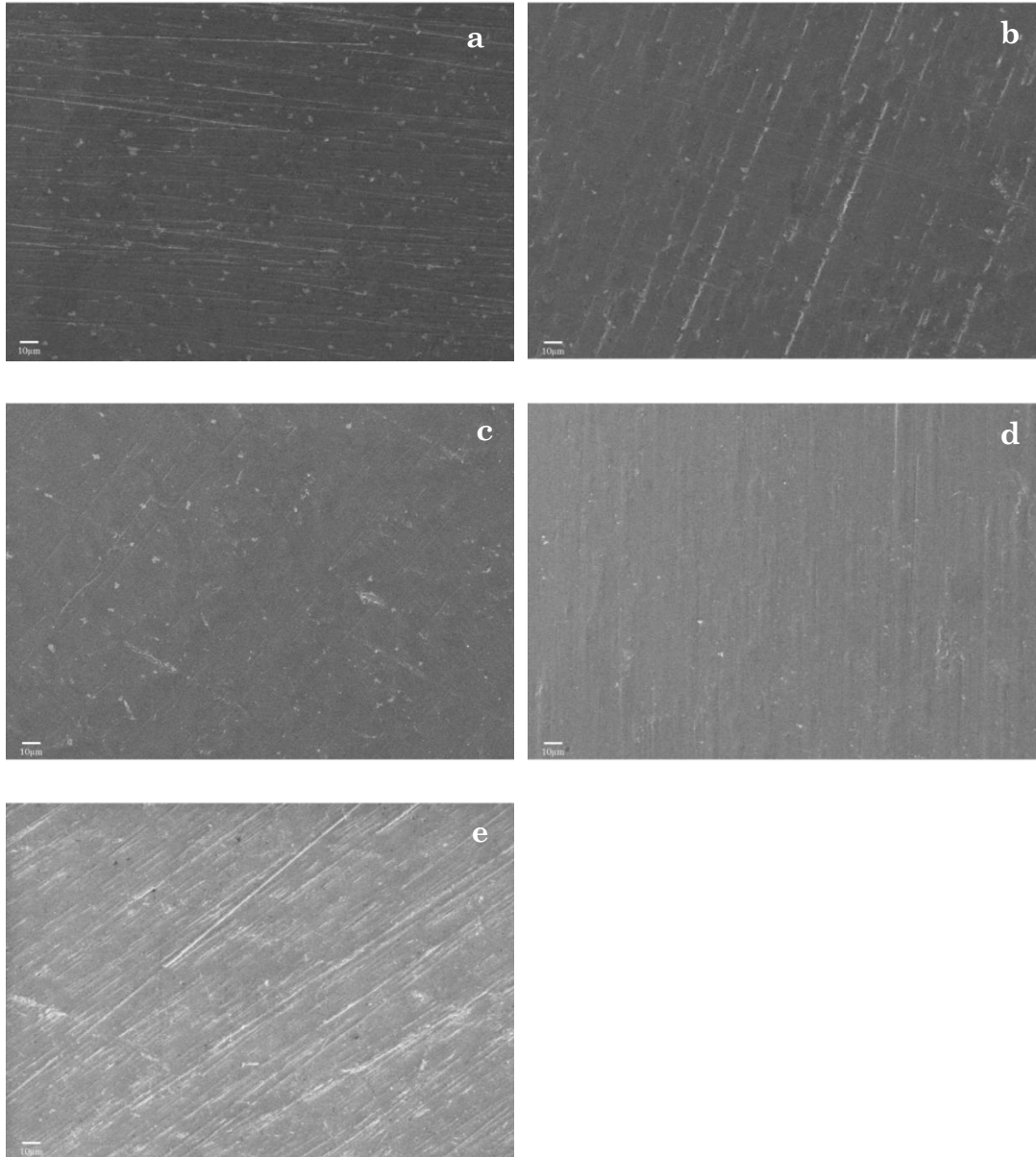
### **3.15. SEM analysis of surface topography of commercially pure (Grade IV) Ti, commercially pure Zr and TiZr alloys after complete polishing**

Scanning electron microscopy (SEM) was conducted to observe the surface of each of the different discs following complete polishing using the method described in Section 2.25.

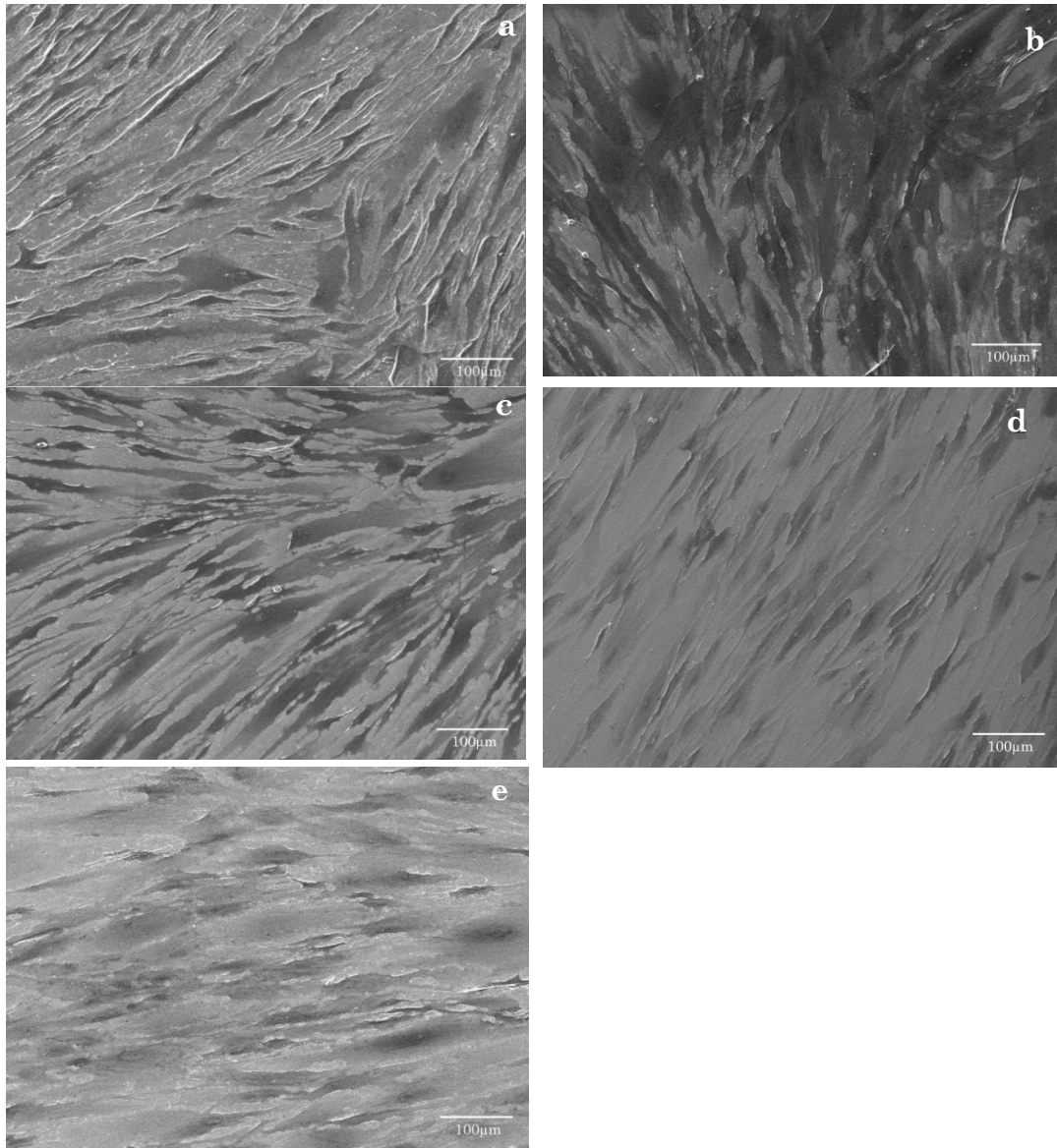
The images in Figure 43 demonstrate that despite the apparent observed mirror-like finish of the discs after polishing, scratches and imperfections remained, with 100% Zr (Figure 43e) having the most apparent scratches and imperfections compared with the other TiZr discs. Figures 43c and 43d (5% and 15% Zr) had the fewest observable number of scratches and imperfections. The visible difference in apparent scratches and imperfections could be attributed to the Zr% within the overall alloy as it has been shown that hardness of a TiZr increases as Zr composition increases (Gottlow *et al.*, 2012).

Figure 44a-e shows representative SEM images of pHGFs grown on the different TiZr surfaces for 7 days. It can be seen that for all TiZr alloys, pHGFs were able to attach and proliferate on to the surface. pHGFs grown on 5% Zr (Figure 44b) appeared to grow on top of each other and lacked orientation whereas on the other TiZr surfaces, pHGFs grew in a more uniform direction and were in a monolayer; this

was most apparent in the 0% Zr (Figure 44a) and 15% Zr substrates (Figure 44c).



**Figure 43 (a-e):** Representative SEM images of the surface topography of (a) 0% Zr, (b) 5% Zr (c), 15% Zr, (d) 50% Zr and (e) 100% Zr after polishing with 0.2µm colloidal silica particles to a complete mirror-like finish. Polishing marks were visible on all surfaces, with the most marks apparent on 100% Zr (Figure 43e) and the fewest on 15% Zr (Figure 43c) and 50% Zr (Figure 43d). All images were taken at a magnification of 2000x. Scale bars are shown.



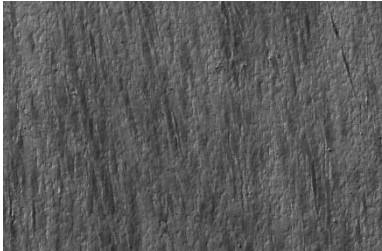
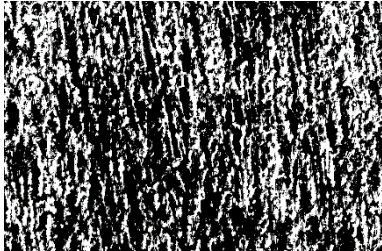
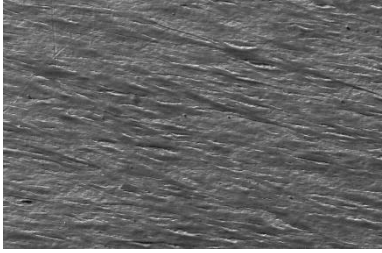
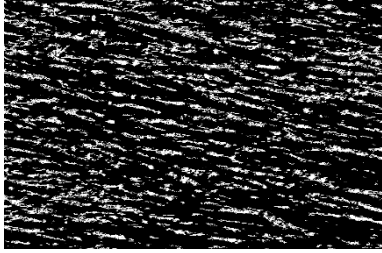
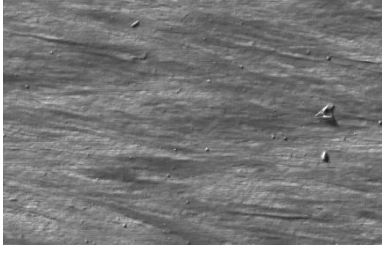
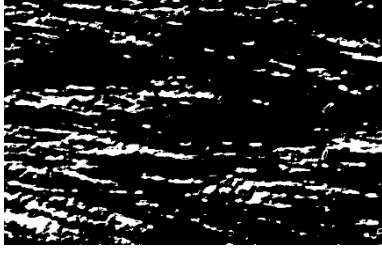
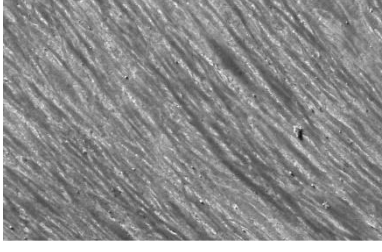
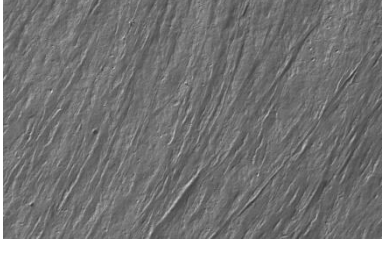
**Figure 44 (a-e):** Representative SEM images of pHGFs grown for 7 days attached to the surface of (a) 0% Zr, (b) 5% Zr (c), 15% Zr, (d) 50% Zr and (e) 100%Zr discs. pHGFs were able to attach and proliferate on to the surface. pHGFs grown on 5% Zr (Figure 44b) appeared to multilayer with lack of orientation whereas on the other TiZr surfaces, pHGFs grew in a more uniform direction as a monolayer; most apparent in 0% Zr (Figure 13a) and 15% Zr (Figure 44c). There also appear to be fewer pHGFs attached to the surface of 50% Zr compared with the other TiZr surfaces. All images were taken at a magnification of 2000x. Scale bars are shown n=3).

### **3.16. Image analysis of pHGF attachment on commercially pure (Grade IV) Ti, commercially pure Zr and TiZr alloy surfaces**

To be able to quantify the SEM images obtained (n=3 for all TiZr discs; represented in Figure 44a-e) the Trainable Weka Segmentation plug-in accessed via FIJI (distribution of the ImageJ software, version 1.15u, National Institutes of Health, Maryland, USA) (Arganda-Carreras *et al.*, 2017) described in Section 2.28, was utilised to calculate the percentage of the surface area covered by attached pHGF cells by segmenting pHGFs from the surface of each disc.

Figure 45 presents example results segmented images of the output from the Trainable Weka Segmentation plug-in. TiZr alloys containing 5% and 15% Zr had the highest surface area covered by attached pHGFs (78±7% and 78±12% of the surface had adherent pHGFs) whereas 100% Zr had the least surface area covered by attached pHGFs (69±8% of the surface had adhered cells). The remaining TiZr alloys, 0%Zr and 50% Zr had similar cell surface area coverage; 70±8% and 78±8% respectively.

A one-way ANOVA revealed that there was no significant difference between the amount of Zr in TiZr alloys and the number of adhered cells to the surface (p=0.245; n=3).

Material	Image before segmentation	Binary segmented image used to calculate surface covered by adhered cells
0% Zr		
5% Zr		
15% Zr		
50% Zr		
100% Zr		

**Figure 45:** Example SEM images of pHGF cells attached to the surface of different TiZr alloys with their corresponding segmented images, where the cells are shown in black and the background in white.

### **3.17. Surface roughness analysis on polished TiZr discs**

Non-contact profilometry was used to analyse the surface roughness of each TiZr discs following complete polishing (see Figure 43 a-e for representative images). From the analysis, three-dimensional surface roughness images were generated for each of the different sections on the TiZr discs, presented in Figure 46. From the three analysed sections on each disc, average surface roughness (mean-Ra) values ( $\mu\text{m}$ ) were calculated; presented in Figure 47.

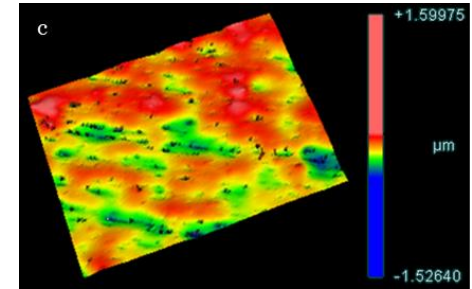
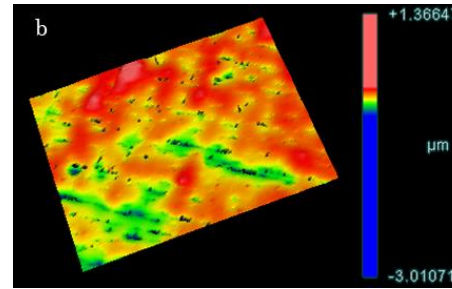
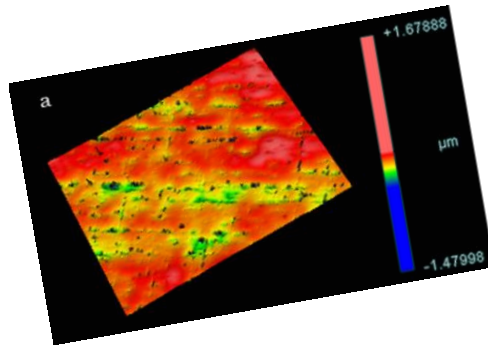
Material

Section a

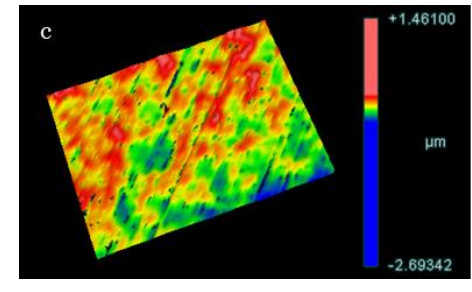
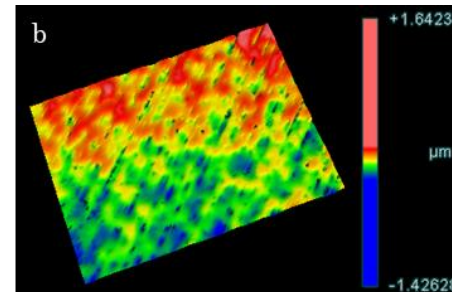
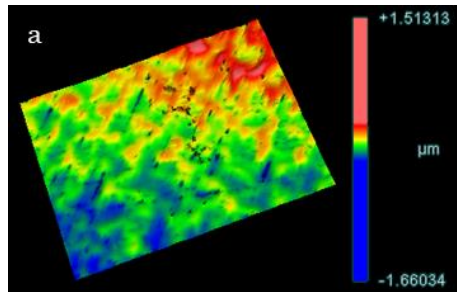
Section b

Section c

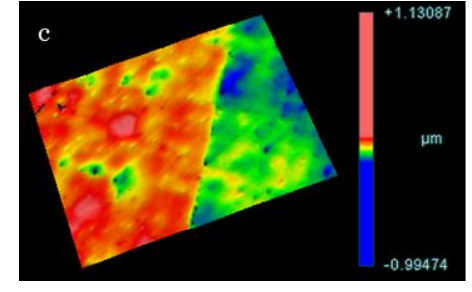
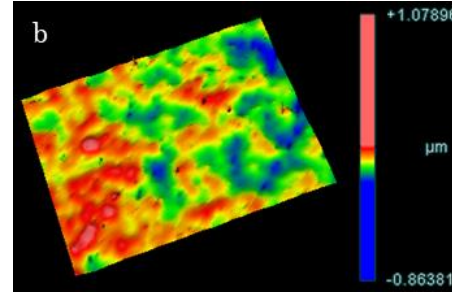
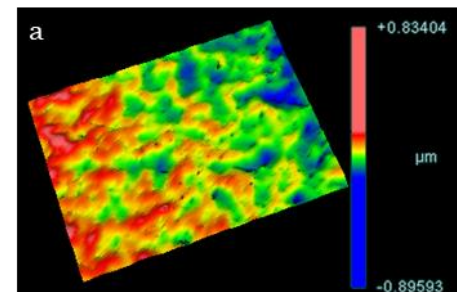
0% Zr



5% Zr



15% Zr



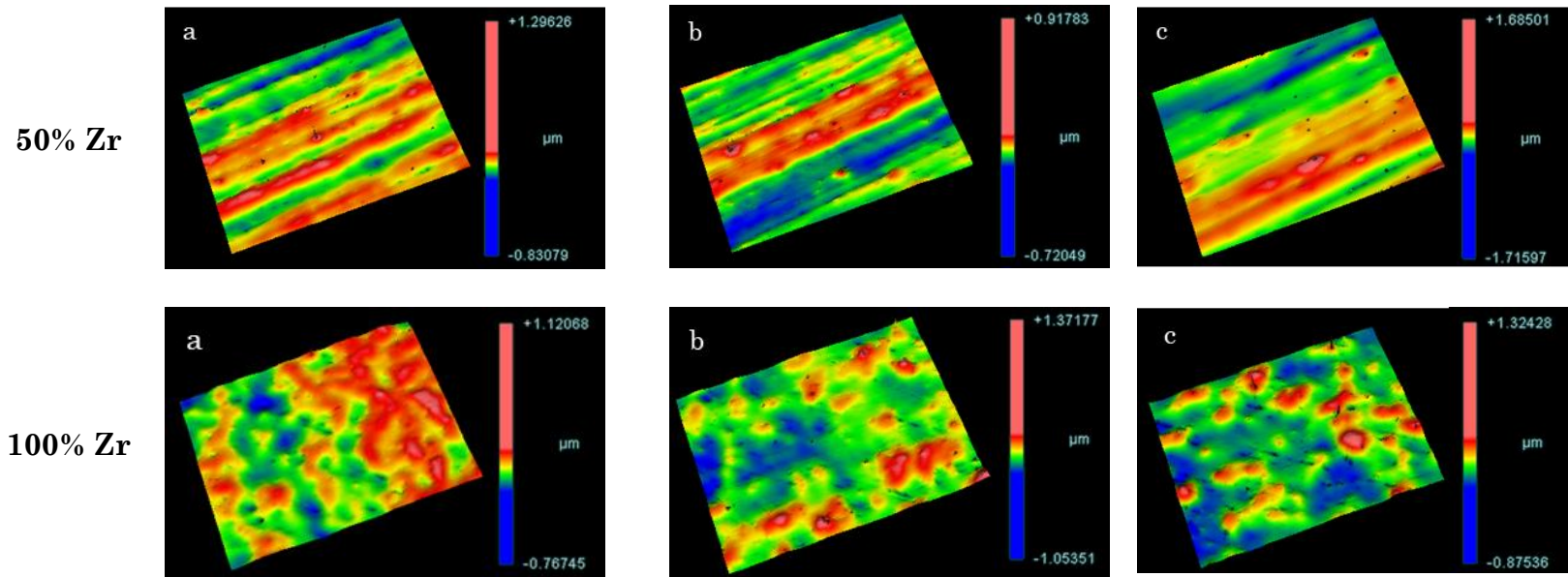


**Figure 46:** Non-contact profilometry representative images showing 3D surface roughness of TiZr discs prepared to a mirror-like finish. Each section is 5x5mm and the colour scale represents depth profiles. The colour scales represent regions of height, with red regions indicated elevated regions from the average (green) and blue regions representing decreased areas of depth from the average.

Figure 47 shows that 15% Zr had the least rough surface, with an average roughness of  $0.047 \pm 0.003 \mu\text{m}$  ( $n=3$ ) whereas 5% Zr had the highest average surface roughness ( $0.070 \pm 0.004 \mu\text{m}$ ;  $n=3$ ). The remaining discs had average surface roughness values of:  $0.064 \pm 0.011 \mu\text{m}$  (0% Zr);  $0.058 \pm 0.021 \mu\text{m}$  (50% Zr) and  $0.068 \pm 0.010 \mu\text{m}$  (100% Zr). Although differences were observed, a one-way ANOVA revealed that there were no significant differences between the surface roughness of the differing TiZr discs ( $p=0.207$ ;  $n=3$ ).

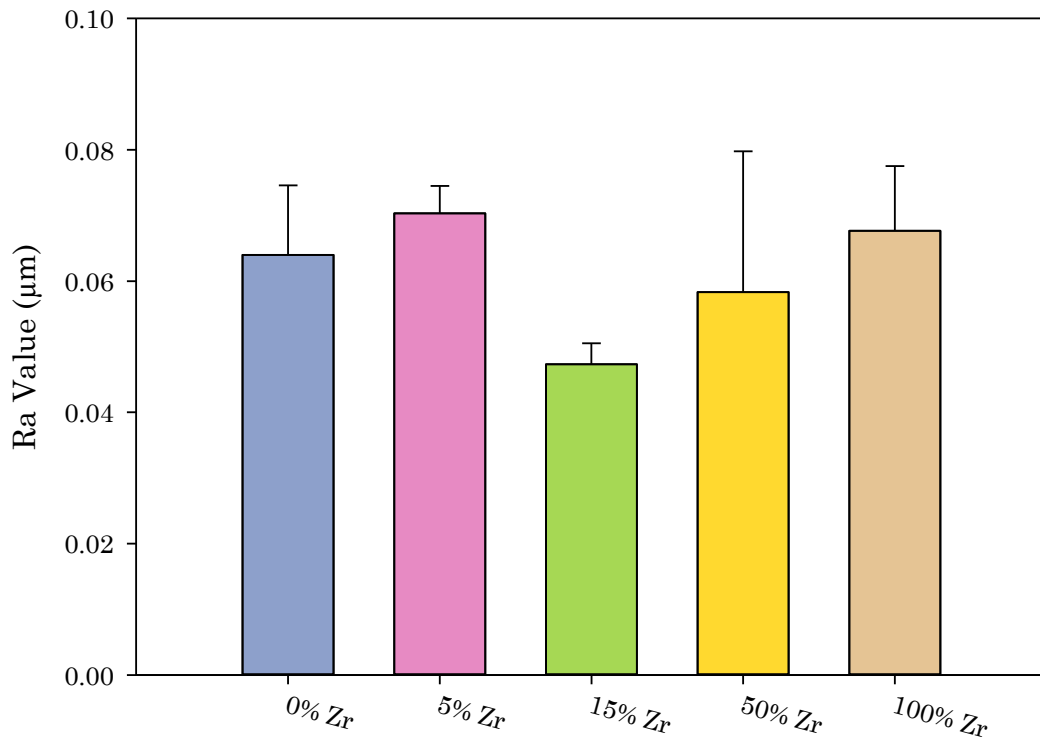


**Figure 47:** Average surface roughness (Ra) values of three 5 x 5 mm sections on prepared mirror-like finished TiZr discs obtained using non-contact profilometry. 15% Zr has the least rough surface, with an average roughness of  $0.047 \pm 0.003 \mu\text{m}$  ( $n=3$ ) whereas 5% Zr has the highest average surface roughness ( $0.070 \pm 0.004 \mu\text{m}$ ;  $n=3$ ). A one-way ANOVA revealed that there were no significant differences between Ra values ( $p=0.207$ ;  $n=3$ ).

The results presented in this section identify that TiZr alloys (5, 15 and 50% Zr) are more favourable substrates when compared to commercially pure grade IV Ti and 100% Zr. Of the TiZr alloys, the results suggest that 15% and 50% Zr induces a more favourable biological responses, in terms of cell attachment, viability and proliferation, which when coupled with the mechanical analysis (detailed and discussed further in Section 4.8) identifies 15% Zr as the more favourable and promising alloy composition.

## Results Section 3

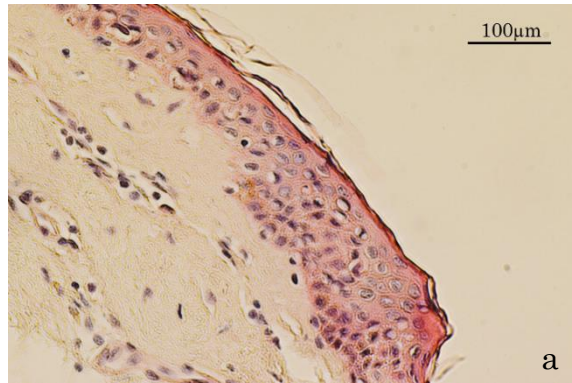
This section presents histological analyses of the efficacy of two commonly used methods to produce de-epidermalised dermis (Takami *et al.*, 1996; MacNeil, Shepherd and Smith, 2011). Data from the 3D oral organotypic cultures that were generated for 7, 14 and 21 days at the air liquid interface (ALI) in different animal-component-free media are presented. Gene expression in the developed 3D oral organotypic cultures were analysed using RT-PCR.

### **3.18. Analysis of the efficacy of preparing de-epidermalised dermis (DED) using two different approaches**

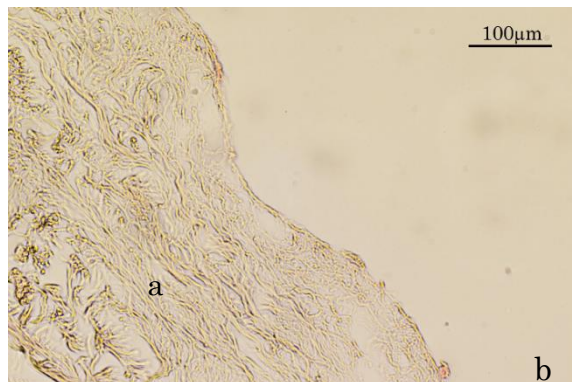
Histological analysis presented in Figure 48 a-c, shows the resultant de-epidermalised dermis after treatment using two commonly used approaches (method one: treatment with dPBS and 1M NaCl; method two: treatment with 0.25% TrypLE, 0.5mM EDTA and 0.5% Triton X-100) (Takami *et al.*, 1996; MacNeil *et al.*, 2011). In comparison with the unprocessed cadaveric skin (Figure 48a), both methods were able to achieve complete de-cellularisation however, small attached fragments of the epidermis were observed; with the most visible attachment apparent on the dermis treated using method two (Figure 48c). Furthermore, the papillary surface of method one processed DED

(Figure 48b) appeared more consistent than the surface generated using method two (Figure 48c), likely due to the ease of separation mechanically following treatment.

**Unprocessed cadaveric skin**



**Processed de-epidermalised dermis using method one (Takami *et al.*, 1996)**



**Processed de-epidermalised dermis using method two (MacNeil, Shepherd and Smith, 2011)**

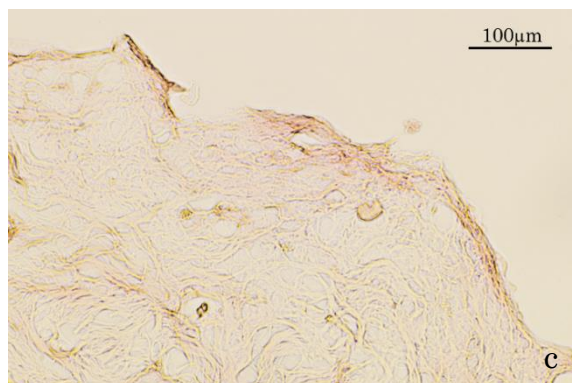


**Figure 48 (a-c):** Representative images of haematoxylin and eosin stained histological sections of unprocessed (a) and processed de-epidermalised dermis (b & c) for the determination of the most effective method of producing DED for use as a 3D oral organotypic models scaffold. Arrows identify epithelium attachment. Sections were cut at a thickness of 4µm. Scale bars are shown.

### **3.19. Histological analysis of 3D oral organotypic models generated in animal-component-free culture media.**

Upon seeding H400 keratinocytes and pHGF cells onto DED, cultures were initially submerged before being raised to the ALI for either 7, 14 or 21 days. Haematoxylin and eosin staining was conducted to analyse the architecture of the developing 3D oral organotypic cultures generated within different the animal-component-free media.

Figure 49 a-f shows H&E stained sections of 3D oral organotypic cultures generated within different animal-component-free media exposed to the air liquid interface (ALI) for 7, 14 and 21 days. Both animal-component-free media were able to generate 3D oral organotypic cultures with varying epithelium thicknesses as exposure time to the ALI was increased. Interestingly, keratinization of the uppermost layer, could be seen in all sections of the 3D models, with more keratinized layers apparent in sections of developed 3D oral organotypic cultures generated in DMEM supplemented with 10% human serum (visible at days 7 and 14). As 3D models were exposed to the ALI for increased time periods, the number of epithelial layers also increased, regardless of culture medium used. Lastly, sections of 3D oral organotypic models cultured in DMEM supplemented with 10% human serum appeared to exhibit more epithelial layers than 3D oral

organotypic models cultured in KGM-CD – which was most apparent at days 14 and 21.

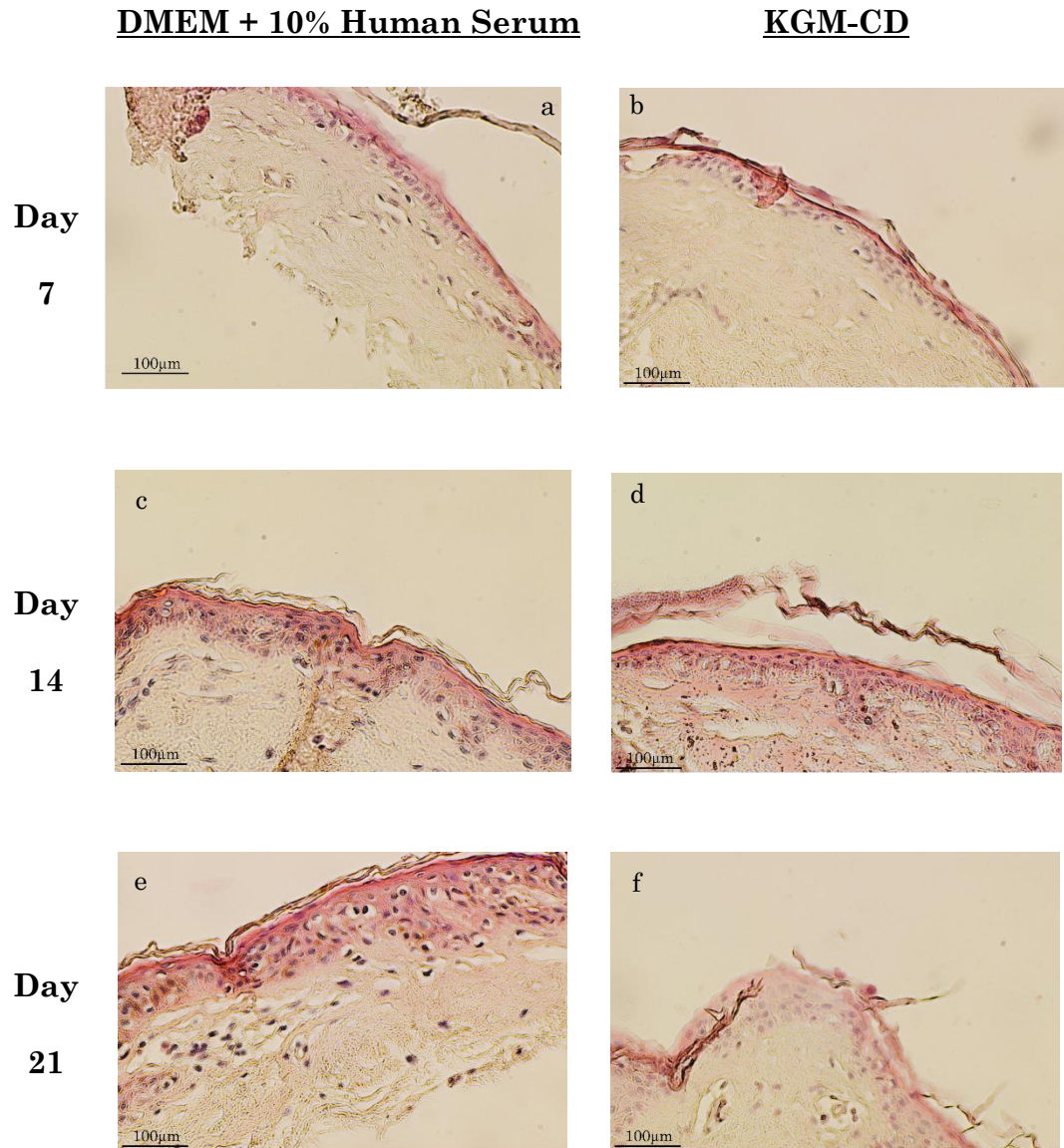


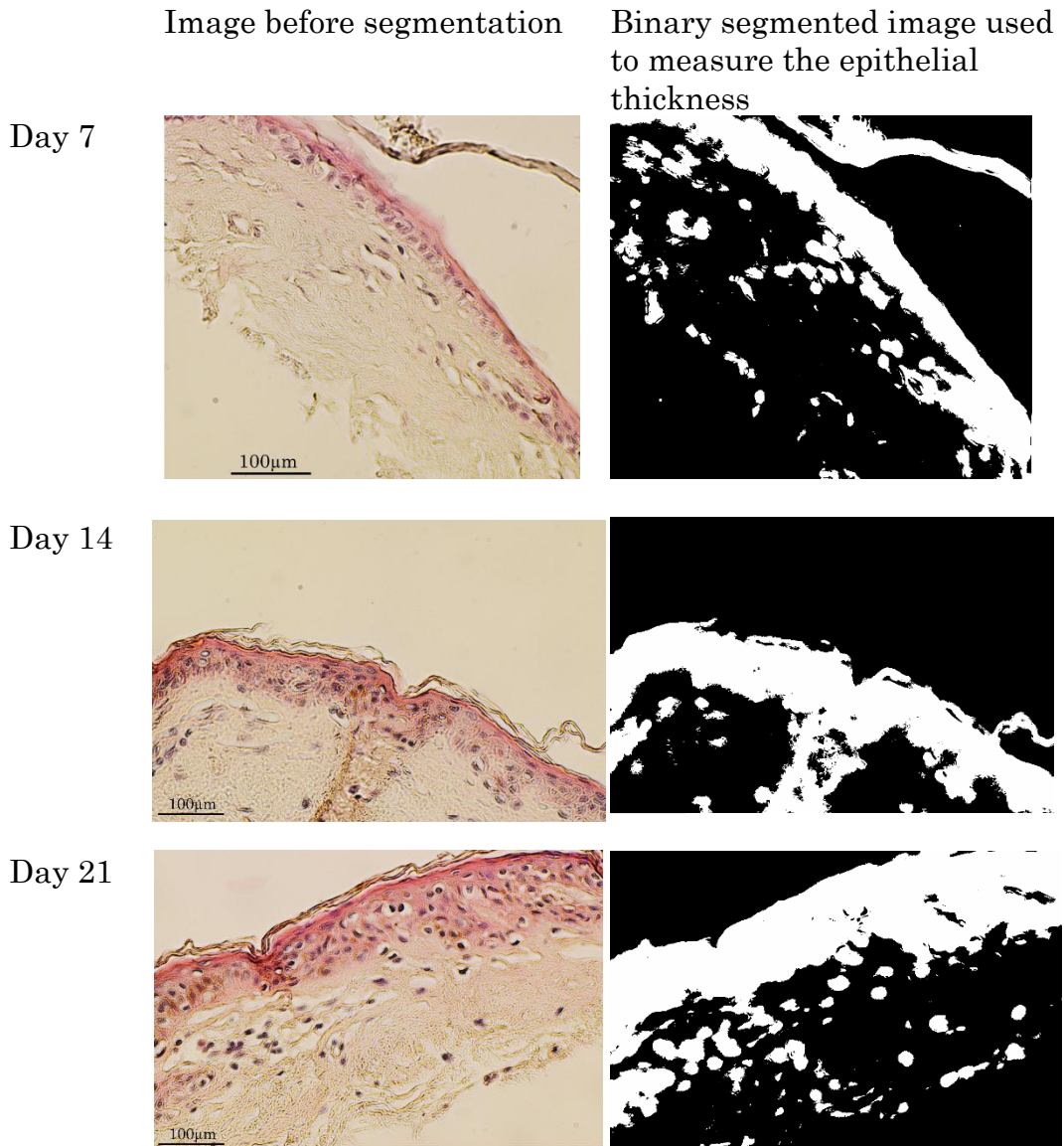
**Figure 49 (a-f):** Haematoxylin and eosin stained sections of 3D oral organotypic models generated within either DMEM supplement with 10% human serum or KGM-CD exposed to the air liquid interface (ALI) for either 7 (a-b), 14 (c-d) or 21 (e-f) days, using DED as the scaffold. Sections were cut at a thickness of 4µm. Scale bars are shown.

### 3.20. Quantification of epithelial thickness

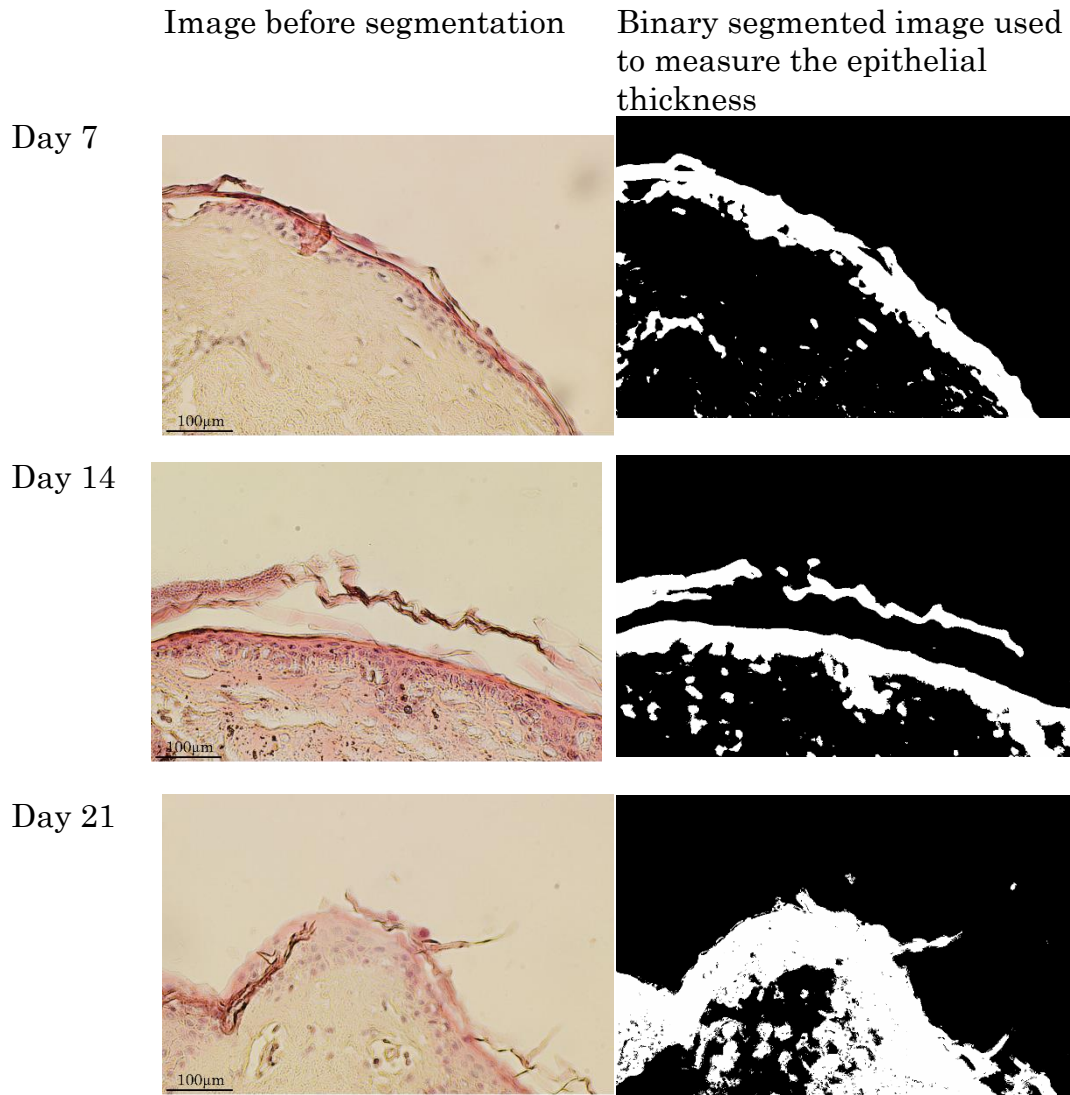
To quantify the H&E stained images obtained (n=3 for all timepoints; represented in Figure 49a-f) the Trainable Weka Segmentation plug-in accessed via FIJI (distribution of the ImageJ software, version 1.15u, National Institutes of Health, Maryland, USA) (Arganda-Carreras *et al.*, 2017) described in Section 2.28 and 2.40, was utilised to measure the epithelial thickness.

Figure 50 and 51 presents the outputted segmented images from the Trainable Weka Segmentation plug-in. and Figure 52 presents the averaged epithelium thickness calculated from the segmented images.

From Figure 52, it can be seen that epithelium thickness increases as the length of time at the ALI increases, regardless of media. Day 21 cultures for both culture environments had the thickest epithelium ( $p < 0.001$ ;  $n=3$ , when compared with Day 7 and 14 epithelium thicknesses). It was also observed that 3D oral organotypic models cultured in DMEM supplemented with 10% human serum generated statically thicker epithelium ( $109.50 \pm 2.94\mu\text{m}$ ) than models cultured in KGM-CD ( $79.45 \pm 4.87\mu\text{m}$ ). This difference was found to be statistically significant upon conduction of a two-way ANOVA, followed by a *post-hoc* Tukey test ( $p=0.012$ ;  $n=3$ ).



**Figure 50:** Haematoxylin and eosin stained sections of 3D oral organotypic models cultured in DMEM supplemented with 10% human serum, with their corresponding segmented images, where the epidermis is shown as white and the background in black.



**Figure 51:** Haematoxylin and eosin stained sections of 3D oral organotypic models cultured in KGM-CD, with their corresponding segmented images, where the epidermis is shown as white and the background in black.

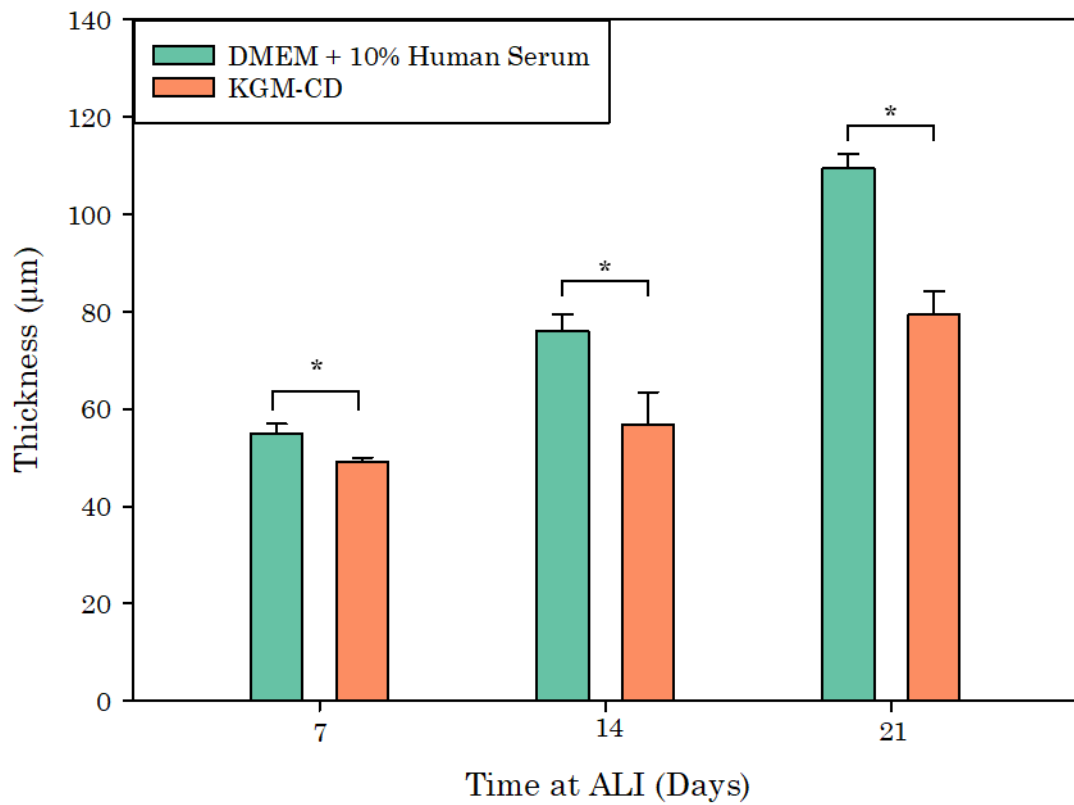


**Figure 52:** Calculated epithelium thickness from the segmented images presented in Figures 50 and 51. 3D oral organotypic models cultured in DMEM supplemented with 10% human serum had statistically significantly thicker epithelium when compared to KGM-CD counterpart ( $p = 0.012$ ; denoted by \*). Error bars represent one standard deviation from the mean ( $n=3$ ).

### **3.21. Gene expression analysis of 3D oral organotypic models generated in animal-component-free culture media.**

Figures 53a-c show data comparing gene expression levels for developed 3D oral organotypic models cultured in either DMEM supplemented with 10% human serum or KGM-CD after being grown at the ALI for 7, 14 and 21 days. Data were analysed using RT-PCR and are expressed as a ratio to the reference housekeeping gene YWHAZ.

It is apparent from Figure 53a, that expression ratios of all genes tested on day 7 - except for vimentin - were expressed at a higher ratio in the developed 3D oral organotypic models cultured in DMEM supplemented with 10% human serum than KGM-CD. A two-way ANOVA followed by *post-hoc* Tukey tests identified that expression ratios of CK1 ( $p=0.009$ ;  $n=3$ ), CK10 ( $p=0.031$ ;  $n=3$ ), CK13 ( $p=0.007$ ;  $n=3$ ) and n-cadherin ( $p=0.05$ ;  $n=3$ ) were statistically significantly higher. No statistical differences were found between transcript levels for CK5, Ki-67, e-cadherin, vimentin or collagen VII between developed 3D oral organotypic models ( $p>0.05$ ;  $n=3$ ).

Figure 53b, provides data indicating that after 14 days, gene expression ratios were at a higher level in 3D oral organotypic models cultured within DMEM supplemented with 10% human serum than 3D

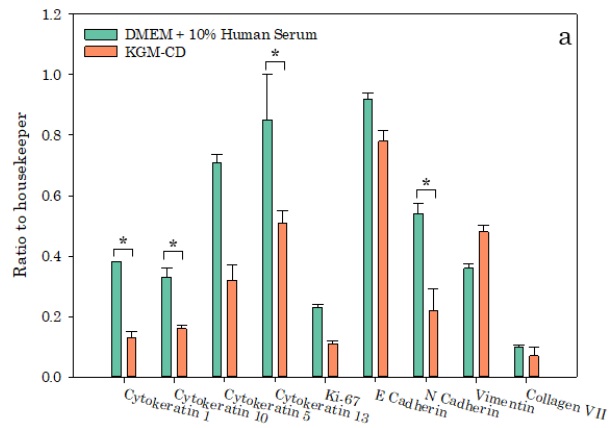
oral organotypic models cultured in KGM-CD. Following statistical analysis (two-way ANOVA followed by *post-hoc* Tukey tests) all gene expression ratios apart from vimentin ( $p > 0.05$ ;  $n=3$ ) were identified to be statistically higher in DMEM supplemented with 10% human serum than 3D oral organotypic models cultured KGM-CD ( $p < 0.05$  (denoted by \*) or  $p < 0.001$  (denoted by \*\*\*)).

Similarly, to Figure 53a and 53b, after 21 days, expression ratios presented in Figure 53c show that levels of all transcripts were higher in 3D oral organotypic models cultured within DMEM supplemented with 10% human serum. A two-way ANOVA followed by *post-hoc* Tukey tests identified that the aforementioned observation was statistically significant;  $p < 0.05$  (denoted by \*) or  $p < 0.001$  (denoted by \*\*\*), in all expression ratios apart for n-cadherin and vimentin ( $p > 0.005$  ;  $n=3$ ).

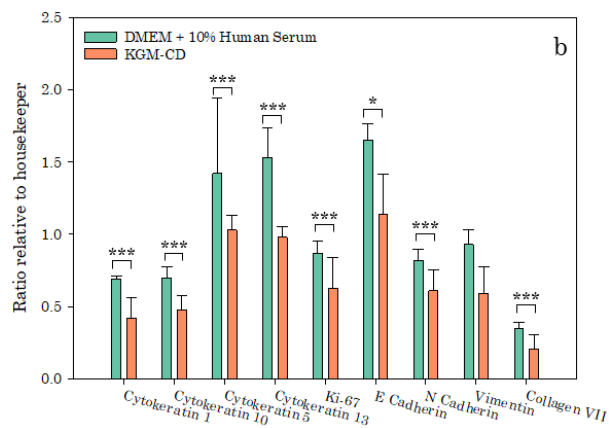
Two-way ANOVA was also used to compare expression ratios of the gene expressed in the 3D oral organotypic models in the same culture medium from all three time-periods. In general the gene expression ratios in 3D oral organotypic models cultured in DMEM supplemented with 10% human serum significantly increased as the number of days at the ALI increased (all p-values were less than 0.05) with the exception of the vimentin expression ( $p > 0.05$ ;  $n=3$ ) and n-cadherin ( $p < 0.05$ ;  $n=3$ ) ratios, where no significant differences were found.

For the analysis of the 3D oral organotypic models in KGM-CD, it was found that there were no statistical significance differences between gene expression ratios on day 7 ( $p>0.05$ ;  $n=3$ ) or day 14 ( $p>0.05$ ;  $n=3$ ) for the genes analysed, however when compared with the day 21 expression ratios it was found that day 21 exhibited statistically higher expression ratios for all genes, apart from vimentin, than day 14 and day 7 expression ratios ( $p>0.05$ ;  $n=3$ ).

Day 7



Day 14



Day 21

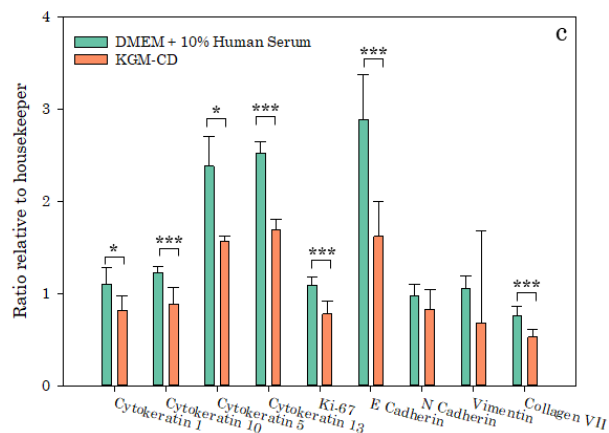


**Figure 53 (a-c):** Gene expression levels in 3D oral organotypic models grown at the air liquid interface for (a) 7, (b) 14 and (c) 21 days expressed as a ratio relative to the housekeeper gene *YWHAZ*. Statistical significance was determined using a two-way ANOVA followed by post-hoc Tukey test (\*  $p < 0.05$ , \*\*\*  $p < 0.001$ ). Error bars represent one standard deviation from the mean ( $n = 3$ ).

## Results Section 4

The results presented in this section are generated from experiments designed to investigate the use of hydrogels as potential scaffolds for the development of a 3D oral organotypic culture model. To determine scaffold suitability for this application, mechanical and biological tests were undertaken.

### **3.22. Mechanical properties of RGD modified alginate**

Compressive testing is important in the identification of a suitable scaffold as it provides insight towards the scaffold's ability to withstand compressive forces, particularly the range that oral mucosa is exposed to. Figure 54 presents stress-strain curve data for 1, 3 and 5 wt% alginate and RGD modified alginate hydrogel discs under compressive load. Despite varying weight percentages and modifications, all four hydrogel discs generated similar overall stress/strain profiles. 5 wt% alginate discs were able to withstand more compressive load compared with all the other samples.

Due to the unequal and non-parametric nature of the datasets, determined by failure of Shapiro-Wilk test, a Kruskal Wallis-H test followed by a Student Newman-Keuls *post-hoc* test was conducted which identified that 5wt% alginate had a statistically significantly higher elastic modulus than all other alginates ( $p < 0.001$ ;  $n=3$ ). 3wt%

alginate had a statistically higher modulus compared with 1wt% alginate ( $p < 0.001$ ;  $n = 3$ ) and RGD modified alginate ( $p < 0.001$ ;  $n = 3$ ).

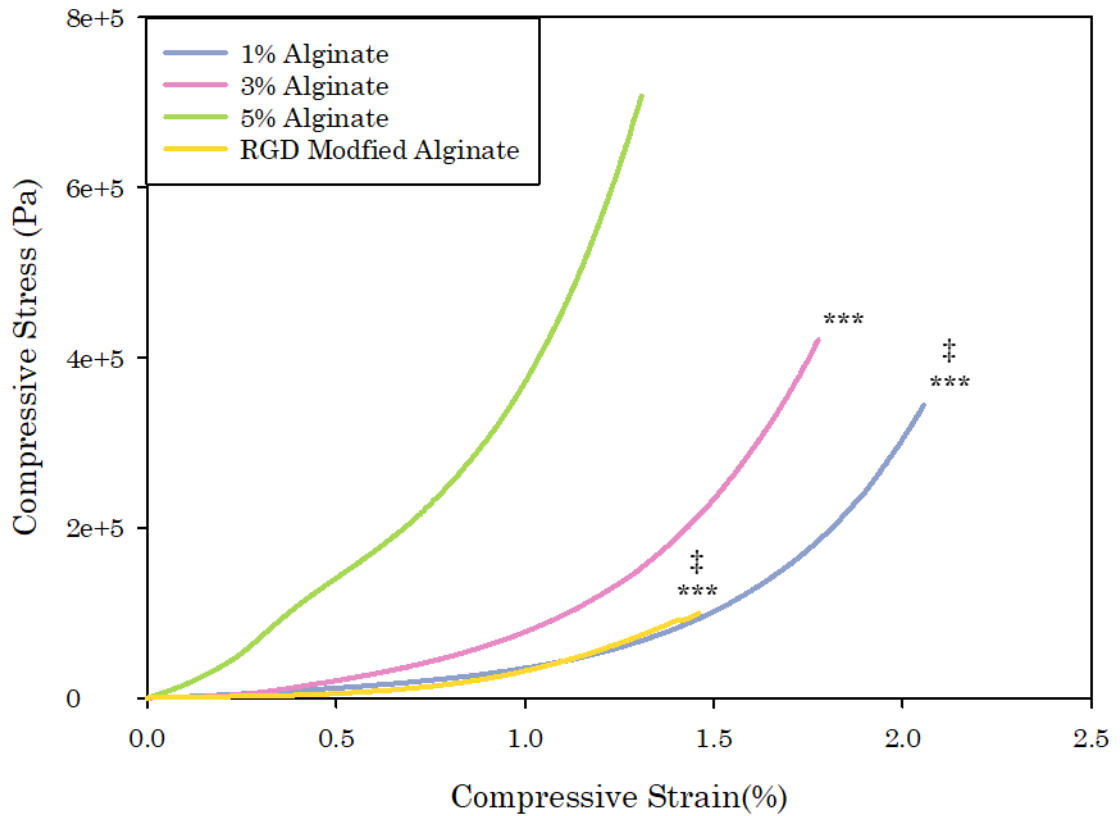


**Figure 54:** Stress-strain curves of different weight percent alginate hydrogel discs and RGD modified alginate hydrogel discs under compressive force. All hydrogel curves had similar overall shapes and all curves are plotted until fracture point. Kruskal Wallis-H test followed by a Student Newman-Keuls *post-hoc* test identified that 5wt% alginate had a significantly higher elastic modulus than all other alginates ( $p < 0.001$ , denoted by \*\*\*) and 3wt% alginate had a statistically higher modulus compared with 1wt% and RGD modified alginate ( $p < 0.001$ , denoted by §) ( $n = 3$ ).

Table 16 presents the calculated compressive strength moduli for the different wt% alginates and RGD modified alginate. Using the Kruskal

Wallis-H test followed by a Student Newman-Keuls *post-hoc* test, due to the non-parametric nature of the data, it was found that 1wt% alginate exhibited a significantly lower compressive modulus when compared with 5wt% alginate ( $p=0.012$ ;  $n=3$ ), 3wt% alginate ( $p=0.020$ ;  $n=3$ ) and RGD modified alginate ( $p=0.05$ ;  $n=3$ ). The compressive modulus of RGD modified alginate was significantly lower when compared with 3wt% alginate ( $n=0.05$ ;  $n=3$ ) and 5wt% alginate ( $n=0.020$ ;  $n=3$ ). 3wt% alginate had a significantly lower compressive modulus than 5wt% alginate ( $p=0.050$ ;  $n=3$ ).

**Table 16:** Calculated compressive moduli of the different weight percent alginate hydrogel discs and RGD modified alginate hydrogel discs

<b>Alginate type</b>	<b>Compressive modulus <math>\pm</math> standard error (MPa)</b>
1wt% Alginate	1.43 $\pm$ 0.11
3wt% Alginate	2.42 $\pm$ 0.08
5wt% Alginate	2.47 $\pm$ 0.14
RGD Modified Alginate	1.65 $\pm$ 0.05

The mass loss studies of the different alginate hydrogels incubated in saline for either 1 or 7 days showed that RGD modified alginate discs experienced the greatest loss of mass when compared with the other alginate discs on both days (shown in Figure 55). Furthermore, regardless of composition or weight percentage, hydrogel discs experienced the most mass loss after 7 days when compared with day 1

samples; with the most evident mass loss occurring in hydrogels discs made from 3wt% alginate. A two-way ANOVA revealed that the observed trends were not statistically significant ( $p>0.05$ ;  $n=3$ ).

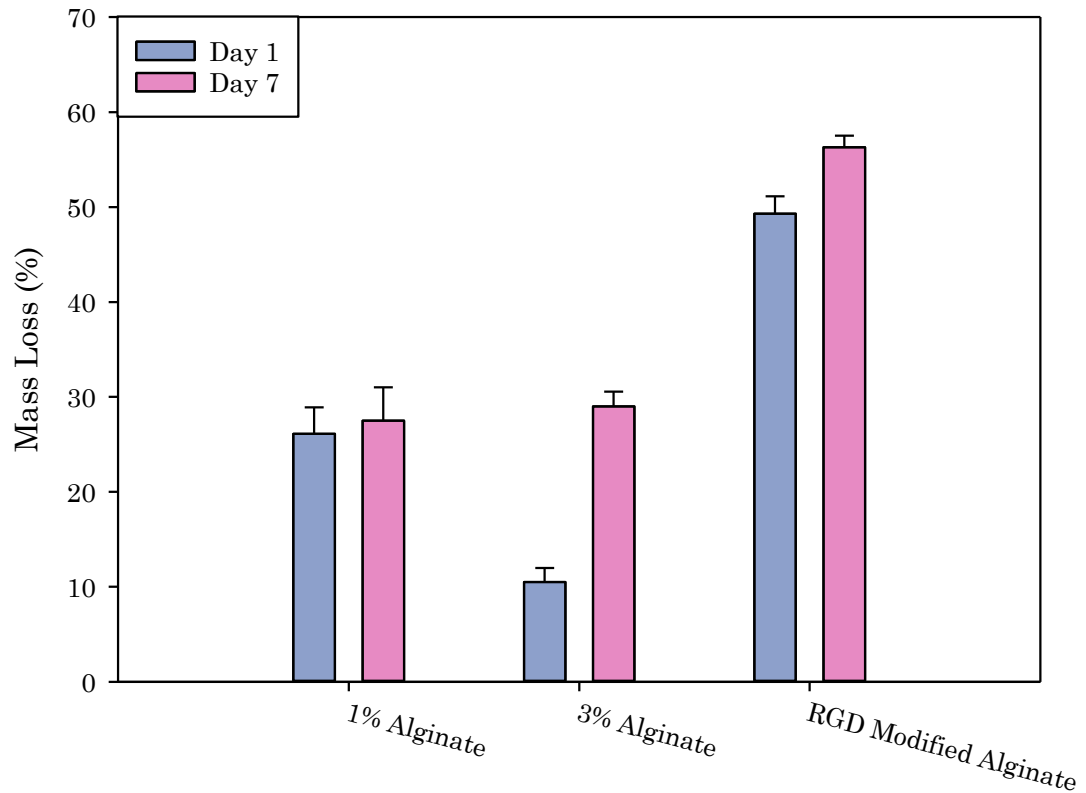


**Figure 55:** Mass loss graphs for different weight percent alginate hydrogel discs and RGD modified alginate hydrogel discs. All hydrogel discs decreased in mass after 7 days incubation compared with day 1 samples, with the most noticeable difference in loss of mass occurring in 3wt% alginate discs. RGD modified alginate decreased with the most mass during the experimental period. A two-way ANOVA revealed that observations were not statistically significant ( $p>0.05$ ) Error bars represent one standard deviation from the mean ( $n=3$ ).

### 3.23. The effect of hydrogel reagents on pHGF cultures

Alginate hydrogels are widely used within biomedical research due to favourable properties and biocompatibility when used in several applications (Lee and Mooney, 2012; Sun and Tan, 2013). However, it is imperative to understand how the reagents used to fabricate and dissolve these hydrogels affect cell cultures especially if used as a potential scaffold when developing 3D oral organotypic cultures.

Figure 56 presents growth curves of pHGF cultures exposed to either 0.1M calcium chloride, which was used to cross-link and form the hydrogel and 0.1M sodium citrate used to dissociate hydrogels after which cells were grown for 21 days. Cultures exposed to 0.1M calcium chloride apparently were able to proliferate and yield similar numbers of viable cells when compared with the unexposed control whereas cultures exposed to 0.1M sodium citrate appeared to be growth inhibited and did not reach similar numbers of viable cells. A Kruskal-Wallis H test followed by a Student Newman-Keuls *post-hoc* test was conducted which revealed that cultures exposed to 0.1M sodium citrate had significantly lower numbers of viable cells when compared with both the control ( $p=0.037$ ;  $n=3$ ) and cultures exposed to calcium chloride ( $p=0.004$ ;  $n=3$ ). No significant difference was found between the number of viable cells exposed to 0.1M calcium chloride or the control at any time point.

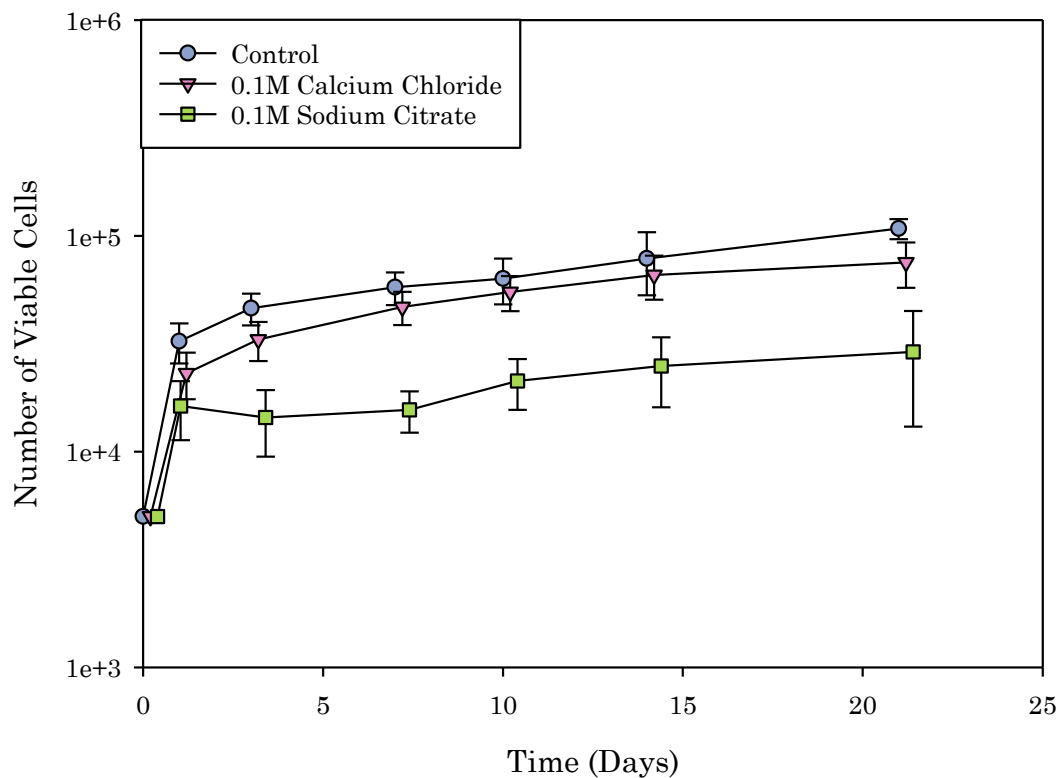


**Figure 56:** pHGF growth curves after exposure to different reagents involved in fabricating and dissolving alginate hydrogel discs (0.1M calcium chloride and 0.1M sodium citrate) for 21 days. A Kruskal-Wallis H test followed by a Student Newman-Keuls *post-hoc* test, identified that pHGF cultures exposed to 0.1M sodium citrate generated statically significant lower cell numbers compared with pHGF cultures grown in supplemented culture media (control) and pHGF cultures exposed to 0.1M calcium chloride ( $p=0.037$  and  $p=0.004$  respectively;). No significant difference in viable cell numbers was identified between the control cell cultures and cultures exposed to 0.1M calcium chloride ( $p=0.447$ ). Error bars represent one standard deviation from the mean and each group has been jittered 0.2 days along the x-axis for presentation ( $n=3$ ).

Cell viability was also monitored during the experimental period and data is presented in Figure 57. There was minimal apparent difference between the viability of pHGF cultures exposed to 0.1M calcium

chloride and the controls which was further supported by the statistical analysis; a one-way ANOVA followed by a *post-hoc* Tukey test (0.883; n=3). Additionally, the observed reduction in viability of pHGF cultures exposed to 0.1M sodium citrate when compared with the control and cultures exposed to 0.1M calcium chloride- was also found to be statistically significant ( $p < 0.05$  for both comparisons).

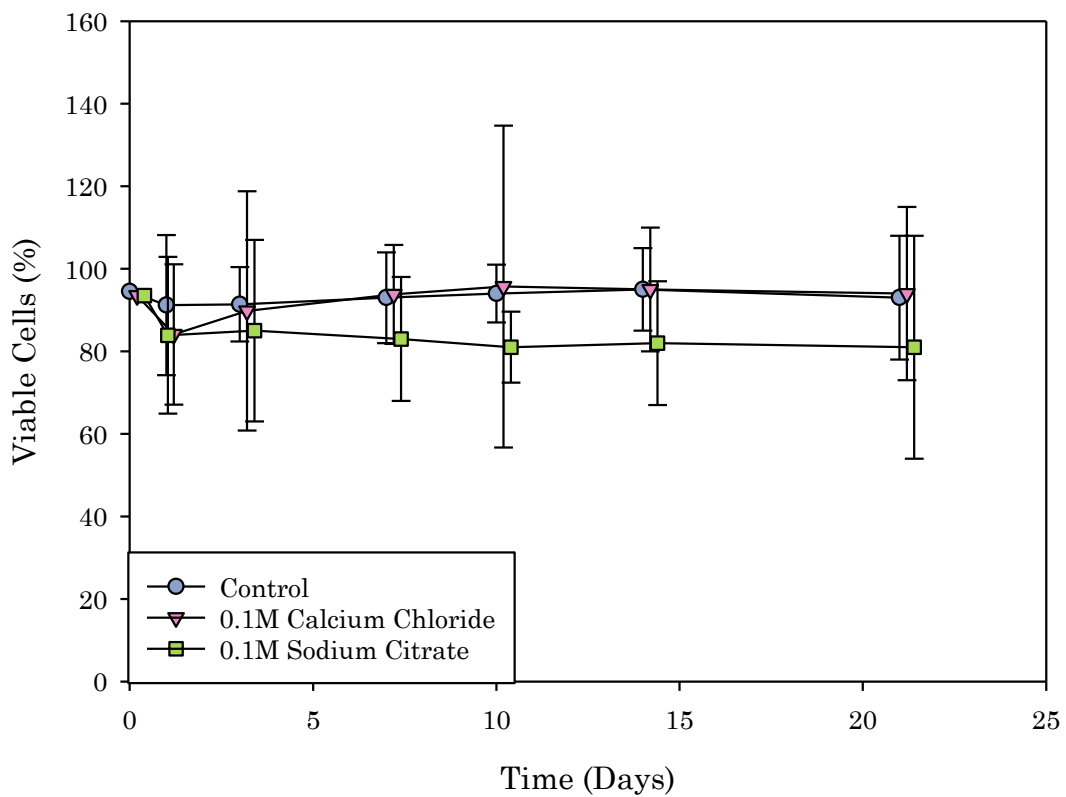


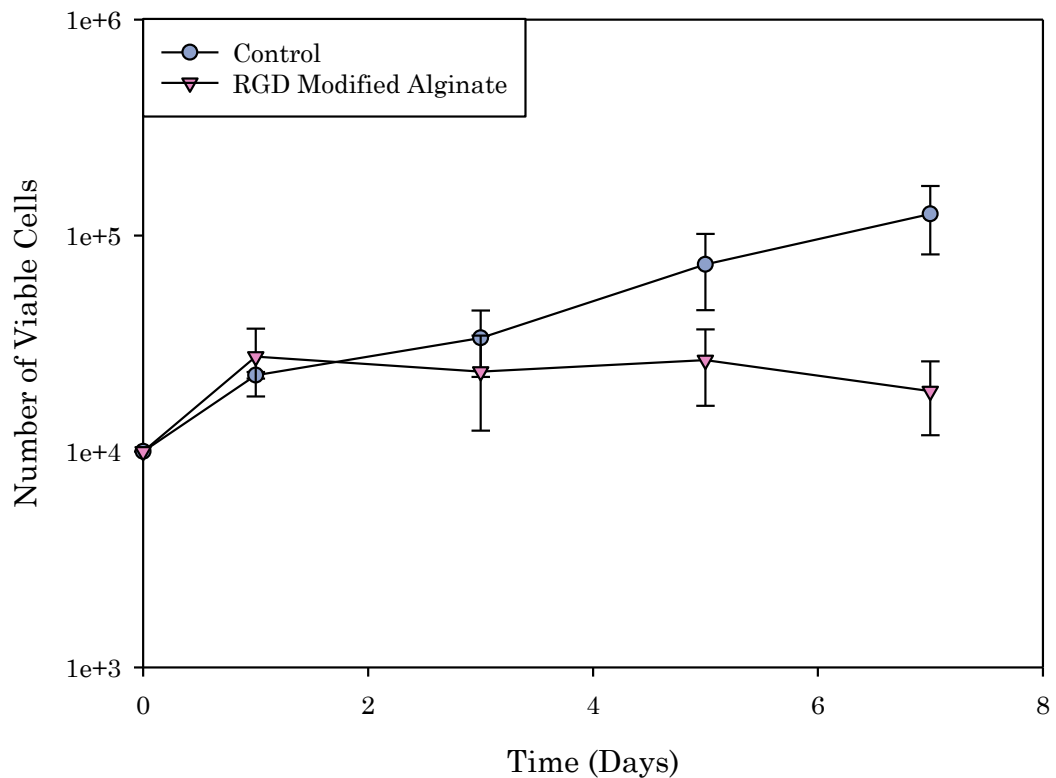
**Figure 57:** Viability of pHGF cultures exposed to either 0.1M calcium chloride or 0.1M sodium citrate for 30 minutes and subsequently grown in KGM-CD for 21 days. A one-way ANOVA followed by a *post-hoc* Tukey test revealed that pHGF cultures exposed to 0.1M sodium citrate exhibited lower yields of viable pHGF cells when compared with both the control and cultures exposed to 0.1M calcium chloride ( $p < 0.001$ ). No statistically significant differences were detected in cell viability between the control and cultures exposed to 0.1M calcium chloride ( $p = 0.883$ ). Error bars represent one

standard deviation from the mean and each group has been jittered 0.2 days along the x-axis for clarity (n=3).

### **3.24. Biological influence of RGD modified alginate**

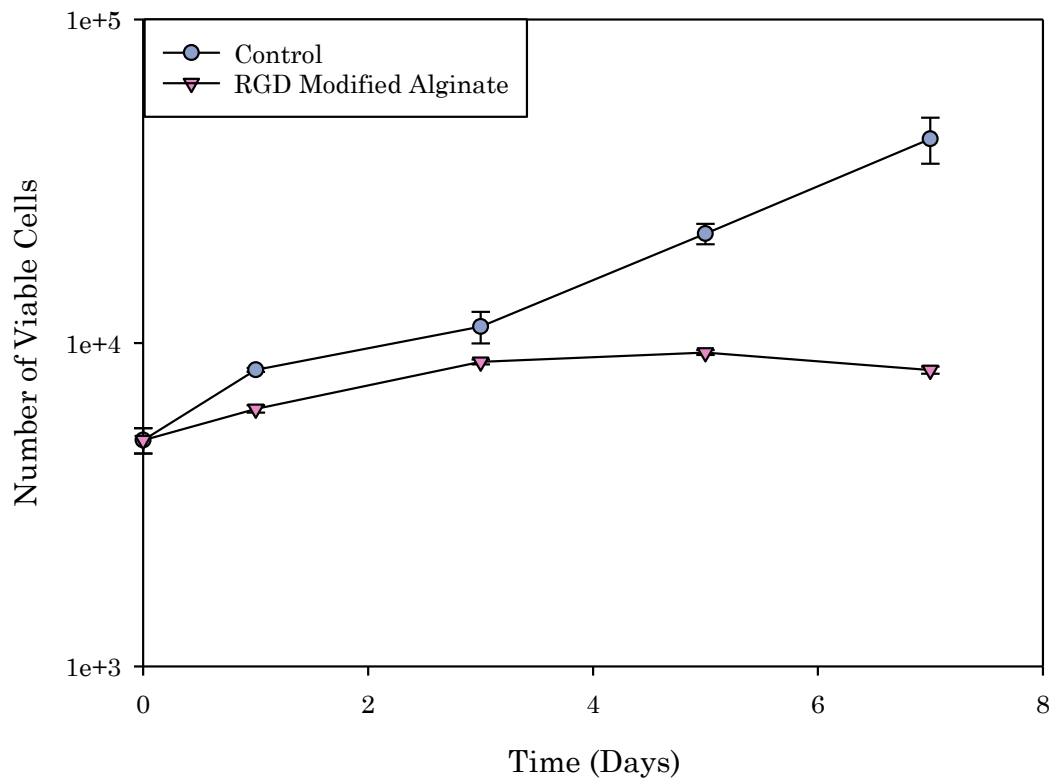
Cells are unable to directly attach to the alginate matrix due to no adhesion motifs being present along the polysaccharide backbone, therefore to encourage cell attachment which in some circumstances positively affect cell viability, alginates are commonly modified with adhesion promoting peptides (Rosso *et al.*, 2004; Khan and Ahmad, 2013; Andersen *et al.*, 2015).

Figure 58 depicts the growth curves of pHGFs cultured following release from RGD modified alginate encapsulation. Although there appeared to be a difference in number of viable cells from day 3, which increased as the experimental period progressed, a one-way ANOVA revealed that this difference was not significant as  $p=0.174$  (n=3).



**Figure 58:** Growth curves of pHGF cell cultures following release from encapsulation within RGD modified alginate hydrogel discs for 7 days. No statistical difference in terms of the number of viable cells was found using a one-way ANOVA ( $p=0.174$ ). Error bars represent one standard deviation from the mean ( $n=3$ ).

Figure 59 presents data obtained from H400 cell cultures attached to the surface of RGD modified alginate hydrogels discs. There was an apparent difference in viable cell numbers from day 1, which identified that more viable cells were encapsulated within the control than modified RGD alginate, however, a one-way ANOVA revealed that this difference was not significant as  $p=0.150$ .



**Figure 59:** Growth curves of H400 cell cultures attached to the surface of RGD modified alginate hydrogel discs for 7 days. No statistically significant differences were detected between groups using a one-way ANOVA ( $p=0.150$ ). Error bars represent one standard deviation from the mean ( $n=3$ ).

Despite the results presented in Figures 58 and 59 not being statistically significant, the results are biologically relevant, and suggest that both cell types struggle to adapt to the RGD modified alginate; signified as a reduced number of viable cells when compared to the control.

### **3.25. Mechanical properties of polyethylene glycol di-methacrylate**

Unlike alginate, polyethylene glycol di-methacrylate (PEG-DM) is a commonly used non-degradable synthetic polymer, which can be modified and adapted for long term use in biomedical research (Zhu and Marchant, 2011; Parlato *et al.*, 2014). Prior to modification, understanding the polymer's mechanical properties is essential to initially assess the suitability of PEG-DM as a potential scaffold material and to provide insight towards the effects of functionalising with bioactive proteins.

Figure 60 presents stress-strain curves for different modulations of PEG-DM hydrogels under compressive force. Table 17 presents the calculated compressive strength moduli based on the data presented in Figure 57. Data indicated that both 20wt% PEG-DM hydrogels had higher yield strengths and compressive moduli when compared with 10wt% PEG-DM hydrogels. Data presented in Figure 57 demonstrated that the 10wt% PEG-DM hydrogels were more ductile than 20wt% gels. A two-way ANOVA followed by a *post-hoc* Tukey test revealed that the observations were statistically significant and that 20wt% PEG-DM hydrogels were able to withstand greater compressive loads ( $p < 0.001$ ;  $n = 3$ ) and had higher compressive moduli ( $p = 0.012$ ;  $n = 3$ ) than 10% PEG hydrogels. Interestingly, varying the percentage of

photoinitiator had no effect on the overall yield strength or compressive moduli as  $p > 0.05$  for either result ( $n=3$ ).

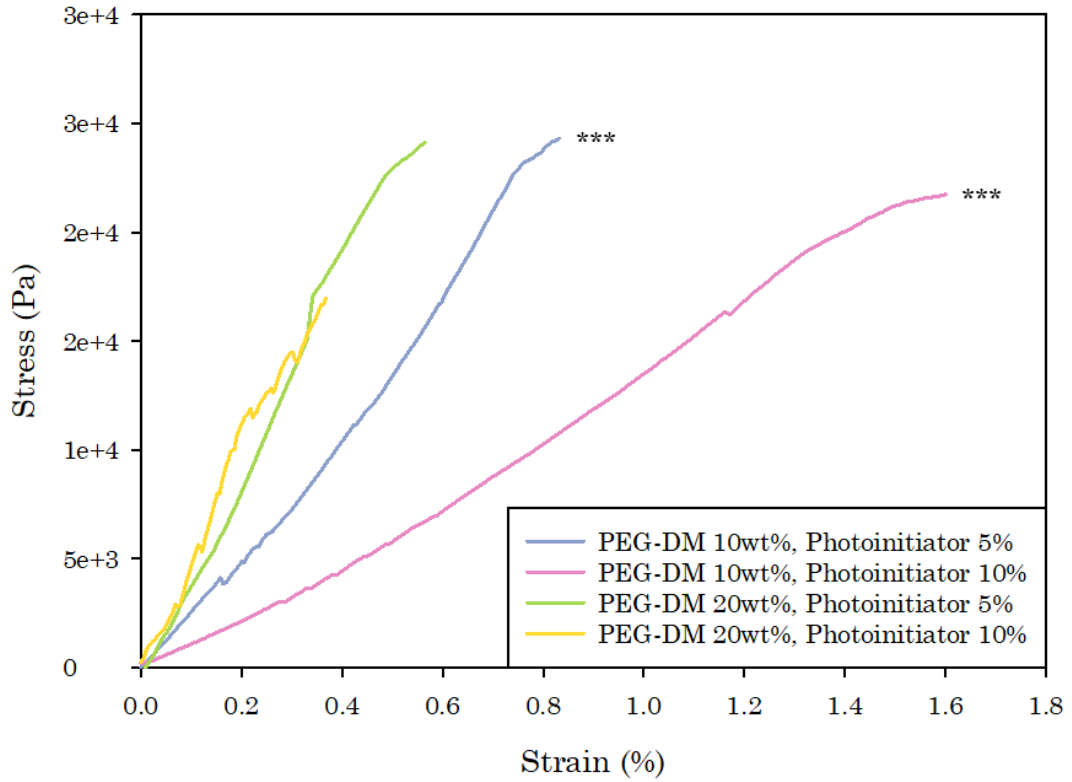


**Figure 60:** Stress-strain curves of different modulations of PEG-DM hydrogels under compressive force. All hydrogel curves had similar overall shapes and all curves are plotted until fracture point. A two-way ANOVA followed by a *post-hoc* Tukey test revealed that 20wt% PEG-DM hydrogels were able to withstand greater compressive loads ( $p < 0.001$ , denoted by \*\*\*) ( $n=3$ ).

**Table 17:** Calculated compressive moduli of different compositions of PEG-DM hydrogel discs

<b>Hydrogel composition</b>	<b>Compressive modulus <math>\pm</math> standard error (KPa)</b>
PEG-DM 10wt%; 5% Photoinitiator	0.94 $\pm$ 0.08
PEG-DM 10wt%; 10% Photoinitiator	1.58 $\pm$ 0.10
PEG-DM 20wt%; 5% Photoinitiator	3.74 $\pm$ 0.07
PEG-DM 20wt%; 10% Photoinitiator	2.89 $\pm$ 0.06

Figure 61 shows the mass loss studies of the different modulations of PEG-DM hydrogels incubated in saline for either 1 or 7 days. It can be seen that 20wt% PEG-DM hydrogel discs experienced the greatest loss of mass when compared with 10wt% PEG-DM hydrogels. It can also be seen that although 10wt% PEG-DM hydrogel initially lost mass after 1 day in incubation, after 7 days, the hydrogels appeared to gain approximately 5% in mass. Analysis using one-way ANOVA- revealed that the observed differences were not statistically significant as  $p > 0.05$  ( $n=3$ ).

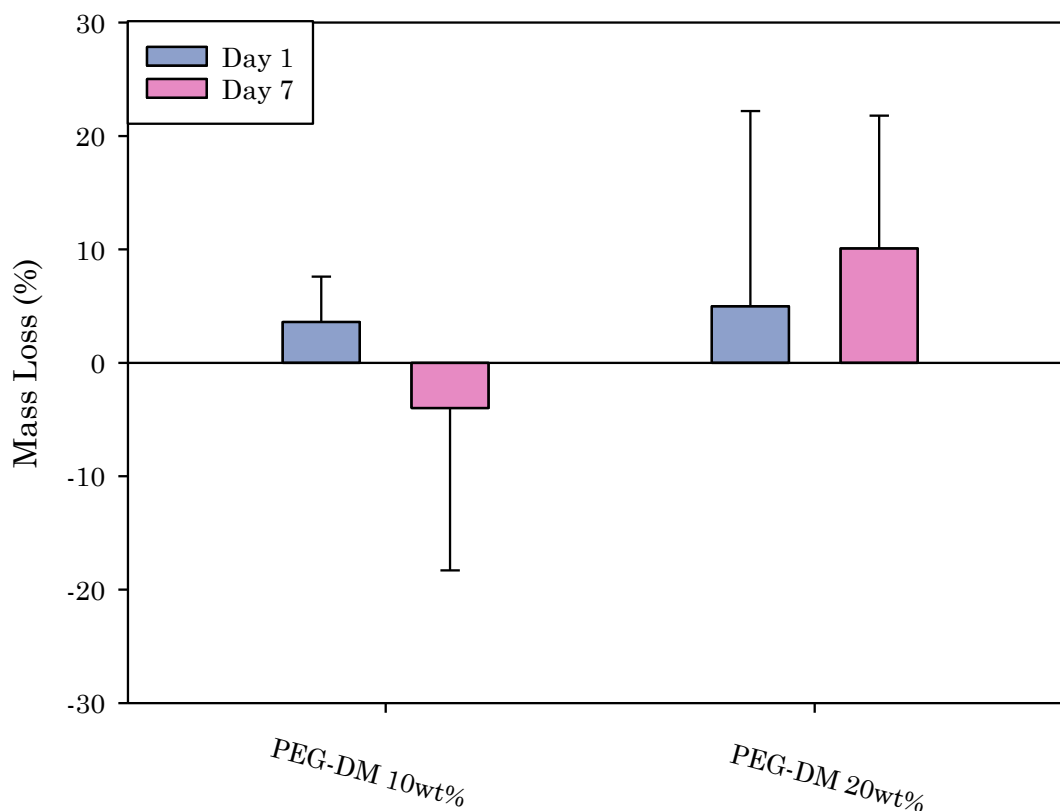


**Figure 61:** Mass loss graphs for 10wt% or 20wt% PEG-DM hydrogel discs. PEG-DM 20wt% hydrogels appeared to lose the most mass, with the greatest mass loss occurring up to Day 7. PEG-DM 10wt% hydrogels appeared to initially lose mass after 1 day of incubation however gained approximately 5% mass after 7 days. Statistical analysis revealed that observations were not significantly different as  $p > 0.05$ . Error bars represent one standard deviation from the mean ( $n=3$ ).

The results presented in this results section indicate that all the mechanically tested hydrogels have the potential to be used as scaffolds when looking to construct a 3D oral organotypic model that is biologically similar. This is due to the tested hydrogels having compressive strength capacity that falls in line with the reported strength capacity of oral mucosa.

CHAPTER 4:  
DISCUSSION

# Discussion of Section 1 Results

The results discussed in this section arise from research aimed at identifying a suitable commercially available animal-component free media for the development of a 3D model of oral mucosa using organotypic cultures. Prior to generating these cultures, it was essential to understand how an animal-component free environment affected behaviour of keratinocyte and fibroblast cultures; with the results obtained, dictating subsequent culture conditions for future experimental work.

## **4.1. The effects of human serum supplementation**

Cultures grown in 10% human serum were able to proliferate unrestrictedly and maintain a high percentage (>75%) of viable keratinocytes for up to 21 days in comparison with both 5% and 2% serum supplementation. The differences in cell number observed could be attributed to 10% serum supplementation providing necessary growth factors and hormones required to support culture proliferation and growth, resulting in the increase of cell numbers observed.

Furthermore, it could be speculated that 2% and 5% serum supplementation, only provided the necessary nutrition for cultures of initial seeding number with minimal support increases in cell number.

The findings of the growth curve analysis concur with previous research conducted by Naseer *et al.* (2009), which identified that increasing the FBS supplementation from 1% to 5% increased both the cell number and viability of seeded cultures. It should be highlighted that Naseer *et al.* (2009) used FBS, rather than human serum and whilst there are compositional differences between both, Isaac *et al.* (2011) identified that there was no significant differences in proliferation between human fibroblasts cultures grown in DMEM supplemented with human serum or FBS.

The findings from the growth curve and viability experimental work led to the suggestion that 10% human serum supplementation was the most appropriate percentage of serum supplementation to be used as control for future experimental work.

#### **4.2. Identification of a suitable mitomycin C concentration for the generation of pHGF feeder layers**

Mitomycin C is commonly used to arrest proliferation of fibroblasts to generate mitotically inactive feeder layers used to support the culturing of primary keratinocytes. Concentrations and exposure time widely vary within the literature, from 0.4µg/ml to 4mg/ml and 30 minutes to 24 hours, therefore identification of a suitable concentration

for this research was essential (Ponchio *et al.*, 2000; Li *et al.*, 2014; Llamas *et al.*, 2015).

All of the concentrations of mitomycin C tested inhibited proliferation of fibroblast cultures. The results of the Kruskal-Wallis H test revealed that there were no significant differences in cell number or viability between the experimental cultures. This observation was consistent with the work of Ponchio *et al.* (2000), who found that concentrations of mitomycin C at a range between 0.2 and 10 µg/ml exposed to cultures for 3 hours, were able to inhibit proliferation without adverse effects on cell viability. Furthermore, sensitivity to the dose of mitomycin C was dependant on cell type and line, which therefore suggests that fibroblasts isolated from different anatomical sites could have different sensitivities to mitomycin C, thus highlighting the importance of investigating concentration prior to further experimental work. Interestingly, Chen *et al.* (2006), explored the effects of reduced exposure times (4 minutes) and higher mitomycin C concentrations (4 mg/ml, 0.4 mg/ml, 0.04 mg/ml, and 0.004 mg/ml), on viability and gene expression in adult dermal fibroblast cultures. It was found that 0.4 mg/ml was the only concentration to significantly inhibit proliferation, with higher mitomycin C concentrations (4 mg/ml) resulting in cell death and the lower concentrations (0.04 mg/ml and 0.004 mg/ml) having negligible effect on cellular responses. Whilst these findings highlighted that 4 µg/ml had minimal effect on

proliferation inhibition, a major difference in methodology compared with this study was the length of exposure time. An exposure time of 4 hours were used in this research, therefore suggesting that exposing fibroblast cultures to lower concentrations of mitomycin C for long periods (4 hours), was as effective as a shorter exposure time (less than 4 hours), with a higher concentration of mitomycin C (>4 µg/ml). From these findings, it was decided for future experimentation that the lowest effective concentration of mitomycin C treatment (4 µg/ml) would be used, due to the potential adverse effects that mitomycin C exposure can have on cultures; such as induction of cell death (Blacker *et al.*, 1987).

### **4.3. Influence of commercially available animal-component free culture media on H400 keratinocyte cultures**

Keratinocyte cultures grown in KGM-CD proliferated to an extent that outperformed the other commercially available animal-component free media being tested, despite identical seeding numbers. This suggested that that KGM-CD has been optimised to yield high cell numbers of keratinocyte cultures. Whilst there is no published research directly comparing the efficacy of commercially available keratinocyte animal-component free media, the data presented here is similar to that reported by Tan *et al.* (2015), who investigated the proliferation of

mesenchymal stromal cells in six serum free media optimised for mesenchymal stromal cultures. Tan *et al.* (2015) found that out of the tested media, only one yielded cell numbers and viability comparable with cultures grown in serum supplemented media, highlighting that not all specifically optimised serum-free media can promote cell growth and maintain cell viability. Additionally, Swamynathan *et al.* (2014) examined the influence of serum and xeno-free culture conditions in stem cells and found that cultures grown in xeno-free media proliferated at a quicker rate, yielding higher cell numbers. Furthermore, when comparing the different xeno-free culture media, one medium supported significantly increased levels of culture proliferation and cell number, similar to the findings in this present work. Whilst both Tan *et al.* (2015) and Swamynathan *et al.* (2014) support the findings of this work, similarities should be interpreted with caution, owing to the differences in cell type and species of origin.

It is difficult to draw any conclusions from culture viability, which could be attributed to the use of Trypan Blue to assess viability.

Tennant (1964), identified that Trypan Blue data only became highly inaccurate following immediate traumatic cell treatment, such as dissociation from the culture vessel. However it has been argued by Altman *et al.* (1993) that use of the Trypan Blue exclusion method, 'yields an erroneous estimation of the overall viability of the culture due to lack of ambiguity in the identification of stained, non-viable

cells' and alternatives such as fluorometric assays, should be used to determine cell viability. It could be suggested that a change to methodology, such as a delay after dissociation would benefit the accuracy of cell viability counts.

Gene expression analysis (Figures 30 and 31) revealed that keratinocytes grown in KGM-CD appeared to follow the patterns of expression seen in keratinocytes cultured in DMEM supplemented with 10% human serum, suggesting normal expression of the tested genes. This finding is similar to that reported by Hannoun *et al.* (2010) who found that human embryonic stem cells cultured in a serum-free environment, retained normal expression of the tested genes and any differences were insignificant. Additionally, Skottman *et al.* (2006) also cultured human embryonic stem cells in both serum supplemented and serum free media and found that whilst the expression of common stem cell markers were similar, over 1400 other genes were expressed at different levels (many were up-regulated), highlighting that serum free environments can directly affect gene expression.

KGM-CD is reported to have been refined to enable improved keratinocyte growth, more so than commercially available counterparts; CnT-Pr or Epilife supplemented with S7. These properties have made it the most suitable tested animal-component free medium - among those investigated in the present study - for

culturing H400 keratinocytes in an animal-component free environment and this offers the potential for use as a culture medium to develop 3D oral organotypic cultures.

#### **4.4. Influence of commercially available animal-component free culture media on pHGF cultures**

The selected animal-component free media have been specifically formulated and optimised to support keratinocyte cultures. Alongside keratinocyte cultures, fibroblasts were also necessary to generate 3D oral organotypic cultures so an understanding of how fibroblast cultures behave when cultured in these media was essential.

All the commercially available animal-component free media tested in this work inhibited proliferation of fibroblasts cultures. However, it appears that KGM-CD did not inhibit fibroblast proliferation to the same extent as the other tested media. Whilst this may have appeared an unfavourable outcome, fibroblast cultures have a shorter population doubling time than keratinocyte cultures and tend to be the dominant cell type when grown as a co-culture in a non-specific environment (Clark, Ghosh and Tonnesen, 2007). Therefore, selecting an appropriate culture medium that acted as a partial limiting factor towards fibroblast growth was favourable, as this reduced fibroblast outgrowth. Whilst a reduced proliferation was desirable, considerably reduced proliferation may not be beneficial as the 3D oral organotypic

cultures generated may not then reflect the tissues that were being designed to be replicated.

It is difficult to compare the present work with previous research, due to a lack of published data exploring the effect of culturing cells in media specialised for other cell types, however it could be argued that culturing in non-specific environments is routinely performed within cell culture. An example of this is the use of DMEM supplemented with FBS, which is widely used to culture fibroblasts, as well as other cell types including keratinocytes, embryonic stem cells and mesenchymal stem cells (Bukovsky *et al.*, 2006; Mazlyzam *et al.*, 2008).

Gene expression analysis of pHGF cultures, revealed that despite culturing within a keratinocyte specific medium, fibroblastic markers were strongly expressed whilst epithelial markers were not.

#### **4.5. Influence of commercially available animal-component free culture media on pHGK cultures**

Cell lines are commonly used to generate 3D oral organotypic cultures due to cost effectiveness, ease of use, infinite lifespan and ability to conduct long term research; however, there are arguments against their use which have been detailed in Section 1.6.2.1. Understanding how primary cells respond to animal-component free environments is

essential for providing insight into selecting the most appropriate media for developing a 3D organotypic model of oral mucosa.

Unlike the H400 growth curves (Figure 13), pHGK growth (Figure 23) did not differ between any of culture media. H400 keratinocytes are an immortalised cell line which are often used in scientific research instead of primary epithelial cells (Kaur and Dufour, 2012). Whilst cell line use has advantages, translating results to primary cells must be done with care. Olschälger *et al.* (2009) compared the sensitivity in terms of cytotoxicity and cell growth inhibition, using neutral red uptake cytotoxicity assay, of immortalised keratinocyte and fibroblast cell lines and primary human fibroblast and keratinocytes to sodium dodecyl sulphate (SDS) and found that primary keratinocyte cultures were more susceptible to SDS in comparison with the cell lines due to increased cell death. This indicated that primary cells were more sensitive to changes of the culture environment than cell lines. Since growth between all the tested culture environments in the present study were on a comparable level, it could be suggested that any of the tested media could be used to generate 3D oral organotypic models, when using pHGK cultures, reinforcing the suitability of KGM-CD as an appropriate culture medium.

No conclusions could be deduced from the viability analysis of pHGK cultures due to the high degree of variability recorded from all experimental environments. However, the overall trend identifies that

pHGK cultures are able to remain viable in all media tested, further reinforcing the idea that any of the tested media could be used to generate 3D oral organotypic models.

#### **4.6. Calcium concentration of commercially available animal-component free culture media**

Detailed chemical compositions for CnT-PR, Epilife supplemented with S7 and KGM-CD are a trade secret and therefore not available within the public domain. To determine why differences in proliferation, viability, and gene expression occur, media calcium concentrations were measured. Surprisingly, all the selected commercially available animal-component-free media had lower calcium concentrations when compared with human serum supplemented media. The effects of calcium on cell proliferation and viability have been documented previously. Leigh and Watt (1995) found that keratinocyte cultures proliferated at an increased rate when cultured in low calcium containing media when compared with high calcium media.

Furthermore, Huang *et al.* (2006) investigated keratinocyte behaviours and found that primary keratinocytes cultured in media with high concentrations of calcium ions (1.2 mM) experienced inhibition of proliferation and had reduced viability. The data obtained is not in agreement with these observations due to cultures grown in DMEM supplemented with human serum (which had the highest calcium concentration) generating high cell numbers. This discrepancy

therefore indicates that it is likely that other specific keratinocyte factors including amino acids, hormones and growth factors are present within the composition of KGM-CD.

## Discussion of Section 2 Results

The results discussed in this section are the focus of experimental work aimed at understanding cell responses to novel TiZr alloys for the potential use as dental implants. Titanium and its alloys have been used to fabricate dental implants for over 40 years due to favourable properties such as mechanical strength, development of an oxide layer that prevents corrosion, and demonstration of osseointegration (Osman and Swain, 2015). As the number of placed dental implants increases, research focused on understanding, promoting, and improving the interactions between the implant surface and epithelial tissues, to prevent tissue recession causing exposure of the metal components. This, coupled with increasing numbers of Ti allergies reported, has led to the investigation of novel implant materials for clinical application such as TiZr alloys.

### **4.7. Understanding pHGF and H400 keratinocyte culture growth on commercially pure (Grade IV) Ti**

Prior to investigating how H400 keratinocyte and pHGF cultures respond to novel TiZr alloys, it is essential to understand how these cells respond to existing Ti dental implant material.

pHGF and H400 keratinocyte cultures formed attachments and proliferated on the surface of the commercially pure (Grade IV) Ti discs

which concurred with previous research (Kimura *et al.*, 2012; Dorkhan *et al.*, 2014) and were expected due to the long history and clinical success of the use of commercially pure (Grade IV) Ti as an implant material (Saini *et al.*, 2015).

#### **4.8. Understanding pHGF culture response to TiZr metals**

Initial short-term responses were evaluated using 24 and 48-hr attachment studies, which highlighted that after 24 hours, 50% Zr alloys had the greatest cell attachment compared with the other alloys, however after 48 hours, the highest number of cells attached to the 5%, 15% and 50% Zr surfaces; higher than the commercially pure (Grade IV) Ti and 100% Zr discs. Growth curves of 20 days revealed that cultures grown on the novel TiZr alloys (5%, 15% and 50% Zr) had shorter population doubling times compared with 0%, 100% Zr and the control. Furthermore, fibroblasts cultured on 15% Zr showed significantly ( $p < 0.05$ ) shorter population doubling times when compared with the other culture studies. These data suggested that TiZr alloys demonstrate better biocompatibility than commercially pure (Grade IV) Ti (0% Zr), which is in agreement with current research and previous findings (Ikarashi *et al.*, 2007; Sista *et al.*, 2011; Grandin *et al.*, 2012).

Sista *et al.* (2011) compared the attachment of osteoblasts to TiZr (50% Zr), TiNb and commercially pure Ti discs and found that higher numbers of osteoblasts were attached to the TiZr surfaces in comparison with commercially pure Ti and TiNb. Additionally, *in vivo* research conducted by Ikarahi *et al.* (2005) found that TiZr had the lowest score of adverse tissue responses; with fewer immune cells observed around the fibrous capsule, a thinner fibrous capsule and no discernible systemic toxicity. The authors concluded that '*TiZr had better biocompatibility than Ti*' indicating it may be a suitable implant material. However, despite these studies suggesting that TiZr implants promoted improved cell attachment than commercially pure Ti, *in vivo* research conducted by Thoma *et al.* (2011) found that healing in terms of bone loss surrounding TiZr implants was directly comparable with the bone levels found adjacent to Ti implants and no statistical differences were found. However, it could be argued that the lack of significance could be attributed to the use of dogs as the test clinical model, where it has been identified that bone apposition and remodelling rates can greatly vary between dogs and between individual dogs (Anderson and Danylchuk, 1978). Whilst dogs are a commonly used animal model within dental implant research, Bloebaum *et al.* (1991) indicated that bone turnover rate in dogs is higher than in humans and Magee *et al.* (1989) demonstrated that bone-implant interfaces reduced in strength with increasing age of the

test animal; thus indicating caution required in the interpretation of data (Thoma *et al.*,2011).

The superior attachment promoting properties and cell interactions observed could be attributed to the physio-chemical properties of TiZr alloys. Physio-chemical properties such as surface energy, topography, and chemistry, have been shown to influence initial attachment and subsequent cell adhesion by adsorption of proteins affecting these biological processes (Wilson *et al.*, 2005).

Zhang *et al.* (2018) investigated the behaviour of TiZr alloys within artificial corrosive environments. Replicating both acidic and inflammatory simulated environments associated with implant placement, corrosion, ion release and oxide layer behaviour were examined. It was found that as the percentage of Zr increased the passivity of the oxide layer increased and a reduction in metal ion release was observed. However, 50% Zr alloys demonstrated increased pitting susceptibility, therefore Zhang *et al.* (2018) concluded that 15% Zr optimised both oxide passivity and pitting resistance without compromising the physio-chemical properties. Additionally, research conducted by Sista *et al.* (2011) concluded that surface energy, wettability, and oxide layer composition of TiZr implants were more favourable to cells due to increased adhesion, differentiation and proliferation, positively influencing the superior biological properties

observed. Both Zhang *et al.* (2018) and Sista *et al.* (2011) highlighted the enhanced physio-chemical properties of TiZr alloys in comparison with commercially pure (Grade IV) Ti, that generated increased cell attachment.

Alongside growth curves, cell attachment was also analysed in the present study in the form of surface coverage (Figure 45). Image analysis suggested that TiZr alloys had improved cell attachment promoting properties in comparison with the commercially pure metals (0% and 100% Zr) due to the greater surface coverage calculated, however these values were not statistically significantly different. The differences could be attributed to ground truth imaging not being conducted in this research. Ground truth imaging is the process that compares new segmentation methods to the gold standard method, determining whether the new segmentation method is correct and an improvement on current methodology. For the type of image analysis used within this research, the gold standard method is for a user to manually distinguish between cells attached to the surface and the remaining exposed surface of the TiZr alloy discs. The resultant image would then be used to compare the resultant image of the new segmentation method and where applicable, facilitate any necessary adjustment to the new methodology to improve and correct the final output.

By not conducting this initial process the efficacy and potential value of the data set obtained is debatable. However, the methodology outlined in Section 2.28 has been previously compared with ground truth segmentation techniques by Vyas *et al.* (2017) and shown to be an accurate and tested segmentation method that has been previously utilised for similar applications; including the calculation of area covered by attached bacteria on Ti discs (Vyas *et al.*, 2017; Zhang *et al.*, 2018).

Another explanation for the differences observed in both surface coverage and growth curves could be attributed to surface finish of the TiZr discs. Whilst methodology was standardised to produce mirror like finish surfaces, slight variability in surface roughness (presented in Figure 46) occurred, with 15% Zr presenting the most even surface finish and 5% and 100% Zr with the most inconsistent. Research by Pendegrass *et al.* (2008), identified that surface roughness of Ti had a direct effect on cell attachment; with reduced surface roughness (polished finish) improving overall cell attachment. Whilst this observation supports the data in the present study, statistical analysis revealed that there were no significant differences in the surface roughness of the samples. It was therefore concluded that surface roughness had a minimal effect on the cell culture variations observed

between TiZr alloys. This therefore implied that other physio-chemical factors influenced cell behaviour, e.g. oxide composition, however further analysis exploring this will be required to be able to draw further conclusions.

The results obtained here and presented in previously published research, suggest that 15% Zr provides the greatest potential for use as a dental implant material owing to favourable biological and physio-chemical responses.

## Discussion of Section 3 Results

This section discusses the findings of histological analyses on the efficacy of two commonly used approaches to produce de-epidermalised dermis as well as data from 3D oral organotypic cultures that were generated for 7, 14 and 21 days at the air liquid interface (ALI) in different animal-component-free media.

### **4.9. Analysis of the efficacy of preparing de-epidermalised dermis (DED) from two approaches**

Over the last 10 years, research focused on developing 3D oral organotypic cultures has progressed significantly. Of the available biomaterials that are used as scaffolds, de-epidermalised dermis (DED) is commonly used due to providing necessary tissue architecture, ease of production (relative to other scaffolds) and bioactive properties including promotion of cell adherence. Several approaches such as repeated freeze-thaw treatments, detergent treatment and enzymatic treatment have been employed to prepare DED from cadaveric skin. It was therefore important to identify a suitable approach for the current research.

Both approaches tested in the present study (method one: treatment with dPBS and 1M NaCl; method two: treatment with 0.25% TrypLE, 0.5mM EDTA and 0.5% Triton X-100) were capable of complete de-

cellularisation. Small fragments of epidermis could be seen on the processed samples, however more fragments were visible on DED processed using method two. One explanation for this was the increased difficulty of mechanical separation of the epidermis from the dermis after method two reagent treatment. Furthermore, because of this increased difficulty, the papillary surface of samples processed using method two, resulted in an irregular appearance.

Comparisons of two different DED preparation approaches (disperse treatment, or NaCl treatment), have been previously undertaken by Ghosh *et al.* (1997) who found that all three treatments were able to produce organotypic cultures that shared many structural features observed in normal skin, highlighting the inconsequential differences between the different approaches. Therefore, due to the difficulties in cleaning and separating the epidermis from the dermis and the mechanical disruption to the remaining dermis, method one was used for all subsequent experimental work.

#### **4.10. Analysis of 3D oral organotypic cultures in animal-component-free culture media**

Oral organotypic cultures have been increasingly utilised within scientific research, with multiple methodologies and applications documented (Moharamzadeh, 2017). To test the conclusions from previously obtained data, 3D oral organotypic cultures were developed

within KGM-CD and DMEM supplemented with human serum for 7, 14 or 21 days at the ALI.

The results suggest that KGM-CD had the capability to support the development of 3D oral organotypic cultures and cultures exhibited epithelium stratification, which to the best of current knowledge is the first time that this has been reported. Measurements of the epithelial thickness identified that thickness increased as the number of days at ALI increased, however the thickness of the epithelium was significantly thinner than 3D oral organotypic cultures grown in DMEM supplemented with 10% human serum. Furthermore, observed stratification within 3D oral organotypic cultures generated with KGM-CD was in direct contrast with previous research (Lamb and Ambler, 2013). Briefly, Lamb and Ambler (2013), seeded neonatal human epidermal keratinocyte cultures (NHEK), previously cultured in a serum-free and feeder free environment, onto DED and cultured in serum free environments using KGM-Gold or Epilife and serum supplemented equivalents as well as complete FAD medium (a 3:1 mixture of Dulbecco's modified Eagle's medium and Ham's F12 medium). Epithelium stratification did not occur; with the generated epithelium consisting of up to two layers of nucleated cells. Furthermore, cornification of the superficial layer was not apparent. However, organotypic cultures grown in the serum free media

supplemented with 10% human serum generated stratified epithelium, although only consisting of a minimal number of layers.

The difference in observations could be attributed to the selection of the particular cell lines, used for the respective research objectives necessary here. In this research, the H400 oral keratinocyte cell line was used, which is an immortalized gingival keratinocyte cell line established from a human squamous cell carcinoma, whereas research by Lamb and Ambler (2013) used neonatal human epidermal keratinocytes; cultures that have been optimised for growth. The differences in derivation may affect cell behaviour within specific environments specifically serum and animal-component free conditions.

Research by Turabelidze *et al.* (2014) analysed at the intrinsic differences between human skin and oral keratinocytes and found that there were significant differences in gene expression, proliferation, and migration. Oral keratinocyte cultures proliferated and migrated at a rapider rate than skin keratinocyte cultures. Additionally, over 100 genes were found to be upregulated in oral keratinocyte cultures compared with skin keratinocyte cultures and baseline values of genes that responded to stimuli from wound healing were elevated in oral keratinocyte cultures. These findings highlighted the apparent differences between oral and skin keratinocytes when cultured *in vitro*.

It could be suggested that due to the slower proliferation capacities of skin keratinocyte cultures, the developed skin organotypic model would have taken greater time to not only stratify but also develop a similar epithelial thickness as seen in the serum supplemented cultures.

Whilst immortalised cell lines are commonly used to develop organotypic models of both skin and oral mucosa, cell lines have been genetically altered which in turn could potentially alter behaviour and responsiveness to stimuli such as ALI exposure therefore, it is more beneficial to use primary human keratinocyte cultures to develop 3D oral organotypic models. Earlier experimental work presented in this thesis, utilised pHGK cells however due to difficulties faced, specifically low cell yields, and short culture life span, it was decided to use H400 keratinocytes to develop 3D oral organotypic models. The difficulties outlined above, are not synonymous to this work and have been previously reported by Daniels *et al.* (1996).

Another possible explanation for the difference in epithelium stratification could be associated with culture media. In this research KGM-CD was used, whereas Lamb and Ambler (2013) used KGM-Gold- which requires supplementation with BPE plus other hormones- and Epilife. The developed skin organotypic cultures grown in both the serum free media failed to stratify, where serum supplemented counterparts yielded stratified epithelium. This suggested that both

media lacked key nutrients and hormones necessary for stratification, which was observed in subsequent experiments by Lamb and Ambler (2013). It was found that epithelial stratification and thickness of skin organotypic cultures increased when cultured in serum, and this was suggested to contain components such as amino acids, and growth factors that facilitated stratification.

The generation of 3D oral organotypic cultures, with apparent stratification, suggested that KGM-CD contained the necessary factors required to induce this process. Growth factors and hormones thought to be involved in epithelial stratification include, epidermal growth factor (EGF), a protein that stimulates epithelial cell growth and proliferation and, keratinocyte growth factor (KGF/FGF7), a growth factor secreted by fibroblasts that enhances keratinocyte cell proliferation, however complete analysis of the media and further testing to identify the roles of the different growth factors in epithelial stratification needs to be conducted to firmly conclude this (Ganapathy *et al.*, 2012).

#### **4.11. Gene expression analysis of 3D oral organotypic cultures in animal-component-free culture media**

Expression of CK 1, 5, 10, and 13, Ki-67, e-cadherin, n-cadherin, vimentin and collagen VII were analysed in 3D oral organotypic cultures grown in either DMEM supplemented with 10% human serum

or KGM-CD at 7, 14, and 21 days at the ALI. Transcription ratios of the tested cytokeratins were statistically higher in 3D oral organotypic cultures grown in DMEM supplemented with 10% human than cultures developed in KGM-CD on all days. Expression of Ki-67, e-cadherin and collagen VII were expressed at higher ratios again in DMEM supplemented with 10% human serum cultures, however this was only found to be statistically higher in cultures grown at the ALI for either 14 or 21 days. No statistical difference in vimentin expression ratios was found at any time point and n-cadherin was initially (day 7 and 14) expressed at a higher ratio in cultures grown in DMEM supplemented with 10% human serum however, by day 21 no statistically significant difference were found between the cultures.

Significant differences in expression ratios for cytokeratins, Ki-67, e-cadherin and n-cadherin between 3D oral organotypic cultures grown in either DMEM supplemented with 10% human serum and cultures grown in KGM-CD could be attributed to differences in calcium concentration of the culture media. It is known that calcium is a fundamental regulator of both proliferation, and differentiation (Tu and Bikle, 2013). Braga *et al.* (1995) identified that culturing keratinocytes within a low calcium environment (<0.07mM), induced accelerated proliferation and expression of basal layer cytokeratins (CK 5 and 14) was raised. Increasing calcium concentrations above 0.1 mM, initiated keratinocyte differentiation by inducing stratification,

indicated by an increase of suprabasal cytokeratin expression (CK1 and 10). However, expression of CK1 and 10 and obvious stratification observed in 3D oral organotypic cultures grown using KGM-CD, suggest that other compositional elements could be attributed to epithelial stratification, as concluded by Lamb and Ambler (2013). Since the complete composition of KGM-CD is unavailable, further testing would be necessary to clarify what factors could be contributing to the results obtained.

Alongside keratinocyte differentiation, calcium is also required for cell-cell junction formation; especially desmosome and adherens junctions. Calcium concentration has been found to influence the conformational organisation of cell-cell junctions, particularly affecting the cadherin proteins. Notably, calcium binds to the extracellular domain of a cadherin which initiates cadherin interaction between cells, enabling the arrangement of the adherens junctions (Hartsock and Nelson, 2008).

No statistically significant differences in vimentin expression were found between either 3D oral organotypic cultures. Vimentin is typically expressed in cells of mesenchymal origin such as fibroblasts and the observed variations, could be attributed to the effect of the culture media on fibroblast proliferation and doubling time as discussed in Section 4.4.

Collagen VII is an integral component of anchoring junctions such as hemidesmosomes and has been found to be expressed by both basal keratinocytes and fibroblasts located within the lamina propria (Ryynänen *et al.*, 1992). The obvious expression differences of collagen VII could be attributed to the culture medium's ability to support growth and proliferation of pHGF cultures. From previous experimental work, it was identified that KGM-CD was able to support reduced pHGF growth and proliferation. Increased numbers of pHGF cells within 3D oral organotypic cultures, would naturally influence the increased expression of genes expressed by fibroblast cultures.

In summary, it has been shown that that animal-component free medium, KGM-CD, induced keratinocyte differentiation within 3D oral organotypic cultures, inclusive of stratified epithelium.

## Discussion of Section 4 Results

Scaffolds are used within tissue engineering to provide structure to the developing tissue by acting as a representative extracellular matrix.

There are several types of scaffold available, including natural, synthetic and hybrid; each with their own advantages and disadvantages. Natural scaffolds, specifically acellular dermal matrix materials, such as DED, are considered to be the 'gold standard' and are commonly used as scaffolds owing to retention of structural and functional proteins following processing (Chaudhari *et al.*, 2016).

However, the cost of these scaffolds have led to research utilising alternatives such as natural and synthetic derived hydrogels (Cheng and Saint-Cyr, 2012). Prior to utilisation, understanding the basic mechanical properties is key to the process of developing a scaffold that not only biologically, but also mechanically mimics the extracellular matrix found in oral mucosa to enable a more complete representation of the developed 3D oral organotypic model.

### **4.12. Understanding the mechanical properties of RGD modified alginate**

Hydrogels have emerged as potential scaffolds that have been utilised in the development of 3D oral organotypic cultures (Khan *et al.*, 2012).

Alginate is a naturally occurring polysaccharide that is commonly used

as a scaffold owing to favourable mechanical and biological properties, low cost and abundance (Sun and Tan, 2013). Alginate hydrogels do not contain bioactive motifs, permitting cellular attachments to the polymer chain, however, alginate polymer chains can be functionalised with bioactive groups such as amino acid sequence arginine-glycine-aspartate (RGD) to promote cell attachment. Whilst conjugation with bioactive moieties improve the biological properties in terms of cell attachment, understanding how this in turn affects mechanical properties, is of equal importance as this can affect cell behaviour.

As expected from previous research, increasing the wt% of alginate within the hydrogel system, increased the stress that can be exerted on the hydrogel system before failing (Lee and Mooney, 2012). This is due to an increase in the number of cross-linked polymer chains which is the main contributor to the overall systems mechanical strength.

Swelling ratio results indicated that RGD modified alginates significantly lost the most mass after 1 and 7 days. This result is in agreement with previous research conducted by Ferris *et al.* (2015) who found that RGD conjugation prevented ionic crosslinking which resulted in polymer chains leaching out of the hydrogel systems causing RGD modified alginate hydrogels to lose the most mass when compared to unmodified counterparts. Since, fewer cross-links are formed within the RGD modified hydrogel, degradation of the system

occurs at an accelerated rate in comparison with the traditional alginate systems hence an increased percentage of mass lost Figure 52.

The biological implications of the mechanical results have identified that RGD modified alginate has the potential to be used as a scaffold for developing 3D oral mucosa models due to the ability of the scaffold to withstand compressive forces similar to that experienced by oral mucosa. However, long term culture development (in excess of 21 days) is not suitable use of the alginate scaffold systems investigated, due to the accelerated rate of degradation. This conclusion is in alignment with the conclusions drawn by Lee and Mooney (2012) who identified that alginate based scaffolds readily dissolve in media by ionic exchange (divalent cations are replaced with monovalent cations) causing the breakdown of the ionic crosslink.

#### **4.13. Understanding the biological properties of RGD modified alginate**

To identify whether alginate was successfully modified with RGD, surface and encapsulation release cell growth curves were conducted. There was a noticeable lack of proliferation in H400 keratinocyte cultures grown on the surface and pHGF cultures encapsulated and released, no significant differences were found. However, the trends observed do have biological significance. Figures 58 and 59 show that both pHGF and H400 cell cultures struggle to retain viability when

attached to the surface of encapsulated within RGD-modified alginate, which could be due to reagents used for peptide conjugation not being effectively removed during the purification process. In this research, RGD-modified alginate was purified by means of dialysis, using a cellulose tubing with a MW of 14,000Da in water for 3 days; with 3 water changes performed per day. Despite dialysis purification being a reliable and commonly used purification method for RGD-modified alginate solutions (Taketa *et al.*, 2016), it could be suggested that the duration and frequency of water changes during the purification process was not enough to yield an RGD-modified alginate solution with the required purity for biological experiments. Furthermore, Sandvig *et al.* (2015) identified that coal filtration prior to dialysis was more effective at removing by products from the carbodiimide reaction than dialysis alone and it is therefore suggested coal filtration should be included in the purification methodology of RGD-modified alginate.

To develop this work further, it is suggested that polymer characterisation using nuclear magnetic resonance (NMR) spectroscopy be conducted to analyse the molecular structure enabling quantitative identification of RGD. Following this, adaptations to the polymer conjugation technique should be conducted to enhance the biological properties, due to the mechanical results discussed in Section 4.12 highlighting scaffold suitability for short term culture development.

#### 4.14. Understanding the effect of hydrogel reagents on pHGF cultures

Owing to routine use within tissue engineering, differing approaches have been reported to cross-link alginate polymer chains, with ionic crosslinking being the most common method. Calcium chloride ( $\text{CaCl}_2$ ) is frequently used to cross link with divalent cations, which are required to directly bind to guluronate regions on the polymer backbone, in turn forming, ionic links between the polymer chains (Grant *et al.*, 1973).

Destabilisation of the alginate hydrogel occurs in the presence of chelating agents such as sodium citrate. Disintegration of the hydrogel via chelation occurs by ionic exchange, where divalent cations are replaced with monovalent cations such as  $\text{Na}^+$ , which ultimately breaks the ionic crosslink (Kikuchi *et al.*, 1999). pHGF cultures were exposed to both sodium citrate and  $\text{CaCl}_2$  to gain an understanding of the effect that these reagents potentially have on cell proliferation and viability.

Exposure of pHGF cultures to  $\text{CaCl}_2$  had minimal effect on cell proliferation or viability. Cao *et al.* (2012) conducted a similar experiment which investigated the effect of calcium ions on viability and proliferation of Schwann cells encapsulated within alginate hydrogels. It was found that upon an initial exposure to the differing

CaCl<sub>2</sub> solutions (0.1M, 0.5M and 1M) viability dropped by 50%.

However, the viability of cultures exposed to 0.1M CaCl<sub>2</sub> after 24 hours increased to 80%, whereas cultures exposed to higher concentrations, did not recover and viability remained at 50%. A possible explanation for the difference in biological effects could be attributed to exposure time.

In the current research pHGF cultures were only exposed to CaCl<sub>2</sub> for the minimum gelation period (3 minutes), whereas Cao *et al.* (2012) used exposure times of 5, 10 and 30 minutes. Although calcium is necessary for intercellular functions, exposure to high concentrations is known to induce cell death caused by osmotic stress (Demaurex and Distelhorst, 2003). This finding was significant, as it suggested that the fabrication method used to construct RGD modified hydrogels in the present research, had minimal effect on pHGFs encapsulated within the hydrogel, thus highlighting suitability for use. Additionally, it was found that sodium citrate inhibited proliferation and reduced culture viability. Whilst there is no published research exploring the effect of sodium citrate on normal fibroblasts cultures, in cancer research, there have been extensive studies investigating the potential use of sodium citrate as an anti-cancer drug. Sodium citrate inhibits tumour growth by inhibiting the enzyme phosphofructokinase, which prevents glycolysis and leads to apoptosis (Guo *et al.*, 2016). However, this suggestion for reduced cell number and viability observed in the present research should be applied with caution as cancer

experimental work has not been replicated within non-cancerous cultures of cells. Based on the results and previous literature, it is suggested that sodium citrate exposure should be kept to a minimum and should be considered when dissociating the 3D oral organotypic cultures in future experimental work.

#### **4.15. Understanding the mechanical properties of PEG-DM**

Despite the various advantages of utilising RGD modified alginate, it is a degradable hydrogel system, making it unsuitable for long term experimental work. Of the numerous synthetic polymers, PEG is a promising choice due to the possibility of manipulating its chemical composition by modifying the polymer backbone with methacrylate groups (PEG-DM), making the system photopolymerizable, and leading to a more homogenous hydrogel formation as well as the presence of functional groups that promote cell attachment. Prior to modification, understanding the unmodified mechanical properties, to initially assess the suitability of PEG-DM as a potential scaffold material and to provide insight towards the effects of functionalising with bioactive proteins is needed.

20wt% PEG-DM hydrogels had higher yield strengths and compressive moduli when compared with 10wt% PEG-DM hydrogels, which concurred with previous studies (Martens and Anseth, 2000; Killion *et al.*, 2011; Nguyen *et al.*, 2012). Furthermore, increasing photoinitiator

content within the 20wt% PEG-DM hydrogel systems, reduced the compressive modulus, also in agreement with published data (Killion *et al.*, 2011). The role of the photoinitiator is to start photopolymerization by producing free radicals. However, despite increased free radical generation, the overall compressive modulus of the hydrogel becomes weaker due to fewer polymer chains within the hydrogel system.

The relevance of the compressive testing experimental work was to identify whether PEG-DM has the potential to be a suitable scaffold material for 3D oral organotypic cultures. At present, published data has yet to identify conclusive data concerning the compressive strength capacity of oral mucosa, reporting ranges from as little as 0.06MPa to 8.89MPa (Kydd and Daly, 1982; Lacoste-Ferré *et al.*, 2011). The findings of the compressive studies presented in

Table 17 demonstrated that all the PEG-DM hydrogel formations tested could potentially be used as a scaffold due to each of the calculated compressive moduli were within the reported range of oral mucosa .

Monitoring the swelling of these hydrogels over 7 days provided an insight into the nature of these particular polymers systems. PEG-DM 10wt% hydrogels gained mass after 7 days (Figure 61) and generated large standard error bars. A possible and likely explanation for this result is methodical error; incomplete removal of excess water prior to weighing, which could have an effect on the weight recorded. In contrast, PEG-DM 20wt% hydrogel swelling was in accordance with previous work of Cruise, Scharp and Hubbell (1998), who found that decreasing the macromer percentage of PEG-DM especially molecular weight 4000 kDa, increased the volumetric swelling ratio. From this it could be concluded that the different hydrogel systems behaved in a way that was expected and in agreement with previous research.

# CHAPTER 5:

# CONCLUSIONS

The overall aim of this thesis was to develop 3D oral organotypic cultures using an entirely animal-component-free environment, and ultimately to use this as a research tools to analyse implant-soft tissue interactions.

Using the thesis objectives to design suitable experiments it was found that:

- Monolayer studies using H400 keratinocyte and pHGK cultures identified that KGM-CD medium showed the most suitability for development of 3D oral organotypic cultures, by generating results comparable with human serum supplemented media. Additionally, studies demonstrated that KGM-CD limited proliferation in pHGF cultures; a favourable response required when developing 3D oral organotypic cultures, to prevent fibroblast overgrowth.
- Short- and long-term culture studies investigating cell responses to novel TiZr alloys identified increased growth rates on novel TiZr alloys compared with commercially pure Ti or Zr. Furthermore, 15% Zr had the greatest potential as an implant material owing to increased cell proliferation on the surface.
- 3D oral organotypic cultures in KGM-CD developed mature stratified epithelium based upon histological analysis. Additionally, gene expression analysis determined the expression of CK1 and CK10, suprabasal cytokeratins, an indication of epithelium stratification. However due to expression of these cytokeratins being

weaker than basal cytokeratins, (CK5 and CK13), it is suggested that further characterisation of protein expression of the generated 3D oral organotypic cultures be conducted and compared with natural oral mucosa.

- Compressive analysis of both RGD modified alginate and PEG-DM hydrogel systems, suggested that both have the potential to be used as scaffolds to develop 3D oral organotypic cultures due to similar compressive moduli of that reported range for oral mucosa.

## Future Work

To build on the work presented in this thesis, the following research studies are proposed:

### **Optimisation of animal-component-free environments:**

- Full characterisation of the tested commercially available animal-component-free media should be conducted using chemical analysis such as mass spectrometry. This will potentially aid the identification of any differences in composition which could be attributed to differences seen in cell responses in terms of proliferation, viability, and gene expression.

- Analysis of the expression of mesenchymal–epithelial transition induction and apoptosis markers in pHGF cultures to identify any changes in expression which could be used to understand the limiting impact of culturing pHGF cultures within keratinocyte specific media.

### **TiZr analysis**

- Oxide layers should be analysed to identify any variations such as wettability, oxide thickness and surface chemistry that could be attributed to the differences in observed cell attachment.
- Short and long-term growth (21 days) curves be replicated on TiZr alloys that have sustained different surface treatments specifically sandblasting, acid- etching and anodization. This should enable full optimisation of surface characteristics of TiZr alloys which may enable the attachment of keratinocyte and fibroblast cultures to the metal surface in situ.
- Replication of experiments listed above within a 3D oral organotypic culture using simulated implant structures is proposed. This will provide insight into the relationship between the TiZr alloy implant surfaces and engineered oral soft tissue, this may enable the development of a highly optimised surface composition that encourages periodontal tissue attachment.

### **3D oral organotypic culture development**

- Transmission electron microscopy could be employed to analyse the collagen fibres of processed DED, to gain an understanding of the potential effect the different epithelium removal approaches have on scaffold architecture.
- Immunofluorescence studies on protein expression relating to epithelial stratification, proliferation and structural proteins be conducted upon the developed 3D oral organotypic cultures to understand the localisation of expression to determine if epithelial stratification occurs.
- pHGK cultures could be utilised to develop 3D oral organotypic cultures and fully analysed using histology, immunofluorescence, and gene expression techniques. This will allow direct comparisons to be made with the organotypic cultures generated in this research and determination of the suitability of H400 keratinocyte cultures for use in this model system.
- The developed 3D oral organotypic cultures should be directly compared with natural oral mucosa using histology, gene expression analysis and immunofluorescence to understand any similarities and differences between the engineered structure in terms of architecture and protein expression. From this comparison, investigations focused on further developing the engineered structures could occur.

- Exploration of epithelial thickness using optical coherence tomography and image analysis techniques to identify any quantitative differences between the generated 3D oral organotypic cultures in the respective animal-free environments as well as natural mucosa.

### **Hydrogel scaffold development**

- Long term growth curves (up to 21 days) and viability analysis using pHGF cultures could be conducted for all hydrogel scaffolds previously investigated including DED to identify if encapsulation or scaffold seeding has an effect on these cultures.
- Scaffolds could be used to construct 3D oral organotypic cultures and resultant structures could be compared with cultures developed using DED and natural oral mucosa to identify if synthetic animal-component-free 3D oral organotypic cultures can be developed.
- Comparison of the engineered 3D oral organotypic cultures mechanical properties, such as static and cyclic compressive testing, with natural oral mucosa leading to the development of optimised scaffolds through adjustments to the hydrogel chemical composition.
- Adaption of natural and synthetic scaffolds to further improve soft tissue architecture and biomechanical properties including functionalisation of PEG-DM.

LIST OF  
REFERENCES

- Abraham, C. M. (2014) 'A brief historical perspective on dental implants, their surface coatings and treatments', *The Open Dentistry Journal*. Bentham Science Publishers, 8(1), 50–55.
- Adell, R., *et al.* (1981) 'A 15-year study of osseointegrated implants in the treatment of the edentulous jaw', *International Journal of Oral Surgery*, 10(6), 387–416.
- Aktary, Z. and Pasdar, M. (2012) 'Plakoglobin: Role of tumorigenesis and metastasis', *International Journal of Cell Biology*, 1, 1-14.
- Alberts, B.*et al.*, (2002) 'Cell junctions', in *Molecular Biology of the Cell*. 4th edn. Connecticut, USA: Garland Science, pp. 1035-1081.
- Albrektsson, T. *et al.*, (2009) 'A requiem for the periodontal ligament revisited', *The International Journal of Prosthodontics*, 22(2), 120–122.
- Albrektsson, T. and Isidor, F. (1994) 'Consensus report of session IV', in Lang, N. P. and Karring, T. (eds) *Proceedings of the First European Workshop on Periodontology*. London, UK: Quintessence, pp. 365–369.
- Albrektsson, T. and Wennerberg, A. (2004). 'Oral implant surfaces: part 1-review focusing on topographic and chemical properties of different surfaces and in vivo responses to them'. *International Journal of Prosthodontics*, 17(5): 536-543.
- Altman, S. A. *et al.*, (1993) 'Comparison of Trypan Blue dye exclusion and fluorometric assays for mammalian cell viability determinations',

*Biotechnology Progress*, 9(6), 671–674.

Alturkistani, H. A. *et al.*, (2015) ‘Histological stains: A literature review and case study.’, *Global Journal of Health Science*. 8(3), 72–79.

Andersen, T. *et al.*, (2015) ‘3D cell culture in alginate hydrogels.’, *Microarrays*. 4(2), 133–161.

Anderson, C. and Danylchuk, K. D. (1978) ‘Bone-remodeling rates of the Beagle: a comparison between different sites on the same rib.’, *American Journal of Veterinary Research*, 39(11), 1763–1765.

Animals (Scientific Procedures) Act 1986, c. 6. Available at:

<https://www.legislation.gov.uk/ukpga/1986/14/contents> (Accessed: 13 September 2018).

Annibali, S. *et al.* (2008) ‘Local complications in dental implant surgery: prevention and treatment.’, *ORAL & Implantology*. 1(1), 21–33.

Arganda-Carreras, I. *et al.* (2017) ‘Trainable Weka Segmentation: a machine learning tool for microscopy pixel classification’., *Bioinformatics*. 33(15), 2424–2426.

el Askary, A. S. *et al.*, (1999) ‘Why do dental implants fail? Part I.’, *Implant Dentistry*, 8(2), 173–185.

Bain, C. A. and Moy, P. K. (1993) ‘The association between the failure of dental implants and cigarette smoking.’, *The International Journal*

*of Oral & Maxillofacial Implants*, 8(6), 609–615.

Balcombe, J.P. *et al.*, (2004). 'Laboratory routines cause animal stress'.

*Contemporary Topics in Laboratory Animal Science*, 46(6): 42-51.

Barczyk, M. *et al.*, (2013) 'Role of integrins in the periodontal ligament:

Organizers and facilitators', *Periodontology 2000*, 63(1), 26–47.

Barnes, D. and Sato, G. (1980) 'Serum-free cell culture: A unifying approach', *Cell*, 22(3), 649–655.

Barrila, J. *et al.* (2010) 'Organotypic 3D cell culture models: using the rotating wall vessel to study host-pathogen interactions.', *Nature Reviews. Microbiology*, 8(11), 791–801.

Baylink, D. J. *et al.* (1993). 'Growth factors to stimulate bone formation'. *Journal of Bone and Mineral Research*, 8 (Suppl 2): 565-572.

Belaldavar, C. *et al.* (2016) 'Cytokeratins: Its role and expression profile in oral health and disease', *Journal of Oral and Maxillofacial Surgery, Medicine, and Pathology*, 28(1), 77–84.

Blacker, K. L. *et al.*, (1987) 'Mitomycin c-treated 3T3 fibroblasts used as feeder layers for human keratinocyte culture retain the capacity to generate eicosanoids', *Journal of Investigative Dermatology*. 89(6), 536–539.

Bloebaum, R. D. *et al.* (1991) 'Retrieval analysis of a hydroxyapatite-

coated hip prosthesis.’, *Clinical Orthopaedics and Related Research*, 267, 97–102.

Boadi, J., *et al.*, (2015). ‘Imaging of 3D tissue-engineered models of oral cancer using 890 and 1300 nm optical coherence tomography’.  
*Sovremennyye Tehnologii v Medicине*, 7(1): 60 - 67.

Bosshardt, D. and Lang, N. (2005) 'The junctional epithelium: From health to disease', *Journal of Dental Research*, 84(1), 9–20.

Brånemark, P. I. *et al.* (1969) ‘Intra-osseous anchorage of dental prostheses. I. Experimental studies.’, *Scandinavian Journal of Plastic and Reconstructive Surgery*, 3(2), 81–100.

Brånemark, P. I. *et al.* (1977) ‘Osseointegrated implants in the treatment of the edentulous jaw. Experience from a 10-year period.’, *Scandinavian Journal of Plastic and Reconstructive Surgery. Supplementum*, 16, 1–132.

Braga, V. M. M. *et al.*, (1995) ‘Calcium-induced changes in distribution and solubility of cadherins, integrins and their associated cytoplasmic proteins in human keratinocytes’, *Cell Communication and Adhesion*, 3(3), 201–215.

Brogden, K. and Squier, C. (2011) *Human Oral Mucosa: Development, Structure, and Function*. Oxford, UK: Wiley-Blackwell.

Bukovsky, A. *et al.* (2006) ‘Ovarian germ cells’, *Methods in Enzymology*,

419, 208–258.

Buskermolen, J. K. *et al.* (2016). ‘Development of a full-thickness human gingiva equivalent constructed from immortalized keratinocytes and fibroblasts’. *Tissue Engineering Part C Methods*, 22(8): 781 -791.

Cao, N. *et al.*, (2012) ‘Influence of calcium ions on cell survival and proliferation in the context of an alginate hydrogel’, *ISRN Chemical Engineering*, 2012, 1–9.

Carrel, A. (1912). ‘On the permanent life of tissues outside of the organism’. *The Journal of Experimental Medicine*, 15(5): 16-28.

Cekici, A. *et al.*, (2014). ‘Inflammatory and immune pathways in the pathogenesis of periodontal disease’. *Periodontology 2000*, 64(1): 57-80.

Chai, W. L. *et al.* (2010) ‘Development of a novel model for the investigation of implant-soft tissue interface.’, *The Journal of Periodontology*, 81(8), 1187–1195.

Chai, W. L. *et al.* (2011) ‘Ultrastructural analysis of implant-soft tissue interface on a three dimensional tissue-engineered oral mucosal model.’, *Journal of Biomedical Materials Research. Part A*. 269–277.

Chai, W. L. *et al.* (2012) ‘The biological seal of the implant-soft tissue interface evaluated in a tissue-engineered oral mucosal model.’, *Journal of the Royal Society, Interface*, 9(77), 3528–3538.

Chaudhari, A. A. *et al.* (2016) 'Future prospects for scaffolding methods and biomaterials in skin tissue engineering: A review', *International Journal of Molecular Sciences*, 17(12), 1974-2005.

Chen, J. *et al.* (2015) 'Biomechanics of oral mucosa.', *Journal of the Royal Society, Interface*, 12(109), p. 20150325.

Chen, T. *et al.*, (2006) 'Effects of mitomycin-C on normal dermal fibroblasts', *Laryngoscope*, 116(4), 514–517.

Cheng, A. and Saint-Cyr, M. (2012) 'Comparison of different adm materials in breast surgery', *Clinics in Plastic Surgery*, 39(2), 167–175.

Ciba Speciality Chemicals (2011) 'Ciba® IRGACURE® 2959'.

Available at: <http://www.xtgchem.cn/upload/20110629045632.PDF>.

(Accessed: 27 February 2018).

Clark, R. A. F. *et al.*, (2007) 'Tissue engineering for cutaneous wounds', *Journal of Investigative Dermatology*, 127(5), 1018–1029.

Collins, L. M. C. and Dawes, C. (1987) 'The surface area of the adult human mouth and thickness of the salivary film covering the teeth and oral mucosa', *Journal of Dental Research*, 66(8), 1300–1302.

Costea, D. E. *et al.* (2005) 'The phenotype of in vitro reconstituted normal human oral epithelium is essentially determined by culture medium', *Journal of Oral Pathology and Medicine*, 34(4), 247–252.

Cruchley, A. T. and Bergmeier, L. A. (2018) 'Structure and functions of

- the oral mucosa', in *Oral Mucosa in Health and Disease*. Basel, Switzerland: Cham: Springer International Publishing, pp. 1–18.
- Daniels, J. T. *et al.*, (1996) 'Human keratinocyte isolation and cell culture: a survey of current practices in the UK', *Burns*, 22(1), 35–39.
- Demaurex, N. and Distelhorst, C. (2003) 'Cell biology: Apoptosis - The calcium connection', *Science*, 65–67.
- Delva, E. *et al.*, (2009) 'The desmosome', *Cold Spring Harbour Perspective in Biology*, 1(2), a002543.
- Dhir, S. *et al.* (2013) 'Peri-implant and periodontal tissues: a review of differences and similarities.', *Compendium of Continuing Education in Dentistry*, 34(7), e69-75.
- Dongari-Bagtzoglou, A. and Kashleva, H. (2006) 'Development of a novel three-dimensional in vitro model of oral Candida infection.', *Microbial Pathogenesis*, 40(6), 271–278.
- Donos, N. and Calciolari, E. (2014) 'Dental implants in patients affected by systemic diseases', *British Dental Journal*, 217(8), 425–430.
- Dorkhan, M. *et al.* (2014) 'Adherence of human oral keratinocytes and gingival fibroblasts to nano-structured titanium surfaces.', *BMC Oral Health*, 14(1), 14–75.
- Dulbecco, R. and Freeman, G. (1959). 'Plaque production by the polyoma virus'. *Virology*, 8(3): 396-397.

Durham, A. C. and Walton, J. M. (1982) 'Calcium ions and the control of proliferation in normal and cancer cells.', *Bioscience Reports*, 2(1), 15–30.

Eagle, H. (1955). 'Nutrition needs of mammalian cells in tissue culture'. *Science*, 122(3168): 501-514.

Edmondson, R. *et al.* (2014) 'Three-dimensional cell culture systems and their applications in drug discovery and cell-based biosensors', *ASSAY and Drug Development Technologies*. 12(4), 207–218.

Elias, C. N. *et al.* (2012) 'Influence of implant shape, surface morphology, surgical technique and bone quality on the primary stability of dental implants.', *Journal of the Mechanical Behavior of Biomedical Materials*, 16, 169–180.

Eriksson, R. A. and Albrektsson, T. (1984) 'The effect of heat on bone regeneration: an experimental study in the rabbit using the bone growth chamber.', *Journal of Oral and Maxillofacial Surgery*, 42(11), 705–711.

Esposito, M. *et al.* (1998) 'Biological factors contributing to failures of osseointegrated oral implants, (II). Etiopathogenesis', *European Journal of Oral Sciences*, 106(3), 721–764.

Ferris, C. J. *et al.* (2015) 'Peptide modification of purified gellan gum', *Journal of Materials Chemistry B*, 3(6), 1106–1115.

- Fini, M. *et al.* (2004) 'Osteoporosis and biomaterial osteointegration', *Biomedicine and Pharmacotherapy*, 58(9), 487–493.
- Franco, N. H. (2013) 'Animal experiments in biomedical research: A historical perspective', *Animals*, 3(1), 238–273.
- Fukuyama, K. and Epstein, W. L. (1986) 'Keratohyalin', in *Biology of the Integument*. Berlin, Germany: Springer Berlin Heidelberg, pp. 739–751.
- Ganapathy, N. *et al.*, (2012). 'Molecular biology of wound healing', *Journal of Pharmacy and BioAllied Sciences*, 4 (Suppl 2): S334 – s337.
- Garrod, D. and Chidgey, M. (2008) 'Desmosome structure, composition and function', *Biochimica et Biophysica Acta (BBA) - Biomembranes*, 1778(3), 572–587.
- Gervaso, F. *et al.*, (2013) 'The biomaterialist's task: Scaffold biomaterials and fabrication technologies', *Joints*, 1(3), 130–137.
- Giepmans, B. N. G. and van Ijzendoorn, S. C. D. (2009) 'Epithelial cell-cell junctions and plasma membrane domains', *Biochimica et Biophysica Acta - Biomembranes*, 1788(4), 820–831.
- Gotfredsen, K. *et al.*, (2001). 'Bone reactions adjacent to titanium implants subjected to static load. A study in the dog (I)'. *Clinical Oral Implants Research*, 12(1): 1-8.
- Gotman, I. (1997) 'Characteristics of metals used in implants', *Journal*

of *Endourology*, 11(6), 383–389.

Gottlow, J. *et al.* (2012) ‘Evaluation of a new titanium-zirconium dental implant: A biomechanical and histological comparative study in the mini pig’, *Clinical Implant Dentistry and Related Research*, 14(4), 538–545.

Gowers., K. H. C *et al.* (2018). ‘Optimized isolation and expansion of human airway epithelial basal cells from endobronchial biopsy samples’. *Journal of Tissue Engineering and Regenerative Medicine*, 12(1): 313-317.

Grandin, M. H. *et al.*, (2012) ‘A review of titanium zirconium (TiZr) alloys for use in endosseous dental implants’, *Materials*, 5(8), 1348–1360.

Grant, G. T. *et al.* (1973) ‘Biological interactions between polysaccharides and divalent cations: The egg-box model’, *FEBS Letters*, 32(1) 195–198.

Guo, X. *et al.* (2016) ‘3-Bromopyruvate and sodium citrate induce apoptosis in human gastric cancer cell line MGC-803 by inhibiting glycolysis and promoting mitochondria-regulated apoptosis pathway’, *Biochemical and Biophysical Research Communications*, 475(1), 37–43.

Hakkinen. K.M. *et al.* (2011). ‘Direct comparisons of the morphology, migration, cell adhesions, and actin cytoskeleton of fibroblasts in four

different three-dimensional extracellular matrices'. *Tissue Engineering Part A*, 17(5-6): 713-724.

Hamid, R. *et al.* (2004) 'Comparison of alamar blue and MTT assays for high through-put screening', *Toxicology in Vitro*, 18(5), 703–710.

Hand, A. R. and Frank, M. E. (eds) (2015) *Fundamentals of Oral Histology and Physiology*. Iowa, USA: John Wiley & Sons, Inc.

Harris, T. J. C. and Tepass, U. (2010) 'Adherens junctions: From molecules to morphogenesis', *Nature Reviews Molecular Cell Biology*, 11(7), 502–514.

Hannoun, Z. *et al.* (2010) 'The comparison between conditioned media and serum-free media in human embryonic stem cell culture and differentiation', *Cellular Reprogramming*, 12(2), 133–140.

Harrison, R. G. *et al.*, (1907). 'Observation on the living developing never fiber'. *The Anatomical Record*, 1(5): 116-128.

Hartsock, A. and Nelson, W. J. (2008) 'Adherens and tight junctions: Structure, function and connections to the actin cytoskeleton', *Biochimica et Biophysica Acta - Biomembranes*, 1778(3), 660–669.

Hernández, M. *et al.* (2011) 'Host-pathogen interactions in progressive chronic periodontitis', *Journal of Dental Research*, 90(10), 1164–1170.

Hosseinkhani, M. *et al.* (2014) 'Tissue engineered scaffolds in regenerative medicine', *World Journal of Plastic Surgery*, 33(11), 3–7.

- Huang, Y. *et al.* (2006) 'Effect of calcium ion concentration on keratinocyte behaviors in the defined media', *Biomedical Engineering - Applications, Basis & Communications*, 18(1), 37–41.
- Hughes, F. J. (2014) 'Periodontium and Periodontal Disease', in *Stem Cell Biology and Tissue Engineering in Dental Sciences*, 433–444.
- Hwang, N. S. *et al.*, (2007) 'Cartilage tissue engineering: Directed differentiation of embryonic stem cells in three-dimensional hydrogel culture.', *Methods in Molecular Biology*, 407, 351–373.
- Ikarashi, Y. *et al.* (2007) 'Improved biocompatibility of titanium-zirconium (Ti-Zr) alloy: Tissue reaction and sensitization to Ti-Zr alloy compared with pure Ti and Zr in rat implantation study', *Material Transactions*, 71(4), 395–401.
- Ikeda, H. *et al.* (2000) 'Ultrastructural and immunoelectron microscopic studies of the peri-implant epithelium-implant (Ti-6Al-4V) interface of rat maxilla.', *The Journal of Periodontology*, 71(6), 961–973.
- Isaac, C. *et al.* (2011) 'Replacement of fetal calf serum by human serum as supplementation for human fibroblast culture', *Revista Brasileira de Cirurgia Plástica*, 26(3), 379–384.
- Ivanovski, S. and Lee, R. (2018) 'Comparison of peri-implant and periodontal marginal soft tissues in health and disease', *Periodontology 2000*, 76(1), 116–130.

- Izumi, K. *et al.* (2000) 'Development and characterization of a tissue-engineered human oral mucosa equivalent produced in a serum-free culture system', *Journal of Dental Research*, 79(3), 798–805.
- Javed, F. *et al.* (2013) 'Role of primary stability for successful osseointegration of dental implants: Factors of influence and evaluation.', *Interventional Medicine & Applied Science*, 5(4), 162–167.
- Jedrzejczak-Silicka, M. (2017) 'History of cell culture', *InTech*, 3, 1–42.
- Jochems, C. E. A. *et al.* (2002) 'The use of fetal bovine serum: Ethical or scientific problem?', *ATLA*, 30(2), 219–227.
- Johnston, R. B. and Johnston, R. B. (2012) 'Disorders of epidermal maturation and keratinization', in *Weedon's Skin Pathology Essentials*. Churchill Livingstone, Florida, USA, pp. 193–219.
- Kaur, G. and Dufour, J. M. (2012) 'Cell lines: Valuable tools or useless artifacts.', *Spermatogenesis*, 2(1), 1–5.
- Khan, E. *et al.* (2012) 'Architectural characterization of organotypic cultures of H400 and primary rat keratinocytes.', *Journal of Biomedical Materials Research. Part A*, 100(12), 3227–3238.
- Khan, F. and Ahmad, S. R. (2013) 'Polysaccharides and their derivatives for versatile tissue engineering application', *Macromolecular Bioscience*, 13(4), 395–421.
- Kikuchi, A. *et al.* (1999) 'Effect of Ca<sup>2+</sup>-alginate gel dissolution on

- release of dextran with different molecular weights', *Journal of Controlled Release*, 58(1), 21–28.
- Killion, J. A. *et al.* (2011) 'Mechanical properties and thermal behaviour of PEGDMA hydrogels for potential bone regeneration application', *Journal of the Mechanical Behavior of Biomedical Materials*, 4(7), 1219–1227.
- Kimura, Y. *et al.* (2012) 'Initial attachment of human oral keratinocytes cultured on zirconia or titanium.', *Dental Materials Journal*, 31(3), 346–353.
- Kortegaard, H. E. *et al.* (2008). 'Periodontal disease in research beagle dogs--an epidemiological study'. *The Journal of Small Animal Practice*, 46(12): 610-616.
- Kydd, W. L. and Daly, C. H. (1982) 'The biologic and mechanical effects of stress on oral mucosa', *The Journal of Prosthetic Dentistry*, 47(3), 317–329.
- Lacoste-Ferré, M.-H. *et al.* (2011) 'Dynamic mechanical properties of oral mucosa: Comparison with polymeric soft denture liners.', *Journal of the Mechanical Behavior of Biomedical Materials*, 4(3), 269–274.
- Lamb, R. and Ambler, C. A. (2013) 'Keratinocytes propagated in serum-free, feeder-free culture conditions fail to form stratified epidermis in a reconstituted skin model.', *PloS one*, 8(1), e52494.

Lambert, P. M., Morris, H. F. and Ochi, S. (1997) 'The influence of 0.12% chlorhexidine digluconate rinses on the incidence of infectious complications and implant success', *Journal of Oral and Maxillofacial Surgery*, 55(12 SUPPL.), 25–30.

Lamouille, S., Xu, J. and Derynck, R. (2014) 'Molecular mechanisms of epithelial-mesenchymal transition.', *Nature Reviews Molecular Cell Biology*, 15(3), 178–196.

Larsson, C. et al. (1996) 'Bone response to surface-modified titanium implants: studies on the early tissue response to machined and electropolished implants with different oxide thicknesses', *Biomaterials*, 16(6), 605–616.

Lee, D., et al. (2016). 'Effects of untreated periodontitis on osseointegration of dental implants in a beagle dog model'. *Journal of Periodontology*, 87(10): 1141-1148.

Lee, K. Y. and Mooney, D. J. (2012a) 'Alginate: properties and biomedical applications.', *Progress in Polymer Science*, 37(1), 106–126.

Leigh I. M. and Watt F. M. 1995) 'The culture of human epidermal keratinocytes'. In Leigh, I.M, Lane, E.B and Watt, F. M (eds.) *The Keratinocyte Handbook*, Cambridge, UK: Cambridge University Press, pp. 43-153.

Lekhanont, K. et al. (2009) 'A serum- and feeder-free technique of culturing human corneal epithelial stem cells on amniotic membrane.',

*Molecular Vision*, 15, 1294–1302.

Leonhardt *et al.* (1992) 'Putative periodontal and teeth in pathogens on titanium implants and teeth in experimental gingivitis and periodontitis in beagle dogs', *Clinical Oral Implants Research*, 3(3), 112–119.

Levin, L. (2008) 'Dealing with dental implant failures.', *Journal of Applied Oral Science*, 16(3), 171–175.

Lewis, W. H. and Lewis, M. R. (1912). 'The cultivation of chick tissues in media of known chemical constitution'. *The Anatomical Record*, 6(5): 207-211.

Li, N. Y. K. *et al.* (2014) 'Dose-dependent effect of mitomycin C on human vocal fold fibroblasts.', *Head & Neck*, 36(3), 401–410.

Li, Y. *et al.* (2010) 'Cytotoxicity of titanium and titanium alloying elements', *Journal of Dental Research*, 89(5), 493–497.

Li, Y. and Kilian, K. A. (2015) 'Bridging the gap: from 2D cell culture to 3D microengineered extracellular matrices', *Advanced Healthcare Materials*, 4(18), 2780–2796.

Lim, K. S. *et al.* (2015) 'Promoting cell survival and proliferation in degradable poly(vinyl alcohol)-tyramine hydrogels', *Macromolecular Bioscience*, 15(10), 1423–1432.

Liñares, A. *et al.* (2013) 'Peri-implant soft tissues around implants with

a modified neck surface. Part 1. Clinical and histometric outcomes: A pilot study in minipigs', *Journal of Clinical Periodontology*, 40(4), 142–420.

Lindhe, J. *et al.*(eds) (2015) *Clinical Periodontology and Implant Dentistry*. Oxford, UK: John Wiley & Sons.

Llames, S. *et al.* (2015) 'Feeder layer cell actions and applications.', *Tissue Engineering. Part B, Reviews*, 21(4), 345–353.

Lu, R. *et al.* (2012) 'Identification of human fibroblast cell lines as a feeder layer for human corneal epithelial regeneration.', *PloS one*, 7(6), e38825.

MacNeil, S. *et al.*, (2011) 'Production of tissue-engineered skin and oral mucosa for clinical and experimental use.', in Haycock, J. (ed.) *3D Cell Culture: Methods and Protocols*. New York, USA: Humana Press, pp. 129–53.

Malik, R. *et al.* (2010) 'Success or failure of a dental implant: its relationship to bone density: a case report of a failed implant.', *The Journal of Contemporary Dental Practice*, 11(6), e065-72.

Martens, P. *et al.* (2007) 'Effect of poly(vinyl alcohol) macromer chemistry and chain interactions on hydrogel mechanical properties', *Chemistry of Materials*, 19(10), 2641–2648.

Martens, P. and Anseth, K. (2000) 'Characterization of hydrogels

formed from acrylate modified poly(vinyl alcohol) macromers', *Polymer*, 41(21), 7715–7722.

Matalová, E. *et al.*, (2014) 'Development of tooth and associated structures', in *Stem Cell Biology and Tissue Engineering in Dental Sciences*, 335–346.

Mateo, M. *et al.* (2015) 'Connections matter – how viruses use cell–cell adhesion components', *Journal of Cell Science*, 128(3), 431–439.

Mazlyzam, A. L. *et al.* (2008) 'Human serum is an advantageous supplement for human dermal fibroblast expansion: clinical implications for tissue engineering of skin', *Archives of Medical Research*, 39(8), 743–752.

McGinley, E. L. *et al.*, (2013) 'Biocompatibility effects of indirect exposure of base-metal dental casting alloys to a human-derived three-dimensional oral mucosal model.', *Journal of Dentistry*, 41(11), 1091–1100.

McGrath, J. A. (2005) 'Inherited disorders of desmosomes', *Australasian Journal of Dermatology*, 46(4), 221–229.

Merker, H.-J. (1994) 'Morphology of the basement membrane', *Microscopy Research and Technique*, 28(2), 95–124.

Moharamzadeh, K. (2017) 'Oral mucosa tissue engineering', in Taybi, L. and Moharamzadeh, K. (eds.), *Biomaterials for Oral and Dental*

*Tissue Engineering*. Cambridge, UK: Woodhead Publishing, pp. 223–244.

Monjo, M. *et al.* (2008). 'In vivo expression of osteogenic markers and bone mineral density at the surface of fluoride-modified titanium implants'. *Biomaterials*, 29(28): 3771-3780.

Mosmann, T. (1983) 'Rapid colorimetric assay for cellular growth and survival: Application to proliferation and cytotoxicity assays', *Journal of Immunological Methods*. Elsevier, 65(1–2), 55–63.

Nanci, A. (2008) *Ten Cate's Oral Histology*. 6th edn. Missouri, USA: Mosby.

Nanci, A. and Bosshardt, D. D. (2006) 'Structure of periodontal tissues in health and disease', *Periodontology 2000*, 11–28.

Naseer, M. I. *et al.* (2009) 'Effect of fetal calf serum on cellular proliferation of mouse y1 adrenocortical cells in vitro', *Pakistan Journal of Medical Sciences*, 25(3), 500–504.

National Center for Biotechnology Information (2018) 'Gene'. Available at: <https://www.ncbi.nlm.nih.gov/gene>. (Accessed: 6 February 2017).

National Center for Biotechnology Information (2018) 'Primer-BLAST'. Available at: <https://www.ncbi.nlm.nih.gov/tools/primer-blast/>. (Accessed: 6 February 2017).

National Center for Biotechnology Information (2018) 'BLAST:

Standard Nucleotide BLAST'. Available at:

[https://blast.ncbi.nlm.nih.gov/Blast.cgi?PAGE\\_TYPE=BlastSearch](https://blast.ncbi.nlm.nih.gov/Blast.cgi?PAGE_TYPE=BlastSearch).

(Accessed: 6 February 2017).

National Centre for the Replacement Refinement & Reduction of Animals in Research (2018) 'The 3Rs'. Available at:

<https://www.nc3rs.org.uk/the-3rs>. (Accessed 13 September 2018)

Newman, M. G., Takei, H. H. and Carranza, F. A. (2015) *Carranza's Clinical Periodontology*. 6 edn. Sydney, Australia: Saunders.

Nguyen, Q. T. *et al.* (2012) 'Cartilage-like mechanical properties of poly (ethylene glycol)-diacrylate hydrogels', *Biomaterials*, 33(28), 6682–6690.

Noort, R. (1987) 'Titanium: The implant material of today', *Journal of Materials Science*, 22(11), 3801–3811.

O'Brien, J. *et al.* (2000) 'Investigation of the Alamar Blue (resazurin) fluorescent dye for the assessment of mammalian cell cytotoxicity', *European Journal of Biochemistry*, 5421–5426.

Office of Life Sciences (2016) '*Public attitudes to animal research in 2016*' Ipsos MORI. Available at:

<https://www.ipsos.com/sites/default/files/publication/1970-01/sri-public-attitudes-to-animal-research-2016.pdf>. (Accessed: 13 September 2018).

Ölschläger, V. *et al.*, (2011) 'Comparison of primary human fibroblasts

and keratinocytes with immortalized cell lines regarding their sensitivity to sodium dodecyl sulfate in a neutral red uptake cytotoxicity assay', *Arzneimittelforschung*, 59(03), 146–152.

Ophof, R. *et al.* (2002) 'Oral keratinocytes cultured on dermal matrices form a mucosa-like tissue.', *Biomaterials*, 23(17), 3741–3748.

Orimo, H. (2010) 'The mechanism of mineralization and the role of alkaline phosphatase in health and disease'. *Journal of Nippon Medical School*, 77(1): 4-12.

Osman, R. B. and Swain, M. V (2015) 'A critical review of dental implant materials with an emphasis on titanium versus zirconia.', *Materials*, 8(3), 932–958.

Page, R. C. and Kornman, K. S. (1997) 'The pathogenesis of human periodontitis: an introduction.', *Periodontology 2000*, 14(1), 9–11.

Parlato, M. *et al.* (2014) 'Poly(ethylene glycol) hydrogels with adaptable mechanical and degradation properties for use in biomedical applications.', *Macromolecular Bioscience*. 14(5), 687–698.

Paulsen, F. and Thale, A. (1998) 'Epithelial-connective tissue boundary in the oral part of the human soft palate.', *Journal of Anatomy*, 193 (3), 457–467.

Payne, K. F. B. *et al.* (2014) 'Tissue engineering technology and its possible applications in oral and maxillofacial surgery.', *The British*

*Journal of Oral & Maxillofacial Surgery*, 52(1), 7–15.

Pfaffl, M. W. *et al.* (2004) ‘Determination of stable housekeeping genes, differentially regulated target genes and sample integrity: BestKeeper – Excel-based tool using pair-wise correlations’, *Biotechnology Letters*, 26, 509–515.

Pinto, M. C. X. *et al.* (2015) ‘Calcium signaling and cell proliferation’, *Cellular Signalling*, 27(11), 2139–2149.

Ponchio, L. *et al.* (2000) ‘Mitomycin C as an alternative to irradiation to inhibit the feeder layer growth in long-term culture assays’, *Cytotherapy*, 2(4), 281–286.

Presland, R. B. and Dale, B. A. (2000) ‘Epithelial structural proteins of the skin and oral cavity: Function in health and disease’, *Critical Reviews in Oral Biology and Medicine*, 383–408.

Prime, S. S. *et al.* (1990) ‘The behaviour of human oral squamous cell carcinoma in cell culture.’, *The Journal of pathology*, 160(3), 259–269.

Rheinwald, J. G. and Green, H. (1975) ‘Serial cultivation of strains of human epidermal keratinocytes: the formation of keratinizing colonies from single cells.’, *Cell*, 6(3), 331–343.

Richard, M. H. *et al.* (1990) ‘Vimentin expression in normal human keratinocytes grown in serum-free defined MCDB 153 medium’, *Archives of Dermatological Research*, 282(8), 512–515.

Roed-Petersen, B. and Renstrup, G. (1969) 'A topographical classification of the oral mucosa suitable for electronic data processing. Its application to 560 leukoplakias.', *Acta Odontologica Scandinavica*, 27(6), 681–695.

Rohrbach, D. H. and Martin, G. R. (1982) 'Structure of basement membrane in normal and diabetic tissue.', *Annals of the New York Academy of Sciences*, 401, 203–211.

Rosso, F. *et al.* (2004) 'From cell-ECM interactions to tissue engineering', *Journal of Cellular Physiology*, 199(2), 174–180.

Rutkovskiy, A *et al.* (2016). 'Osteoblast differentiation at a glance'. *Medical Science Monitor Basic Research*, 22(1): 95-106.

Ryynänen, J. *et al.* (1992) 'Type VII collagen gene expression by cultured human cells and in fetal skin. Abundant mRNA and protein levels in epidermal keratinocytes', *Journal of Clinical Investigation*, 89(1), 163–168.

Saini, M. *et al.* (2015) 'Implant biomaterials: A comprehensive review', *World Journal of Clinical Cases*, 3(1), 52–57.

Saintigny, G *et al.* (1993) 'Reconstruction of epidermis on a chitosan cross-linked collagen-GAG lattice: effect of fibroblasts', *Acta dermatovenereologica*, 73(3), 175–180.

Sakka, S. *et al.*, (2012) 'Factors associated with early and late failure of

dental implants', *Journal of Investigative and Clinical Dentistry*, 3(4), 258–261.

Salvi, G. E. *et al.* (2008) 'One-year bacterial colonization patterns of *Staphylococcus aureus* and other bacteria at implants and adjacent teeth', *Clinical Oral Implants Research*, 19(3), 242–248.

Salvi, G. E. *et al.*, (2012) 'Reversibility of experimental peri-implant mucositis compared with experimental gingivitis in humans', *Clinical Oral Implants Research*, 23(2), 182–190.

Sandvig, I. *et al.*, (2014). 'RGD-peptide modified alginate by a chemoenzymatic strategy for tissue engineering applications'. *Journal of Biomedical Materials Research Part A*. 103(3): 896–906.

Sartoretto, S. C. *et al.* (2015) 'Early osseointegration driven by the surface chemistry and wettability of dental implants', *Journal of Applied Oral Science*, 23(3), 279–287.

Schindelin, J. *et al.* (2012) 'Fiji: An open-source platform for biological-image analysis', *Nature Methods*, 9(7), 676–682.

Schweizer, J. *et al.*(2006). 'New consensus nomenclature for mammalian keratins', *The Journal of Cell Biology*, 174(2), 169–174.

Shen, L. (2012) 'Tight junctions on the move: Molecular mechanisms for epithelial barrier regulation', *Annals of the New York Academy of Sciences*, 1258(1), 9–18.

- Shetty, S. and Gokul, S. (2012) 'Keratinization and its disorders', *Oman Medical Journal*, 27(5), 348–357.
- Sigurdson, L. *et al.* (2002) 'A comparative study of primary and immortalized cell adhesion characteristics to modified polymer surfaces: toward the goal of effective re-epithelialization.', *Journal of Biomedical Materials Research*, 59(2), 357–365.
- Sista, S. *et al.* (2011) 'The influence of surface energy of titanium-zirconium alloy on osteoblast cell functions in vitro', *Journal of Biomedical Materials Research - Part A*, 97(1), 27–36.
- Skottman, H. *et al.* (2006) 'Unique gene expression signature by human embryonic stem cells cultured under serum-free conditions correlates with their enhanced and prolonged growth in an undifferentiated stage', *Stem Cells*, 24(1), 151–167.
- Smeets, R. *et al.* (2016) 'Impact of dental implant surface modifications on osseointegration', *BioMed Research International*, 6285620.
- Song, J. *et al.* (2004) 'Development and characterization of a canine oral mucosa equivalent in a serum-free environment.', *Journal of Biomedical Materials Research. Part A*, 71(1), 143–153.
- Sorsa, T. *et al.*, (2004). 'Matrix metalloproteinases (MMPs) in oral diseases'. *Oral Diseases*. 10(6): 311-318.
- Squier, C. A. and Kremer, M. J. (2001) 'Biology of oral mucosa and

esophagus.’, *Journal of the National Cancer Institute. Monographs*, 2001(29), 7–15.

Subramani, K. *et al.* (2009) ‘Biofilm on dental implants: A review of the literature.’, *The International Journal of Oral & Maxillofacial Implants*, 24(4), 616–626.

Sun, J. and Tan, H. (2013a) ‘Alginate-based biomaterials for regenerative medicine applications’, *Materials*, 1285–1309.

Sun, T. *et al.* (2006) ‘Culture of skin cells in 3D rather than 2D improves their ability to survive exposure to cytotoxic agents’, *Journal of Biotechnology*, 122(3), 372–381.

Swamynathan, P. *et al.* (2014) ‘Are serum-free and xeno-free culture conditions ideal for large scale clinical grade expansion of Wharton’s jelly derived mesenchymal stem cells? A comparative study’, *Stem Cell Research & Therapy*, 5(4), 88-105.

Takami, Y. *et al.* (1996) ‘Dispase/detergent treated dermal matrix as a dermal substitute’, *Burns*, 22(3), 182–190.

Taketa, H. (2015). ‘Peptide-modified substrate for modulating gland tissue growth and morphology *in vitro*’. *Scientific Reports*, 5(1): 11468.

Tan, K. Y. *et al.* (2015) ‘Serum-free media formulations are cell line-specific and require optimization for microcarrier culture’, *Cytotherapy*, 17(8), 1152–1165.

- Teitelbaum, S.L. (2000). 'Bone resorption by osteoclasts'. *Science*, 289(5484): 1504-1508.
- Tennant, J. R. (1964) 'Evaluation of the trypan blue technique for determination of cell viability', *Transplantation*, 2(6), 685–694.
- Tu, C. L. and Bikle, D. D. (2013) 'Role of the calcium-sensing receptor in calcium regulation of epidermal differentiation and function', in *Best Practice and Research: Clinical Endocrinology and Metabolism*. Oxford, UK: Baillière Tindall, pp. 415–427.
- van der Valk, J. *et al.* (2004) 'The humane collection of fetal bovine serum and possibilities for serum-free cell and tissue culture', *Toxicology in Vitro*, 18(1), 1–12.
- van der Velden, L.-A. *et al.* (2001) 'Expression of cytokeratin subtypes and vimentin in squamous cell carcinoma of the floor of the mouth and the mobile tongue', *Oto-Rhino-Laryngologia Nova*, 11(3), 186–192.
- Vyas, N. *et al.* (2017) 'Penetration of sub-micron particles into dentinal tubules using ultrasonic cavitation', *Journal of Dentistry*, 56, 112–120.
- Walko, G., Castañón, M. J. and Wiche, G. (2015) 'Molecular architecture and function of the hemidesmosome', *Cell and Tissue Research*, 360(2), 363–378.
- Wehrle-Haller, B. (2012) 'Structure and function of focal adhesions', *Current Opinion in Cell Biology*, 24(1), 116–124.

Wennerberg, A. *et al.* 'A histomorphometric evaluation of screw-shaped implants each prepared with two surface roughnesses', *Clinical Oral Implants Research*, 9(1), 11–19.

Williams, C. G. *et al.* (2005) 'Variable cytocompatibility of six cell lines with photoinitiators used for polymerizing hydrogels and cell encapsulation', *Biomaterials*, 26(11), 1211–1218.

Wilson, C. J. *et al.* (2005) 'Mediation of biomaterial–cell interactions by adsorbed proteins: A review', *Tissue Engineering*, 11(1), 1–18.

Yadev, N. P. *et al.* (2011) 'Evaluation of tissue engineered models of the oral mucosa to investigate oral candidiasis.', *Microbial Pathogenesis*, 50(6), 278–285.

Yamamoto, T. *et al.* (2016) 'Histology of human cementum: Its structure, function, and development', *Japanese Dental Science Review*, 52(3), 63–74.

Yamaza, T. and Kido, M. A. (2011) 'Biological sealing and defense mechanisms in peri-implant mucosa of dental implants', in Turkyilmaz, I. (ed.) *Implant Dentistry - The Most Promising Discipline of Dentistry*. London, UK: Intech Open, pp. 219–242.

Yoshizawa, M. *et al.* (2004) 'Ex vivo produced human conjunctiva and oral mucosa equivalents grown in a serum-free culture system', *Journal of Oral and Maxillofacial Surgery*, 62(8), 908–988.

Yao, T. and Asayama, Y. (2017). 'Animal-cell cultures media: History, characteristics and current issues'. *Reproductive Medicine and Biology*, 16(2): 99-117.

Young, C. J., Poole-Warren, L. A. and Martens, P. J. (2012) 'Combining submerged electrospray and UV photopolymerization for production of synthetic hydrogel microspheres for cell encapsulation.', *Biotechnology and Bioengineering*, 109(6), 1561–1570.

Yurchenco, P. D. and Patton, B. L. (2009) 'Developmental and pathogenic mechanisms of basement membrane assembly', *Current Pharmaceutical Design*, 15(12), 1277–1294.

Zhang, Y. *et al.* (2018) 'Effect of zr addition on the corrosion of Ti in acidic and reactive oxygen species (ros)-containing environments', *ACS Biomaterials Science and Engineering*, 4(3), 1103–1111.

Zhu, J. and Marchant, R. E. (2011) 'Design properties of hydrogel tissue-engineering scaffolds.', *Expert Review of Medical Devices*, 8(5), 607–626.

Zillikens, D. (1999) 'Acquired skin disease of hemidesmosomes', *Journal of Dermatological Science*, 20(2), 134–154.

Zitzmann, N. U. and Berglundh, T. (2008) 'Definition and prevalence of peri-implant diseases', *Journal of Clinical Periodontology*, 35(SUPPL. 8), 286–291.

# APPENDIX

## **Outputs from this research.**

### **Conference Presentations (Oral)**

Animal Replacement Science 2016 – Advances, Awareness, Applications, 9 December 2016, London

- C L White, O Addison, G Landini, P R Cooper & R M Shelton. Identification of suitable culture medium for the development of an animal-free oral mucosa model.

---

### **Introduction**

Tissue engineering recreates complex 3D tissue within an in vitro environment. Animal-derived products such as foetal calf/bovine serum are commonly used to support the engineered tissue. However, their use has many disadvantages, including potential disease transmission, contamination, inter-batch variability and ethical concerns.

### **Aim**

This study aimed to identify a suitable animal-free culture medium that can be used to develop long-term 3D cultures of human oral mucosa. This model will then be used to analyse mucosal soft tissue interactions with dental implant surfaces.

### **Materials and Methods**

Primary human gingival fibroblasts (pHGFs) and H400 cells (human keratinocyte cell lines isolated from an oral squamous cell carcinoma) were maintained in three commercially available keratinocyte chemically defined culture media; Epilife® supplemented with S7, CnT-04 and KGM®-CD and DMEM supplemented with 10% human serum (used as a comparator). Doubling-time and viability of cultures were analyzed for 21 days from growth curves established using trypan blue dye exclusion and Alamar Blue assays. Gene expression analyses of cytokeratins-1, -5, -10, -14, and -19, vimentin, and e-cadherin were performed using semi-quantitative RT-PCR.

### **Results and Discussion**

KGM®-CD exhibited highest growth rates for both cell types during the experimental period. There was minimal difference between cytokeratin expression levels of cultures grown in KGM®-CD and the control, and these cultures expressed similar levels of vimentin and e-cadherin.

### **Conclusion**

The animal-free culture medium KGM®-CD has the potential to support development of a 3D model of oral mucosa. The ability to construct oral mucosa without using animal products would enhance the relevance of tissue engineering research and reduce animal use.

### **Conference Presentations (Poster)**

United Kingdom Society for Biomaterials 15<sup>th</sup> Annual Conference, 30 June- 1 July 2016, London.

- C L White, O Addison, G Landini, P R Cooper & R M Shelton. . Identification of a suitable animal-free culture medium for the development of 3D oral mucosa models.

---

### **Introduction**

Animal-derived products such as foetal bovine/calf serum (FBS/FCS) are routinely used to culture cells in vitro. Drawbacks in using serum supplementation include potential risk of disease transmission and contamination, inter-batch variability and ethical concerns. The use of serum free or chemically defined media as an alternative is currently being investigated. The aim of this research is to identify a suitable animal-free culture medium that supports and sustains primary human gingival keratinocytes and fibroblasts in the development of 3D oral mucosa models.

### **Materials and Methods**

The H400 human oral keratinocyte cell line<sup>3</sup> and primary human gingival fibroblasts, isolated from biopsies (approved by the University of Birmingham Ethics Committee: RG\_12-020), were grown as monolayer cultures. Cultures were maintained in three commercially

available keratinocyte chemically defined culture media; Epilife® supplemented with S7 (Gibco®, Life Technologies, Paisley, UK), CnT-04 (CellnTec, Advanced Cell Systems AG, Bern, Switzerland) and KGM®-CD (Lonza, Switzerland) and DMEM (Gibco®, UK) supplemented with 10% human serum (Sigma-Aldrich, Paisley, UK), which was used as a control. Doubling-time and viability of the monolayers were analyzed up to 21 days in culture, from growth curves established using trypan blue dye exclusion. Gene expression analysis of cytokeratin-1, -5, -6, -13, -16 and -19 as well as vimentin, n-cadherin and e-cadherin were performed using semi-quantitative reverse transcription-polymerase chain reaction.

## **Results**

KGM®-CD showed the greatest potential to support both human oral keratinocytes and fibroblasts for 21 days from analysis of viable cell growth curves. KGM®-CD enhanced growth rates in keratinocytes ( $p < 0.05$ ) whilst limited growth in fibroblasts when compared with controls. Cultures grown in Epilife® supplemented with S7 and CnT-04, exhibited significantly ( $p < 0.05$ ) slower growth and exhibited variable viability during the culture period in comparison with the control and KGM®-CD. Analysis of cytokeratins alongside other epithelial and fibroblastic markers in the cells maintained in the different oral keratinocyte media, revealed minimal difference in expression levels between cultures grown in KGM®-CD and the control. However, expression of the cytokeratins in cultures grown in Epilife® supplemented with S7, appeared to have increased compared with the control whereas cultures grown in CnT-04 decreased expression cytokeratins compared with the control. All cultures exhibited like expression levels for epithelial and fibroblastic markers.

## **Discussion**

Growth curve analyses were in agreement with previous research conducted by Sun et al (2004) who demonstrated that cultures were able to grow in serum-free culture conditions, however when directly comparing with serum supplemented cultures, growth was slightly inhibited.

It appeared likely that the different growth and gene expression within the media used could have resulted from the differences in formulation of the chemically defined culture media. The composition of each of the commercial chemically defined media was not provided by the

manufacturers, making definitive conclusions regarding the impact of particular components difficult.

## **Conclusion**

KGM®-CD has the capacity to support growing cultures of human gingival keratinocytes and fibroblasts for up to 21 days, whilst maintaining a high level of viability (>80%). This suggested that KGM®-CD can be used as a serum-free culture medium for the necessary expansion of primary human gingival keratinocytes and fibroblasts and can be potentially used to develop 3D models of oral mucosa

Animal Replacement Science 2016 – Advances, Awareness, Applications, 9 December 2016, London

- C L White, O Addison, G Landini, P R Cooper & R M Shelton. Identification of suitable culture medium for the development of an animal-free oral mucosa model.

---

## **Introduction**

Tissue engineering recreates complex 3D tissue within an in vitro environment. Animal-derived products such as foetal calf/bovine serum are commonly used to support the engineered tissue. However, their use has many disadvantages, including potential disease transmission, contamination, inter-batch variability and ethical concerns.

## **Aim**

This study aimed to identify a suitable animal-free culture medium that can be used to develop long-term 3D cultures of human oral mucosa. This model will then be used to analyse mucosal soft tissue interactions with dental implant surfaces.

## **Materials and Methods**

Primary human gingival fibroblasts (pHGFs) and H400 cells (human keratinocyte cell lines isolated from an oral squamous cell carcinoma) were maintained in three commercially available keratinocyte chemically defined culture media; Epilife® supplemented with S7, CnT-04 and KGM®-CD and DMEM supplemented with 10% human

serum (used as a comparator). Doubling-time and viability of cultures were analyzed for 21 days from growth curves established using trypan blue dye exclusion and Alamar Blue assays. Gene expression analyses of cytokeratins-1, -5, -10, -14, and -19, vimentin, and e-cadherin were performed using semi-quantitative RT-PCR.

## **Results and Discussion**

KGM®-CD exhibited highest growth rates for both cell types during the experimental period. There was minimal difference between cytokeratin expression levels of cultures grown in KGM®-CD and the control, and these cultures expressed similar levels of vimentin and e-cadherin.

## **Conclusion**

The animal-free culture medium KGM®-CD has the potential to support development of a 3D model of oral mucosa. The ability to construct oral mucosa without using animal products would enhance the relevance of tissue engineering research and reduce animal use.

Annual Scientific Cranofacial Conference, 5 – 7 April 2017, Newcastle

- C L White, O Addison, G Landini, P R Cooper & R M Shelton.  
Determining a suitable culture medium for the development of an animal-free oral mucosa model.

---

## **Introduction**

3D tissue engineering aims to recreate complex tissues in vitro. Foetal calf/bovine serum and other animal derived products are commonly used to support development of these tissues. However, there is now a shift to use animal-free cultures due to intra-batch variations, ethical issues, and increased awareness to reduce animal use. This has led to the development of serum-free or chemically defined culture conditions.

## **Aim**

This research aimed to identify a suitable animal-free culture medium that supports and sustains human oral keratinocytes and fibroblasts, which will be used to develop long-term 3D oral mucosa models.

## **Materials and Method**

Primary human gingival fibroblasts (pHGFs) and H400 cells (human keratinocyte cell line isolated from an oral squamous cell carcinoma) were cultured in three commercially available keratinocyte chemically defined media; Epilife® supplemented with S7, CnT-04 and KGM®-CD. DMEM supplemented with 10% human serum was used for comparison. Over 21 days, cell number and viability were measured using Trypan blue dye exclusion and gene expression of cytokeratins-1, -5, -10, -14, and -19, and e-cadherin were analysed using semi-quantitative RT-PCR.

### **Results and Discussion**

KGM®-CD demonstrated the greatest potential to support populations of pHGFs and H400 cells, as growth curves, viability and doubling times of these cultures were comparable with cultures grown in human serum supplemented medium. There was also minimal difference between these two culture conditions in terms of cytokeratin and e-cadherin expression profiles.

### **Conclusion**

Data indicate that KGM-CD could be used as an animal-free alternative culture medium to support the development of 3D models of oral mucosa.